

Structural and functional analysis of the guidance
cue molecule netrin-1 in complex with its receptor
DCC unravels the molecular mechanisms of
interaction

Dissertation

with the aim to achieve the doctoral degree at the Faculty of Mathematics,
Informatics and Natural Sciences
Department of Biology, University Hamburg

-Korrigierte Fassung-

submitted by

Nina Krüger

March, 2014

Gutachter : Dr. Rob Meijers, EMBL Hamburg

Gutachter : JProf. Dr. Christian A. Voigt, Universität Hamburg

Vorsitzender : Prof. Dr. Christian Lohr, Universität Hamburg

Disputation : 23.05.2014

›Dem Gehenden schiebt sich der Weg unter die Füße‹

Martin Walser

Confirmation of linguistic accuracy by a native speaker

I hereby declare that I have read the PhD thesis “*Structural and functional analysis of the guidance cue molecule netrin-1 in complex with its receptor DCC unravels the molecular mechanisms of interaction*” by Nina Krüger. I confirm its accuracy with regard of application of the English language.

Hamburg, 18.03.2014

Mr. Matthew S. Dunne
Predoctoral Student
EMBL Hamburg c/o DESY
Notkestraße 85
22603 Hamburg
Germany

Index

I.	Confirmation of linguistic accuracy by a native speaker	4
II.	Abbreviations	7
1.	Abstracts	10
a.	Summary	10
b.	Zusammenfassung	12
2.	Introduction	14
a.	Basics	14
1.	Discovery of chemotropic guidance	14
2.	Basic principles of neuronal development	15
b.	Netrins and receptors	18
1.	Netrins are highly conserved guidance cues for migrating cells	18
2.	Netrin-1 and its receptors	19
3.	Deleted in colorectal cancer	22
4.	Neogenin	25
5.	UNC5	25
6.	Down syndrome cell adhesion molecule	26
c.	Netrin-1's functions outside the nervous system	27
d.	Aim of study	29
3.	Material and Methods	33
a.	Material	33
1.	Chemicals	33
2.	Buffers	34
3.	Media	34
4.	Enzymes	37
5.	Antibodies	37
6.	Kits	37
7.	Equipment	38
8.	HEK media	39
9.	Columns	40
10.	Proteins	40
b.	Methods	41
1.	Molecular cloning and DNA preparation	41
2.	Expression	51
3.	Protein purification	53
4.	Protein characterisation	58
5.	Binding assays	60
6.	Functional assays	62
7.	Crystallisation and SAXS	66
8.	Sequence alignment	70
9.	Programs	70
4.	Results	71
a.	Netrin-1	71
1.	Small scale expression and initial purification	71
2.	Improving affinity purification	76

3. Ion exchange	81
4. Protein precipitation	83
5. Reducing FCS minimised contamination	84
6. Biophysical protein characterisation	87
7. Expression and purification of Netrin _{VIV} mutants and GFP-fused construct	90
8. Crystallisation of Netrin _{VIV}	93
b. Netrin-1 and DCC	95
1. DCCs fibronectin domains 5 and 6 are sufficient to bind Netrin _{VIV}	95
2. Netrin _{VIV} crystallises with DCC _{FN56}	98
3. Netrin _{VIV} -DCC _{FN56} complex reveals two distinct binding sites	101
4. A generic receptor binding site is mediated by a cluster of sulphate ions	105
5. The DCC specific binding site is a hydrophobic hot spot	109
6. The two receptor binding sites are differentiated by individual affinities	111
7. Signal transduction is dependent on clustering by both binding sites of Netrin _{VIV} /DCC _{FN56}	118
8. Clustering in solution requires both binding sites and is netrin-1 dependent	126
c. Analysis of binding site conservation	129
1. Conservation of DCC binding sites on netrins	129
2. Conservation of netrin-1 binding sites on DCC and neogenin	132
5. Discussion and Conclusion	134
a. Discussion	134
1. Expression, purification and characterisation of Netrin _{VIV}	134
2. Netrin-1 and DCC	138
b. Conclusion	143
6. Acknowledgements	144
7. References	145
8. Appendix	155
a. Publication	155
b. Eidesstattliche Versicherung	156
c. SAXS data table	157
d. Crystallisation data table	160

I. Abbreviations

6xHis tag	Hexa-histidine tag
AB	Antibody
Anti-His	Antibody against a poly histidine motif
Anti-BSA	Antibody against bovine serum albumin
BSA	Bovine serum albumin
ConA	Concanavalin A
CV	Column volume
DCC	Deleted in colorectal cancer
DMEM	Dulbecco's modified eagle medium
DNA	Deoxyribonucleic acid
dNTP	Deoxynucleotide triphosphate
DSCAM	Down syndrome cell adhesion molecule
DTT	Dithiothreitol
E	Elution
EC	Effective concentration
EDTA	Ethylenediaminetetraacetic acid
EGF	Epidermal growth factor domain
FCS	Foetal calf serum
Fc-tag	Immunoglobulin soluble constant fragment tag
Fig	Figure
FN	Fibronectin domain
FPLC	Fast protein liquid chromatography
FT	Flow-through
GFP	Green fluorescent protein
GlcNAc	N-acetyl-D-glucosamine
GPI	Glycosylphosphatidylinositol
HA-tag	Human influenza hemagglutinin tag
HEK293T	Human embryonic kidney cells
HRP	Horseradish peroxidase
Hrs	Hours
HSPG	Heparan sulphate proteoglycan

Ig	Immunoglobulin domain
IMAC	Ion mobility affinity chromatography
IP	Immunoprecipitation
ITC	Isothermal titration calorimetry
K _d	Dissociation constant
LED	Light-emitting diode
MALDI TOF	Matrix-assisted laser desorption/ionisation time of flight
Med	Medium
min	Minute
MS	Mass spectrometry
MSC	Multiple cloning site
MST	Microscale thermophoresis
MUT	Mutant
Myc-tag	Myelocytomatosis oncogene tag
Ni-X	Nickel Sepharose™ excel
NTR	Netrin-like domain
p53	Phosphoprotein 53
PBS	Phosphate buffered saline
PBS	Phosphate buffered Saline
PBS-T	Phosphate buffered saline-Tween20
PCR	Polymerase chain reaction
PEI	Polyethylenimine
pI	Isoelectric point
PSG1	Human pregnancy-specific glycoprotein 1
RGMB	Repulsive guidance molecule B
Rpm	Rounds per minute
RT	Room temperature
S75	Superdex 75
SAXS	Small angle X-ray scattering
SDS-PAGE	Sodium dodecyl sulphate polyacrylamide gel electrophoresis
SEC	Size exclusion chromatography
siRNA	Small interfering ribonucleic acid
SPC	Sample preparation and characterisation
TAE	Tris acetate buffer with EDTA

TBS	Tris buffered saline
TBS-T	Tris buffered saline-Tween20
TSP	Thrombospondin
UNC	Uncoordinated
V	Volt
V ₀	Void volume
W	Wash
WB	Western blot
WT	Wildtype

1. Abstracts

1.a. Summary

The development of the nervous system involves complex cell signalling and generations of scientists have engaged in understanding these processes. The study presented here concentrates on the investigation of the molecular binding mechanisms between human netrin-1 and its receptor DCC to contribute to a better comprehension of developing neuronal networks.

Netrins belong to the laminin family and were firstly described as chemical guidance cues for migrating commissural and motor axons. Among bilaterally symmetric animals, from *C. elegans* to humans, they are highly conserved to play modulating roles in cell migration, proliferation and adhesion. They are involved in the organisation of neuronal connections, tissue patterning during organogenesis, angiogenesis, inflammation and cancer. Migrating nerve cells are attracted or repelled by netrin gradients respective to the receptors they are expressing, revealing them as bi-functional chemotropic factors. Netrin-1 is to date their best characterised representative. Among the receptors that have been identified to bind netrin-1 are deleted in colorectal cancer (DCC), neogenin, down-syndrome cell adhesion molecule (DSCAM) and uncoordinated 5A-D (UNC5A-D). Failure of the netrin-1 signalling leads to severe developmental defects during embryogenesis and, if occurring later in life, can lead to cancer. Therefore, a more detailed determination of the molecular interactions between netrin-1 and its cell-surface binding partners is of particular interest.

The domains taking part in these interactions between netrin-1 and its receptors have been the target of several studies. Using this information truncated constructs were designed for recombinant expression in human embryonic kidney cells (HEK293T). A construct comprised of the VI and V laminin-like domains, both proposed to be involved in DCC binding, was chosen for further studies according to the observed expression yields. Verification of different affinity and gel filtration chromatography techniques led to adjustment of the expression conditions and the establishment of a convenient and reproducible purification protocol. The described construct was confirmed to bind to the fifth and sixth fibronectin domain of DCC by two *in-vitro* binding assays. The crystal structure of a complex of netrin-1 and DCC revealed two distinct binding sites utilising different binding mechanisms and

affinities. Binding site 1 involves exclusively the third EGF-domain of netrin-1 and fibronectin domain 5 of DCC. This DCC-specific binding site resembles, based on its architecture, a hydrophobic hotspot. SAXS experiments and binding studies by thermophoresis showed a preference for the occupation of this binding site in solution.

Binding site 2 engages negatively charged ions in a unique way to mediate binding between positively charged surface patches on both, receptor and ligand. This generic binding site could interact with heparan sulphates to mediate the association with various other receptors to determine the fate of migrating cells, depending on the receptor composition. The effects of binding site specific mutations were tested in cell based and axon guidance assays. It was shown that the integrity of both binding sites is essential for path finding and signal transduction. Together the results of this study gave an insight into the molecular mechanisms of receptor/ligand interactions and a perspective on understanding netrin-1's bi-functionality.

1.b. Zusammenfassung

Generationen von Wissenschaftlern haben sich mit dem Studium der komplexen Signalwege während der Entwicklung neuronaler Netzwerke beschäftigt.

Um zu einem besseren Verständnis der Entstehung des Nervensystems beizutragen, beschäftigt sich die hier vorliegende Arbeit mit der Untersuchung der molekularen Bindungsmechanismen zwischen dem humanen Netrin-1 und seinem Rezeptor DCC.

Netrine gehören zur Familie der Laminine und wurden zunächst als chemische Leitmoleküle für kommissurale und motorische Axone beschrieben, später zeigte sich aber auch ihre Beteiligung in der Organentwicklung, der Angiogenese, bei Entzündungsprozessen und bestimmten Krebsformen. Migrierende Nervenzellen werden von Netrin Gradienten, in Abhängigkeit von ihren Zelloberflächenrezeptoren, angezogen oder abgestoßen. Dies verdeutlicht die Bi-Funktionalität dieser chemotropen Signalmoleküle. In bilateral symmetrisch organisierten Organismen, vom Wurm bis zum Menschen, sind diese Proteine in hohem Maße evolutionäre konserviert. Netrin-1 stellt bis heute den bestcharakterisierten Vertreter der Netrine dar. Zu den Netrin-1 bindenden Rezeptoren zählen *Deleted in colorectal cancer* (DCC), Neogenin, *Down-syndrome cell adhesion molecule* (DSCAM) und *uncoordinated 5A-D* (UNC5A-D). Da verschiedene Formen schwerer neuronale Entwicklungsfehler sowie einige Krebsarten mit einer Unterbrechung des Netrin-1 Signalweges in Verbindung gebracht werden können, ist eine genauere Bestimmung der molekularen Mechanismen, denen die Interaktionen zwischen Rezeptor und Ligand unterworfen sind, von großem Interesse.

Die Definition der Domänen, die an den genannten Interaktionen beteiligt sind, war Gegenstand etlicher vorangegangener Studien. Mit Hilfe der dort gewonnenen Erkenntnisse wurden verschiedene Konstrukte erstellt und in humanen embryonalen Nierenzellen (HEK293T) rekombinant expremiert. Besonders ein Konstrukt, das die VI und die V Laminin Domänen aufwies, fiel durch seine gute Expression auf. Für beide Domänen wurde schon früher eine Beteiligung in der Rezeptorenbindung vermutet. Zur Erstellung eines praktikablen und reproduzierbaren Reinigungsprotokolls wurden zahlreiche chromatographische Affinitäts- und Gelfiltrationstechniken untersucht und schließlich eine Adaptation der Expressionsbedingungen vorgenommen. Durch *in-vitro* Studien wurde die Bindung

des beschriebenen Netrin-1 Konstrukts an die fünfte und sechste Fibronectin-Domäne der Rezeptors DCC bestätigt. Die Kristallstruktur eines Komplexes aus Netrin-1 und DCC zeigte zwei, in Mechanismus und Affinität unterschiedliche, Bindungsstellen. An Bindungsstelle 1 interagieren ausschließlich die dritte EGF-Domäne des Netrin-1 und die Fibronectin-Domäne 5 des DCCs. Diese DCC-spezifische Bindungsstelle wurde anhand ihrer Architektur als hydrophober Hotspot identifiziert. Die Präferenz für diese Bindungsstelle in Lösung wurde durch SAXS Experimente und thermophoretische Messungen gezeigt.

Bindungsstelle 2 weist in einzigartiger Weise eine Akkumulation negativer Ionen auf, welche die Bindung zwischen positiv geladener Oberflächenbereiche des Rezeptors und des Ligand ermöglichen. Diese vielseitige Bindungsstelle könnte auf eine Interaktion mit Heparansulfaten hindeuten mit deren Hilfe die Bindung zu unterschiedlichen Rezeptoren vermittelt werden könnte, um so das Schicksal der migrierenden Zellen zu bestimmen. Zellbasierte Bindungsversuche und funktionale Untersuchungen an Axonen mit bindungsstellen-spezifischen Mutanten haben gezeigt, dass beide Bindungsstellen für die Wegfindung und Signaltransduktion essentiell sind. Zusammenfassend ermöglicht die vorliegende Studie einen Einblick in die molekularen Mechanismen der Rezeptor/Liganden Interaktionen die ein besseres Verständnis der Bi-Funktionalität von Netrin-1 ermöglicht.

2. Introduction

2.a. Basics

2.a.1. Discovery of chemotropic guidance

The brain has always been in the spiritual and scientific focus of interest. The first descriptions of brain organisation can be dated to 5000 years BC (Breasted, 1980). Nevertheless, for a long time the heart was seen as the base of soul and feelings. For Aristotle (384-322 BC) the brain was no more than a cooling organ but Hippocrates (460-370 BC) recognised it as the origin of intelligence and cognition (Oeser, 2010). How the brain and the nervous system are organised and developed remained a mostly unanswered question. After centuries of controversial speculations, Santiago Ramón y Cajal first visualised axons and dendrites by improving Golgi's staining methods. Both were honoured with the Noble prize in medicine and physiology in 1906 (Oeser, 2010). Cajal also developed the concept of chemotropic selection during neuronal development to explain his observations but came under attack during the 1930's and 1940's when mechanical theories were more in favour to describe neuronal networking (Sperry, 1963). Today, Roger Wolcott Sperry (Noble prize, 1981) is seen as the father of the chemo-affinity theory, postulating that nerve cells must carry chemical tags that distinguish them from one another and allow them to find their target destination by following morphogenic gradients (Sperry, 1963). He performed experiments on amphibian and fish eyes to investigate the regeneration of neuronal connections after injuries. Nerve fibres originating from the retina were disconnected, interchanged or scrambled but still managed to find their matching target region in the midbrain tectum during regeneration. Surprisingly, even when the retina was turned 180°, they would rather connect to this region, than to the region that would now make functional sense. He concluded that the selective determination of the path these fibres are taking is following chemical guidance (Sperry, 1963). Nirenberg's experiments with antibodies against cell surface molecules of avian retinal neurons then showed that their position can be identified by the molecules they carry on the cell surface, supporting the 'chemical stamp' postulated by Sperry (Trisler et al., 1981). It was not until a decade later that chemical guidance by morphogenic gradients was more specified

by the discovery of molecules that provide complementary gradients to establish the retinotectal and other topographically organised maps (Drescher et al., 1995; Zipursky and Sanes, 2010). Further identification of guidance molecules and their receptors, which combine short range contact-mediated and long range diffusible cues to guide axons to their targets, have led to the current understanding of the organisation of neuronal development, leaving Sperry's findings largely unchallenged (Zipursky and Sanes, 2010).

2.a.2. Basic principles of neuronal development

The development of the brain is a complex process. The human brain contains more than 100 billion neurons each contacting on average 1000 others to guarantee a complete and regular wiring (Alberts (2004) p. 1430). The development of the nervous system follows a three step process. Neurons are born and follow in a morphogenic phase distinct guidance cues to form a network of high order to connect all parts of the organism. In the last step, continuing into adulthood, these connections are adjusted depending on the signals they receive (Alberts (2004) p. 1431).

Neurons are, together with glia cells which form the insulating surrounding of the nerve cells, descendent from the ectoderm. In vertebrates the cells of the central nervous system are formed by the neural tube while the cells of the peripheral nerves are formed by the neural fold (Alberts (2004) p. 1432). Neuronal growth occurs into two directions. The axon extends into the direction of signal transduction and the dendrites are sent out to collect these signals by connecting to the axons of other neurons. Extension in either direction requires the formation of a spinose structure, called growth cone, with long, thin spikes, the lamellipodia. The growth cone organises the direction of migration, while dragging an axon or dendrite along (Alberts (2004) p. 1435). Nerve cells find their target regions with remarkable precision. Attached to the extracellular matrix or along other axons, the growth cones follow specific paths (Kolodkin and Tessier-Lavigne, 2011). Some matrix molecules (e.g. laminins) promote growth, while others (e.g. chondroitin sulphate proteoglycans) act as inhibitors (Siebert and Osterhout, 2011). Axons are not only influenced by the surface they are migrating on. Chemotropic factors can also attract or repel the

direction of growth. The movement of the growth cone is directed actively by short- and long range guidance cues. These cues can be contact-mediated (short range) or diffusible (long-range) and, depending on the origin of the growth cone, chemo-attractive or chemo-repulsive (Kolodkin and Tessier-Lavigne, 2011; Tessier-Lavigne and Goodman, 1996).

This behaviour is promoted by a number of receptors present on the lamellipodia of the growth cone which initiate the reorganisation of the cytoskeleton by the GTPases Rho and Rac according to a signals they receive (Alberts (2004) p. 1435). Upon reaching their final target they also initiate the growth cone to collapse (Jin and Strittmatter, 1997).

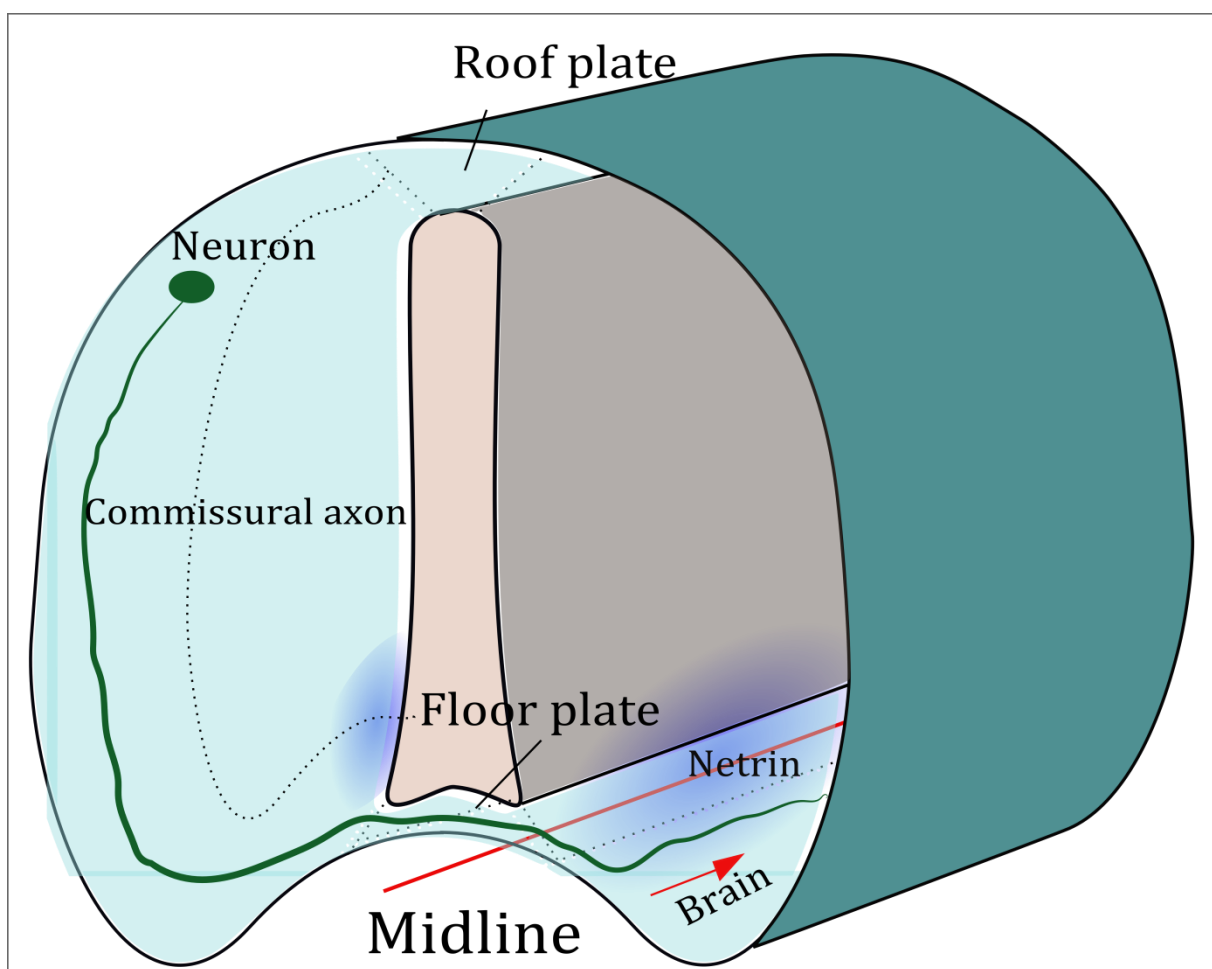


Figure A Guidance of commissural axons in the neural tube. Neurons send their axons ventrally in the direction of the floor plate, attracted by a netrin-1 gradient. They cross the midline and turn in a 90° angle to follow parallel to the floor plate. Here they lose their sensitivity for netrin-1 and migrate away from the gradient in the direction of the brain (adapted from (Alberts, 2004))

A highly conserved process that follows the described mechanisms is in bilaterally organised organisms the mechanism of transversal connection of an organisms two sides. Therefore, commissural axons are send from the spinal cord ventral in the

direction of the floor plate. After crossing the midline through the floor plate they change their direction in a 90° angle to proceed along the neural tube towards the brain (Fig. A). The growth cones of commissural axons express specific receptors that are responsive to guidance molecules secreted by the floor plate. Axons not expressing these receptors are not attracted and non-commissural neurons that express a different subset of receptors can even be rejected and sent to the roof plate instead. One of the guidance cue molecules expressed ventrally by the floor plate midline is netrin-1. This gradient is bi-functional and its attracting or repelling effect depends on the present receptors (Moore et al., 2007). The selection of receptors expressed in the growth cone can change during migration to alter the direction of migration after midline and floor plate crossing. Sensitivity for the attractive signals from the floor plate is lost, while the sensitivity for floor plate derived repellent signals arises to prevent back crossing over the midline (Alberts (2004), p. 1436 f.).

After reaching their target destination, neurons form contacts. Two events take place to adjust the innervation of a region. Firstly, many nerve cells die competing for growth factors, ensuring that the wiring in the target region resembles the respective requirements. Secondly, synapses are formed and enhanced depending on the intensity of signals they are receiving (Alberts (2004), p. 1446).

Four major families of guidance cues are known to date: Netrins, slits, semaphorins and ephrins. These cues are called the canonical cues. The draxin guidance cue shows no sequence similarity with the other guidance cues and is believed to stand therefor on its own (Ahmed et al., 2011; Islam et al., 2009).

2.b. Netrins and receptors

2.b.1. Netrins are highly conserved guidance cues for migrating cells

The name netrin derived from the Sanskrit word “netr” which means “one who guides”. Netrins belong to the superfamily of laminin-related proteins and were first described as chemical guidance cues for migrating commissural and motor axons (Hedgecock et al., 1990). They were discovered in the 1990’s during a genome search in *Caenorhabditis elegans* (*C. elegans*). The loss of the homologues gene uncoordinated-6 (*unc-6/netrin*) resulted in uncoordinated movement of the worms. This is due to misguidance of commissural axons during midline crossing (Chan et al., 1996; Culotti, 1994). Shortly after the presence of netrins were confirmed in fruit flies (*Drosophila melanogaster*, (Harris et al., 1996)), frogs (*Xenopus laevis*, (de la Torre et al., 1997)), chicken (*Gallus gallus*), mice (*Mus musculus*) and humans (Serafini et al., 1996), revealing the high conservation of this chemotropic factors in axon guidance and cell migration. Even a sea anemone, an organism with only basic characteristics of bilateral organisation, was confirmed to express netrin homologues (Matus et al., 2006). As secreted morphogenes they do not just guide growing axons to connect the brain with the periphery, it has become more and more clear that netrins are also involved in the patterning of tissues during organogenesis (Lai Wing Sun et al., 2011). Furthermore, netrins promote angiogenesis during embryonic development (Castets et al., 2009), Coissieux et al. 2009), inflammation (Ramesh et al., 2010) and cancer (Fitamant et al., 2008).

In mammals, four secreted netrins (netrin-1, netrin-3, netrin-4 and netrin-5) are described along with two membrane associated glycoposphatidylinositol (GPI)-linked representatives, netrinG1 and netrinG2. The membrane-anchored netrins are believed to have evolved independently (Lai Wing Sun et al., 2011). They are only found in the central nervous system of vertebrates and do not seem to have the same function as the secreted netrins (Lai Wing Sun et al., 2011; Rajasekharan and Kennedy, 2009).

Netrin-1 is express in developing and adult neuronal tissues and has diverse functions outside the nervous system during organ development and angiogenesis

(Lai Wing Sun et al., 2011; Wilson et al., 2006). Netrin-3 is present on motor neurons and neurons in sensory and sympathetic ganglia, implying a role in the development of the peripheral nervous system (Seaman and Cooper, 2001). Netrin-4 has anti-angiogenic effects and stimulates vascular smooth muscle cells (Lejmi et al., 2014). There is not much known about expression and function of Netrin-5.

2.b.2. Netrin-1 and its receptors

The best characterised representative of the secreted family members remains netrin-1, a glycoprotein composed of ~600 amino acids. It contains four predicted glycosylation sites (Lai Wing Sun et al., 2011) (Fig. B). The N-terminal domain is homologous to the laminin VI domain, followed by three EGF-like domains resembling the laminin domain V. This domain of EGF repeats is also called EGF-hand motif. The N-terminal domains are linked to a C-terminal Netrin-like module (NTR) also known as C345 (C3, C4, and C5 are also found in the complement proteins (Serafini et al., 1994). The C-terminus is believed to interact with heparan sulphate proteoglycan, while the VI and V domains were proposed to take part in specific receptor-ligand interactions (Lai Wing Sun et al., 2011).

Among the receptors (Fig. B) that have been identified to bind netrin-1 are deleted in colorectal cancer (DCC, (Chan et al., 1996); Keino-Masu et al. (1996)), neogenin (Keino-Masu et al., 1996), down-syndrome cell adhesion molecule (DSCAM, (Ly et al., 2008)) and uncoordinated 5A-D (UNC5A-D, (Geisbrecht et al., 2003; Leonardo et al., 1997a)). DCC and UNC5 belong to the dependence receptor family. Receptors of this family share the property to induce cell death by apoptosis when not bound to their ligand, but ligand binding triggers a different signalling pathway leading to migration and differentiation. Therefore, ligand binding ensures cell survival in diverse contexts (Bagri and Ashkenazi, 2010).

To reach their target region, axons might need to change direction of migration as described previously. This involves turning and losing sensitivity for one guidance cue, while the sensitivity for another might rise (Culotti and Merz, 1998). Axons projecting towards the floor plate are attracted to a netrin-1 gradient, but lose this attraction after midline crossing. Changes in receptor expression patterns could be responsible for that. While neogenin and DCC, alone or together with DSCAM,

expressing axons are attracted to netrin-1 (Ly et al., 2008), DCC in combination with UNC5 has a repelling effect ((Hong et al., 1999)Fig. C and E).

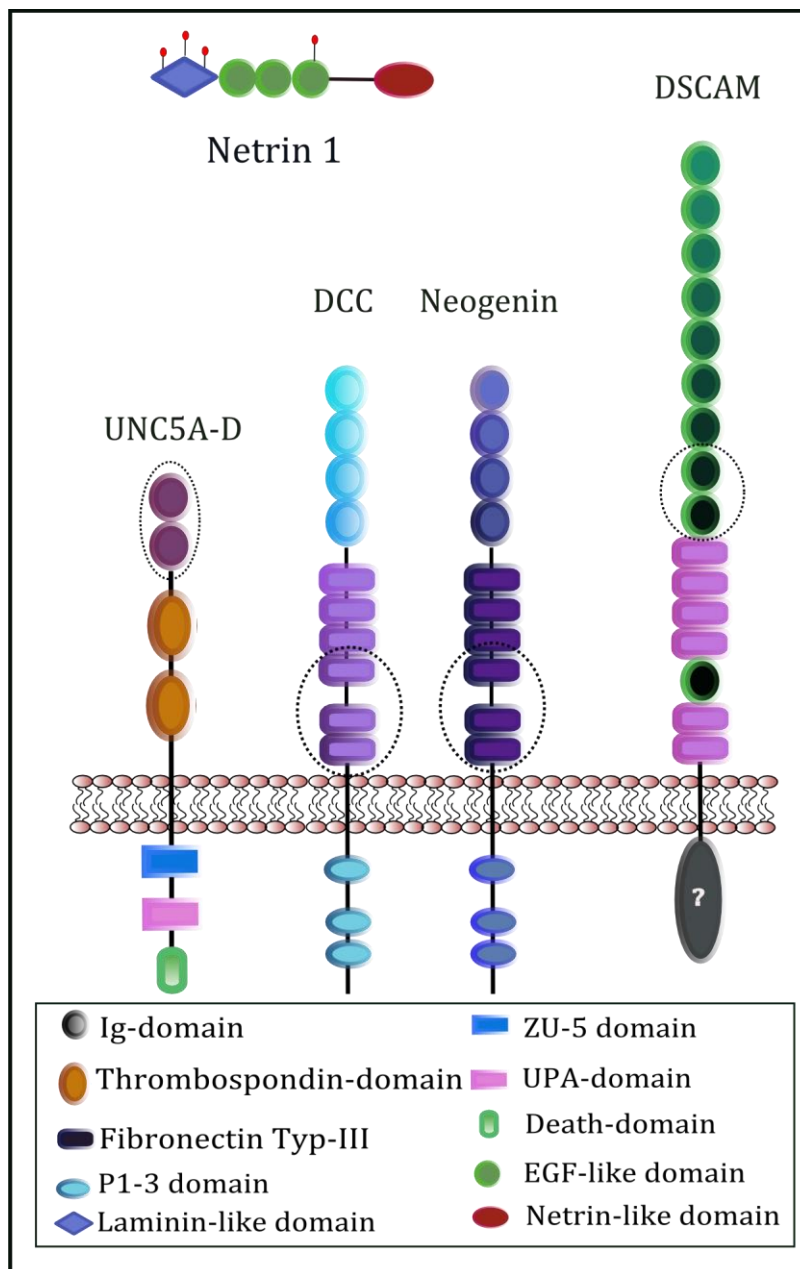


Figure B Netrin-1, its receptors and their domain organisation. Glycosylation sites for netrin-1 are indicated by lollipops. Sites of proposed interactions between receptor and ligand are indicated in dotted circles (adapted from: (Mehlen et al., 2011))

Netrin-1 directs migrating cells during neuronal development as well as in adulthood (Lai Wing Sun et al., 2011). Progenitor cells of the cerebellum and commissural axons express DCC and are attracted by a netrin-1 gradient from the ventral midline (Alcantara et al., 2000; Kennedy et al., 1994). This is mediated by activation of microtubule reorganisation (Del Rio et al., 2004). In contrast, the motor axons

innervating the muscles of the ear are repelled by netrin-1 mediated through UNC5, that guides them dorsally away from the ventral midline (Burgess et al., 2006). Postnatal maturation of the cerebellar progenitors and migration of adult neuronal stem cells after injuries are also regulated by UNC5 expression (Alcantara et al., 2000; Petit et al., 2007). This shows the bi- functionality of the netrin-1 guidance cue (Rajasekharan and Kennedy, 2009) (Fig. C & E). Furthermore, Netrin-1 is involved in the processes of axon branching, innervation and synaptogenesis (Lai Wing Sun et al., 2011). On migrating glia precursor cells, developing later into oligodendrocytes, netrin-1 has a repelling effect and contributes to regulation of their maturation (Jarjour et al., 2003; Rajasekharan et al., 2009; Tsai et al., 2006). These cells provide the insulating myelin sheet of the axons in the central nervous system.

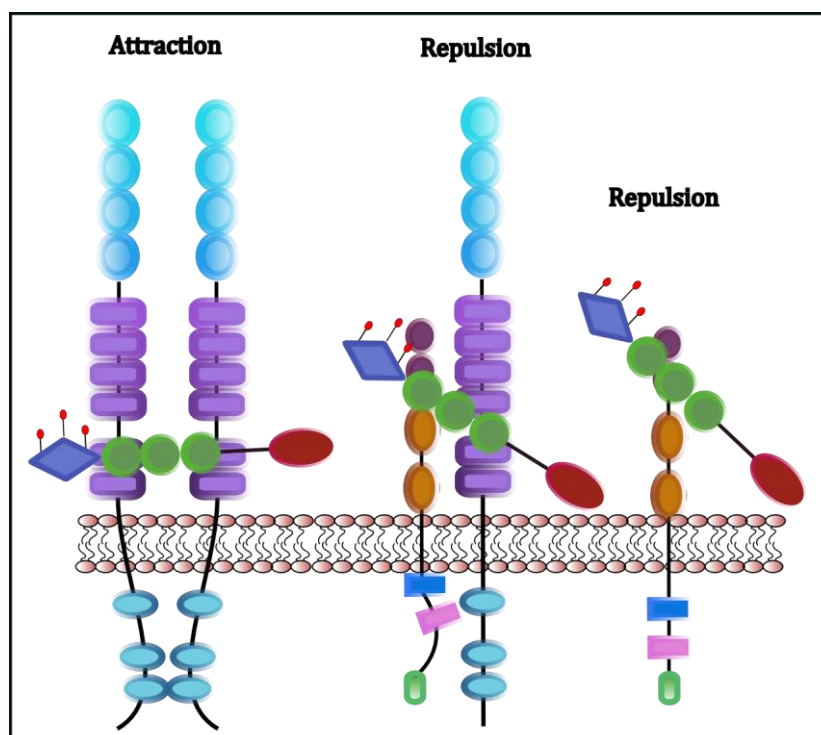


Figure C Netrin-1 and interaction with its receptors DCC and UNC5 **Attraction** is mediated by homo-dimerisation of DCC **Repulsion** is mediated by UNC5 alone or by hetero-dimerisation with DCC. Interaction sites may not be correctly resembled.

Failure of netrin signalling causes severe developmental defects during embryogenesis and, if occurring later in life, can lead to cancer. Genetic studies in humans have also shown that nucleotide polymorphism in netrin-1 and DCC genes can be linked to the risk of developing Parkinson and amyotrophic lateral sclerosis (Lesnick et al., 2007; Lesnick et al., 2008). Future investigations studying the role of netrin-1 in synaptogenesis and related pathologies might unravel netrin-1's influence

in the development and progression of neurodegenerative diseases (Lai Wing Sun et al., 2011). Some disorders observed in Down's syndrome might be related to impaired netrin-1 signalling resulting from chromosome duplication (Ly et al., 2008). Therefore, a greater understanding of the molecular interactions between netrins and their cell-surface binding partners is of particular interest. The domains of receptors and ligand taking part in the interactions have been investigated in a number of publications ((Lim and Wadsworth, 2002); (Geisbrecht et al., 2003)), but the molecular details have remained elusive.

2.b.3. Deleted in colorectal cancer

DCC is the vertebrate homologue of UNC40 in *C. elegans* (Chan et al., 1996). It is a single pass transmembrane receptor (Fig. B). The four N-terminal Ig-domains adopt a horseshoe-like conformation by folding back on each other. This conformation is evolutionary conserved in neuronal receptors and functionally necessary (Chen et al., 2013; Meijers et al., 2007). This motif is followed by six type-III fibronectin domains (FN) connected through a helical transmembrane domain with the conserved cytosolic domains called P1, P2 and P3. Through these domains DCC forms homo- or hetero-dimers for signal transduction (Stein and Tessier-Lavigne, 2001; Stein et al., 2001; Xie et al., 2006) (Fig. C, D and E). Association of the cytosolic domains occurs after a triggering signal from the ligand is received, however, it can still happen independently of ectodomain association (Stein et al., 2001).

DCC was first described as a candidate for tumour suppression located on the chromosome 18q (Fearon et al., 1990). It is frequently lost in several kinds of cancers, such as colorectal carcinoma due to allele depletion (Cho and Fearon, 1995). DCC is widely express in low amounts in adult tissues, but is mainly studied in the developing nervous system (Cooper et al., 1995). During migration of spinal commissural axons DCC is present on the axon and the growth cone and binds to netrin-1 specifically and with high affinity in the Nano molar range (Keino-Masu et al., 1996). It has been reported that less than five netrin-1 molecules are necessary to mediate a positive response towards the signal (Pinato et al., 2012).

Interaction of DCC and netrin-1 is further supported by the observation, that the absence of DCC during neuronal development resembles certain netrin-1 and unc6 mutants, lacking the ability of commissural axon path finding (Hedgecock et al., 1990;

Serafini et al., 1996). These interactions have been limited to appear within the basal fibronectin domains FN4-FN6 (Geisbrecht et al., 2003; Kruger et al., 2004).

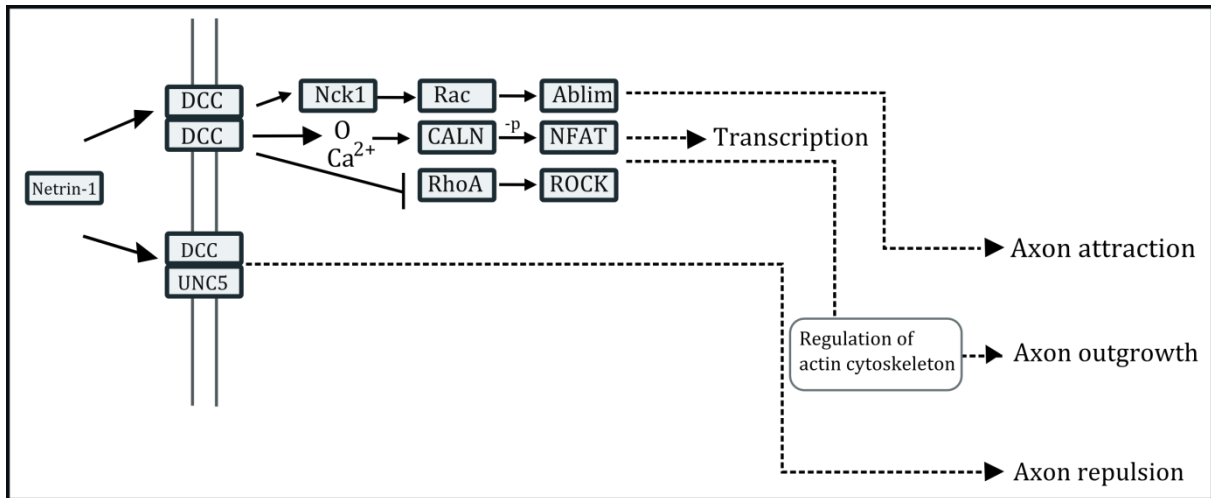


Figure D Signalling pathways initiated by netrin-1 binding to DCC/DCC or DCC/UNC5 and growth cone response to the signal. Figure has been adapted from the axon guidance map of the KEGG database (Kanehisa et al., 2014).

Netrin-1 initiates several signalling pathways upon binding to DCC and subsequent receptor dimerisation, including the activation of kinases that are involved in the initiation of cytoskeleton rearrangements and release of Ca^{2+} (Ko et al., 2012) (Fig. D) as an essential process for axon movement and path finding (Qu et al., 2013). (Fig. D). Homo-dimerisation leads to the intracellular association of adaptor proteins (Nck1) followed by GTPase (Rac) activation that promotes actin polymerisation (Ablim) and membrane folding, necessary for the forward movement towards an attractive gradient (p. 1099 ff. Alberts (2004); (Round and Stein, 2007)). A calcium dependent pathway, involved in desensitization or resensitization during axon turning, requires MAP-tyrosine phosphorylation (CALN) of the receptor triggering then the activation of the NFAT transcription complex (Round and Stein, 2007). Also calcium dependent is the down regulation of the GTPase RhoA which controls protein kinases that influence the actin cytoskeleton and therefore axon expansion. Once axons reached their target region, DCC mediates axon branching (Tang and Kalil, 2005) and formation of synapses (Manitt et al., 2009). through a netrin-1 induced increase of intracellular Ca^{2+} . DCC also binds to other guidance cues, such as draxin (Ahmed et al., 2011; Islam et al., 2009) and was proposed to bind heparan sulphate proteoglycans (Bennett et al., 1997). Heparan sulphate proteoglycans (HSPG) act as cell surface or extracellular matrix bound ligands responsible for receptor multimerisation (Gallagher, 2001). They are involved in angiogenesis, cell migration and cell adhesion (Gallagher, 2001) and could be

necessary to mediate interactions between netrin-1 and DCC (Geisbrecht et al., 2003). The interaction of netrin-1 with DCC is not limited to the developing nervous system. Several studies support the evidence that they are influencing synaptogenesis and their plasticity in the adult brain (Horn et al. (2013), Horn and Kennedy (2012)) as well as the mesocortical dopamine circuitry (Manitt et al., 2011).

In colorectal cancer the deletion of DCC leaves the colon cells unresponsive to netrin-1 (Fig. F). With the receptor deletion, so is their dependence function lost. The characteristic of dependency is initiated when netrin-1 is not bound. Caspase activity cleaves the cytosolic part of the receptor when not dimerised by ligand binding to activate apoptosis (Ko et al., 2012).

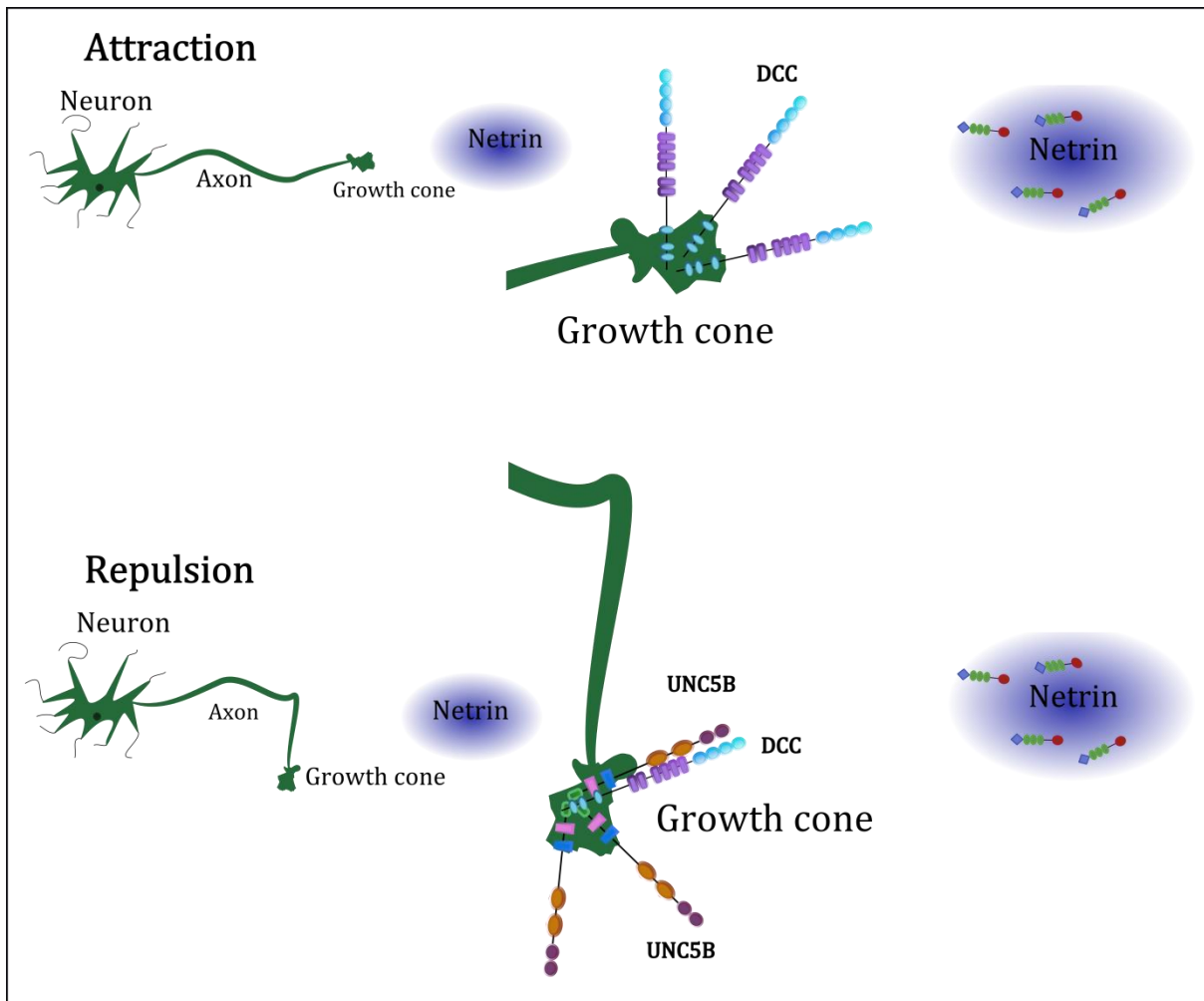


Figure E Growth cone response to a netrin-1 gradient is dependent on the receptors expressed **Attraction** of the migrating axon is mediated when DCC is present on the growth cone **Repulsion** is mediated by UNC5 alone or by hetero-dimerisation with DCC.

2.b.4. Neogenin

Neogenin belongs to the DCC family and shares ~50% sequence similarity (Vielmetter et al., 1997). The domain organisation is similar to DCC (Fig. B) consisting of four Ig-domains followed by six fibronectin type-III domains connected through a transmembrane domain to the cytosolic domains. Like DCC, neogenin is highly conserved in vertebrates (Vielmetter et al., 1997). Similar to DCC, neogenin mediates an attractive response to a netrin-1 gradient when not interacting with UNC5. Studies of the axon guidance in chicken suggest that neogenin may act as a substitution for DCC (Phan et al., 2011) in binding to netrins. In mammals neogenin is involved in the development of the forebrain, the olfactory bulb (Bradford et al., 2010) and in interaction with netrin-4 to inhibit angiogenesis (Lejmi et al., 2008).

Together with the repulsive guidance molecule (RGM), a membrane-bound protein known for its axon guidance ability, neogenin is mediating cell survival in a dependence receptor/ligand manner (Matsunaga, Tauszig-Delamasure et al. 2004). Binding creates a repulsive response leading to collapse of the growth cone (Conrad et al., 2007).

2.b.5. UNC5

UNC-5 was discovered together with netrin/UNC-6 in *C. elegans* and found to be crucial for correct neuronal wiring. During axon migration it was observed that UNC-5 expressing growth cones are rejected by UNC-6 (Hedgecock et al., 1990). In vertebrates, four orthologues of the Ig-superfamily members are known, UNC5A, UNC5B, UNC5C and UNC5D (Lai Wing Sun et al., 2011). All four receptors are composed of two N-terminal Ig-domains which are believed to contain the netrin binding motif (Geisbrecht et al., 2003). Two following thrombospondin (TPS) type I domains are then connected through a transmembrane domain with the intracellular domains. They are composed of a ZU-domain, the DCC-P1 binding domain UPA and a death domain (Fig. B) (Leonardo et al., 1997b). Like DCC and neogenin, UNC5 homologues are dependence receptors that mediate apoptosis when not bound to their ligand (Castets et al., 2009). Similar to DCC, UNC5 expression is down regulated in several cancers (Thiebault et al., 2003).

As mentioned before, axons that express UNC5 are rejected by netrin gradients as a short or long range effect (Fig. E). In some cases the response is dependent on the

presence of DCC as well (Keleman and Dickson, 2001). The interaction with DCC might be responsible for the switch of sensitivity to netrin-1 gradients when commissural axons have crossed the midline of the floor plate (Culotti and Merz, 1998; Su et al., 2000).

UNC5B is also expressed outside the nervous system, more specifically during angiogenesis (Lu et al., 2004). UNC5B is normally down-regulated in the adult vasculature but reinitiated during sprouting angiogenesis (Larrivee et al., 2007). Upon binding to netrin-1 it mediates filopodia retraction leading to a repellent effect (Lu et al., 2004). Interestingly, a positive effect in angiogenesis is mediated by DCC (Nguyen and Cai, 2006) and other, not yet identified, receptors (Wilson et al., 2006).

2.b.6. Down syndrome cell adhesion molecule

The DSCAM gene is located on the human chromosome 21 which causes Down's syndrome when duplicated (Yamakawa et al., 1998). In the fruit fly *D. melanogaster* Dscam has with over 38 000 splicing variants an extraordinary variation that contributes to the development of the nervous system (Schmucker et al., 2000), whereas in mammals only two variants are known. Human DSCAM (Fig. B) is composed of nine N-terminal Ig-domains, separated by four fibronectin domains from the tenth Ig-domain and followed by two more fibronectin domains. Through a transmembrane domain the cytosolic part is connected (Yamakawa et al., 1998). *D. melanogaster* Dscam adopts a similar horseshoe conformation as described for DCC (Meijers et al., 2007). It has been proposed that netrin-1 binds to the basal Ig-domains Ig7-Ig9 (Ly et al., 2008).

DSCAM is expressed by commissural axons of the spinal cord. Upon binding to netrin-1 it can mediate a positive turning response guiding the migrating growth cone through the ventral midline. It was also demonstrated that DSCAM can form receptor complexes with DCC through their ectodomains or transmembrane domains, but unlike the DCC homo- or hetero-dimers with UNC5 not through the cytosolic domains (Ly et al., 2008). This suggests that DSCAM holds DCC in a resting state by silencing the dependence receptor activity that would initiate apoptosis when netrin-1 or another ligand is not present (Ly et al., 2008). DSCAM is also involved in a process called self-avoidance to prevent neurons of the same kind to connect to each other in order to mediate a specific wiring pattern (Millard and Zipursky, 2008)

2.c. Netrin-1's function outside the nervous system

Netrin was confirmed to be expressed also in numerous tissues outside the nervous system, and not exclusively during development (Lai Wing Sun et al., 2011). Cell adhesion in mammary gland development, a process occurring during end bud formation, is mediated by netrin-1 through binding to neogenin (Srinivasan et al., 2003). Another interaction is observed during lung development (Fig. F), where netrin-1 and netrin-4 bind to UNC5B to inhibit local changes of cell shapes to prevent the extending bud from inappropriate branching (Liu et al., 2004).

Netrins play also a bi-functional role in angiogenesis (Fig. F) and neovascularisation similar to axon guidance. It has been reported that netrin-1 inhibits endothelial cell migration and blood vessel branching (Larrivee et al., 2007). Through inhibition of neovascularisation, anti-inflammatory effects have been observed after corneal injury (Han et al., 2012). Both processes are mediated by UNC5B expression. Furthermore, netrin-1 is expressed abundantly in the adult kidney and was observed to reduce oxidative stress and inflammation as a result of ischemic kidney damage (Liu et al., 2013). Therefore, a role for netrin-1 as a biomarker for tissue injury and a target for inflammatory diseases has been proposed (Ramesh, 2012). On the other hand the promotion of angiogenesis, migration of endothelial cells and tube formation was reported together with DCC and an uncharacterised receptor (Wilson et al., 2006).

It was discussed earlier that deletions of DCC and UNC are related to certain cancers (Banerjee, 1997; Coissieux et al., 2011). UNC5B is a transcriptional target of p53, an apoptosis inducer. In tumour cells, UNC5B expression is often missing or down regulated and this apoptosis inhibition is promoting tumour growth (He et al., 2011).

The same is true for late-stage colorectal carcinoma. Netrin-1 expresses in the intestine epithelium where it provides a gradient from the base to the tip of the villi. DCC expressing cells, which receive netrin-1, survive while the cells outside the gradient at the tip of the epithelial villi undergo apoptosis (Fig. F). This function is lost in colorectal carcinoma leading to uncontrolled cell growth (Mazelin et al., 2004).

Finally, netrins are implicated to be involved in fertility, both in vertebrates and invertebrates (Newquist et al., 2013).

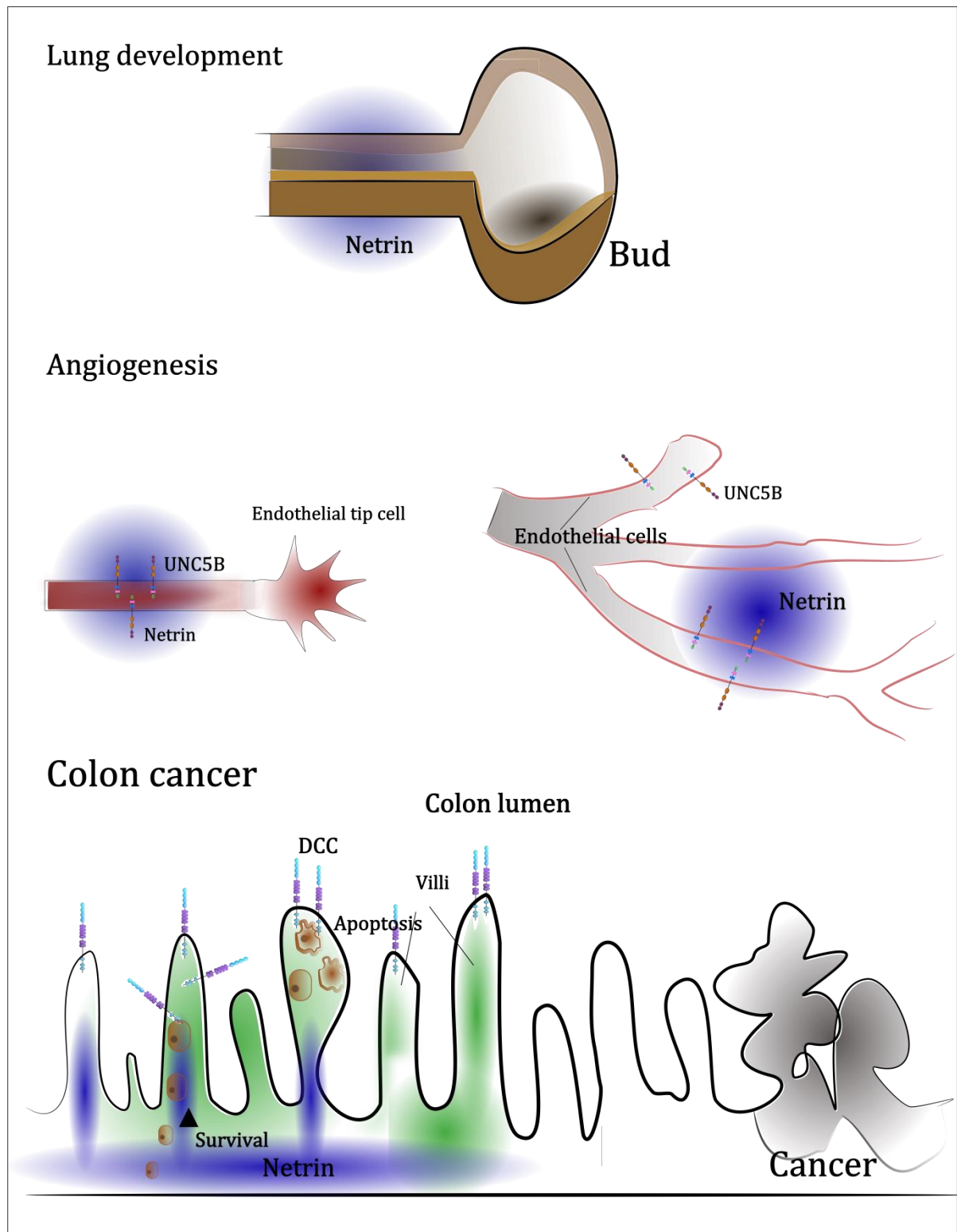


Figure F Netrin-1's function outside the nervous system **Lung development** During the development of the bronchial tree a netrin-1 gradient is preventing the bud cells to branch. **Angiogenesis** Similar to axon growth endothelial migrate during angiogenesis. Here a netrin-1 gradient is inhibiting endothelial tip cells from branching (right). Cells that express UNC5B but do not receive netrin-1 signalling undergo apoptosis; cells that receive netrin-1 continue extending. **Colon cancer** Netrin-1 is expressed at the base of the colon epithelium where stem cells proliferate and migrate to the tip of the villi. Here, cells that do express DCC but are outside the netrin-1 gradient undergo apoptosis. This signalling pathway is eliminated in certain cancers. (Lung development and angiogenesis adapted from (Lai Wing Sun et al., 2011))

2.d. Aim of study

The present study concentrated on the characterisation of the interaction between the human guidance cue molecule netrin-1 and its receptor DCC.

Netrin-1 has four predicted glycosylation sites and several cysteine-cysteine disulphide bonds (Lai Wing Sun et al., 2011; Serafini et al., 1994). It has been reported before that soluble constructs of netrin-1 were successfully expressed using mammalian expression (Keino-Masu et al., 1996). Therefore, HEK293T were chosen as a well-established mammalian system for transient expression (Aricescu et al., 2006a; Baldi et al., 2007). Previous studies (unpublished) have shown that the expression yield of secreted recombinant proteins can be enhanced by utilising the signal peptide from a high expressing pregnancy-specific glycoprotein (PSG1). The first aim of the study was the design full-length and truncated constructs of netrin-1 containing or excluding the proposed receptor binding regions secreted using the native or the PSG1 signal peptide. The previously presented constructs were expressed fused to a solubility tags like the human IgG1 constant region (Fc)-tag (Keino-Masu et al., 1996), this tag might be a hindrance in protein characterisation, protein interaction studies and crystallisation due to its size. For this study the use of a hexa-histidine affinity tag was chosen. The procedure was followed by the aim to establish a reproducible and convenient protocol for purification of stable, crystallisation grade protein. This included ion affinity purification and gel filtration (size exclusion) chromatography, as well as biophysical characterisation methods such as SDS-PAGE, Western blot, MALDI TOF, mass spectrometry and thermal denaturation assays (thermofluor). These methods can aid in monitoring protein purity and stability, as well as improving purification conditions such as pH and salt content / ionic strength of buffers (Boivin et al., 2013). Proteins that could be purified to a degree of 95% or higher were then tested in high-throughput crystallisation trials and promising conditions further optimised by hand to obtain crystals for diffraction studies.

The structure of a neogenin/ligand complex was recently presented (Bell et al., 2013), but no structural information of a netrin-1/DCC complex was available before to answer the rising question what the molecular interaction of netrin-1 and DCC may look like. The neogenin/ligand complex, together with other already available structures of guidance cue complexes, made a number of different models of binding

events leading to an active signalling complex seem plausible (Fig. G).

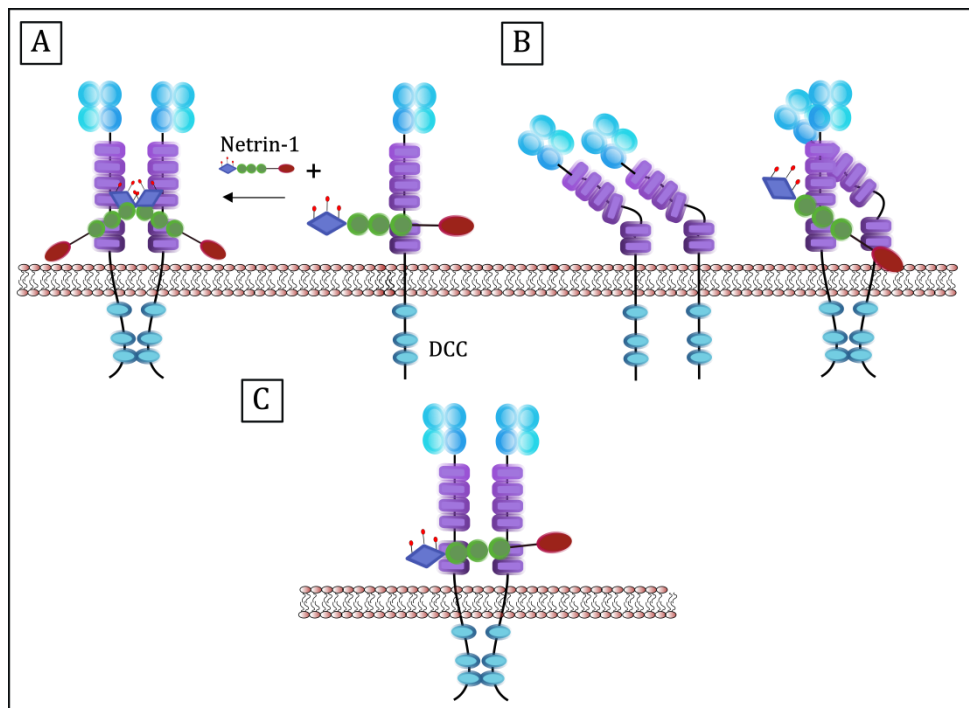


Figure G Models of receptor ligand interactions between netrin-1 and DCC/DCC. **A** Netrin-1 binds to DCC and dimerises with a second netrin-1 molecule bound to another receptor. **B** The receptor adapts a conformation that prevents dimerisation when no ligand is bound. Netrin-1 binding to one of the receptor molecules is changing its conformation to mediate ectodomain association to promote intracellular dimerisation. **C** A single netrin-1 molecule binds to DCC and recruits a second receptor through a second binding site.

Experimental receptor clustering showed that two DCC molecules are required for signal transduction (Stein et al., 2001) but the number of netrin-1 molecules has not been determined. Neogenin forms a 2:2 complex with its ligand repulsive guidance molecule B (RGMB) and netrin-1 was shown to compete with this ligand (Bell et al., 2013). The binding between netrin-1 and DCC could occur in a similar way, providing the start point of a multi-molecular cluster. Therefore, a model is conceivable where netrin-1 would bind to a receptor molecule and recruit a second receptor by dimerising with another netrin-1 molecule in order to bring the receptors in close proximity to initiate cytosolic association (Fig. G A). Semaphorin, another guidance cue molecule involved in growth cone migration, forms a similar 2:2 complex with its receptor plexin (Janssen et al., 2010). A second possibility is shown in Fig. G B, here the receptor molecules adapt a conformation in solution that inhibits cytosolic dimerisation when no ligand is bound. Upon binding of a netrin-1, one of them changes its conformation to allow ectodomain association and cytosolic dimerisation. This model is supported by observations, where binding to one DCC ectodomain is sufficient to cause dimerisation of DCCs cytosolic P3 domains (Stein et al., 2001). A

third binding model (Fig. G C) shows the binding of one netrin-1 molecule to two DCC ectodomains. This could occur through two similar or two distinct binding sites without the necessity to form netrin-1 dimers for receptor binding. However, based on the current understanding of guidance cue complexes this model seemed less likely. Therefore, the further aim of the study was to unravel the molecular receptor-ligand principles by crystallisation studies and subsequent functional confirmation of binding modalities.

To verify the proposed binding sites (Bennett et al., 1997; Geisbrecht et al., 2003) for DCC, binding assays and thermofluor, as well as co-crystallisation studies were performed in collaboration with Prof. Jia-huai Wang (Harvard, Boston, USA) and Dr. Lorenzo Finci (Peking University, China) . They kindly provided *E.coli* expressed and purified constructs of DCC containing the fibronectin domains FN4-FN6. To gain deeper insight into binding, their structure was studied by X-ray crystallography. To verify if netrin-1 and DCC alone occur monomeric in solution and could form clusters together, small-angle X-ray scattering (SAXS) methods were used (in collaboration with Dr. Dmitri Svergun, Dr. Haydyn Mertens and Dr. Gundolf Schenk, EMBL Hamburg). After observation of two binding sites by solving the crystal structure, key residues were altered by site-directed mutagenesis for further analysis.

In-vivo cell binding and axon guidance assays were performed in collaboration with Dr. Yan Zhang (Peking University, China). These experiments were designed to verify that the used construct of netrin-1 was indeed sufficient to mediate specific signalling on one hand and on the other hand to confirm the influence of the observed binding sites in axon guidance *in-vivo*. The binding affinities that were reported in earlier studies (Keino-Masu et al., 1996) were sought to be critically investigated by microscale thermophoresis and isothermal titration calorimetry with wild-type and mutant constructs. The newly acquired insights into receptor ligand binding events will aid in verification of the hypothesised binding models (Fig. G) and in the identification of the residues and co-factors necessary for binding to occur. Moreover, this would provide fundamental information about how netrins could act as a scaffold for different receptors to create a signalling cluster on the cell surface of tissues influenced by netrin gradients. Although netrin's involvement in neurodegenerative diseases (Lesnick et al., 2008) and several cancers (He et al., 2011; Mazelin et al., 2004) was described, current understanding of the molecular mechanisms is not very detailed. The results obtained from this study could

contribute to a better comprehension of how the multiple events during neuronal development, angiogenesis and cancer are mediated by diffusible netrin-1 gradients and therefore promote new ideas for subsequent drug targeting.

3. Material and Methods

3. a. Material

All chemicals were obtained from Carl Roth GmbH & Co. KG (Germany), if not otherwise specified.

3.a.1. Chemicals

Table A Chemicals, Application and Source

Chemical	Application	Source
GeneRuler™ 1 kb Plus	DNA ladder	Thermo scientific cat# SM0311
Fermentas 6x DNA loading dye	DNA loading dye	Thermo scientific cat# R1151
ColorPlus Prestained Protein Marker	Protein ladder	NEB cat# P7709V
PageRuler Plus Prestained ProteinLadder	Protein ladder	Thermo scientific cat# 26619
NuPage® LDS Sample 4x buffer	Protein loading dye	Life technologies cat#NP0008
Roti®Mark 10-150	His-tagged protein ladder for Western blot	Carl Roth cat# T850.2
Instantblue™ coomassie	SDS-PAGE stain	Expedeon ISB1L
Dimethylsulfoxid (DMSO)	Anti-freezing agent for cell storage	Sigma Aldrich cat#D2438-50ML
dNTPs	Nucleotides for PCR	Thermo scientific cat# R0181
β-mercaptoethanol	Reducing agent	Sigma Aldrich cat# M6250-100ML
Monolith™ NT.115 Protein Labelling Kit RED-NHS	Protein labelling	Nanotemper Technologies Cat# L001
Polyethylenimine (PEI), 25 kDa branched	Transfection agent for HEK cells	Sigma Aldrich cat# 408727-250ML
Triton X-114	Endotoxin removal	Sigma cat# T-7003
Trypan Blue 10x Trypsin-EDTA	Cell counting Cell detachment from surfaces	Biochrom cat# L 6323 Biochrom cat# L 2153

3.a.2. Buffers

Table B Buffers, Composition and Application

Buffer	Composition	Application
5x Bis-tris gel buffer pH 6.5	1.8 M Bis-Tris	Bis-Tris Acrylamid gels
5% stacking gel	125 mM TRIS pH 6.8 0.5 % SDS 5 % Acrylamide/Bis Solution	Tris-Glycine gels
12% stacking gel	125 mM TRIS pH 8.8 0.5 % SDS 12 % Acrylamide/Bis Solution 20 % Glycerol	Tris-Glycine gels
20x MES running buffer	1 M MES 600 mM Bis Tris 70 mM SDS 20 mM EDTA	Bis-Tris SDS-PAGE running buffer
Running Buffer	200 mM Glycine 25 mM TRIS 0.1% SDS	Tris-Glycine SDS-PAGE running
Coomassie Standard stain	0.1 % Coomassie R-250 40 % Ethanol 10 % Acetic acid	SDS-PAGE gel staining
Coomassie Destain	20 % Ethanol 10 % Acetic acid	SDS-PAGE gel destaining from standard stain
TAE Buffer	40 mM TRIS pH 8.5 1 mM EDTA- Na^2 -salt 20 mM Acetic acid	Agarose gel electrophoresis
Blot Buffer	192 mM glycine, 25 mM Tris-base, 20 % Ethanol	Western blot transfer buffer
10x PBS	20 mM KH_2HPO_4 80 mM $\text{Na}_2\text{HPO}_4 \cdot 2\text{H}_2\text{O}$ 1,37 M NaCl, 25 mM KCL	Stock for PBS
PBS-T	1x PBS 0.1 % Tween-20	Wash buffer
25mM Phosphate Buffer pH 8.0	1.7 mM NaH_2HPO_4 , 23.3 mM $\text{Na}_2\text{HPO}_4 \cdot 7\text{H}_2\text{O}$ 250 mM NaCl	Dialysis, Talon purification (Wash Buffer 1)
Talon Wash Buffer 2 pH 8.0	25 mM Phosphate Buffer 10 mM TRIS 10 mM Imidazole	Talon purification
Talon Elution Buffer pH 8.0	50 mM HEPES 250 mM NaCl 250 mM Imidazole	Elution from Talon beads

Buffer	Composition	Application
20mM Phosphate Buffer pH 7.4	1.7 mM NaH ₂ HPO ₄ 23.3 mM Na ₂ HPO ₄ *7H ₂ O	Dialysis, Ni-X purification
Ni-X Wash Buffer 1	20 mM Phosphate Buffer pH 7.4 500 mM NaCl	Ni-X purification
Ni-X Wash Buffer 2	20 mM Phosphate Buffer pH 7.4 500 mM NaCl 50 mM Imidazole	Ni-X purification
Ni-X Elution Buffer	20 mM Phosphate Buffer pH 7.4 500 mM NaCl 500 mM Imidazole	Ni-X purification
Netrin _{VIV} Ion exchange Buffer 1	50 mM Tris pH 7.4	Ion Exchange equilibration
Netrin _{VIV} Ion exchange Buffer 2	50 mM Tris pH 7.4, 2M NaCl	Ion Exchange gradient
Ion Exchange Buffer A	20 mM HEPES pH 7.4	Ion Exchange equilibration
Ion Exchange Buffer B	20 mM HEPES pH 7.4, 2 M NaCl	Ion Exchange gradient
ConA Binding Buffer	20 mM TRIS-HCL pH 7.4 500 mM NaCl 1 mM CaCl ₂ 1 mM MnCl ₂	Equilibration of ConA column, washing, dialysis
ConA Elution Buffer 1	20 mM TRIS-HCl pH 7.4 500 mM NaCl 500 mM α-D-Glucose	Elution from ConA column
ConA Elution Buffer 2 pH 6.0	20 mM Citric acid 500 mM NaCl 500 mM α-D-Glucose	Elution from ConA column
ConA Elution Buffer 3 pH 5.4	20 mM Citric acid 500 mM NaCl	Elution from ConA column
ConA Elution Buffer 4 pH 4.5	20 mM Citric acid 500 mM NaCl	Elution from ConA column
HEPES buffer pH 7.4	20 mM HEPES pH 7.4 500 mM NaCl 1 mM DTT	Size exclusion chromatography
Netrin SEC Buffer Na-citrate	50 mM Na-citrate pH 6.0 250 mM NaCl 1 mM DTT	Size exclusion chromatography
Netrin SEC Buffer Tris	20 mM Tris pH 6.5 500 mM NaCl 1 mM DTT	Size exclusion chromatography
Netrin SEC Buffer MES 1	50 mM MES pH 6.0 250 mM NaCl 1 mM DTT	Size exclusion chromatography

Buffer	Composition	Application
Netrin SEC Buffer MES 2	50 mM MES pH 6.0 250 mM NaCl 1 mM DTT 2 mM CaCl ₂	Size exclusion chromatography
DSCAM9 SEC Buffer HEPES	20 mM HEPES, pH 7.5 100 mM NaCl 1 mM DTT	Size exclusion chromatography
PBS SEC Buffer	1x PBS pH 8.0 1 mM DTT	Size exclusion chromatography for ITC
DCC SEC Buffer	100 mM Tris 150 mM NaCl	Size exclusion chromatography
Strep Elution Buffer	100 mM Tris/HCl, pH 8.0 150 mM NaCl 1 mM EDTA 2.5 mM desthiobiotin	Strep pull down assay
Thermophoresis reaction buffer 1	50 mM HEPES pH 7.4 250 mM NaCl, 200 mM (NH ₄) ₂ SO ₄ , 2 mM CaCl ₂	Thermophoresis
Thermophoresis reaction buffer 2	1x PBS pH 8.0 0.5 mg/ml BSA 0.1 % Tween 20	Thermophoresis

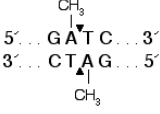
3.a.3. Media

Table C Media used for bacterial cultures, composition and application

Medium	Composition	Application
SOC medium	2 % Tryptone 0.5 % Yeast Extract 10 mM NaCl 2.5 mM KCL 10 mM MgCl ₂ 10 mM MgSO ₄ 20 mM Glucose	Bacterial transformation
LB medium – Lennox pH 7.0	10 g/l Tryptone 5 g/l Yeast Extract 5 g/l NaCl 25 mg/l Ampicillin-Na ²⁺	Bacterial cultures
LB plates	LB medium 15 g/l Agar agar 35 mg/l Ampicillin-Na ²⁺	Bacterial cultures

3.a.4. Enzymes

Table D Enzymes, recognised sequence, application and source

Enzyme	Sequence	Application	Source
AgeI	ACCGGT	Restriction Digest	NEB #R0552S
KpnI	GGTACC	Restriction Digest	NEB #R3142S
SacI	GAGCTC	Restriction Digest	NEB #R3156S
NotI	GCGGCCGC	Restriction Digest	NEB #R3189S
HindIII	AAGCTT	Restriction Digest	NEB # R3104S
DpnI		Digest of parental DNA	NEB #R0176S
Phusion® Fidelity Polymerase	High DNA	PCR	NEB #M0530S
T4 Ligase		Ligation of DNA fragments	NEB # M0202S

3.a.5. Antibodies

Table E Antibodies, origin, application and source

Antibody	Origin	Application	Source
Penta-His Antibody	mouse	Primary Western blot antibody	Qiagen cat# 34660
Anti-BSA Antibody	mouse	Primary Western blot antibody	Pierce cat# MA5-15238
HRP-linked Anti-mouse antibody	goat	Secondary Western blot Antibody	Pierce cat# 32230

3.a.6. Kits

Table F Kits, applications and sources

Kit	Application	Source
QIAquick® Gel Extraction Kit	DNA extraction from agarose gel	Qiagen cat# 28704
QIAprep® Spin Miniprep Kit	DNA extraction from bacterial cells	Qiagen cat# 27104
QIAGEN Plasmid <i>Plus</i> Midi Kit	DNA extraction from bacterial cells	Qiagen cat# 12943

Kit	Application	Source
QIAGEN Plasmid Plus Giga Kit	DNA extraction from bacterial cells	Qiagen cat# 12991
SuperSignal West Femto Chemiluminescent Substrate	Western blot	Pierce cat# 34094
SuperSignal West Pico Chemiluminescent Substrate	Western blot	Pierce cat# 34077
Qiagen Protein Complex Suite	Crystallisation	Qiagen cat# 130715
Qiagen Classic II Suite	Crystallisation	Qiagen cat# 130723
Qiagen Classic I Suite	Crystallisation	Qiagen cat# 130701
Qiagen AmSO ₄ Suite	Crystallisation	Qiagen cat# 130705
Qiagen PhClear Suite	Crystallisation	Qiagen cat# 130709
Qiagen PEG II Suite	Crystallisation	Qiagen cat# 130716

3.a.7. Equipment

Table G Equipment, applications and sources

Equipment	Application	Source
ÄKTA FPLC	Chromatography	GE healthcare Life Science
ÄKTA purifier	Chromatography	GE healthcare Life Science
Amicon stirred cell model 8400	Concentration	Millipore
Amicon® Ultra-4 Centrifugal Filter	Concentration	Millipore, cat# UFC800324
Regenerated cellulose membrane	Concentration with Amicon cell	Millipore cat# PLGC07610
ZelluTrans/Roth dialysis membranes T2 MWCO 8000 Da	Dialysis	Carl Roth cat# E670.1
Eppendorf Mastercycler	PCR machine	Eppendorf AG
Eppendorf Centrifuge 5415R (rotor: eppendorf F45-21-11)	Centrifugation	Eppendorf AG
Eppendorf Centrifuge 5810R (rotor: eppendorf A-4-81)	Centrifugation	Eppendorf AG
BECKMAN-COULTER Avanti J-20 XP Centrifuge (rotor JLA-8.1000)	Centrifugation	BECKMAN-COULTER
1 l centrifuge bottles	Centrifugation	BECKMAN-COULTER

Equipment	Application	Source
HT Infors Multitron 25 shaker	Bacterial cultures	Infors HT
HLC heatblock	Transformations, Digests, Gel extraction	Biofrontier Technology
Nanodrop spectrophotometer ND1000	UV absorbance measurement	PeQlab biotech GmbH, Germany
QIAvac 24 Plus manifold Mini-PROTEAN® Tetra Cell	DNA purification SDS-PAGE	Qiagen Biorad Life Science
BioRAD PowerPAC 300	Power supply for electrophoresis	Biorad Life Science
Protran Nitrocellulose membrane	Western blot membrane	Sigma Aldrich cat# Z670952
6 well tissue culture plate	2 ml HEK cell culture	TPP cat# 92006
T175 tissue culture flask	25 ml HEK cell culture	greiner Bio one cat# 660175
Polysterol roller bottles surface area of 2125 cm ²	250ml HEK cell culture	greiner Bio one cat# 681070
Wheaton incubator Monolith™ NT.115	HEK cell culture	Wheaton Industries Inc.
Standard treated capillaries	Thermophoresis	Nanotemper Technologies cat# K002
Hydrophilic capillaries	Thermophoresis	Nanotemper Technologies cat# K004
VP-ITC	Isothermal titration calorimeter	MicroCal, LLC

3.a.8. HEK media

Table H HEK293T cell culture medium, content, application and source

Medium	Content	Application	Source
Dulbecco's Modified Eagle's Medium (DMEM)	2 mM L-glutamine 1x non-essential amino acids 10% FCS	HEK 239T transfection	Biochrom cat# F 0435 cat# K 0283 cat# K 0293
	2 % FCS 0.5 % FCS 0.2 % FCS	HEK293T cell maintenance Expression Expression Expression	cat# S 0615
PBS		Dilution and washing	cat# L 1825

3.a.9. Columns

Table I Column/Resin , application and source

Column	Application	Source
S75 GL 10/300	Analytical size exclusion chromatography	GE healthcare cat# 17-5174-01
HiLoad S75 prep grade 16/60	Prep grade size exclusion chromatography	GE healthcare cat# 28-9893-33
Mono Q™ 5/50 GL	Anion exchange	GE healthcare cat# 17-5166-01
Strep-Tactin® 50% suspension	Strep-tag pulldown	Iba cat# 2-1201-002
Talon®Metal Affinity resin	Affinity purification	Clontech Laboratories inc. Cat# 635501
NiSepharose™ HighPerformance	Affinity purification	GE healthcare cat#17-5268-01
NiSepharose™excel	Affinity purification	GE healthcare cat# 17-3712-02
Con A Sepharose	Affinity purification	GE healthcare #17-0440-01
PD-10 Desalting column	Desalting/Buffer exchange	Bio-rad cat# 732-210

3.a.10. Proteins

Table J Recombinant Proteins, origin, expression host, and source

Protein	Origin	Expression host	Source
Netrin-1	Human	Murine myeloma	R&D cat# 6419-N1
Netrin-1 and truncated constructs and mutants	Human	HEK293T cells	Own production
DCC _{FN56} WT and mutants	Human	<i>E.coli</i>	Provided by L.I. Finci
DCC _{FN456} WT	Human	<i>E.coli</i>	Provided by L.I. Finci
DCC _{FN56} WT and mutants	Human	HEK293T cells	Own production,
DCC ectodomains and mutants	Human	HEK293T cells, COS cells, embryonic murine neurons	DNA provided by L.I. Finci/ Y. Zhang

3. b. Methods

3. b.1. Molecular cloning and DNA preparation

Synthetic genes, optimized for mammalian expression by GenScript

The amino acid sequence of the full-length precursor of human Netrin1 was obtained from Uniprot.org, entry: O95631 (NET1_HUMAN). To guarantee high expression yields, the construct was reverse translated to the nucleotide sequence and codon optimized with the OptimumGene™ algorithm provided by GenScript (USA Inc.). For cloning purposes, a KpnI site was introduced at position 22 of the construct positioned just after the native signalling peptide, which is necessary for secretion. At position 604, a SacI site is followed by a hexa-histidine tag, and a double stop codon.

The amino acid sequence of the truncated UNC5B construct was obtained from Uniprot.org entry Q8IZJ1 (UNC5B_HUMAN). The sequence that was ordered from GenScript for reverse translation and codon optimisation contains the two extracellular immunoglobulin domains (Ig) and the native signalling peptide. The secretion signal is followed by a KpnI site at position 25. The domain boundaries suggested by Uniprot were extended to position 245, after which a TEV cleavage site and a SacI site were introduced.

All constructs were received lyophilized in a pUC57 holding vector cloned between a NotI and HindIII restriction site.

The DCC constructs were designed from the Uniprot entry P43146 (DCC_HUMAN) for *E.coli* expression. The DCC_{ecto} domain constructs were cloned into the pXLGsec vector for expression in mammalian cells. Construct design, cloning and expression in *E.coli* from a pET21a vector was performed by Dr. Lorenzo Finci and colleagues (Peking University/Harvard Medical School) and purified protein and DNA was kindly provided by them.

Vector design

The mammalian pXLG_eGFP expression vector that was used as backbone for vector design was a gift from Dr. David Hacker (École Polytechnique Fédérale der Lausanne, Switzerland). The eGFP construct was excised with the restriction enzymes NotI and KpnI. For enhanced expression and secretion of full-length and truncated constructs, the signalling peptide of the human pregnancy-specific

glycoprotein-1 (PSG1) was introduced. This signal sequence is known from previous experiments (Krüger, 2011) to produce high yield expression *in vivo* and *in vitro*. Together with a Kozak start-codon, it was inserted between the NotI and KpnI site of the multiple cloning site (MCS) of the vector. For subsequent affinity purification of constructs cloned before the SacI site, the vector was equipped with a hexa-histidine (6xHis) tag followed by a double stop codon. Cloning was performed as described later in this section. The modified vector was named pXLGsec.

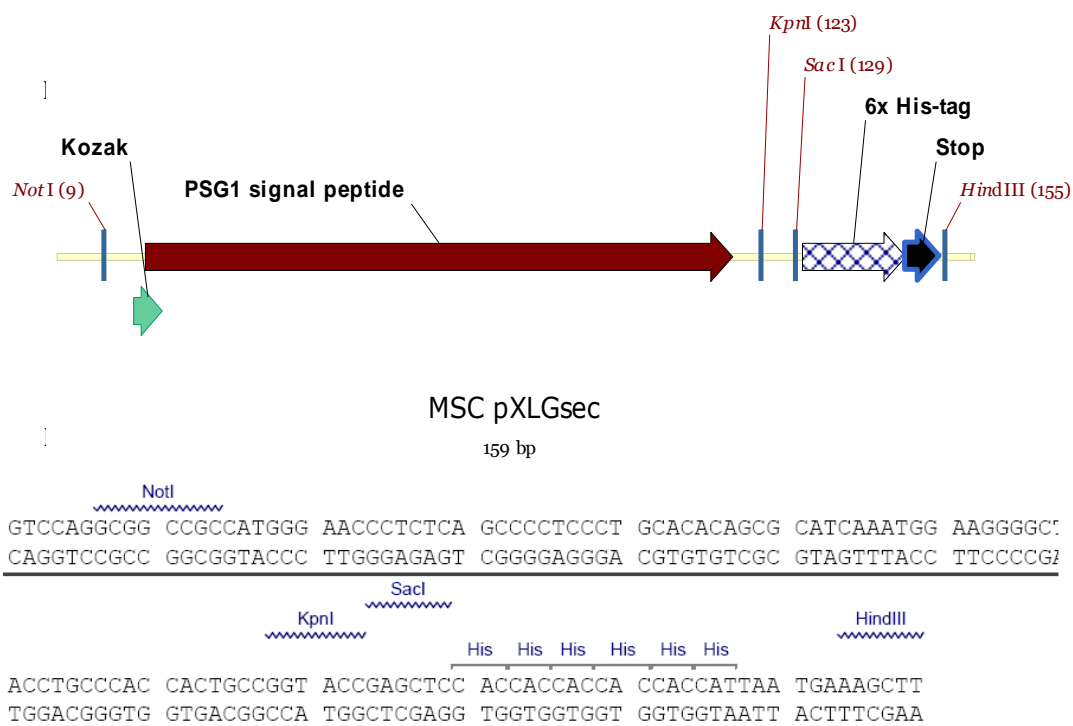


Figure A I Multiple cloning site pXLGsec vector I Schematic display of the features in the MCS of pXLGsec showing restriction sites, Kozak sequence, secretion signal and C-terminal 6x His-tag, II Sequence of the important attributes in the MCS, both images were designed with Vector NTI Advance® 11.5.

Primer	PSG1sec NotI/KpnI
Forward	5'-ACAGGTGTCCAGGCGGCCGCCATGGGAACC-3'
Reverse	5'-AGGGGTACCGCAGTGGTGGCAGGTTCC-3'

Construct design

Table K Netrin1 and DCC constructs

Construct	Domains	Domain boundaries
Netrin1	Native signal peptide	1-604
Netrin _V	V domains + PSG1 signal	280-484
Netrin _{VI}	VI domain + PSG1 signal	25-284
Netrin _{VII}	VI domain + V ₁ domain + PSG1 signal	1-340
Netrin _{VIII}	VI + V domains	25-453
Netrin _{VIV}	VI + V domains + PSG1 signal	25-453
Netrin _{VIVR349A/R351A}	VI + V domains + PSG1 signal Mutations of the arginine residues 349 and 351 to alanine	25-453
Netrin _{VIVR349D/R351D}	VI + V domains + PSG1 signal Mutations of the arginine residues 349 and 351 to aspartic acid	25-453
Netrin _{VIVY323A}	VI + V domains + PSG1 signal Mutation of the tyrosine residue 323 to alanine	25-453
Netrin _{VIVQ443A}	VI + V domains + PSG1 signal Mutation of the glutamine residue 443 to alanine	25-453
eGFP_Netrin1	eGFP + Netrin1	1-604
eGFP_Netrin _{VIV}	eGFP + VI + V domains + PSG1 signal	25-453
DCC _{FN56wt}	Fibronectin domains 5 and 6	846-1044
DCC _{FN56M933A}	Fibronectin domains 5 and 6, methionine 933 mutated to an alanine	846-1044
DCC _{FN56M933D}	Fibronectin domains 5 and 6, methionine 933 mutated to aspartic acid	846-1044
DCC _{FN56M933R}	Fibronectin domains 5 and 6, methionine 933 mutated to arginine	846-1044
DCC _{FN56H857A}	Fibronectin domains 5 and 6, histidine 857 mutated to alanine	846-1044
DCC _{FN56D858R}	Fibronectin domains 5 and 6, aspartic acid 858 mutated to arginine	846-1044
DCC _{FN456wt}	Fibronectin domains 4, 5 and 6	728-1044
DCC _{FN4wt}	Fibronectin domain 4	728-821
DCC _{ecto}	DCC full ectodomains	26-1044
DCC _{ectoV848}	DCC full ectodomains, valine 848 mutated to arginine	26-1044
DCC _{ectoH857A}	DCC full ectodomains, histidine 857 mutated to alanine	26-1044
DCC _{ectoD858R}	DCC full ectodomains, aspartic acid 858 mutated to arginine	26-1044
DCC _{ectoM933R}	DCC full ectodomains, methionine 933 mutated to arginine	26-1044

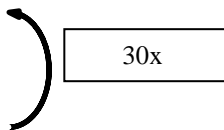
The construct netrin-1 contains the full-length sequence of the synthetic gene described above with the sequence of its native signal peptide. The truncated constructs Netrin_V - Netrin_{VIV} are based on this sequence and were defined by Dr. Jonathan Rapley (EMBL, Hamburg) who was working on this project before. The primers were designed with Vector NTI and can be found in Table K. The construct Netrin_V contains the three EGF-hand domains, plus the linker region between the

motif V and the NTR-domain, since this construct does not contain a native secretion signal it was cloned into the pXLGsec vector between the KpnI and SacI site, to utilise the sequence of the PSG1 signal peptide and the 6xHis-tag. The boundaries of the laminin-like N-terminal domain outline the Netrin_{VI} construct, here again the PSG1 secretion signal was used in the same way. The Netrin_{VII} construct is comprised of the N-terminal laminin-like domain (residues 24-284) and the first EGF-hand domain (residues 285-340). This construct was cloned between the NotI and the SacI site. Both constructs, Netrin_{VIII} and Netrin_{IV} contain the VI-domain (25-284) and the V-domain (285-484), with the variation that Netrin_{IV} was fused with the PSG1 secretion signal by cloning it between the KpnI and the SacI site contrary, to Netrin_{VIII}, which was cloned between NotI and SacI. The eGFP_Netrin constructs were both obtained by adding a KpnI site to the N-terminus of the eGFP and an AgeI site between eGFP and the Netrin, to clone both into the pXLGsec vector for expression and secretion as described above. Cloning of DCC constructs for *E.coli* expression, the DCC_{ecto} constructs and site directed mutagenesis was performed as described in Appendix A.

Molecular cloning & PCR

For cloning the constructs described above, the necessary DNA fragments were obtained by PCR using the primers listed in Table L. All PCR reactions were performed according to the Phusion® High-Fidelity DNA Polymerase manufacturer's protocol in 50µl preparations in an Eppendorf Mastercycler. The dNTPs were added to a final concentration of the 10 mM, forward and reverse primer at a final concentration of 5 µM. The standard PCR program described below was used if not otherwise specified.

PCR steps	Standard PCR for truncated Netrin constructs
Initial denaturation	98°C 2min
Denaturation	98°C 30sec
Annealing	63°C 15sec
Elongation	72°C 30sec per kb
Final elongation	5 min



To obtain pure DNA fragments for the following enzymatic reactions by removal of polymerase and primers, a PCR purification step was performed with the QIAquick PCR purification Kit according to the manufacturer's protocol and the concentration was measured by Nanodrop. To utilise the previously described PSG1 signal peptide for protein secretion, the corresponding PCR products as well as the pXLGsec vector were digested with the restriction enzymes KpnI and SacI. The reaction was carried out with 500ng-1µg of DNA overnight at 37°C in a 20 µl set up in the buffer provided and recommended by the manufacturer. For constructs with the native signal the digest was performed with NotI and SacI. Digested vectors and inserts were purified from a 0.8% agarose gel using the QIAquick Gel Extraction. To ligate the vector and the Netrin fragments, they were mixed in a 1:3 ratio with the ligation buffer provided with the T₄-ligase in a 20µl reaction mix and incubated for 2 hours at room temperature. The correct insertion of the construct was confirmed by sequencing (MWG eurofins) with primers up- and down-stream of the MCS as described in Table M.

Table L Constructs and their primers

Construct	Primer	
Netrin _V	Forward Reverse	5'-GGGGTACCGGAGGCAGGTGCAAATGTAATG-3' 5'-GCTCGAGCTCCTTGATGCATGGGGCAATAGG-3'
	Netrin _{VI}	Forward Reverse
Netrin _{VII}		Forward Reverse
	Netrin _{VIII}	Forward Reverse
Netrin _{IV}		Forward Reverse
	Netrin _{VIVR349A/R351A}	Forward Reverse
Netrin _{VIVR349D/R351D}		Forward
	2. 5'-TAATCTGCACGCCAGGGACTGTGACTTTAATATGGAG-3'	
	Reverse	1. 5'-CTCCATATTAAGCGACAGTCCCTGGCGTGCAGATTACAG-3'
		2. 5'-CTCCATATTAAGTCACAGTCCCTGGCGTGCAGATTA-3'
Netrin _{VIVY323A}	Forward Reverse	5'-ACAGGTGTAAGCCCTTCCATGCCGATAGACCTTGGCAG-3' 5'-CTGCCAAGGTCTATCGGCATGGAAGGGCTTACACCTGT-3'

Construct	Primer
Netrin _{VIVQ443A}	Forward 5'-GTGCCAAAGGATACCAGGCGTCCCGGTCTCCTATTG-3'
	Reverse 5'-CAATAGGAGACCGGGACGCCTGGTATCCTTTGGCAC-3'
eGFP	Forward 5'-AACGGTACCGTGAGCAAGGGCGAGGAGCTGTTCACC-3'
	Reverse 5'-ATTGAGCTCACCGGTCTTGTACAGCTCGTCCATGCCGAGAGTGAT-3
eGFP_Netrin1	Forward 5'-ATTACCGGTGGACCTGGGCTGTCAATGTTTGCAGGACAGGCA-3'
	Reverse 5'-GGTGGTGGAGCTCAGCCTTTTTACATTTCCCTTTT-3'
eGFP_Netrin _{VIV}	Forward 5'-ATTACCGGTGGACCTGGGCTGTCAATGTTTGCAGGACAGGCA-3'
	Reverse 5'-GTGGTGGTGGAGCTCCTTGATGCATGGGGCAATAGGA-3'
DCC _{FN56wt/mutants}	Forward 5'-TAAGGTACCATGCTCCCACCAGTAGGTGT-3'
	Reverse 5'-GGTAAGCTTTTACTTTTCGAAGTGGGGGTGG-3'

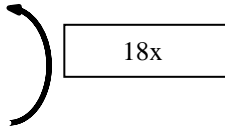
To obtain an N-terminal GFP-tagged Netrin_{VIV} construct primers were designed to introduce the necessary restrictions sites by PCR for cloning into the pXLGsec vector. A KpnI site was added on the 5'end of the eGFP-gen (template pXLGeGFP) and an AgeI site to the 3'end. The Netrin_{VIV} construct was altered with an N-terminal AgeI site and a C-terminal SacI site. The PCRs were performed as described previously. PCR products were purified with the QIAquick PCR purification kit. The purified eGFP product was digested with the enzymes KpnI and AgeI, Netrin_{VIV} with AgeI, SacI and the pXLGsec vector with KpnI and SacI. Both constructs and the pXLGsec vector were ligated after purification from a 0.8% agarose gel in a single reaction. The correct insertion of the eGFP-Netrin_{VIV} construct into the pXLGsec vector was confirmed by sequencing with the described pXLG specific primers and an additional primer specific for eGFP (Table M) to cover the whole sequence of the construct.

For cloning of the DCC_{FN56wt} and mutant constructs from their pET21a origin into the pXLGsec vector for mammalian expression, the constructs were amplified with the primers listed above to introduce an N-terminal KpnI site and a C-terminal HindIII site. The constructs contain a 6xHis-tag followed by a strep-tag and can be secreted through the PSG1 secretion signal.

Site directed mutagenesis

Residues of netrin-1 that are involved, directly or indirectly, in binding to the fibronectin domains 5 and 6 of DCC were mutated by site directed mutagenesis. All primers were designed with the QuikChange Primer Design online tool (Agilent Technologies, <http://www.genomics.agilent.com/primerDesignProgram.jsp>). To change the residues arginine349 (R349) and arginine351 (R351) to alanine (A) a one-step PCR was performed using the primers in Table K. The subsequent construct was named Netrin_{VIVR349A/R351A}. For the construct Netrin_{VIVR349D/R351D} the same residues as described above were changed to aspartic acid (D). This PCR was performed in two steps. The residue tyrosine323 (Y323) was replaced by an alanine to give rise to mutant Netrin_{VIVY323A}. The fourth mutation was made for the residue 443 (Q443). For the construct Netrin_{VIVQ443A} a glutamine was changed again to an alanine. All PCRs were performed with the Phusion® High-Fidelity DNA Polymerase, reaction mixtures were set up according to the manufacturer's protocol in a 50 µl volume using the 5x GC Buffer for GC-rich templates, 10 mM of dNTPS, 5 µM of forward primer and 2.5 µM of reverse primer.

PCR steps	Site-directed mutagenesis
Initial denaturation	98°C 1min
Denaturation	98°C 30sec
Annealing	63°C 35sec
Elongation	72°C 12min
Final elongation	72°C 15min



To select for the mutated PCR product, 25 µl of the reaction mix were digested with the restriction enzyme DpnI. 4 µl of this digest were transformed into the chemical competent *E. coli* strain DH5α and plated on selective agar plates containing 100 mg per ml ampicillin. For plasmid preparation DNA was isolated using the QIAprep Spin Miniprep kit. All constructs were sequenced to confirm the correct alteration of desired amino acids.

Sequencing

For confirmation of the correct insertion of the described constructs and mutations, samples of 1-2 µg plasmid DNA purified by miniprep were sent for sequencing to MWG Eurofins using primers up- and downstream of the multiple cloning site. The obtained sequences were aligned in Vector NTI with the contigExpress to confirm the correctness of the constructs.

Table M Sequencing primer

Primer	pXLG primer
pXLG	
Forward	5'-CAGGTAAGTATCAAGGTTACA-3'
Reverse	5'-GCGTAAAAGGAGCAACATAG-3'
eGFP Forward	5'-CCCTGAGCAAAGACCCCAACGAGA-3'

Plasmid amplification and purification

For transfection grade DNA, plasmid extraction was performed with the QIAGEN Plasmid Plus Giga Kit to obtain high yield, endotoxin free DNA, suitable for transient transfection of mammalian cells. The plasmid was transformed into E. coli DH5α competent cells (Life Tech) and incubated in three litres of conditioned LB medium at 37°C overnight in a shaking incubator, according to the manufactures manual. Only preparations with concentrations over 500 µg/ml and a 260/280 ratio higher than 1.8 were used.

Gel Extraction

Gel extraction was carried out with the QIAquick® Gel Extraction Kit according to the QIAquick® Spin Handbook. The kit was used to extract DNA fragments from an agarose gel (0.8 %) in TAE buffer. After separation by electrophoresis the desired DNA bands were detected by UV-light and cut out with a scalpel. All centrifugation steps were performed in the tabletop Eppendorf Centrifuge 5415R.

Agarose Gel Electrophoresis

Agarose gel electrophoresis was used to separate nucleic acids fragments by size. Electrophoresis was performed using an agarose (0.8 %, Serva) gel submersed in TAE buffer supplemented with 1 drop of ethidium bromide solution (0.025 %). Fermentas GeneRuler™ 1 kb Plus DNA ladder was used as a molecular weight marker (3 µl per gel). Fermentas 6x DNA loading dye was added to the DNA samples

in a 1 to 6 dilution. Electrophoresis was performed at 80 V for 40 minutes with a BioRAD PowerPAC 300 device. Images were taken with a BioRAD ChemiDoc System and BioRAD Quantity One 4.2.3 program.

DNA amplification and purification

Transformation of E. coli Competent Cells

For transformation, 10-50 ng of plasmid DNA was added directly to frozen competent cells and incubated 30 min on ice. The cells were occasionally mixed by gentle vortexing. The plasmid DNA was then introduced into the cells by heat-shocking for 30 seconds at 42°C in a heat block followed by 2 minutes on ice. 80 µl SOC medium was added to the cells prior to incubation at 37°C for 1 hour. Cells were plated on selective LB-agar and incubated overnight at 37°C.

Plasmid DNA Preparation

Plasmid DNA purifications from transformed E. coli DH5-α competent cells were performed using different QIAGEN preparation kits, depending on the amount of plasmid DNA required. Plasmid DNA was quantified and checked for quality with the Nanodrop spectrophotometer for absorbance at 260 and 280 nm. Ratios of 260 to 280 ratios greater than 1.8 guarantee pure enough DNA and were used for further experiments. To guarantee endotoxin free preparations, Midi- and Gigapreps were carried out with the QIAGEN plasmid *Plus* kits.

Minipreps

All minipreps were carried out with the QIAprep® Spin Miniprep Kit according to the QIAprep® Miniprep Handbook.

Midipreps

All Midipreps were carried out with the QIAGEN Plasmid *Plus* Midi Kit according to the Purification Handbook.

Gigapreps

Plasmid preparations from bacterial cultures could potentially be contaminated with significant amounts of endotoxins. Endotoxins are lipopolysaccharide (LPS) complexes associated with the outer membrane of the cell wall of gram-negative

bacteria such as *E. coli*. The toxicity is mediated by the lipid component Lipid A of the LPS complex (Todar, Online Textbook of Bacteriology). In mammalian cell culture, endotoxins can have an effect on the recombinant expression of proteins (Epstein et al., 1990). To avoid negative influences on transfection efficiency or expression yield in mammalian cells endotoxins were removed with the QIAGEN Plasmid *Plus* Giga Kit according to the purification handbook. For the starting culture 10 ml LB media containing a specific antibiotic were inoculated with a single colony from a selective LB-plate and incubated for 8 hours at 37°C in a shaker (180 rpm). Thereafter, 2.5 l of selective LB media split in five 2 l Erlenmeyer flask were inoculated with 2 ml starter culture each and incubated at 37°C overnight shaking. The cells were then harvested in 1 l centrifuge bottles using a BECKMAN-COULTER Avanti J-20 XP Centrifuge at 6000 rpm for 20 minutes at 4°C. Following centrifugation steps were carried out in the Eppendorf Centrifuge 5810R. Vacuum filtration was performed by a WELCH vacuum pump and the QIAvac 24 Plus manifold. Gigapreps are suitable for DNA yields up to 10 mg in 5ml endotoxin free buffer provided with the kit.

3.b.2. Expression

Mammalian Cell Culture

Recombinant protein expression of human constructs of netrin-1 was carried out by transient transfection in adherent growing HEK293T cells ([HEK 293T/17] ATCC® CRL-11268™) stably transfected with the simian virus 40 large-T antigen (T). This cell line allows episomal replication of plasmids carrying the SV40 origin of replication. The robust growth rate, easy handling and high capacity for recombinant protein expression along with low-cost media requirements make them a good expression system for small-scale screening of multiple constructs and large-scale production of up to milligram quantities of secreted protein (Aricescu et al., 2006b).

Cell Culture Maintenance and Storage

HEK293T cells were maintained at 37°C in a Wheaton incubator in a 5 % CO² atmosphere. The cells were grown adherently in 30 ml Dulbecco's modified eagle medium (DMEM), containing 2 mM L-glutamine, 1x non-essential amino acids and 10% foetal calf serum (FCS) in polystyrene cell culture flasks with a surface area of 175cm² (T175). Cells were cultured upon reaching 80-90 % confluency before being passaged. For passaging the cells, the culture media was aspirated and the cells were washed with 10 ml PBS to remove residual FCS. To remove the cells from the flask surface 3 ml 1x Trypsin-EDTA were added and the cells were incubated at room temperature for 5-10 minutes before neutralisation with 7 ml DMEM media. For further culturing, each culture flask was split into five fresh flasks and incubated further as described previously. To determine viability, the cells were counted using a Neubauer improved counting chamber (Carl Roth, Germany) and culture quality was determined by visualisation with 0.4 % Trypan Blue. Trypan Blue is a vital dye that stains dead cells by penetration of the perforated cell membrane. Cultures of less than 90 % viability were discarded

For small-scale expression one fifth of the cells from a T175 flask were resuspended in 12 ml of DMEM containing 10% FCS. Two ml of cell suspension were added then to each well of a 6-well plate 24 hours prior to transfection. The plates were cultured under humidified conditions to prevent dehydration of the media.

Large scale expression was carried out in polystyrene roller bottles with an expanded surface area of 2125 cm². Cells from one 90% confluent T175 flask were transferred as described previously, per roller bottle. Each roller bottle can

accommodate 250 ml of medium. They were then incubated 72 hours prior to transfection in the roller bottle compartment of the incubator at 0.8 rpm.

For long-term storage, trypsinised cells were centrifuged at 800 rpm in an Eppendorf 5810R centrifuge at room temperature (RT) for 5 minutes. Cells from one culture flask were resuspended in 5 ml freezing media (DMEM with 10% DMSO and 10% FBS) and frozen in 1 ml aliquots for storage in liquid nitrogen.

All plastic ware was purchased from Greiner Bio-one.

Transfection and Expression

For expression purposes, only passage numbers between 6 and 15 were used to guarantee high expression levels. Transient gene expression was performed by chemical transfection using the branched cationic polymer Polyethylenimine 25 kDa. Polyethylenimine (PEI) forms complexes with negatively-charged DNA. The positively charged complexes formed, interact with the cell surface and enter the cell via endocytosis. Upon release into the cytoplasm the complex proceeds to the nucleus where it dissociates, allowing DNA to enter the nucleus (Demeneix and Behr, 2005). PEI was dissolved in water to produce 100 mg/ml stock solutions, and then further diluted to a 1 mg/ml working solution (pH 7.0). Previous experiments (Krüger, 2011) showed that the optimal DNA to PEI ratio is 1:2. For all transfections the transfection agent PEI was incubated with the plasmid of choice for 10 minutes in one quarter (500 µl per well) or one fifth (50 ml per roller bottle) of DMEM without FCS of the final expression volume for complex formation. The culture medium was changed to DMEM containing 2% FCS for small scale expression, or 0.2% FCS for large scale transfections.

Small scale expression samples were taken 48 or 72 hours after transfection by centrifugation at 800 rpm at room temperature. A sample of the supernatant was analysed by SDS-PAGE and Western blot as described below to determine expression levels. For samples of the cell, a small swap was resuspended in loading dye.

For preparative large scale expressions, conditioned media were harvested 5 or 6 days post transfection by filtration through filter paper (Whatman) to remove cells that came off the surface by handling of the bottles. Medium was either used directly for subsequent purification or treated with 0.01 M NaN₃ and stored at 4°C to prevent microbial growth.

Culture volume	DNA	PEI	FCS
2 ml	4 µg	8 µg	2 %
250 ml	500 µg	1 mg	2-0.2 %

Expression was confirmed by Western blot analysis using a penta-histidine primary antibody and an HRP-linked secondary antibody.

3.b.3. Protein purification

For further experiments recombinantly expressed proteins secreted into the culture medium needed to be separated from the media components and impurities. A variety of methods were used to establish a protocol to purify the desired proteins from contaminating components. The methods described below utilise different properties of the recombinant proteins like the affinity tag, isoelectric charge and glycosylation.

Protein precipitation

Proteins can be precipitated from solutions by the addition of ammonium sulphate. It is a method to fractionate proteins based on the fact that high salt concentrations can impair the natural ability of proteins to not aggregate by neutralisation of their surface charges. Each protein will start aggregation at a specific salt concentration, so that different proteins can be salted out at different concentrations of ammonium sulphate. This experiment was an attempt to separate the FCS that is necessary for nutrition of the HEK cells during growth and expression from the recombinant proteins. This can be a difficult endeavour, especially when the desired protein is at a similar molecular weight as bovine serum albumin (BSA), the main component in FCS. Preparative ammonium sulphate precipitation can either be performed directly from medium or after an affinity purification step to remove residual BSA from the solution.

Another method to precipitate acidic proteins such as BSA out of solutions is by addition of the positively charged transfection agent PEI at neutral pH. It is based on the same ability to cover surface charges that prevent protein in solution to aggregate.

Ammonium Sulphate Precipitation

For precipitation directly from the culturing medium, ammonium sulphate was added directly to 50 ml of medium, containing Netrin_{VI} in DMEM with 2% FCS to obtain concentrations of 20%, 30%, 35%, 40% and 50% w/v and incubated for 30 minutes with occasionally vortexing at room temperature before brief centrifugation at 4000 rpm for 20 minutes at 4°C. Pellets were then resuspended in HEPES buffer pH 7.4. Samples of supernatant and pellets were taken for an analytical SDS-PAGE gel. For precipitation from the affinity purified protein, the combined fractions of the elution gained from Talon® purification were dialysed overnight into HEPES buffer without DTT pH 7.4. The protein sample was aliquoted into 500 µl fractions and ammonium sulphate was added directly to obtain concentrations of 20%, 30%, 40%, 50% and 60%. Samples were incubated for 30 minutes on ice and vortexed in between. The samples were centrifuged at 13000 rpm for 10 minutes at 4°C. Pellets were resuspended in HEPES buffer without DTT pH 7.4. Samples of supernatant and pellets were taken for an analytical SDS-PAGE gel.

Polyethylenimine Precipitation

For PEI precipitation, the affinity purified protein sample was dialysed as described previously. 60 µl of a 10% PEI solution was added to 2 ml of protein solution, incubated for 5 minutes at room temperature with occasional mixing by vortexing. The sample was then centrifuged at 4000 rpm for 5 minutes at 4°C. Pellets were resuspended in HEPES buffer without DTT pH 7.4. Samples of supernatant and pellets were taken for an analytical SDS-PAGE gel.

Affinity Purification

Immobilized Metal Affinity Chromatography (IMAC) separates proteins based on a reversible interaction between a protein and a specific ligand, in this case a metal ion, which is coupled by a chelator to a sepharose matrix. Protein targets containing a six residue histidine tag (6xHis-tag) have a high affinity for Ni²⁺ or Co²⁺. Proteins with a 6xHis-tag can be purified by binding to nickel-nitrilotriacetic acid (Ni-NTA) or cobalt-carboxymethylaspartate metal affinity chromatography matrix and can be regained after washing out contaminating proteins by competitive elution with imidazole. While nickel binds his-tagged proteins tighter, cobalt is known to bind with higher specificity resulting in purer protein after this purification step. Both methods were used and

compared for their versatility as a first purification step of recombinant protein suitable for crystallisation and functional studies.

Talon Purification

Conditioned medium was concentrated 10 fold in an Amicon stirred cell by filtration through a regenerated cellulose membrane with a molecular cut off of 10 kDa. The concentrated medium was dialysed over night against 25 mM phosphate buffer to prevent stripping of the metal ions from the talon resin using a dialysis membrane with a molecular cut off of 8 kDa. Talon[®] beads were equilibrated in PBS before use. The dialysed medium was then incubated with 1 ml Talon[®] slurry per 100 ml concentrated medium for 1 hour at 37°C shaking or at 4°C overnight on a magnetic stirrer. The flow-through was removed by gravity-flow. The remaining beads were washed with 20 column volumes (CV) of 25mM phosphate buffer, followed by 40 CV of Talon wash buffer 2. Bound protein was eluted with 4x 1 ml Talon elution buffer. Concentration was measured with a Nanodrop. Samples of the flow-through, wash steps and elutions were taken for an analytical SDS-PAGE gel.

Nickel Purification (Ni-X)

For nickel purification NiSepharose™excel (Ni-X) beads were used. This resin is specially designed for samples usually causing stripping of metal ions when loaded directly onto the beads. In Ni-X beads, the nickel is bound strong enough to the sepharose that the medium can be loaded directly without the time consuming concentrating and dialysing steps described for Talon purification (GEHealthcare, 2012).

Ni-X beads were equilibrated in 2x 50 CV PBS before use. Conditioned medium was incubated with 1 ml Ni-X slurry per litre at 4°C overnight on a magnetic stirrer. The flow-through was removed by gravity flow. The column was then washed with 20 CV of wash buffer 1, followed by 20 CV of wash buffer 2. For elution the beads were incubated for 5 minutes with 1 CV of Ni-X elution buffer at a time until no absorbance was measured anymore with a Nanodrop. Elutions were collected in individual Eppendorf tubes. Samples of the flow-through, wash steps and elutions were taken for an analytical SDS-PAGE gel.

Concanavalin A Purification

Con A Sepharose is used to separate and purify glycoproteins by binding molecules containing α -D-mannopyranosyl, α -D-glucopyranosyl and sterically related residues. Concanavalin A (Con A) is a tetrameric metalloprotein isolated from *Canavalia ensiformis* coupled to Sepharose 4B by the cyanogen bromide method. Con A binds molecules containing α -D-mannopyranosyl, α -D-glucopyranosyl and sterically related residues. The binding sugar requires the presence of C-3, C-4 and C-5 hydroxyl groups for reaction with Con A (GEHealthcare, 2011).

Samples of combined elutions from previously performed IMAC purifications were dialysed into Con A binding buffer for 3 hours at RT or at 4°C overnight. A 1 ml Con A column was equilibrated in 20 CV of binding buffer. The dialysed sample was loaded by gravity flow. This step was repeated with the flow-through twice. The column was then washed with 20 CV of binding buffer. Elution was performed either with Con A elution buffer 1, containing α -D-Glucose for competitive elution or with a step wise lowering of the pH (elution buffers 2, 3 and 4) to change binding affinities. For competitive elution 6x 1ml elution buffer 1 was added and fractions were collected separately. For elution by reduction of the pH, a wash step with 10 CV of elution buffer 1 was introduced before 3 CV of elution buffer 2, 3 and 4 were added to the column and fractions were collected separately. In both cases, samples of the flow-through, wash steps and elutions were taken for an analytical SDS-PAGE.

Size Exclusion Chromatography (SEC)

To further purify the proteins that have been concentrated and partly separated from contaminating proteins, gel-filtration chromatography was utilised to separate the remaining proteins by their size. This method can either be used for analytical purposes or for preparation as a final purification step to gain the desired proteins or protein complexes in crystallisation grade purity. The columns used were prepacked with a superdex medium produced by covalent bonding of dextran to highly cross-linked agarose. The S75 columns used a suitable for resolving of peptides and proteins in the molecular weight range of 3 000 to 70 000 Da. For small samples sizes (up to 500 μ l) and analytical experiments the S75 GL 10/300 was used, for preparation of up to 5 ml a HiLoad S75 prep grade 16/60 was used with an ÄKTA purifier system. After verification by SDS-PAGE, 5 ml of the combined elutions containing Netrin_{IV} after affinity purification were loaded onto a HiLoad 16/60

Superdex 75 prep grade column equilibrated in 50mM MES buffer pH 6.0, containing 250mM NaCl and 1 mM DTT. Size exclusion chromatography was carried out at a flow rate of 1 ml per minute. Peak fractions were analysed by SDS-PAGE and Western blot.

All runs were performed at 4°C after equilibration of the column into the desired size exclusion buffer. All buffers can be found in the buffer table below. The flow rate was set to 1 ml/min and 500 µl fractions were collected with a fraction collector, elution length was set to 1.2 CV. Absorbance was measured at 280 nm, 260 nm and 315 nm to determine the peak fractions and aggregation state of the eluted proteins. Samples of the peak fractions were taken for an analytical SDS-PAGE gel.

Table N Protein constructs and size exclusion buffers. Standard buffers indicated in red.

Protein	SEC Buffer
Netrin constructs	Na-citrate, pH 6.0
	TRIS, pH 6.5
	MES, pH 6.0
	PBS, pH 8.0
DCC _{FN56} constructs	TRIS, pH 8.0
	PBS, pH 8.0

Ion Exchange Chromatography

Ion exchange chromatography is a method based on the fact that the net surface charge of a protein varies according to the pH of the surrounding solution. In ion exchange chromatography a protein interacts reversibly with an oppositely charged chromatography medium. Even small differences in the net charge of proteins can reliably separate them with great resolution if the right conditions are chosen. Elution is normally performed by a gradual or stepwise change of salt concentration or pH (GEHealthcare, 2010).

For ion exchange chromatography, around 100 µg of SEC purified Netrin_{VIV} were dialysed into 50 mM Tris buffer pH 7.4 at 4°C overnight. For anion exchange a Mono Q™ 5/50 GL column was washed and equilibrated in Tris buffer pH 7.4 as well. After sample loading the salt concentration was increased by step wise addition of Tris buffer containing 2 M NaCl. The column was washed with 10 CV of 10, 20, 50, 80 and 100% buffer B using an ÄEKTA purifier system at 4°C. UV absorbance was

monitored at 260nm, 280 nm and 305 nm and 500 µl fractions were collected. Samples of the peak fractions were taken for an analytical SDS-PAGE gel.

For UNC5B a Mono S™ 5/50 GL around 500 µg Talon purified UNC5B were dialysed into ion exchange buffer A at 4°C overnight. The column was used with the same protocol described above equilibrated in ion exchange buffer A, elution was performed by step wise addition of buffer B.

3.b.4. Protein characterisation

SDS-PAGE

Sodium dodecyl sulphate polyacrylamide gel electrophoresis (SDS-PAGE) was used as method to separate proteins by size. Analytical SDS-PAGE was performed to confirm expression, monitor purification steps and determine purity grade of proteins for crystallisation and functional studies. Gels with 10% acrylamide were prepared freshly every week. All electrophoresis steps were carried out with the Mini-Protean Tetra Electrophoresis System. Samples were prepared with one part NuPage LDS Sample 4x buffer containing 10 % β-mercaptoethanol to break disulphide bonds. To denature the sample they were incubated 5 to 10 minutes at 75°C in a heat block. Gels were stained with Instantblue™ coomassie stain for 1 hour or with coomassie standard stain overnight on an orbital shaker. Gels were then kept in MilliQ water and scanned with a HP Scanjet 4890 scanner.

Western blot

Western blot analysis was used as a semi-quantitative technique to detect the presence of desired proteins. Therefore, samples were separated by SDS-PAGE as described before and transferred onto a nitrocellulose membrane in a Mini Trans-Blot Tank system for 1 hour at 100 V in transfer buffer. Following protein transfer the membrane was washed in PBS-T (2x 5 minutes) and blocked with 5 % skimmed milk for 2 hours at RT to prevent nonspecific binding of antibodies to the surface of the membrane. Again, the membrane was washed in PBS-T (3x 5 minutes), followed by incubation at 4°C overnight with a primary antibody diluted 1:2000 in PBS-T with 0.05 % skimmed milk. After washing, the secondary horseradish peroxidase(HRP)-conjugated antibody was added in a 1:5000 dilution and incubated 2 hours at RT, followed by 3x 10 minutes washing. For detection the membrane was incubated for 5 min in 10 ml SuperSignal West Pico Chemiluminescent Substrate spiked with 5 %

SuperSignal West Femto Chemiluminescent Substrate. Imaging was carried out using a BioRAD ChemiDoc System with BioRAD Quantity One 4.2.3 software.

Thermal Shift Assay/Thermofluor

The thermal shift assay (thermofluor) screening is used to monitor thermal denaturation. This method can be used to determine thermal protein stability. The fluorescent dye, here SYPRO orange, interacts with hydrophobic regions of the protein exposed by partial or full unfolding during heat denaturation. In aqueous solution the fluorescent of this dye is quenched, but regains fluorescence upon interaction with the hydrophobic core of a protein when unfolding. The assay can be performed in a real-time PCR machine (Boivin et al., 2013). This makes thermofluor screening a suitable method to test the influence of buffer conditions and additives on the stability of proteins to optimise storage and purification conditions. Furthermore the influence of protein-protein interactions on the thermal stability of a formed complex can be visualised by this method. For standard quality control the assay was performed in 100 mM HEPES pH 7.0 and 150 mM NaCl. For more detailed screening, the buffer screen and additive screen or selected conditions of those were used as described by Boivin, Kozak and Meijers (Boivin et al., 2013).

Mass Spectrometry

To determine the mass of proteins, the presence of contaminating proteins and the degree of degradation MALDI-TOF (matrix assisted laser desorption and ionisation - time of flight) mass spectrometry was used. All mass spectrometry analysis was performed in the in-house SPC facility by the SPC staff.

GFP verification

Confirmation of the GFP-construct was performed by fluorescence measurement at 510 nm in a Tecan plate reader after exciting GFP at 395 nm in triplicate. Buffer and a non-fluorescent protein were used to compare intensities.

3.b.5. Binding assays

Pull-down assay

This assay uses the strep-(II)-tag that was fused to the DCC constructs to perform a pull-down of Netrin_{VIV} constructs by binding and eluting from a Strep-Tactin[®] column. Therefore 3.2 nM of the DCC_{FN56} construct (kindly provided by L.I. Finci, Peking University) was mixed with Netrin_{VIV} in a 1:1 stoichiometry and filled to 100 µl with Streptag wash buffer. All samples were incubated 2 hours on ice before use. In the meantime, 50 µl of Strep-Tactin[®] resin was filled into spin columns and washed with 10 CV wash buffer by centrifugation for 1 min at 4°C. After loading of the samples, the columns were washed with 2x 10 CV wash buffer. For elution the competitive compound D-Desthiobiotin was added in buffer at 6x 0.5 CV. Fractions were collected individually and samples were taken for an analytical SDS-PAGE gel.

Thermophoresis

Thermophoresis is a relatively new method that recognises changes in the hydration shell of molecules during interactions with ligands. A laser creates a precise micro temperature gradient along which biomolecules in solution migrate. Even slight changes in the hydration shell of these proteins, due to changes in secondary, tertiary or quaternary structure alter the thermophoretic movement of molecules (Wienken et al., 2010). This makes thermophoresis a very sensitive method to determine binding affinities of protein-protein interactions.

For determining binding affinities between netrin-1 and DCC microscale thermophoresis was performed with a Monolith NTTM. 115 instrument. Therefore, size exclusion purified Netrin_{VIV} was labelled with the Monolith NTTM Protein Labelling Kit RED-NHS according to the manufacturer's protocol in its native buffer (50 mM MES, 250 mM NaCl, 2 mM CaCl₂, 1 mM DTT, pH 6.0) at a concentration between 20-34 µM. This method exclusively labels primary amines, as found in solvent accessible lysines, with a fluorescent dye. After verification of labelling efficiency by absorption measurement at 280nm and 647 nm with a Nanodrop, Netrin_{VIV} was diluted into the reaction buffers described in table B to 100 nM prior to mixing with DCC_{FN56} or mutants. DCC_{FN56WT} and mutants (Met933Arg, Met933Asp, Met933Ala all in 100 mM Tris, 150 mM NaCl pH 8.0) were concentrated as described before to 200 µM. The final reaction set up contained 250 mM NaCl, 100 mM

$(\text{NH}_4)_2\text{SO}_4$, 2 mM CaCl_2 , 0.05 % Tween for reaction buffer 1 (DCC wt and mutants). For the first binding reaction Netrin_{VIV} was mixed with the respective binding partner in a 1:1 stoichiometry. Further dilutions of the potential binding partners (50 μM to 300 pM) were made in the reaction buffer and labelled Netrin_{VIV} was added to a final concentration of 50 nM to each binding reaction. Previous experiments showed that Netrin_{VIV} behaves optimal in capillaries coated with a hydrophilic polymer when no BSA is added, but standard capillaries could also be used if the amount of BSA was at least 0.25 mg per ml in the final reaction mix. Additionally, Netrin_{VIV}/DCC_{FN56}Wt and Netrin_{VIV}/DCC_{FN56 M933R} (all proteins expressed in HEK239T cells and purified as described above) were also measured in PBS (thermophoresis buffer 2). Measurements were carried out at 20°C in triplicates after an initial capillary scan if not otherwise described. LED power was adjusted to 50% of full intensity and measurements were performed with 20% and 40% power. Results were analysed with the NTAanalysis software (Nanotemper technologies GmbH, Germany) using the Kd Fit algorithm and plotted with Graphpad PRISM (GraphPad Software, Inc., LaJolla, USA) using the Hill equation.

Isothermal titration calorimetry (ITC)

Isothermal titration calorimetry (ITC) is a method to determine the thermodynamic properties of protein-protein interactions. These thermodynamic properties are determined by the stoichiometry of the interaction, the association constant, the free energy and heat capacity of binding. ITC measures the binding equilibrium by determining the heat evolved upon binding of ligands with their binding partner and can therefore help to elucidate the forces behind the stabilising effect of protein-protein binding (Pierce et al., 1999). The following experiments were carried out in a VP-ITC micro calorimeter. To verify the interactions between Netrin_{VIV} and DCC_{FN56} both proteins were purified from conditioned DMEM as described before. Size exclusion chromatography was performed in PBS pH 8.0 with 1 mM DTT for both proteins to ensure that no false heat production by differences of buffer concentrations would disturb the experiment. Netrin_{VIV} was kept at constant concentration in the sample cell at 9 μM , DCC_{FN56} was concentrated to 82 μM and titrated in 27, 10 μl steps into the sample cell. The temperature was set to 25°C and the time between the individual injections was 360 seconds. A control experiment

was performed with DCC_{FN56} alone. Analysis of the result was done with the Origin® scientific plotting software.

3.b.6. Functional assays

All cell culture based functional assays described in this section have been performed in collaboration with Dr. Yan Zhang (Peking University, China). Netrin_{VIV} wt, as well as the mutants Netrin_{VIV} R439A/R351A, Netrin_{VIV} R349D/R351D and Netrin_{VIV} Q443A were expressed and purified as previously described and sent to Dr. Zhang. Experimental procedure and statistical analysis was carried out at Peking University by Dr. Y. Zhang and Xiaqin Sun.

DCC-netrin binding assay

COS-7 cells were transfected with wild-type or mutant DCC constructs by lipofectamine 2000 at 50% confluency. After 24 hours, wild-type netrin-1 (Enzo, #522-100-C010, 10 µg/ml), Netrin_{VIV} or mutant Netrin_{VIV} (10 µg/ml) was added to the culture medium. After 24 hours' incubation, the medium was removed and cells were washed 5 times by PBS and fixed for immunostaining with netrin-1 (Abcam, #ab78854) antibody against the VI domain of netrin-1.

Immunocytochemistry

Cells were fixed in fresh 4% paraformaldehyde, 4% sucrose in PBS for 20 minutes at room temperature and permeabilised in PBS-Triton at 4°C, blocked in 10% donkey serum at room temperature, followed by incubation with the netrin-1 antibody (1:500) at 4°C for 24 hours. Cy2-conjugated donkey anti-rabbit antibody was applied as the secondary antibody. The nuclei were then stained with Hoechst 33258 (1 µg/ml, Sigma) for 15 minutes in the dark. The cover slips were mounted with ImmunonTM mounting medium (Shandon, Pittsburgh, PA) onto glass slides. The results were analyzed by using a fluorescence microscope (Olympus BH2-RFCA, Olympus, Tokyo, Japan) with digital camera (Olympus DP70 Digital Microscope Camera, Olympus, Tokyo, Japan).

Pull-down assay

COS-7 cells were transfected with the wild-type DCC construct and after 24 hours the cellular extracts were collected with the cell lysis buffer (50 mM Tris pH8.0, 150 mM

NaCl, 1% NP-40, 0.1% SDS, with fresh protease inhibitor cocktail, Roche). Protein A sepharose beads were first soaked with netrin-1 antibody against the VI domain, and then coated with wild-type netrin-1, Netrin_{VI}, or mutant Netrin_{VI}. The respective beads were incubated with the cellular extracts. After rotating overnight, the beads were collected by centrifugation. The proteins that bound to the beads were then removed by adding loading buffer (2% SDS, 50 mM Tris pH6.8, 0.2 mg/ml bromphenol blue, 0.2 M DTT, 10% glycerol) and heated at 95°C for 10 min. The proteins were separated by SDS-PAGE (15% acrylamide) at 70 volts for about 2 hour. The proteins were transferred to Immobilon-P™ polyvinylidene fluoride (PVDF) membrane (Millipore, Billerica, MA) at 100 milliamps for 2 hours. The membrane was then blocked with 5% skimmed milk in Tris buffered saline (TBS) with 0.1% tween20 (TBS-T) at room temperature for 1 hour. Anti-DCC (Abcam ab16793), anti-netrin (Abcam) anti-HA (Millipore, 07-221) or anti-myc (Millipore, 4A6) antibodies were diluted at 1:1000 for Western blots as primary antibodies. After 3 washes of 10 minutes each with TBS-T, Clean-Blot IP Detection Reagent conjugated with horseradish peroxidase (HRP) (Thermo, 21230) was added in a dilution of 1:10000 as the secondary antibody. The secondary HRP was detected by enhanced chemiluminescence. The optical density was analysed by BioRad ChemiDox (BioRad, Hercules, CA).

DCC clustering assay

COS-7 cells were transfected with either a HA or myc tagged full length wild-type or mutant DCC constructs and incubated with or without the presence of netrin-1. After 24 hours the cellular extracts were collected with the cell lysis buffer. The protein A sepharose beads were coated either with anti-HA or anti-myc antibody described in the pull-down assay. After incubation of the beads and the cellular extracts for overnight, the beads were collected as described above. The proteins bound to the beads were extracted and subjected to Western Blot analysis.

Neuronal cell culture for axon guidance, DCC-netrin binding, pull-down and clustering assays

Mouse primary neurons were cultured from the dorsal horn of the spinal cord of E15 embryos of wild-type or DCC^{-/-} mice (Rigato et al., 2011), following the regulations of the Peking University Animal Care and User Committee. In brief, fresh mouse dorsal horn tissues were dissociated with 0.25% trypsin (Invitrogen, Carlsbad, CA), and then

inactivated by 10% decompemented foetal calf serum (FCS, HyClone, Logan, UT). The mixture was triturated through a pipette to make a homogenous mixture. After filtering the mixture through 70 μm sterilized filters, the flow-through was centrifuged. The pellet was then washed once by phosphate buffer saline (PBS) and once by DMEM in Earle's balanced salt solution containing 0.225% sodium bicarbonate, 1 mM sodium pyruvate, 2 mM L-glutamine, 0.1% dextrose, 1x antibiotic Pen-Strep (all from Invitrogen, Carlsbad, CA) with 5% FCS. Cells were then plated on poly-L-lysine (Sigma, St. Louis, MO) coated plates at a density of 3×10^6 cells/ml. Neurons were incubated at 37°C in DMEM without phenol red with 5% FCS and with 5% circulating CO₂. Cytarabine was added to culture media 24 hours after plating at 10 μM to inhibit cell division. Medium was changed every 48 hours. Cells were treated for experiments at 2 days in culture. COS-7 cells (purchased from the ATCC) were maintained in DMEM medium on plates or glass cover slips.

Microinjection

Thin-walled Borosilicate glass capillaries (outer diameter=1.0 mm, inner diameter=0.5 mm) with microfilament (MTW100F-4, World Precision Instrument, Sarasota, FL) were pulled with a Flaming/Brown Micropipette Puller (P-97, Sutter, Novato, CA) to obtain injection needles with a tip diameter of $\sim 0.5 \mu\text{m}$. Microinjections were performed in the cytosol of each cell using the Eppendorf Microinjector FemtoJet and Eppendorf Micromanipulator (Eppendorf, Hamburg, Germany). Neurons were injected with 25 fl/shot at an injection pressure of 100 hPa, a compensation pressure of 50 hPa, and an injection time of 0.1 seconds. The solutions were injected at the indicated concentrations with 100 $\mu\text{g/ml}$ dextran Texas Red (DTR, Molecular Probes, Eugene, OR) as a fluorescent marker to recognize the injected cells. Fifty neurons were injected in each treatment. Approximately 90% neurons survive the injections for at least 16 days (Zhang et al., 2000)

Axon guidance assay

At 2 days in vivo (DIV), the mouse neurons were injected with siRNAs to DSCAM1-4, wild-type DCC/mutant DCC constructs (CMV::DCC in a pCDNA3.1 vector) and 270 kDa ankyrin G (AnkG)-EGFP fusion protein construct (UBC::AnkG-EGFP in a pUB vector) with the marker dye DTR (Molecular Probes). AnkG (270)-EGFP is specifically located at the axon initial segment and is used to indicate the axon. The heparin pre-coated beads were then coated with 100 $\mu\text{g/ml}$ netrin-1, dipped with

0.1% agarose (Sigma) and then placed at one corner of the culture dish. After 24 hours' incubation, the direction of axon (green fluorescent) growth of the injected cells (red fluorescent) toward the beads was observed (S20). A Nikon Super Resolution N-SIM Microscope (Nikon, Japan) was used for analyzing data. Each image was collected using a 40x oil immersion objective. Pictures were taken from the fields of differently treated neurons. The investigators were blinded to the group allocation during the experiment. The direction of the axon was determined by a method previously derived from (Yam et al., 2009).

Statistical evaluation

Statistical significance was assessed using the one-way analysis of variances (ANOVA) technique. The sample size (n) for the cell binding and axon guidance assays was n = 100. The power was estimated as: $\alpha=0.01$, $n=100$, $H_0: X_1=X_2$, $H_1: X_1>X_2$, $Z_\beta=(X_1 - X_2)100^{0.5}/(X_1(1 - X_1)+ X_2(1 - X_2))^{0.5}-Z_\alpha$, giving power=0.879. Therefore, n=100 has adequate power to detect differences between 2 groups. We did not exclude any data. The data meet the assumptions of the tests (giving a normal distribution). The Sheffé's test was then applied *post hoc* for the significant difference shown by ANOVAs. A p value of less than 0.05 was used as an indicator of statistical significance. Power analysis for each experiment was then used for validation, and the group size was then performed by SPSS V13.0.

3.b.7. Crystallisation and Small angle X-ray scattering

All images were taken with the Formulatrix RockImager (Formulatrix, Inc., U.S.) at 19°C. Crystallisation of Netrin_{IV} alone was performed in HTPX-facility in Hamburg as well by the SPC-staff and pictures were taken by the same system. Commercially available screens used can be found in Table F.

Optimisation of promising conditions was performed by hand with Netrin_{IV} purified as described previously. Protein purity was verified by SDS-PAGE and only proteins with less than 5% contamination were used at a concentration of around 100 µM.

Screen 1

Precipitant	L-Proline		Ammonium acetate		MgCl ₂	
0.1 M	0.1 M Hepes pH 7.5 10% PEG 3350	0.1 M Hepes pH 7.5 25% PEG 3350	0.1 M Hepes pH 7.5 10% PEG 3350	0.1 M Hepes pH 7.5 25% PEG 3350	0.1 M Hepes pH 7.5 10% PEG 3350	0.1 M Hepes pH 7.5 25% PEG 3350
0.15 M	0.1 M Hepes pH 7.5 10% PEG 3350	0.1 M Hepes pH 7.5 25% PEG 3350	0.1 M Hepes pH 7.5 10% PEG 3350	0.1 M Hepes pH 7.5 25% PEG 3350	0.1 M Hepes pH 7.5 10% PEG 3350	0.1 M Hepes pH 7.5 25% PEG 3350
0.2 M	0.1 M Hepes pH 7.5 10% PEG 3350	0.1 M Hepes pH 7.5 25% PEG 3350	0.1 M Hepes pH 7.5 10% PEG 3350	0.1 M Hepes pH 7.5 25% PEG 3350	0.1 M Hepes pH 7.5 10% PEG 3350	0.1 M Hepes pH 7.5 25% PEG 3350
0.25 M	0.1 M Hepes pH 7.5 10% PEG 3350	0.1 M Hepes pH 7.5 25% PEG 3350	0.1 M Hepes pH 7.5 10% PEG 3350	0.1 M Hepes pH 7.5 25% PEG 3350	0.1 M Hepes pH 7.5 10% PEG 3350	0.1 M Hepes pH 7.5 25% PEG 3350

Screen 2

Precipitant	L-Proline or Ammonium acetate or MgCl ₂					
0 M	0.1 M Hepes pH 7.5 2.5% PEG 3350	0.1 M Hepes pH 7.5 5% PEG 3350	0.1 M Hepes pH 7.5 10% PEG 3350	0.1 M Hepes pH 7.5 15% PEG 3350	0.1 M Hepes pH 7.5 20% PEG 3350	0.1 M Hepes pH 7.5 25% PEG 3350
0.1 M	0.1 M Hepes pH 7.5 2.5% PEG 3350	0.1 M Hepes pH 7.5 5% PEG 3350	0.1 M Hepes pH 7.5 10% PEG 3350	0.1 M Hepes pH 7.5 15% PEG 3350	0.1 M Hepes pH 7.5 20% PEG 3350	0.1 M Hepes pH 7.5 25% PEG 3350
0.2 M	0.1 M Hepes pH 7.5 2.5% PEG 3350	0.1 M Hepes pH 7.5 5% PEG 3350	0.1 M Hepes pH 7.5 10% PEG 3350	0.1 M Hepes pH 7.5 15% PEG 3350	0.1 M Hepes pH 7.5 20% PEG 3350	0.1 M Hepes pH 7.5 25% PEG 3350
0.3 M	0.1 M Hepes pH 7.5 2.5% PEG 3350	0.1 M Hepes pH 7.5 5% PEG 3350	0.1 M Hepes pH 7.5 10% PEG 3350	0.1 M Hepes pH 7.5 15% PEG 3350	0.1 M Hepes pH 7.5 20% PEG 3350	0.1 M Hepes pH 7.5 25% PEG 3350

Crystallisation of the Netrin_{VIV}/DCC_{FN56} complex

Fractions containing Netrin_{VIV} (in 50 mM MES, 250 mM NaCl₂, 1 mM DTT, pH 6.0) at higher than 90% purity were combined and concentrated in an Amicon® Ultra-4 Centrifugal Filter (Millipore, cat# UFC800324). DCC_{FN56} (in 100 mM Tris, 150 mM NaCl, pH 8.0) was concentrated in the same way and mixed with Netrin_{VIV} in a 1:1 stoichiometry using 100 µM of each protein. Crystallisation trials were carried out in the high-throughput facility for Sample Preparation and Characterization (SPC) at EMBL Hamburg using the Qiagen Protein Complex, Classic I, Classic II, AmSO₄, PhClear and PEG II Suite kits (Table F). The crystal forming condition contained 0.1 M MES pH 6.0, 0.15 M ammonium sulphate and 15% (w/v) PEG 4000 (Protein Complex Suite). Crystals were cryo-protected in 0.1 M MES pH 6.0, 0.25 M ammonium sulphate, 20% (w/v) PEG 4000 and 10 % glycerol prior to flash-cooling to 100 K. X-ray diffraction data were collected with the help of Dr. R. Meijers on the P14 beamline of EMBL Hamburg situated at the PETRA3 synchrotron. The beamline was equipped with a Pilatus 6M detector and an MD3 EMBL diffractometer. The X-ray data was processed by Dr. R. Meijers with XDS (Kabsch, 2010a, b) and merged and scaled with SCALA (Evans, 2006), and the statistics are presented in the appendix (Table S1).

Crystal Structure determination (by R.Meijers)

The structure of the Netrin_{VIV}/DCC_{FN56} complex was solved by Dr. R. Meijers by molecular replacement with MOLREP (Vagin, 2010) using the structure of laminin gamma1 LN-LE1-2 (Carafoli et al., 2012) as a search model for the netrin molecule (PDB code 4AQT) and the FN5 and FN6 domains of Neogenin (Yang et al., 2011)(PDB code 3P4L) as a search model for DCC. The structure was rebuilt using Buccaneer (Cowtan, 2012) and refined with Refmac5 (Murshudov, 2011) and PHENIX (Afonine et al., 2012)(TableS1). Model building was done with Coot (Emsley et al., 2010), and well defined electron density was observed for residues 40 – 455 of Netrin_{VIV} and the residues 844 until 1050 of the DCC_{FN56} receptor construct, except for the BC loop (residues 869 until 874) of the FN5 domain. The stereochemistry was checked with Molprobit (Chen et al., 2010) and Ramachandran statistics are reported in Table S1. The buried surface area of protein-protein interactions alone were calculated using the PISA server (Krissinel, 2011)), using a probe radius of 1.4 Å.

Crystal structure analysis and figures

Analysis of the crystal structure was carried out with PyMOL (www.pymol.org) and the electrostatic surface representations were obtained using the Adaptive Poisson-Boltzmann Equation (APBS) plugin in PyMOL (Unni et al., 2011). Figures were made with Inkscape.

SAXS data collection and analysis

SAXS experiments have been performed and analysed in collaboration with Dr. DI. Svergun, Dr. H. Mertens and Dr. G. Schenk (EMBL, Hamburg). X-ray solution scattering data were collected on the EMBL P12 beamline of the storage ring PETRA III (DESY, Hamburg), using a PILATUS 2M pixel detector (DECTRIS, Switzerland) with 20 frames of 50 msec exposure time. Solutions of all constructs were measured while flowing through a temperature controlled capillary at 10°C in 25 mM MES, 50 mM Tris, 200 mM NaCl, 1 mM CaCl₂, 100 mM ammonium sulphate, pH 7.0. For all constructs, a minimum of four solute concentrations was measured (Appendix, table S2). The sample-to-detector distance was 3.1 m, covering a range of momentum transfer $0.001 \leq s \leq 0.45 \text{ \AA}^{-1}$ ($s = 4\pi \sin\theta / \lambda$, where 2θ is the scattering angle, and $\lambda = 1.24 \text{ \AA}$ is the X-ray wavelength). Based on comparison of successive frames, no detectable radiation damage was observed. The data were radially averaged, processed, normalised and the overall parameters were evaluated using standard procedures by an automated pipeline (Franke, 2012). Molecular masses (MMs) of solutes were estimated from SAXS data by comparing the extrapolated forward scattering $I(0)$ with that of a reference solution of bovine serum albumin.

Low-resolution shape envelopes for DCC_{FN56} and Netrin_{VIV} were determined using the *ab initio* bead-modelling program DAMMIF (Franke, 2009). The results of 10 independent DAMMIF runs were analysed using the program DAMAVER (Volkov, 2003) to identify the most representative/typical models. The scattering patterns from the crystallographic models of DCC_{FN56}, Netrin_{VIV} and of the complexes were computed using CRY SOL (Svergun, 1995). A C-terminal His₆/Strep-tag (20 residues) present in the construct used for solution studies was added to the DCC_{FN56} structure using the program BUNCH (Petoukhov, 2005). The Netrin_{VIV} molecule in the crystal structure contains three glycosylation sites on the VI domain. These sites were used as a basis to extend the glycosylation at each site to contain an oligomannose unit using the website <http://www.glycosciences.de/modeling/glyprot/php/main.php>. The

resulting glycan chains were checked for compatibility within the crystal structure, and the model with extended oligomannose chains was observed to fit well inside the crystal lattice.

For the DCC_{FN56} and Netrin_{VIV} alone in solution, the scattering computed from the high resolution models provided excellent fits to the experimental data with discrepancies of $\chi= 1.2$ and 1.1 , respectively. For the Netrin_{VIV}/DCC_{FN56} sample, the scattering patterns computed from the crystallographic complexes with either site 1, or site 2 or both sites occupied with DCC_{FN56}, yielded significant systematic deviations to the experimental data (discrepancy $\chi= 1.7, 1.4$ and 2.1 , respectively). Data from the Netrin_{VIV}/DCC_{FN56} complex with the M933R mutant cannot be fitted well by any of the single models. The scattering data from the complexes were therefore further analysed in terms of mixtures of different species. The scattering intensity of a mixture of particles is expressed in terms of additive contributions from the different particle type with individual intensities $I_k(s)$, as:

$$I(s) = \sum_{k=1}^K v_k I_k(s)$$

where K is the number of components and v_k are the volume fractions of the components. In this case, form-factors of each of the five possible components were calculated using FFMAKER (Petoukhov, 2012) from the following crystal structures determined in this study: free DCC_{FN56}, free Netrin_{VIV} and the three crystallographic complexes with either, site 1, site 2 or both sites occupied with DCC_{FN56}. The volume fractions yielding the best fits to the experimental data were calculated using the program OLIGOMER (P.V. Konarev, 2003).

3.b.8. Sequence alignment

Sequence alignments of netrin-1, DCC and neogenin

Alignments were done with Clustal Omega (Sievers and Higgins, 2014) and ESPript (Gouet et al., 2003), sequence logo representations were created with Weblogo3 (Crooks et al., 2004).

Sequences were obtained from Uniprot.org. Human netrin-3 (Uniprot: O00634), netrin-4 (Uniprot: Q9HB63) netrin-5 (Uniprot: Q8WTR8), netrinG1 (Uniprot: Q9Y2I2) and netrinG2 (Uniprot: Q96CW9). Netrin-1 of *H. sapiens* (Uniprot: O95631), *M. musculus* (Uniprot: O09118), *D. rerio* (Uniprot: O42203), *X. laevis* (Uniprot: O57339), *D. melanogaster* (Uniprot: Q24567) and *C. elegans* (unc6, Uniprot: P34710). *H. sapiens* (Uniprot: DCC P43146, neogenin Q92859), *M. musculus* (Uniprot: DCC P70211, neogenin P97798), and *D. rerio* (Uniprot: DCC Q49BB0, neogenin Q801M2)

3.b.9. Programs

This thesis was written in Microsoft Word and citations incorporated with Endnote. Figures were made in Inkscape. DNA sequence analysis and primer design was performed with VectorNTI. Agarose gel and Western blot images were taken with BioRAD Quantity One 4.2.3 and visualise with ImageJ. Analysis of thermophoresis and ITC data was performed with NTAAnalysis, Graphpad PRISM and Origin®. Structure analysis was performed in PyMOL.

4. Results

4. a. Netrin-1

Netrin-1 is comprised of an N-terminal laminin-like domain (VI) with three N-glycosylation sites, an EGF hand motif (V) with one N-glycosylation site and a C345 C-terminal domain (Fig.1, Serafini et al. (1994)). It has been of greater interest to investigate which domains are taking part in the interactions of netrin-1 and its receptors. Proteins designated for structural analysis by crystallisation have to be evaluated for stability and homogeneity in milligram quantities. The process of expression, purification and initial crystallisation screening is described in this chapter.

4.a.1. Small scale expression and initial purification

Preliminary experiments have shown that the expression of full-length netrin-1 is low and purification of the protein is difficult to achieve due to instability. To overcome these limitations and address the question which domains are important for stability and function of netrin-1, several truncated constructs have been designed.

The construct Netrin_V consists of the three EGF hand-repeat motifs (V) and a PSG1 signal peptide. Netrin_{VI} contains the N-terminal VI domain and, as well the PSG1 signal peptide. Netrin_{VII} contains the laminin-like VI domain and one EGF-like domain secreted by netrins native signal peptide. The construct VIII contains the VI and the V domains with its native signal peptide, Netrin_{VIV} is of the same composition, but the native signal peptide was exchanged to a PSG1 secretion signal. For expression in human embryonic kidney (HEK) cells these constructs were cloned into a vector derived from the pXLG vector containing a C-terminal hexa-histidine sequence (6xHis tag) for affinity purification.

Expression tests of the constructs described above were carried out by transient transfection of HEK293T cells in small scale (in 6-well plates, 4 µg of plasmid DNA and 8 µg of 25 kDa branched PEI as described in chapter 3. After incubation for 72 hours samples of the culturing medium were taken for analysis.

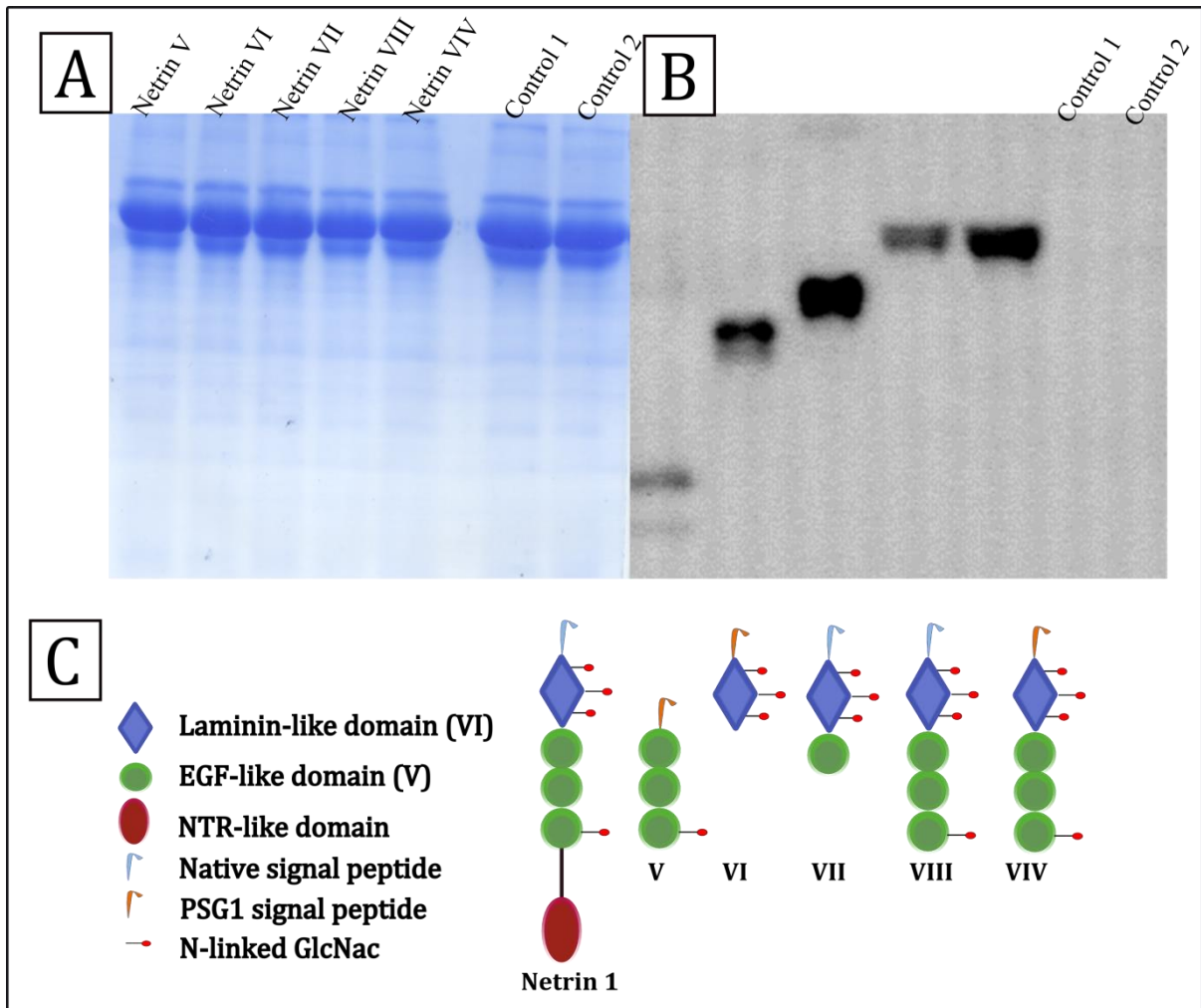


Figure 1 Human netrin-1 domain organisation and small scale expression tests of truncated constructs in HEK 293T cells. **A** SDS-PAGE gel 10% of media samples of small scale expression of netrin-1 constructs stained with coomassie blue. Control 1 medium of non-transfected cells incubated with 8 μ g of PEI, control 2 medium of non-transfected cells not incubated with PEI. **B** Expression was confirmed by Western blot analysis, detection with Anti-His antibody. **C** Domain organisation of human netrin-1 and the composition of truncated constructs.

The coomassie stained SDS-PAGE gel showed two bands between 55 and 70 kDA for all samples. Their presence in the control indicates that they do not resemble recombinant protein expression (Fig.1 A). These bands correspond to the bovine serum albumin (BSA) fraction in the 2 % foetal calf serum (FCS) that is used to supplement the expression medium for HEK293T cells. To confirm netrin expression by immuno detection, a Western blot was performed (Fig. 1 B). All constructs were detected using a primary antibody designed to recognise a penta-histidine motif. The intensity of the signal led to the conclusion, that the constructs Netrin_{VII} and Netrin_{XIV} were best expressed. While Netrin_{VII} is secreted with the native signal peptide, Netrin_{XIV} was cloned into a vector (pXLGsec) containing the signal peptide of PSG1. This protein is known to be expressed in high amounts during pregnancy (Bohn, 1971) and was tested for expression in previous experiments (Krüger (2011), not

published). The expression test of the netrin-1 constructs confirmed that it can be utilised to secrete certain constructs in higher yields than with their native secretion signal. The Western blot analysis also showed that the expression yield of constructs containing the N-terminal laminin-like domain is higher. The Netrin_V, containing only the EGF-hand domains, showed additional, smaller bands that were assumed to indicate degradation. It was therefore concluded that the laminin domain aids in stabilisation of the construct.

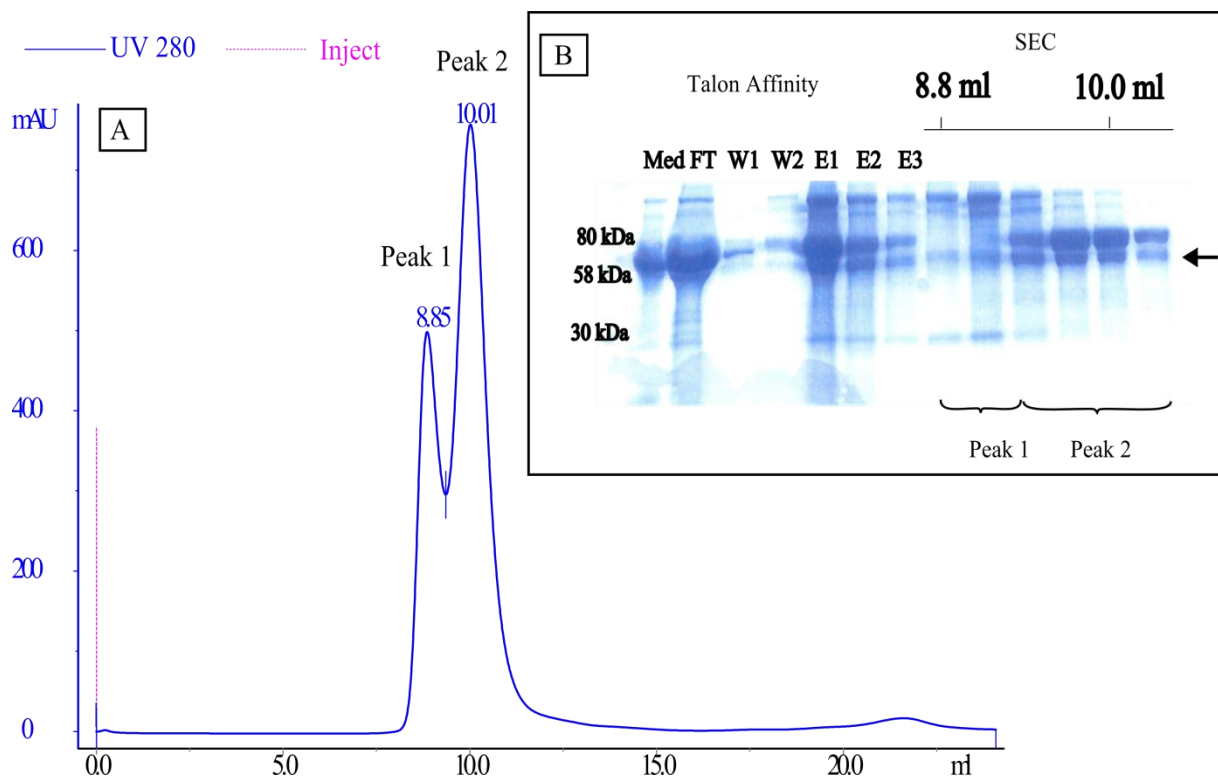


Figure 2 Purification of Netrin_{VIV} in analytical scale, **A** size exclusion chromatography profile, concentrated elutions injected to a Superdex 75 analytical column 10/300 equilibrated in 20 mM Hepes pH 7.5, 500 mM NaCl, 1 mM DTT on an AEKTA FPLC with UV absorbance detection at 280 nm. **B** 10% SDS-PAGE gel stained with coomassie standard stain of Talon affinity purification and samples of the peak fractions of the analytical size exclusion chromatography, FT flow through, W1 wash 1, W2 wash 2, E1-E3 elutions, arrow is indicating Netrin_{VIV}.

After verification of protein expression in small scale, Netrin_{VIV} was chosen to be the best expressing construct. This construct contains the domains proposed for receptor interactions. Evaluation of purification conditions was tested by purification from 1.3 l conditioned medium (Fig. 2 B, Med). Therefore, it was concentrated to 500 ml and dialysed against phosphate buffer to minimize the effect of the medium components such as EDTA, that strip the metal ions (Co²⁺) coupled to the matrix of the Talon affinity column. Following incubation overnight, the Talon beads and

medium were separated by gravity flow (Fig. 2B, FT). The elution fractions were collected after extensive washing of the beads. The combined fractions contained, according to verification of absorbance measured with a Nanodrop, a total amount of 10 mg total proteins. The SDS-PAGE of the samples collected from every affinity purification step showed that not only Netrin_{VIV} was eluted from the beads. A number of bands in the elution fractions were also present in the medium and flow through (Fig. 2 B). These are components of the culture medium. They are known from previous purifications of other proteins from conditioned DMEM (Dulbecco's modified eagle medium). The most prominent band on the gel (Fig. 2 B) was observed between 60 and 80 kDa in all affinity purification fractions. The predicted molecular weight of recombinantly expressed Netrin_{VIV} was calculated to be 49289.43 Da. This is more consistent with the band located below of approximately 55 kDa, if glycosylation of the protein is taken into account. Therefore, the upper band resembles the BSA fractions of the foetal calf serum added to the expression medium in a final concentration of 2%. 500 µl of the combined elution fractions were loaded onto a size exclusion column in the attempt to remove the remaining impurities. The profile showed two defined peaks (Fig. 2 A). The first eluted directly after the void volume of the column indicating that it contained large particles such as aggregates. The SDS-PAGE (Fig. 2 B) confirmed this presumption as it showed a band around 55 kDa among other, much higher components. The second peak around 10 ml contained according to the gel BSA and other medium components along with Netrin_{VIV}. This experiment showed that BSA and other medium contaminants are difficult to remove under standard conditions in an analytical scale.

The resolution of gel filtration columns with a larger diameter and bed volume is higher than the resolution of analytical columns. It has been observed that proteins that separated poorly in small scale purifications were separated better in larger scales. To test if contaminants from the culture medium could be removed by size exclusion in a preparative scale, the combined elutions of affinity purification (Fig. 2) were loaded onto a Superdex 75 prep column in the same buffer as described before. The AEKTA used for this experiment was equipped with UV absorbance detection at 260 nm, 280 nm and 305 nm. The elution profile showed two peaks as seen in analytical scale before (Fig. 3 A). The elution of the first peak was observed close to the void volume (V_0) between 44 and 45 ml. It remained smaller in proportion to peak 1 seen in Fig. 2 A. This first peak contained according to the SDS-PAGE

(Fig. 3 B) mainly bigger contaminants and aggregates. The second peak appeared broader and contained more protein according to the absorbance (Fig. 3 A) and gel analysis (Fig. 3 B). The measurement of the UV absorbance at 305 nm indicated that the proteins in this peak might be aggregated to some extent. However, the SDS-PAGE (Fig. 3 B) of the individual fractions of peak 2 showed no better separation of Netrin_{VIV} from BSA. Both proteins eluted in exactly the same fractions from the column and no improvement of purity was obtained from this experiment.

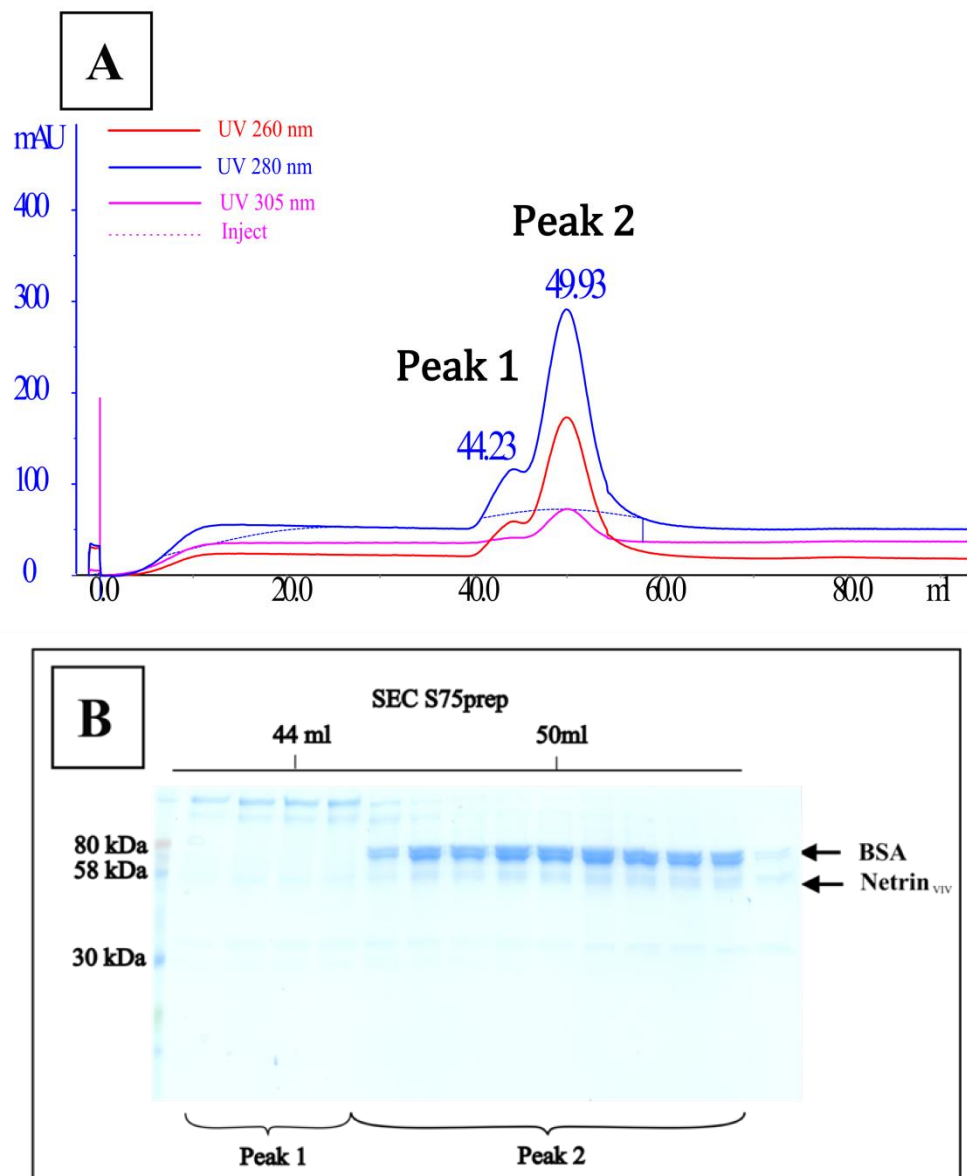


Figure 3 Purification of Netrin_{VIV} in a preparative scale, **A** Size exclusion chromatography profile, concentrated elutions injected to a Superdex 75 prep column 16/60 equilibrated in 20 mM Hepes pH 7.5, 500 mM NaCl, 1 mM DTT on an AEKTA purifier with UV absorbance detection at 260 nm, 280 nm and 305 nm. **B** 10% SDS-PAGE gel stained with coomassie standard stain of peak fraction samples of the size exclusion chromatography, elution volume indicated above. Arrows indicating BSA and Netrin_{VIV} according to the size estimated with marker.

4.a.2. Improving affinity purification

Affinity purification of recombinant proteins secreted into the culture medium of HEK cells is a time and material consuming process when conventional metal ion coupled matrices such as Talon or Ni-NTA sepharose beads are used (as described above). The harvested medium has to be concentrated for more convenient handling and then dialysed excessively to remove chelators that could interact otherwise with the metal ions bound to sepharose matrix. The Ni SepharoseTM excel (Ni-X) was tested for its ability to shorten purification processes in order to increase the productivity. Ni-X is a precharged nickel ion affinity chromatography medium that allows direct loading of mammalian culture media without dialysing. The nickel ions are bound stronger through a special chelating agent to the sepharose beads to prevent stripping (GEHealthcare, 2012). The SDS-PAGE analysis of the purification showed (Fig. 4 A, Ni-X) a comparable ability of the matrix to bind and elute recombinant 6xHis-tagged proteins. Along with the desired protein, contaminating components from the medium were observed (Fig. 2 B). The flow through mainly contained BSA and the wash steps removed only little of the contaminating proteins. The elution fractions showed the double band between 55 kDa and 70 kDa (Fig. 4 A Ni-X, Fig. 2 B) observed for co-purified Netrin_{IV} and BSA before. Even though this method did not lead to improvement of protein purity in this first step of purification, it is suitable to shorten the turnover times of affinity purification.

Separation of Netrin_{IV} from the described contaminants was attempted with another affinity purification method. Concanavalin A (ConA) is a lectin purified from the jack bean *Canavalia ensiformis* that binds to α -D-mannopyranosyl, α -D-glucopyranosyl and sterically related residues identifying it potent to bind glycoproteins such as recombinant Netrin_{IV}. ConA is a metalloprotein and requires Mn^{2+} and Ca^{2+} for binding to sugar residues (GEHealthcare, 2011). Suitability of ConA protein coupled beads was tested by incubation with the combined and dialysed elution fractions of Ni-X purified Netrin_{IV} (Fig. 4 A Ni-X) followed by competitive elution.

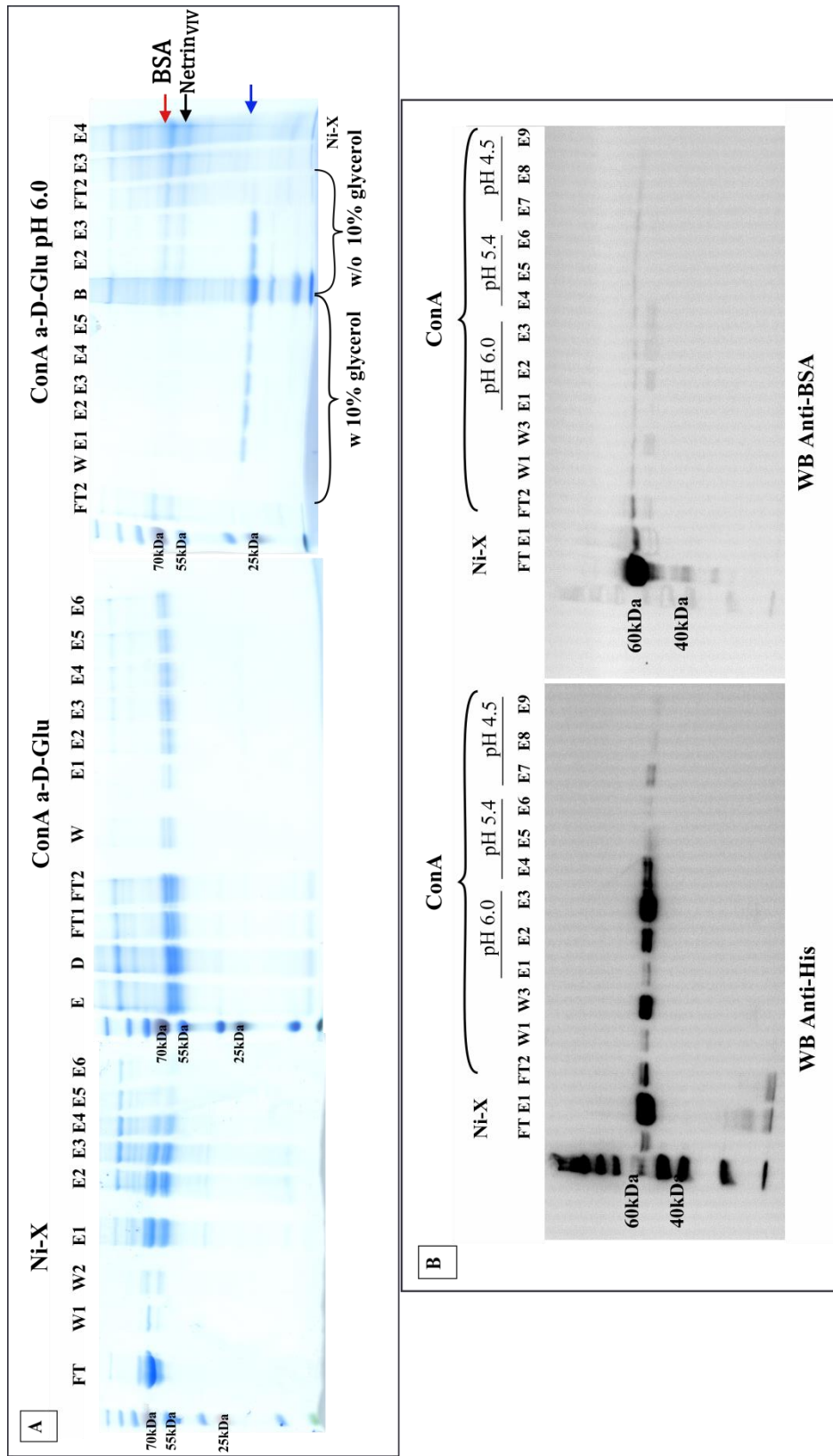


Figure 4 Test affinity purification of Netrin_{vIV} from medium contaminants by Ni-X and subsequent Concanavalin A (ConA) purification, 10% acrylamide gels stained with Instantblue™ coomassie. **A** SDS-PAGE of Ni-X purification, FT: flow through, W1 and W2: wash steps, E1-E6: elutions. SDS-PAGE of ConA purification, elution with **α-D-glucose** at pH 7.4, E: combined elutions from Ni-X, D: dialysed protein, FT1: flow through after loading, FT2: flow through after reloading of FT1, W: wash, E1-E6: elutions with **α-D-glucose**. SDS-PAGE of ConA purification, elution with **α-D-glucose** at pH 6.0 with (w) and without (w/o) 10% glycerol. **B**: boiled beads. Red arrow: BSA, black arrow: Netrin_{vIV}, blue arrow: small fraction **B** Western blot (WB) of Ni-X and ConA purification, elutions at pH 6.0, pH 5.4 and pH 4.5 with antibodies against a penta-His motif (Anti-His) or against bovine serum albumin (Anti-BSA).

Most of the protein was recovered from the dialysis step (Fig. 4 A ConA, E and D). The samples from both flow through fractions (Fig. 4 A ConA, FT1 and FT2) showed the higher bands resembling BSA along with other contaminants (Fig 4 A, Ni-X). Elution was performed by competition with α -D-glucose. These fractions contained Netrin_{VIV}, resembled by the lower band on the gel, but the protein yield was poor. To address the possibility that competition with α -D-glucose was not a sufficient elution method, lowering of the pH along with the effect of the addition of 10% glycerol to stabilise the protein was tested (Fig. 4 A, ConA pH 6.0). Here, the separation of the SDS-PAGE was better compared to the previous one. The elution fractions (same as in Fig. 4 A, Ni-X and ConA) showed both, bands for BSA (red arrow) and Netrin_{VIV} (black arrow) were clearly separated from each other. The elution fractions containing glycerol did not show bands of the size expected for Netrin_{VIV}. A smaller fraction (Fig. 4 A, ConA pH 6.0 E1-E5, blue arrow) of around 25 kDa was present. It could resemble concanavalin A uncoupled from the beads. This is congruent with the sample of the beads (Fig. 4 A, ConA pH 6.0, B) that showed a similar band of this size, together with Netrin_{VIV} and BSA. As a conclusion, glycerol did not seem to improve protein stability. The fractions only contained a smaller fragment of unknown origin. A Western blot of fractions containing the 25 kDa fragment (Fig. 4 B, Anti-His, E1-E3 pH 6.0) showed no 6xHis-tagged protein. Attempts to recover more protein from the ConA column by a pH gradient (Fig. 4 B, Anti-His) were not successful. The fractions showed only little or no 6xHis-tagged protein compared to the Ni-X fractions or the elutions at pH 6.0. The grade of BSA contamination after Ni-X and ConA purification was monitored by Western blot with an antibody against BSA (Fig. 4 B Anti-BSA). Here it turned out that most BSA was already removed in the flow through (Fig. 4 B Anti-BSA, Ni-X FT, ConA FT2) of both subsequent methods. The elution fractions of all ConA test purifications contained no or very little BSA. The experiment described above was repeated in a 1l scale to obtain enough protein to perform a subsequent gel filtration step.

Since Netrin_{VIV} seemed to be present in comparable amounts in the Ni-X elutions (Fig. 5 C, Ni-X Affinity) and in the FT2 from the ConA column (Fig. 5C, ConA) analysis was performed with this sample as well as the elution fractions.

Therefore, the FT2 fraction was loaded on an analytical Superdex 75 gel filtration column. The size exclusion profile showed two peaks (Fig. 5 A). The main peak 1 eluted around 10 ml, while a second peak eluted after 12 ml. According to gel

analysis, the fractions contained for peak 1 Netrin_{VIV} together with BSA (Fig. 5 C, SEC A). Peak 2 exclusively contained smaller fragments of unknown origin.

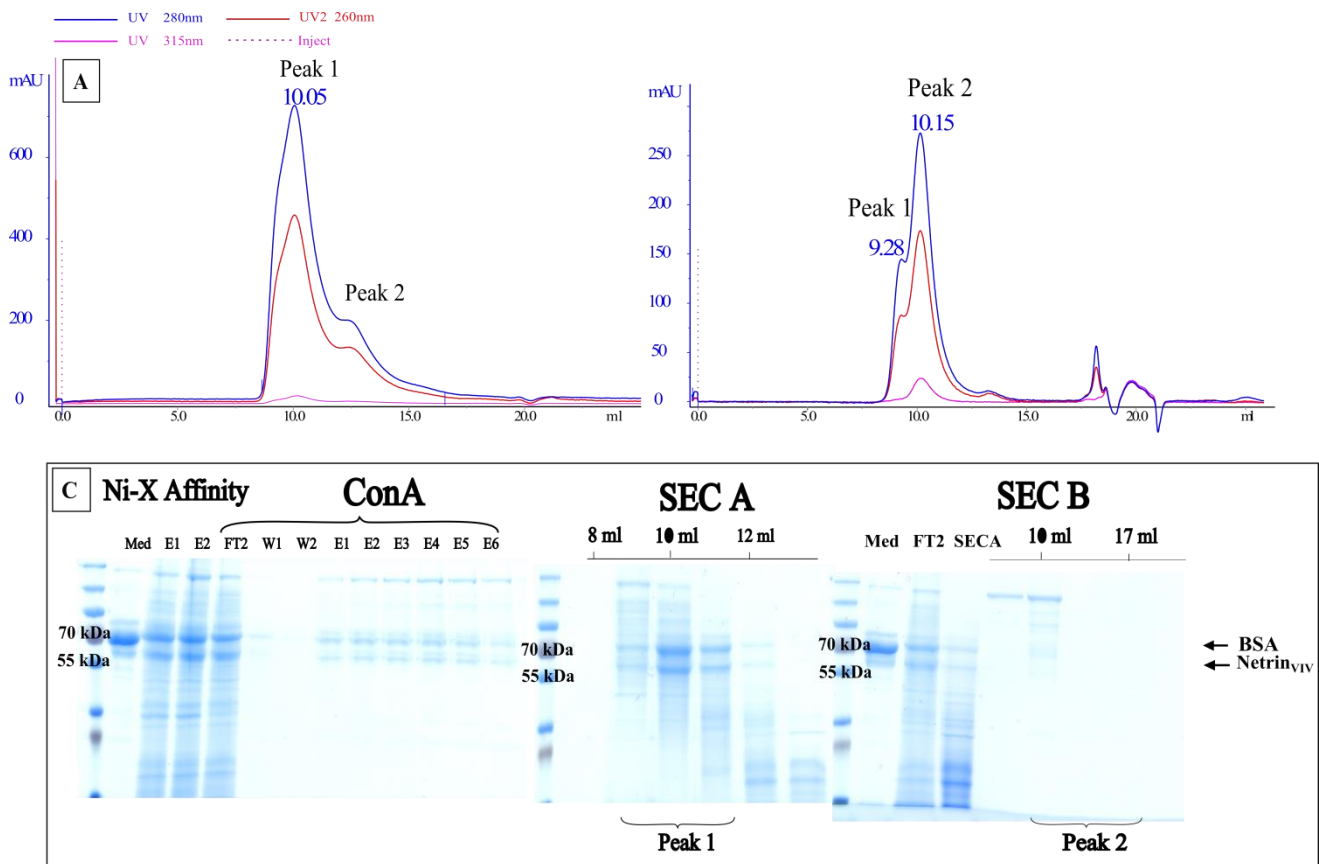


Figure 5 Separation of Netrin_{VIV} from medium contaminants by analytical gel filtration chromatography after Ni-X and subsequent ConA purification. **A** Size exclusion chromatography profile of the ConA flow through, injected to a Superdex 75 analytical column 10/300 equilibrated in 50 mM Na-citrate pH 6.0, 250 mM NaCl, 1 mM DTT on an AEKTA purifier with UV absorbance detection at 260 nm, 280 nm and 315 nm. **B** Size exclusion chromatography profile of the ConA combined and concentrated elutions. **C** 10% SDS-PAGE gels stained with coomassie standard stain of Ni-X and ConA purifications, and peak fraction samples from the size exclusion chromatography **A** and **B**, elution volume indicated above. Arrows indicating BSA and Netrin_{VIV} according to the size estimated using the marker.

The elutions from the ConA column (Fig. 5 C, ConA E1-E6) showed only small amounts of Netrin_{VIV} and BSA. Separation comparable to the separation observed in the previous experiment was not obtained in this case.

Nevertheless, it was attempted to separate Netrin_{VIV} and BSA by size exclusion. The first peak eluted shortly after the V_0 (Fig. 5 B) and contained a high molecular weight fraction that was identified as a medium contaminant (Fig. 5 C, SEC B <10 ml). The second peak eluted around 10 ml as seen in the size exclusion of the FT2 (Fig. 5 A) and seemed to contain only minor amounts of protein (Fig. 5 C, SEC B, peak 2) compared to the same fractions of SEC A. Most of this protein was

accounted to be BSA. After all, it was concluded, that ConA purification is an unreliable method. No consistent separation of Netrin_{VIV} and BSA was obtained.

4.a.3. Ion exchange

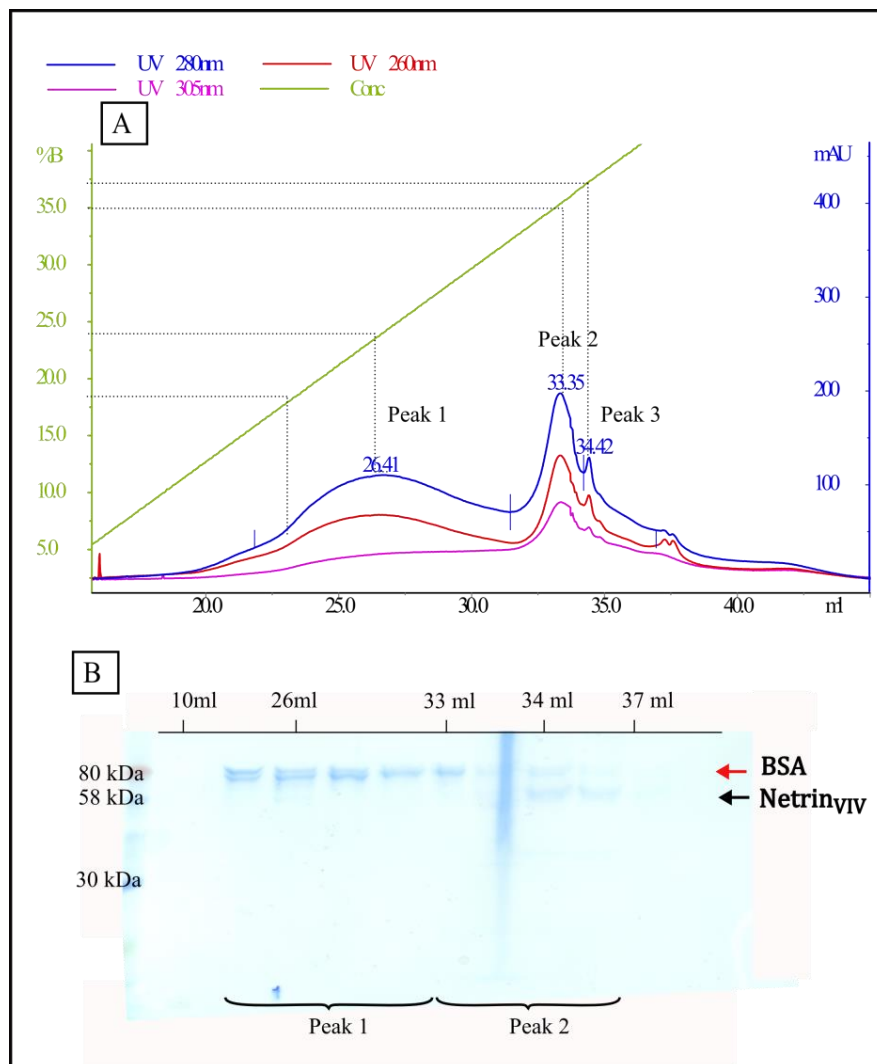


Figure 6 Separation of Netrin_{VIV} from medium contaminants by ion exchange chromatography after Ni-X purification from 11 DMEM containing 2% FCS. **A** Ion exchange chromatography profile of combined and dialysed elutions from Talon purification injected to a MonoQ column equilibrated in 50 mM Tris pH 7.4 on an AEKTA purifier with UV absorbance detection at 260 nm, 280 nm and 305 nm, concentration of elution buffer (2 M NaCl) indicated in green. **B** 10% SDS-PAGE of peak fractions, gel stained with Instantblue™ coomassie, elution volume indicated above. Arrows indicating BSA (red) and Netrin_{VIV} (black) according to the size estimated by marker.

The separation of proteins by ion exchange chromatography is a method based on the different net charges of proteins depending on the pH of the surrounding medium. By binding to differently charged matrix polymers proteins can be separated by anion or cation exchange. Polymers with anionic groups therefore bind positively charged proteins, while polymers with cationic groups bind negatively charged proteins depending on the ionic strength of their charge and the concentration of competing free salt ions (Nelson&Cox, 2005).

BSA is a protein with a predicted isoelectric point (pI) of 6.10 and a negative net charge of -16.0 at pH 7.4. For predictions the sequence of the Uniprot entry P02769 (excluding the signal peptide) was used with the online tool PROTEIN CALCULATOR v3.3. This tool uses the pKa values for the individual amino acids from Stryer Biochemistry, 3rd edition (Stryer, 1988). Although the theoretical calculation of charges is not very accurate for folded proteins and should generally only be used as an indication of the actual charge for experiment planning, in this case the mentioned charges above are experimentally documented (Barbosa et al., 2010). For Netrin_{VIV} a pI of 8.2 was calculated with a positive net charge of 10.2 at pH 7.4. This is quite different from BSA indicating that ion exchange chromatography might be a valuable method for the separation of the two proteins. MonoQ columns, as used for the experiment are packed with an anion exchange matrix that should bind BSA while Netrin_{VIV} should only interact very little if at all with the column matrix if the theoretical charges apply *in-vitro*. A sample containing approximately 100 µg of the fractions from the size exclusion chromatography shown in Fig. 3 were dialysed, filtered and injected to the column. The chromatography profile (Fig. 6 A) showed that the proteins started eluting at approximately 15% buffer B, which corresponded to a NaCl concentration of 300 mM. The first distinct peak eluted at 360 mM, the second at 700 mM and the third at 750 mM NaCl. While the first, very broad peak indicated that it contained a mixture of proteins, the analytical SDS-PAGE (Fig. 6 B, peak 1) showed only a double band below 80 kDa that very likely resembled BSA. Negligible aggregation was indicated by the UV absorbance at 305 nm (Fig. 6 A, UV 305 nm). According to gel analysis, the second peak contained a mixture of BSA and Netrin_{VIV} (Fig. 6 B). The third peak did not contain protein that was visible on the SDS-PAGE gel.

There was no satisfying separation obtained by ion exchange chromatography. This might partially be accounted to the loss of protein during dialysis. Repetition of the experiment with higher amounts of protein failed due to protein precipitation during dialysis or buffer exchange. Another explanation would be that the calculated charge of Netrin_{VIV} does not apply *in-vitro*. Glycosylation can alter the pI of a protein and therefore the net charge at a given pH (Sola and Griebenow, 2009). It is possible that Netrin_{VIV} bound to the column matrix and was subsequently eluted together with BSA.

4.a.4. Protein precipitation

The precipitation of proteins by the addition of ammonium sulphate is another method to separate proteins based on their surface charge, that provides stability and prevents aggregation in solution (Englard and Seifter, 1990). Ammonium sulphate can alter these surface charges, and different proteins can be salted out at different concentrations. Therefore, this method was used in the attempt to separate BSA from Netrin_{VIV}.

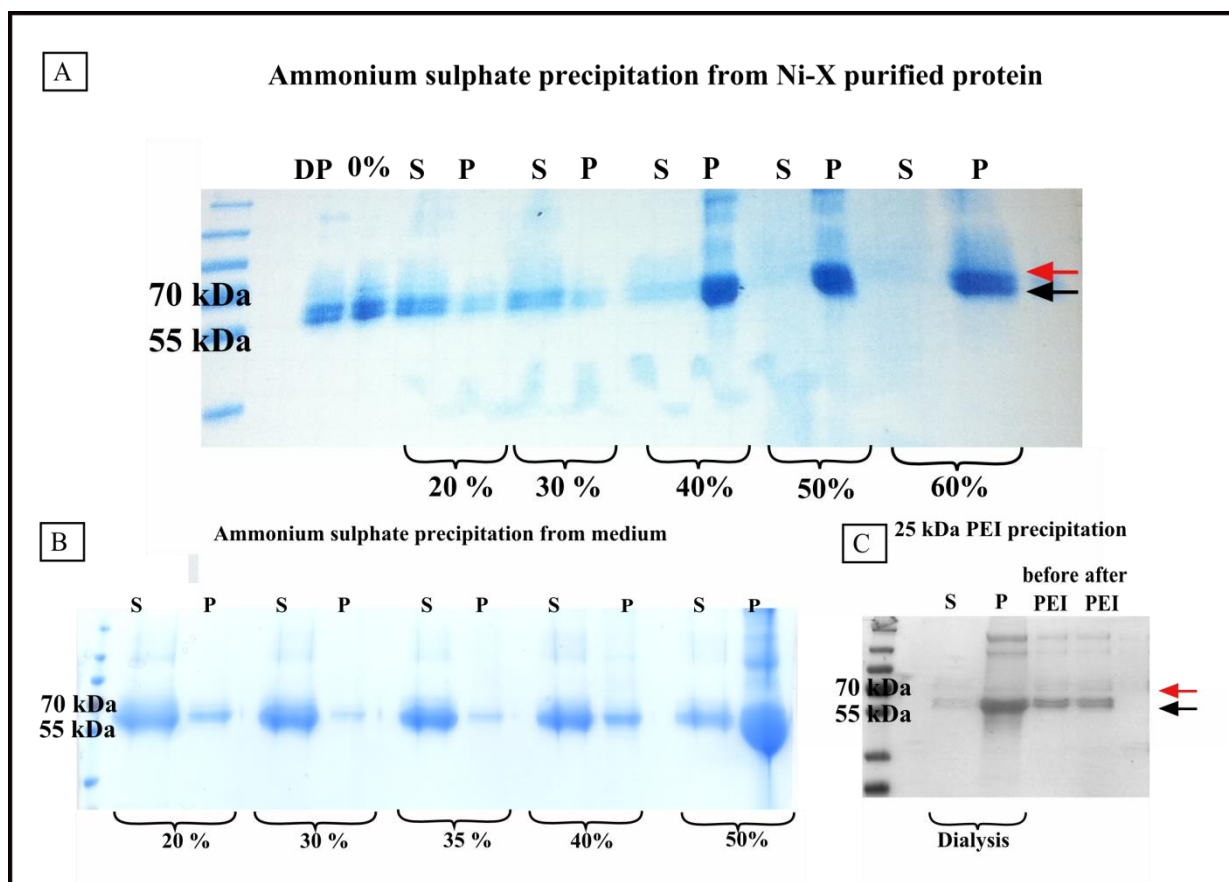


Figure 7 10% SDS-PAGE of fractions from ammonium sulphate and PEI precipitation to separate Netrin_{VIV} from medium contaminants, gels stained with coomassie standard stain. Arrows indicating BSA and Netrin_{VIV} according to the size estimated with marker. **A** Ammonium sulphate (AS) precipitation from Ni-X purified protein, DP: dialysed protein, 0%: no AS added, S: supernatant, P: pellet. **B** Ammonium sulphate precipitation from medium, fractions named as described before. **C** 25 kDa PEI precipitation of Ni-X purified protein, fractions named as described before.

Precipitation was performed after Ni-X purification and dialysis (Fig. 7 A). During dialysis certain proteins precipitated (Fig. 7 A, DP), but enough proteins to conduct the experiment remained in solution (Fig. 7 A, 0%). The addition of 20% and 30% ammonium sulphate had only little effect on the stability of the proteins, and the main fractions remained in the supernatant (Fig. 7 A, 20% S and P, 30% S and P). The

addition of 40% precipitant caused precipitation of almost all proteins in solution (Fig. 7 A, 40% P) without the possibility to distinguish between Netrin_{VIV} and BSA. The same was true for 50% and 60% ammonium sulphate (Fig. 7 A, 50% and 60%). To eliminate the chance that the proteins were already destabilised by the procedure of purification and dialysis, the experiment was also performed by addition of ammonium sulphate directly to conditioned DMEM (Fig. 7 B). Here also, 20%, 30% and even 35% of ammonium sulphate had little effect on the proteins in solution (Fig. 7 B, 20% S and P, 30% S and P and 35% S and P). The addition of 40% salt caused a fraction of approximately 55 kDa to precipitate out which is very likely to be Netrin_{VIV} (Fig. 7 B, 40% P). Most of the other proteins remained in solution (Fig. 7 B, 40% S). These components started precipitation after the addition of 50% ammonium sulphate (Fig. 7 B, 50% P).

No clear separation of Netrin_{VIV} from BSA was obtained from this experiment. The finding that Netrin_{VIV} precipitated before or together with BSA made further analysis, crystallography for example, difficult. A precipitated protein would need resolubilisation or in severe cases even refolding before functional or structural analysis could be performed. This is a process with unpredictable outcome. Therefore, this method was not further considered.

Negative results were obtained by the attempt to precipitate BSA by the addition of the positively charged transfection agent PEI 25 kDa branched (Fig. 7 C). Here dialysis also reduced the amount of protein in solution (Fig. 7 C, Dialysis S) substantially (Fig. 7 C, Dialysis P). The addition of PEI had no effect on the solubility of the proteins in solution (Fig. 7 C, after PEI).

4.a.5. Reducing FCS minimised contamination

BSA was confirmed to be the main contaminant of recombinant Netrin_{VIV} expressed by HEK293T cells. Since removal to an extent suitable for crystallisation was found to be impossible, the logical consequence was to remove or reduce it during expression. The effect on the expression yield by reduction of FCS was investigated by purification of 1 l DMEM containing 0.5% FCS (Fig. 8). Reduction of FCS to a quarter gave already a much purer Netrin_{VIV} after affinity purification (Fig. 8 B, Ni-X Affinity). The BSA present in the culturing medium was mostly removed in the flow

through (Fig. 8 B, Ni-X FT) and further contaminants were eliminated during the subsequent wash steps (Fig. 8 B, Ni-X W2). The main fraction in the elutions (Fig. 8 B, Ni-X E1-E7, E comb) was now observed to run clearly below the band of BSA (Fig. 8 B, SEC: FT) on an analytical SDS-PAGE. Therefore, it was identified to be recombinant Netrin_{VIV} of approximately 55 kDa. Further purification by size exclusion chromatography at pH 6.0 resulted in an elution profile with two peaks (Fig. 8 A). This pH was found to be stabilising in a thermofluor buffer screen during a preliminary study. The first peak at 43.36 ml elution volume contained only proteins of high molecular weight (Fig. 8 B SEC, peak 1) or aggregation. However, the second peak that eluted between 50 ml and 60 ml elution volume (Fig. 8 A) showed a single band on the SDS-PAGE (Fig. 8 B SEC, peak 2). Here again, the band ran below the size of BSA on the SDS-PAGE gel (Fig. 8 B SEC, FT). Netrin_{VIV} was successfully separated from BSA. Later it was found, that 0.2 % (v/v) FCS supplementation is sufficient to express Netrin_{VIV} in milligram quantities (not shown).

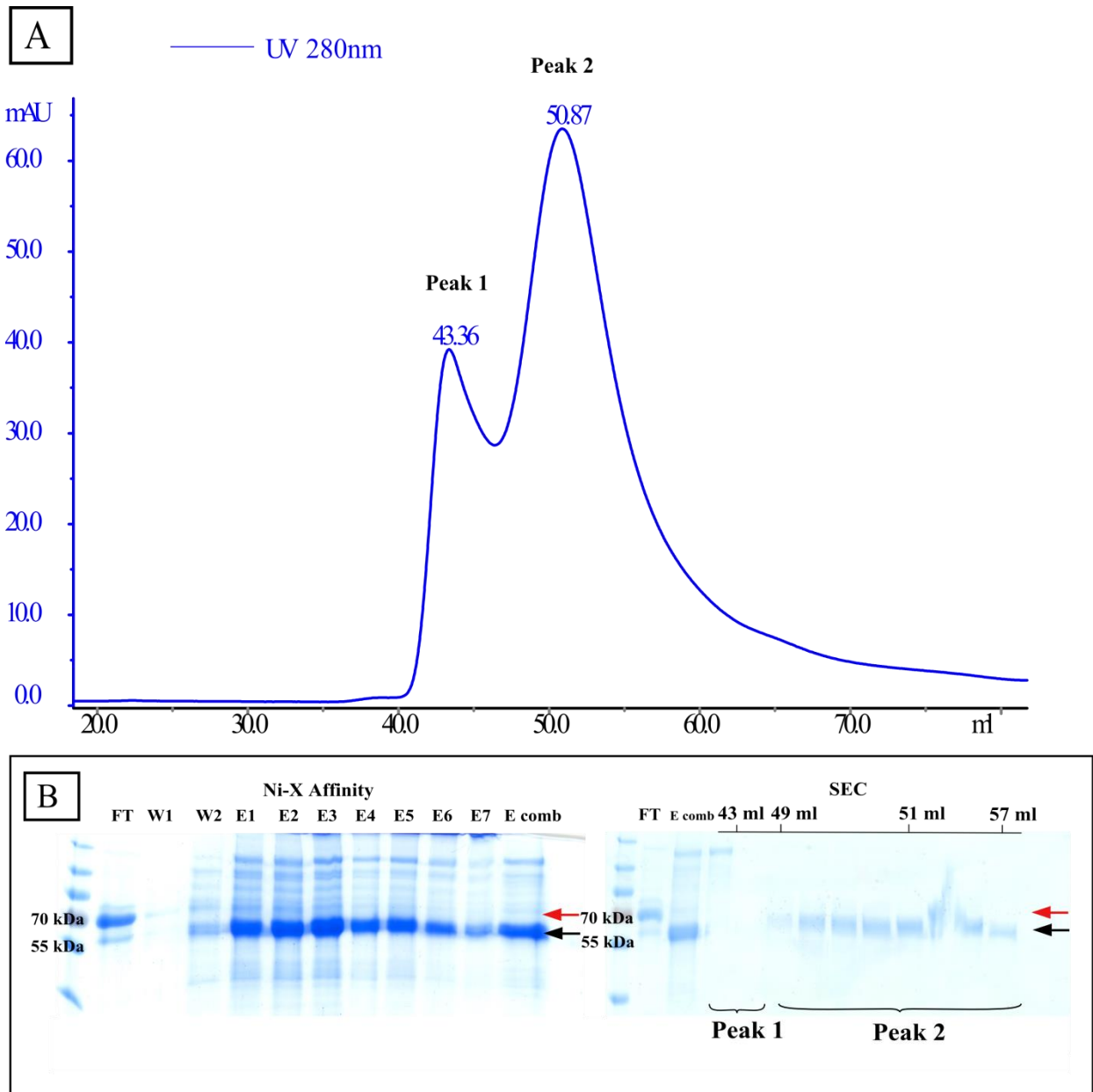


Figure 8 Separation of Netrin_{VIV} from medium contaminants by gel filtration chromatography after Ni-X purification from 1 l DMEM with 0.5% FCS. **A** Size exclusion chromatography profile of combined elutions injected to a Superdex 75 prep column 16/60 equilibrated in 50 mM MES pH 6.0, 250 mM NaCl, 1 mM DTT on an AEKTA FPLC with UV absorbance detection at 280 nm. **B** 10% SDS-PAGE gels stained with InstantblueTM coomassie of **Ni-X Affinity** purification and peak fractions of size exclusion chromatography (**SEC**), FT: flow through, W1 and W2: wash steps, E1-E7: elutions, E comb: combined elutions, size exclusion elution volume indicated above. Arrows indicating BSA (red) and Netrin_{VIV} (black) according to the size estimated with marker.

4.a.6. Biophysical protein characterisation

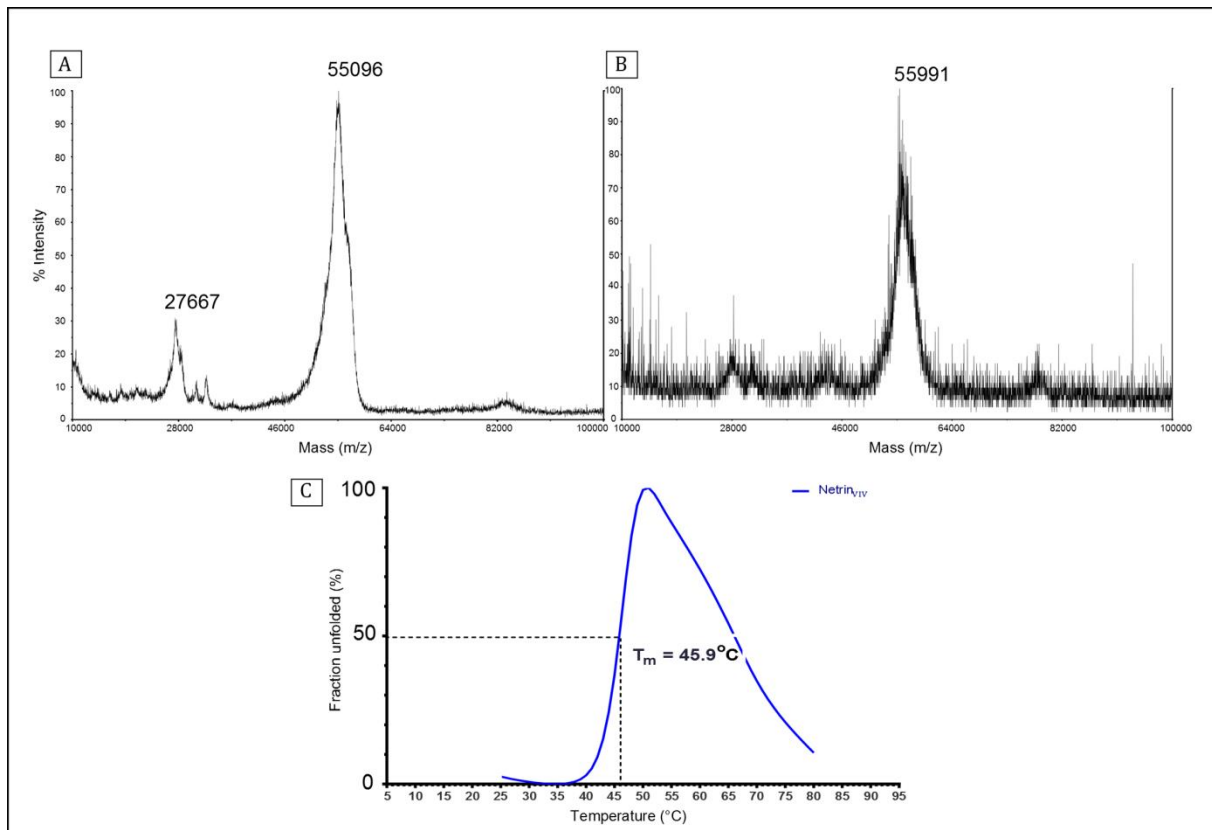


Figure 9 Quality control of Netrin_{VIV} after purification and before crystallisation by mass spectroscopy (MS) and thermofluor (TF). **A** MS of Netrin_{VIV} sample after SEC concentrated to 100 μM , **B** MS of Netrin_{VIV} after SEC concentrated to 20 μM , **C** TF of sample shown in **A** under standard conditions 100 mM Hepes pH 7.5, 150 mM NaCl normalised, unfolded fractions in percent plotted against temperature in $^\circ\text{C}$.

The purity of Netrin_{VIV} was further confirmed by MALDI-TOF mass spectrometric (MS) analysis (Fig. 9 A and B). This method was used as a control step to verify molecular mass, contamination and degradation. BSA is a common standard control protein for MS. It is known to fly well and give distinctive peaks with a molecular mass of 66 kDa. The analysis performed of the concentrated sample (100 μM) described above (Fig. 8) showed two peaks. The highest peak stretched from 52000 to approximately 60000 Dalton with a mean mass of 55096 Daltons (Fig. 9 A). This is consistent with the mass of 49289.43 Da predicted from the amino acid sequence without taking glycosylation into account. The Netrin_{VIV} construct contains four potential N-glycosylation sites which could be responsible for the broad appearance of the main peak, since glycosylation does not necessarily occur homogeneously during expression (Sola and Griebenow, 2009). This could explain the slight variations in mass of samples purified from different expression batches (Fig. 9 B). The second peak (Fig. 9 A) is much lower with a calculated mass of 27667 Dalton. This is close to

half the mass of peak one and can be explained with a higher ionisation state of the sample. However, in none of the samples BSA appeared as a contaminating protein indicating that the described purification is sufficient to reduce it to trace amounts.

The determination of the melting temperature of a protein is another quality control method to verify the stability of a protein. It is performed as a standard procedure to monitor protein quality before crystallisation (Fig. 9 C). The protein is incubated with a fluorescent dye that is quenched in aqueous solution. During heating the protein starts to unfold and the fluorescent signal increases when the dye binds to the gradually exposed hydrophobic core of the protein until the protein is fully unfolded. With increasing temperature the dye dissociates again from the protein and the fluorescence drops (Boivin et al., 2013). The T_m is defined as 50% of the maximum fluorescence intensity corresponding to 50% of the protein being unfolded. The melting curve obtained for Netrin_{VIV} under standard conditions (Fig. 9 C, 100 mM Hepes pH 7.5, 150 mM NaCl) gave a T_m of 45.9 °C. This is just above the recommended minimal temperature for samples dedicated for crystallisation trials. It could indicate instability or partial unfolding of the protein.

The addition of potentially stabilising components was tested separately. The screening (Fig. 10) confirmed that Netrin_{VIV} is more stable in the buffer used for size exclusion chromatography (MES, pH 6.0) than in the standard buffer. The T_m is with 49.5°C (Fig. 10, dotted line) approximately 4 degrees higher than the temperature observed in HEPES buffer at pH 7.5 (Fig. 9 C). The addition of 5 mM EDTA, a chelating agent, destabilised the protein to a degree where a single melting could not be observed anymore. The fluorescence was already very high at low temperatures. Contrary to that, calcium chloride (CaCl₂) added in concentrations between 2 and 10 mM increased the melting temperature up to 52°C. It can therefore be considered to have a stabilising effect on Netrin_{VIV}. This is consistent with reports showing that calcium plays a key role in signal mediation (Wang and Poo, 2005). Netrins contain a calcium binding motif in the laminin domain (Brasch et al., 2011). Here it was shown that it has a stabilising effect as well. The addition of different ammonium sulphate salts did not show a significantly stabilising effect. The resulting temperatures varied between 46°C (100 mM K₂SO₄) and 49°C (200 mM ammonium sulphate). These conditions were chosen according to the observations described in chapter 4.b.4.

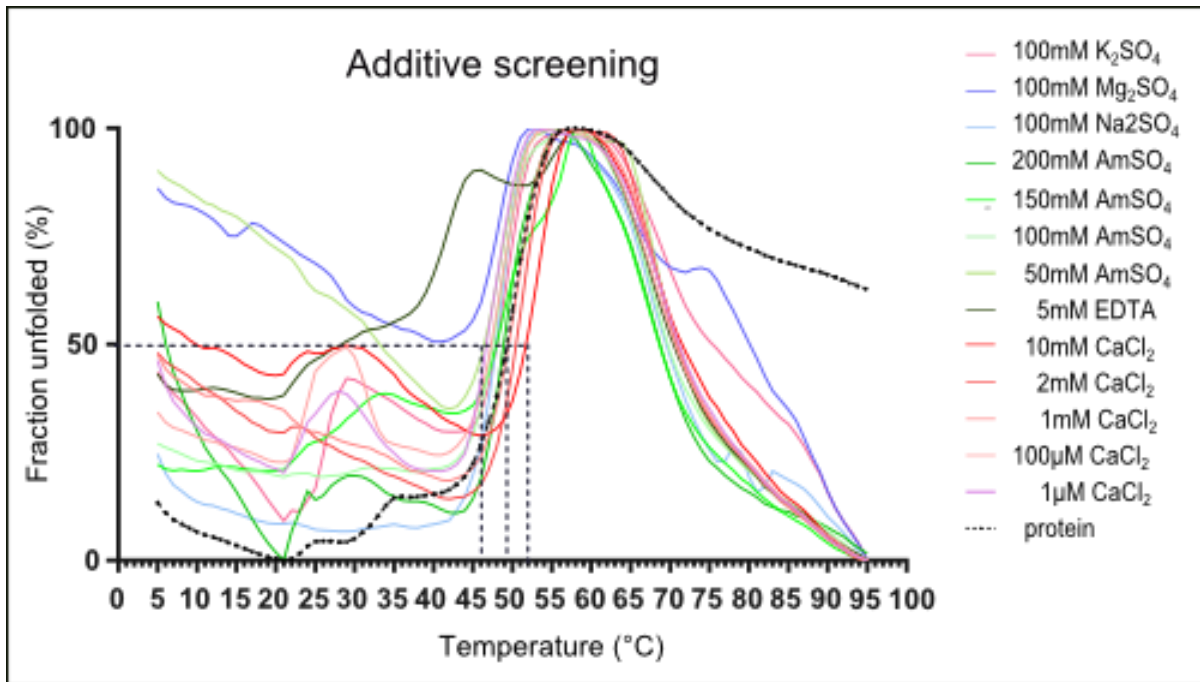


Figure 10 Thermofluor additive screen to test the influence of different sulphate salts and concentrations and calcium chloride on the stability of Netrin_{IV} after SEC purification concentrated to 20 µM in MES buffer pH 6.0, 250 mM NaCl, 1 mM DTT. Controls are 5 mM EDTA and the protein alone in MES buffer. All measurements were normalised.

4.a.7. Expression and purification of Netrin_{VIV} mutants and GFP-fused constructs

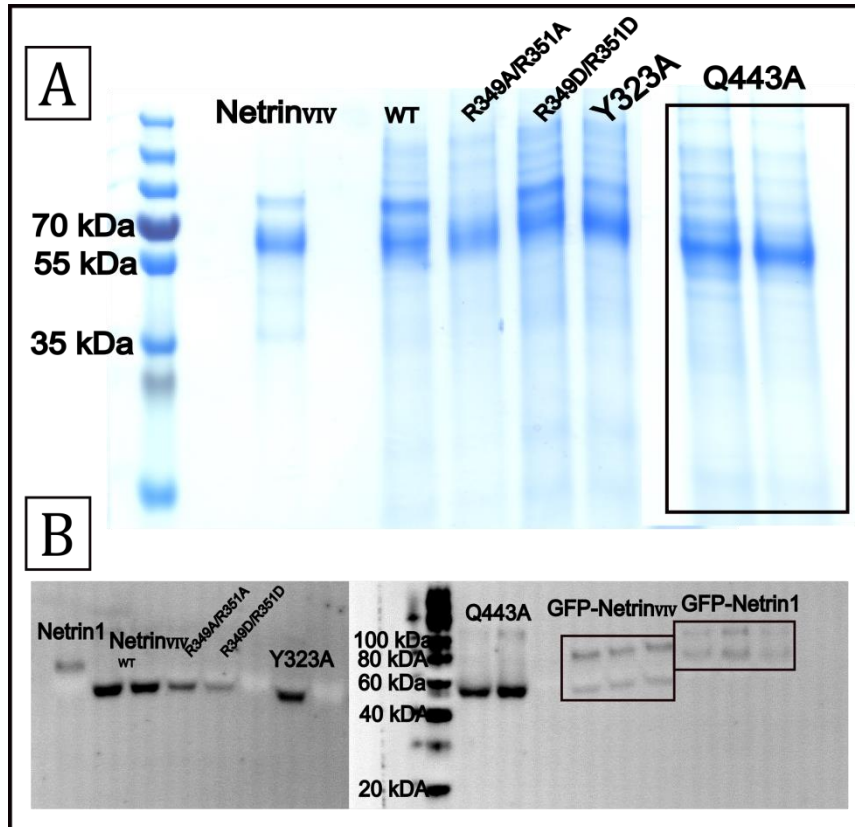


Figure 11 Small scale expression test in HEK 293T cells of Netrin_{VIV} constructs with mutations in two receptor binding relevant areas and purification of these proteins from conditioned DMEM as described before. **A** SDS-PAGE 10% gel of combined elutions samples after Ni-X affinity purification of 11 medium compared to Netrin_{VIV} (after SEC, WT and mutants after Ni-X). Gel stained with Instant blue. **B** Expression of Netrin-1, Netrin_{VIV}, mutations and GFP-fused constructs in small scale 6 well plates, confirmed by Western blot, detection with Anti-His antibody.

Several site-directed mutageneses were performed of the Netrin_{VIV} construct in order to alter areas that were found to be necessary for receptor binding. How these areas and domains of the protein were defined is described in the chapters 4.b.4 and 4.b.5. Amino acids were changed by PCR as described in chapter 3.b.1. . The expression of Netrin_{VIV} mutations and GFP-fusion protein (Fig. 11) was initially tested in a small scale set-up with 2% FCS in the culturing medium and confirm by Western blot analysis with an antibody against the 6xHis-tag (Fig 11 B). To roughly compare the expression yields Netrin_{VIV} *wildtype* (WT= Netrin_{VIV}) was transfected as well as the native full-length netrin-1. The double mutants of the residues arginine 349 and arginine 351 (R349A/R351A and R349D/R351D) showed both reduced expression. The substitution of the arginines by aspartic acid (R349D/R351D) seemed to have a greater effect on the expression yield than the mutation to alanine (R349A/R351A), resulting in an approximately ten times less signal than the WT. The yield was comparable to native full-length netrin-1. Mutations of the residues tyrosine 323

(Y323A) and glutamine 443 (Q443A) to alanine on the other hand showed expression similar to the Netrin_{VIV} wildtype.

Netrin-1 and Netrin_{VIV} WT were both fused to an N-terminal green fluorescent protein (eGFP) by cloning. These constructs were designed for future binding experiments such as thermophoresis to avoid labelling of the interaction partners. GFP has a size of 26.9 kDa, resulting in predicted sizes of the fusion proteins around 80 kDa for GFP-Netrin_{VIV} and 100 kDa for GFP-netrin-1. Both expression trials showed double bands (Fig. 11 B) on the Western blot for all clones (n=3). They could correspond to the fusion protein and the respective netrin-1 construct alone. Since the 6xHis-tag is located C-terminal, Netrin_{VIV} and netrin-1 would be detected alone in the case of degradation but GFP not. The difference in size of the full-length GFP-constructs and degradation product should make it nevertheless possible to separate them during purification.

The purification of the Netrin_{VIV} mutant constructs was performed according to the described protocol for the WT. All mutants behaved similar to the WT during affinity purification and showed comparable SEC profiles and protein yields verified by SDS-PAGE (Fig. 11 A). The culture medium for protein expression dedicated for functional studies described in chapter 4.b.7., was supplemented with 2% FCS. The SDS-PAGE analysis showed BSA contamination (Fig. 11 A WT, R349D/R351D, Y323A and Q443A left lane) by a band occurring above 60 kDa after Ni-X affinity chromatography. For the functional studies in cell culture based assays this is negligible, because the culture medium was supplemented with FCS as well. The experiments described in 4.b.7 are not designed to be concentration dependent either.

GFP-Netrin_{VIV} had to be separated from degradation products and contaminating components during purification (Fig. 12). Samples of the elution fractions from Ni-X (Fig. 12 A) showed contaminating proteins below 70 kDa on the SDS-PAGE gel. These bands could correspond as well to BSA as to Netrin_{VIV} alone as a degradation product as seen in the expression trials (Fig. 11B). The expression yield of the fusion proteins was observed to be lower than the WT. This could have led to co-purification of more contaminants by unspecific binding. Subsequently performed size exclusion chromatography showed two peaks (Fig. 12 C). The first peak at 46 ml just after the V_0 is mainly composed of proteins with high molecular weight (>100 kDa, Fig. 12 B).

Gel analysis showed as well a band that could correspond to the GFP-Netrin_{VIV} compared to the Ni-X elutions. However, the bulk part of the protein was eluted in the second peak after 52 ml (Fig. 12 C). This elution contained the fusion protein as well as smaller contaminating components (Fig. 12 B). Confirmation of the desired GFP-construct was performed by fluorescence measurement at 510 nm in a Tecan plate reader after exciting GFP at 395 nm (Fig. 12 D). Compared to the buffer and Netrin_{VIV} alone, GFP-Netrin_{VIV} showed a hundred times higher fluorescence than the controls and was therefore confirmed to be present in the second eluting peak during size exclusion chromatography.

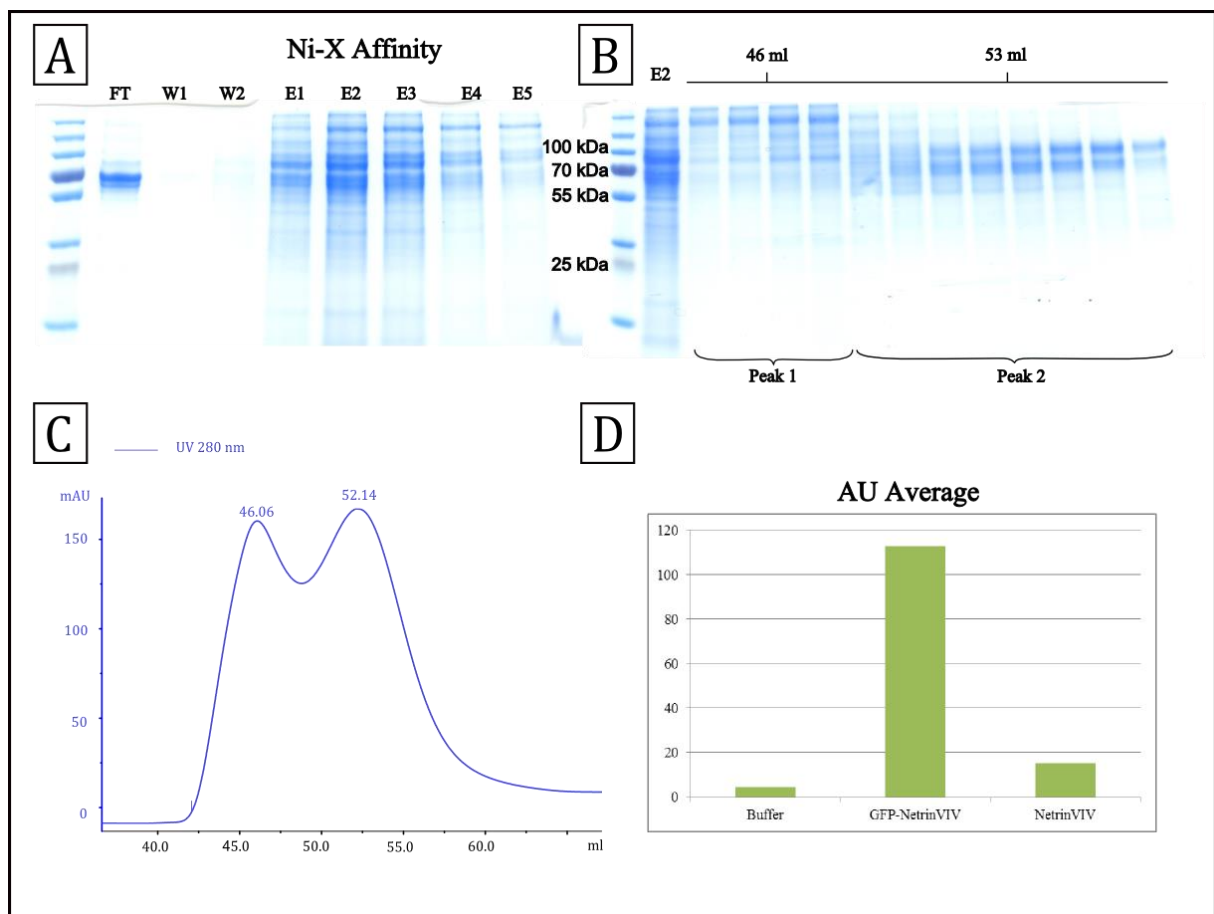


Figure 12 Purification of GFP-Netrin_{VIV} from 2l conditioned DMEM containing 0.2% FCS in a preparative scale and confirmation of GFP activity, gels stained with Instantblue™ coomassie. **A** 10% SDS-PAGE gel of **Ni-X Affinity** purification samples, FT: flow through, W1 and W2: wash steps, E1-E5: elutions. **B** 10% SDS-PAGE gel of peak fraction samples of the size exclusion chromatography (C), elution volume indicated above and elution 2 (E2) from Ni-X affinity purification. **C** Size exclusion chromatography profile, concentrated elutions injected to a Superdex 200 prep column 16/60 equilibrated in 50 mM MES pH 6.0, 250 mM NaCl, 1 mM DTT on an AEKTA FPLC with UV absorbance detection at 280 nm. **D** Confirmation of GFP activity by measuring the emitting fluorescence at 510 nm after excitation at 395 nm, compared to size exclusion buffer (MES pH 6.0, 250 mM NaCl, 1mM DTT) and Netrin_{VIV} alone, averaged (n=3 for all measurements).

4. a. 8. Crystallisation of Netrin_{VIV}

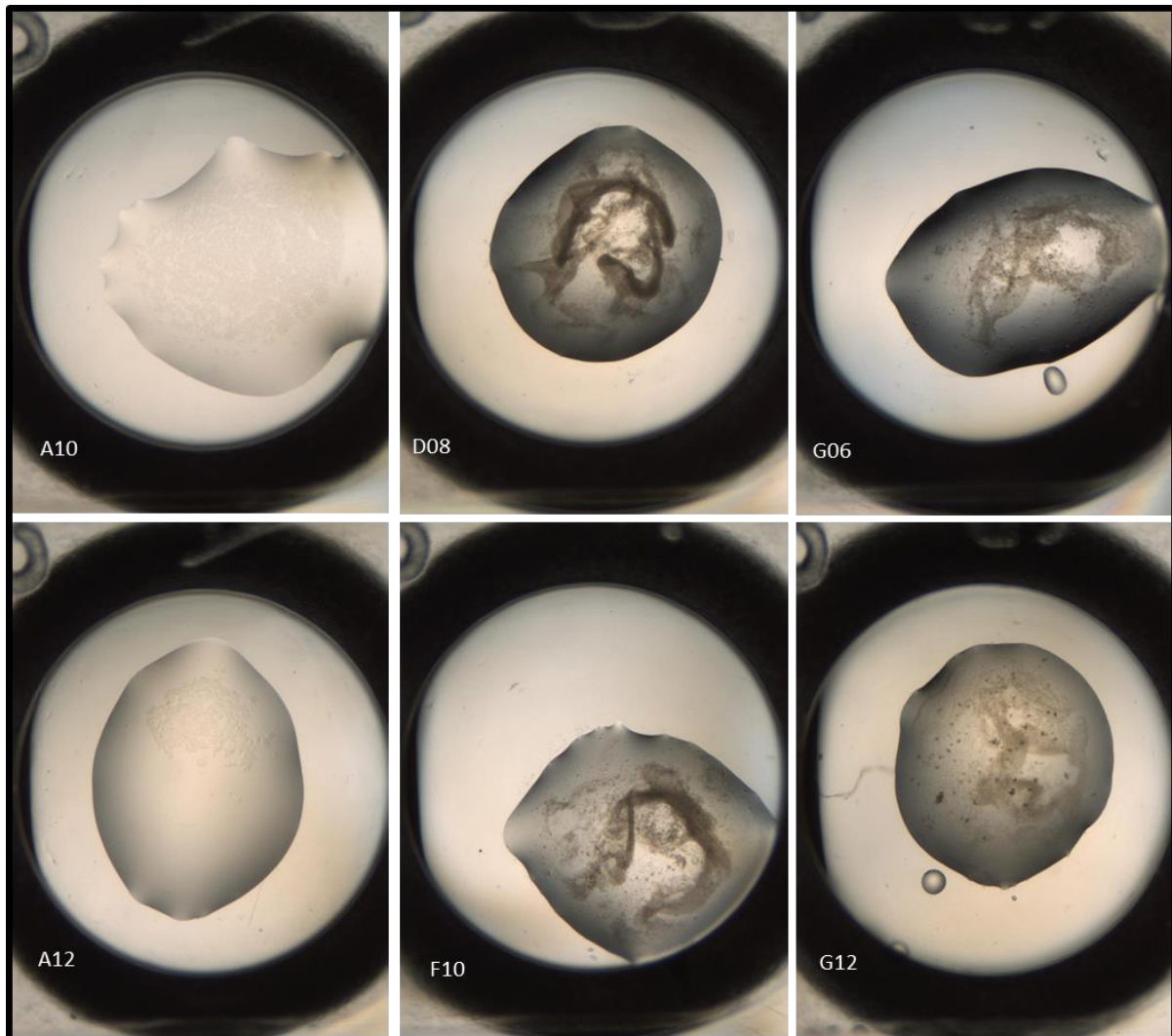


Figure 13 Selection of Qiagen Classic 2 crystallisation screen conditions in a 96-well high-throughput set-up, taken with the Formulatrix RockImager at 19°C. **A10** 0.1 M bis-tris pH 6.5, 3 M sodium chloride, **A12** 0.1 M TRIS pH 8.5, 3 M sodium chloride, **D08** 0.1 M HEPES pH 7.5, 25 % (w/v) PEG 3350 **F10** 0.2 M sodium chloride, 0.1 M bis-tris pH 5.5, 25 % (w/v) PEG 3350 **G06** 0.2 M ammonium acetate, 0.1 M bis-tris pH 5.5, 25 % (w/v) PEG 3350 **G12** 0.2 M magnesium chloride, 0.1 M HEPES pH 7.5, 25 % (w/v) PEG 3350

To crystallise Netrin_{VIV}, the fractions that eluted between 49 ml and 55.5 ml (Fig. 8) during size exclusion were combined and concentrated to 103 μ M (5.8 mg/ml). Crystallisation trials using the Qiagen Classic II screen were performed in a High-throughput crystallisation facility (EMBL, Hamburg). This screen contains a variety of conditions following the sparse matrix principle (Carter and Carter, 1979). The pH ranges between 3.5 and 8.5 were covered. Different salts and polymers, such as PEGs, are components of this screen and many conditions contain ammonium sulphate. None of the conditions gave single crystals (Fig. 13), but approximately half of the wells showed slight (Fig. 13 A10, A12) to heavy precipitation (Fig. 13 D08),

indicating that the concentration of the protein was about right for crystallisation trials. More encouraging than the heavy amorphous precipitations (Fig. 13 D08, F10) were the less amorphous appearing precipitations (Fig. 10 G12) and spherulites (Fig.13 G06). Trials to optimise the most promising conditions (Fig. 13 G06, G12) were performed at pH 7.5 with PEG3350, L-prolin, ammonium acetate and magnesium chloride (as described in chapter 3.b.7., screen 1 and screen 2) but did not show any improvement in the morphology of the crystal precursors or gave rise to single crystals.

4. b. Netrin-1 and DCC

Deleted in colorectal cancer (DCC) has been identified in humans to be a tumour suppressor (Hedrick et al., 1992; Vogelstein et al., 1988) and a netrin-1 receptor. (Keino-Masu et al., 1996). Through attraction and repulsion netrin-1 orchestrates axon migration (Yang et al., 2009) depending on the receptors present on the nerve cells. While DCC alone mediates a positive response towards a netrin-1 gradient, the combination with UNC5 leads to repulsion (Culotti and Merz, 1998; Lai Wing Sun et al., 2011). Which domains are involved in netrin-1 binding, how potential binding sites are constructed and with what affinity receptor and ligand could interact with each other, is presented in this section.

4.b.1. DCCs fibronectin domains 5 and 6 are sufficient to bind Netrin_{VIV}

The netrin-1 receptor DCC (uniprot: P43146) is composed of four N-terminal immunoglobulin domains, which fold back on each other (Chen et al., 2013) to adopt a horseshoe like conformation. This motif is followed by six type-III fibronectin domains (FN) connected through a helical transmembrane domain with the conserved cytosolic domains called P1, P2 and P3. Through these domains DCC forms dimers to initialise signal transduction (Stein and Tessier-Lavigne, 2001; Stein et al., 2001; Xie et al., 2006). Several studies have engaged over the question which domains of the DCC receptor, and more specifically, which parts of those domains are involved in netrin-1 binding. Previous studies attempted to shine light on the mechanisms of interaction but have led to controversial discussions (Geisbrecht et al., 2003; Kruger et al., 2004). While Kruger and colleagues reported that the deletion of domain FN4 abolishes binding, Geisbrecht stated a year earlier that this domain is necessary for interaction. However, the domains involved have been limited to the fibronectin domains close to the cell membrane. On the netrin-1 site it seems to be clear that a construct containing the laminin-like domain VI as well as the V-domain is at least sufficient to bind to the DCC ectodomain (Keino-Masu et al., 1996). To investigate whether fibronectin domain 4 of DCC is necessary or a construct containing FN5 and 6 is sufficient to bind Netrin_{VIV}, a pull down assay was performed. Members of Prof. JH. Wang's laboratory (Dr. Lorenzo Finci, Peking University, China)

provided two recombinantly expressed and purified protein constructs of DCC (Fig. 14). The construct called DCC_{FN456} is comprised of the fourth, the fifth and the sixth extracellular fibronectin domain, DCC_{FN56} only contains FN5 and FN6. Both proteins contain a C-terminal strep-(II)-tag, followed by a 6xHis-tag. The lack of glycosylation sites and disulphide bonds in these domains made it possible to express them in *E.coli*. Purification involved ion affinity purification, followed by Strep-Tactin[®] affinity and size exclusion chromatography to guarantee protein purity in crystallisation grade.

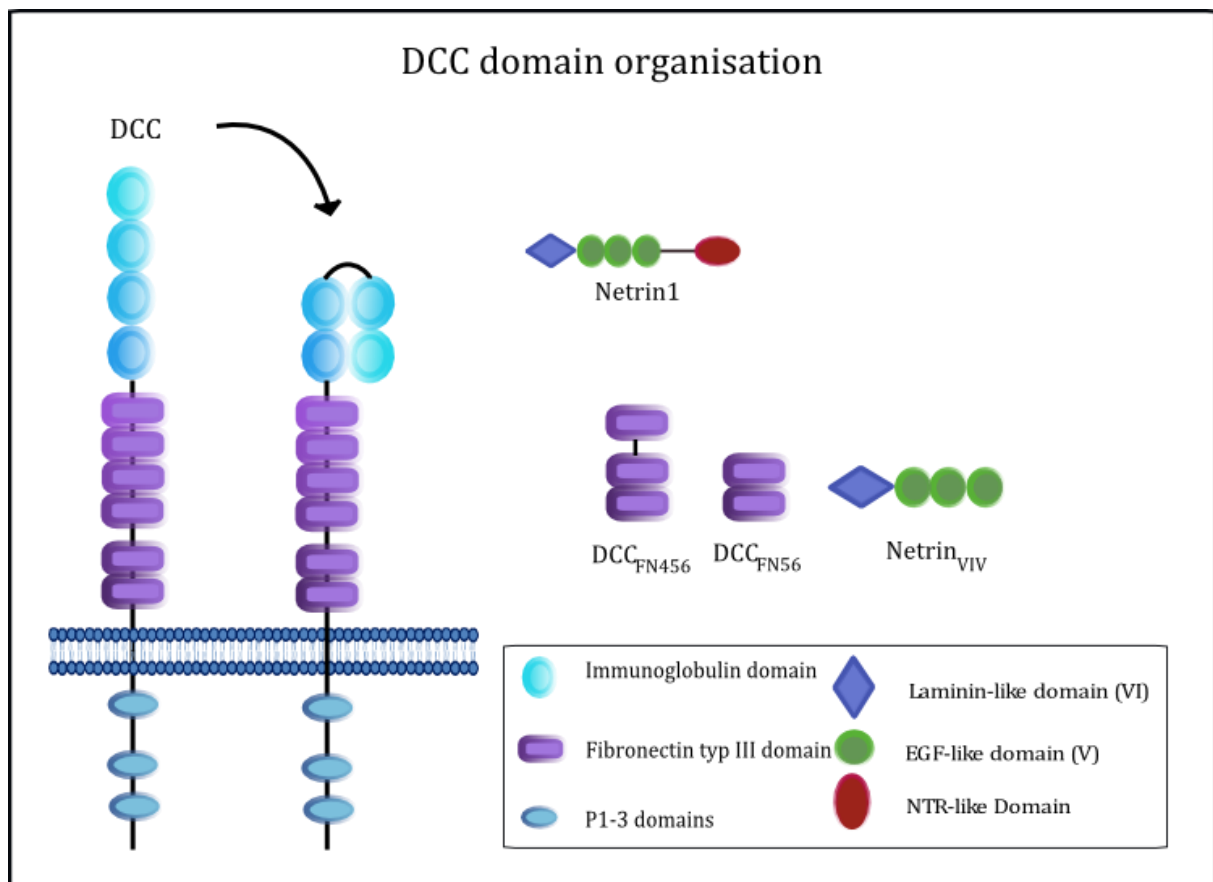


Figure 14 DCC domain organisation and constructs

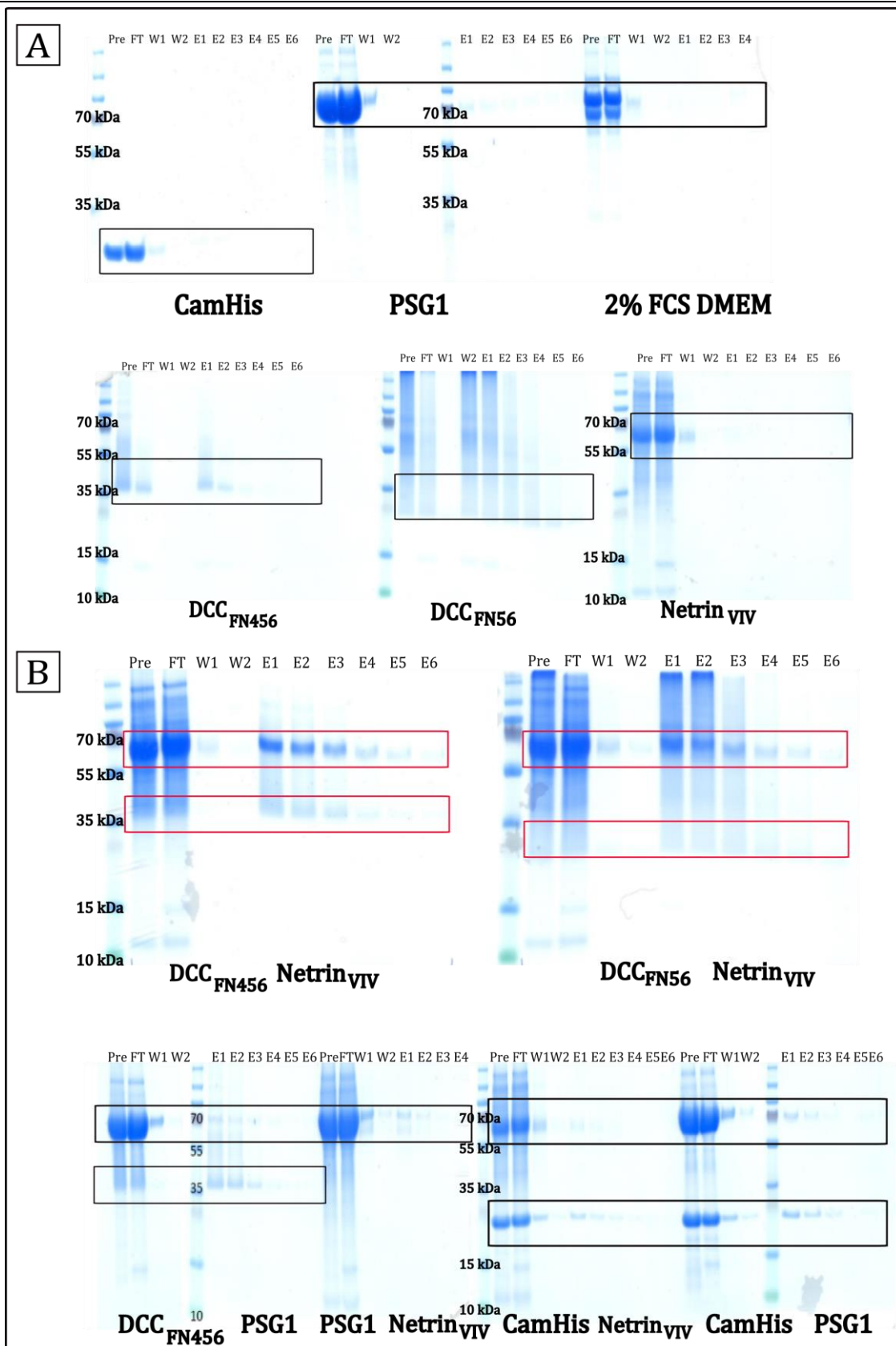


Figure 15 Pull-down assay to identify domains involved in netrin binding. Recombinantly expressed DCC constructs were bound to streptactin sepharose beads via the C-terminal strep-(II)-tag and tested for their ability to bind to Netrin_{VIV}. **A** Control experiments, CamHis (strep-(II)-tagged), PSG1 (6xHis-tag), 2% FCS DMEM (no recombinant proteins), DCC_{FN456} (strep-(II)-tagged), DCC_{FN56} (strep-(II)-tagged), and Netrin_{VIV} (6xHis-tag) were loaded to Strep-Tactin[®] sepharose beads, washed and eluted according to manufactures instructions. **B** For each individual pull-down experiment, 3.2 nM of both potential interaction partners were mixed in a 100 μ l reaction volume before applying to streptactin sepharose. Washing and elutions was performed as described before.

Control experiments confirmed the ability of the constructs DCC_{FN456} and DCC_{FN56} to bind to Strep-Tactin[®] sepharose beads and excluded the possibility that Netrin_{VIV} or control proteins bind unspecifically (Fig. 15 A) leading to false positive results. The pull-down experiment itself showed that both DCC constructs are able to bind Netrin_{VIV} specifically (Fig.15 B) compared to the control experiments where some unspecific binding of DCC_{FN456} to a control protein (PSG1) was observed but no unspecific binding of Netrin_{VIV} (PSG1 and Calmodulin/CamHis). It was concluded that the DCC_{FN56} construct is sufficient to bind and pull-down Netrin_{VIV} *in-vitro*. It cannot be concluded from this experiment if these domains are exclusively involved in binding to netrin-1 *in-vivo* or if the interaction with other parts of the receptor is necessary for signal transduction.

4.b.2. Netrin_{VIV} crystallises with DCC_{FN56}

As mentioned before, the netrin-1 binding domains have been located to the fibronectin repeats of the DCC ectodomain (Geisbrecht et al., 2003). It was even proposed that specific loops within these domains are responsible for heparin mediated (Bennett et al., 1997) or direct binding of netrin-1 (Geisbrecht et al., 2003). However, no structure of a DCC-netrin-1 complex is supporting the evidence of binding sites on these domain parts. After it was shown that the DCC_{FN56} construct is sufficient to bind Netrin_{VIV} in a pull-down assay the question evoked what the binding may look like on a molecular level. To address the possibility that an additional binding site for netrin-1 could be present on the FN4 domain, crystallisation trials were not limited to DCC_{FN56} construct. The fifth FN domain of DCC is closely followed by the sixth FN domain, but between the fifth and the fourth domain a 25 residue linker is present. Flexible or disordered parts of proteins can be challenging to crystallise (Derewenda, 2004). Therefore an additional construct of DCC was tested for co-crystallisation along with the ones introduced previously. DCC_{FN4} consists only of the FN4 domain and was used for complex set ups with Netrin_{VIV} alone and in combination with DCC_{FN56}.

For co-crystallisation all constructs were purified to homogeneity as described before. Purity was monitored by SDS-PAGE (Fig. 16 A) and MS analysis. Previous to complex formation, the constructs were individually concentrated to 100 µM. Netrin_{VIV}

(50 mM MES pH 6.0, 250 mM NaCl, 1mM DTT) was mixed with DCC_{FN56}, DCC_{FN456}, DCC_{FN56} and DCC_{FN4} or DCC_{FN4} respectively (all in 100 mM TRIS pH 8.0, 150 mM NaCl) in a 1:1, in case of DCC_{FN56}/DCC_{FN4} 1:1:1, stoichiometry.

On the SDS-PAGE (Fig. 16 A) of the individual proteins Netrin_{VIV} and DCC_{FN4} appeared as single bands on the gel, indicating protein purity of >95%. DCC_{FN456} and DCC_{FN56} show multiple bands, but the MS (data not shown) quality control confirmed that the samples contained single fractions of 25.7 kDa (DCC_{FN56}) and 37.8 kDa (DCC_{FN456}) respectively. As a standard quality control step a thermofluor assay monitored the melting temperatures of the complex set-ups (Fig. 16 B). This screen gives information about protein stability and complex formation can cause thermal shifting of the melting temperature (Boivin et al., 2013). Netrin_{VIV} alone has a T_m of 45.9°C under standard conditions and was stabilised upon complex formation with DCC_{FN456}, DCC_{FN56} and DCC_{FN56}/DCC_{FN4}. A temperature shift of 8.2°C allowed the conclusion that binding between receptor and ligand formed a complex that is thermally more stable. The curve obtained from a mixture between Netrin_{VIV} and DCC_{FN4} showed no such temperature shift of the melting curve. This observation could indicate that a complex of Netrin_{VIV} and DCC_{FN4} is either not formed or of weaker nature than the complexes between Netrin_{VIV} and DCC_{FN56}. In case of the Netrin_{VIV}-DCC_{FN56}/DCC_{FN4} and the Netrin_{VIV}-DCC_{FN456} set ups, the binding of DCC_{FN56} is most likely causing the increase in thermal stability. The T_m shifts resembled each other and no further increase was observed by addition of FN4. The indication of a double peak in the melting curve of Netrin_{VIV}-DCC_{FN456} could be explained by a stepwise unfolding of firstly the domain FN4 which is separated by an extended linker from the other two domains.

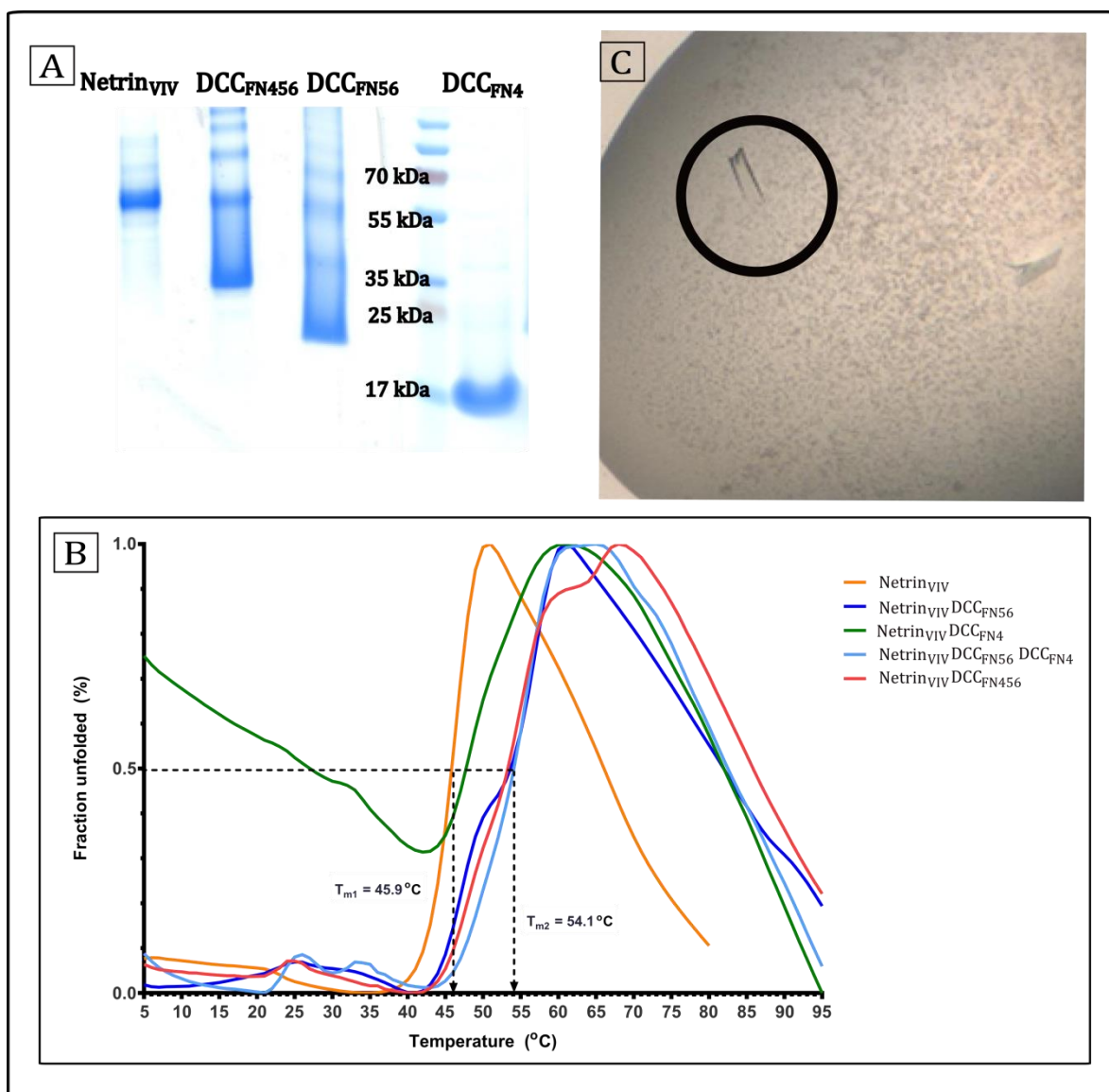


Figure 16 Crystallisation of Netrin_{VIV} in complex with truncated DCC constructs **A** 10% SDS-PAGE gel of purified constructs concentrated to 100 μ M stained with Instant blue. **B** Thermofluor assay of complex mixtures used for crystallisation trials in 100 mM HEPES pH 7.0, 150 mM NaCl. Temperature in $^{\circ}$ C plotted against normalised fluorescence (fraction unfolded in %) to determine T_m . **C** Single crystal in the QIAGEN crystal complex screen of Netrin_{VIV} and DCC_{FN56}, condition: 0.15 M Ammonium sulphate, 0.1 M MES pH6, 15 % (w/v) PEG 4000.

After verification of protein quality, crystallisation screens with 600 nl drops in 96-well plates were performed in a high-through put crystallisation facility (EMBL, Hamburg). Images were taken daily with the Formulatrix RockImager at 19 $^{\circ}$ C. Among the crystallisation screens selected were the Qiagen classic screens, the optimised protein complex screen and the AmSo₄ screen. A minimum of 480 conditions per complex set-up were tested and surprisingly only a single condition gave rise to a single crystal (Fig. 16 C). It appeared after 4 days in a condition containing 0.15 M ammonium sulphate, 0.1 M MES pH 6 and 15 % (w/v) PEG 4000. Consistent with the results from the pull-down assay and the TF assay, the crystal

was found in the screen plate (Qiagen protein complex) that contained the Netrin_{VIV}-DCC_{FN56}.

4.b.3. Netrin_{VIV}-DCC_{FN56} complex reveals two distinct binding sites

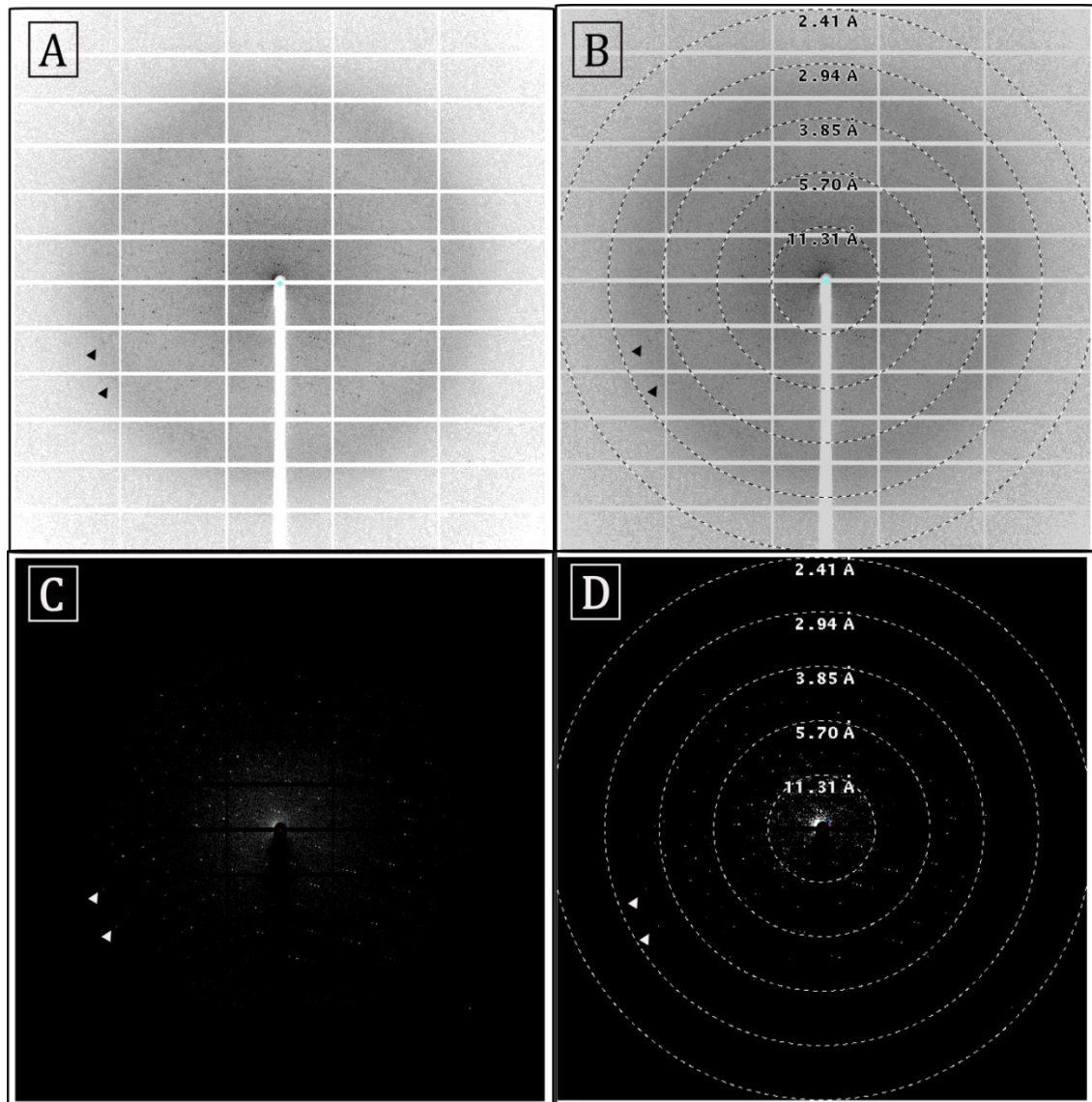


Figure 17 X-ray diffraction pattern of the Netrin_{VIV}-DCC_{FN56} complex crystal collected at the EMBL P14 beamline at the PETRA3 synchrotron using a PILATUS 6 M pixel detector. Examples of reflection spots of scattered x-ray waves by electron clouds indicated by arrow heads (black and white) **A** Diffraction from a Netrin_{VIV}-DCC_{FN56} complex crystal, reflection spots in black. **B** Resolution of diffraction indicated by rings according to dimension in Ångström (Å). **C** Inverted display of figure **A**. **D** Inverted display of figure **B**.

The crystal (Fig. 16 C) was tested at the EMBL P14 beamline at the PETRA3 synchrotron and diffraction data (Fig. 17) was collected using a PILATUS 6 M pixel detector and a MD3 EMBL diffractometer. Diffraction was detected to a resolution of 3.1 Ångström (Å) (Fig. 17 B, D). The distance of 3.1 Å correlates with the typical

distance between the carbon and the nitrogen atom that are covalently bound to the hydrogen and oxygen atoms that form hydrogen bonds as found between the side chains of amino acids (Blow, 2010) p. 4). In terms of resolution this means that two atoms with a distance of 3.1 Å can be recognised as individual. This allows distinguishing between side chains of amino acids. A diffraction pattern like the one observed (Fig. 17) is caused by the coherent scattering occurring when photons from the x-ray beam are absorbed by the electrons in the crystal and the so excited electrons emit photons into a random direction (Blow, 2010) p.15 ff.).

The structure of the proteins in the crystal was determined by Dr. Rob Meijers using laminin γ -1 LN-LE 1-2 as a search model for molecular replacement of Netrin_{VIV} (Carafoli et al., 2012). Electron density was observed for the residues 40 to 455. For DCC_{FN56} the fibronectin domains 5 and 6 of human Neogenin (Yang et al., 2011) were used to resolve the residues 844 to 1050. Details of the data collection and refinement statistics can be found in the appendix (Appendix 8.e.)

The laminin-like VI domain of netrin-1 resembles according to the used model the typical laminin-fold including the anti-parallel β -sandwich (Fig. 18 A, blue) and a calcium binding site (Fig. 18 C). The calcium ion is coordinated by the side chains of the residues aspartic acid (Asp) 110, asparagine (Asn) 112, threonine (Thr) 118 and the carbonyl group of serine (Ser) 277 (Fig. 18 C). Three glycosylation sites at the residues asparagine (Asn) 95, 116 and 131 were also confirmed (not shown in Fig. 18) by the crystal structure. The VI domain sits in the same way as the laminin γ -1 LN-domain like a blossom on its stalk, (Fig. 18 A, green) the V-domain (Carafoli et al., 2012). The V-domain consists of three EGF-hand repeats, named domain EGF1 (Fig. 18 A, green), EGF2 (olive) and EGF3 (dark green). The EGF2 domain exhibits an extended α -helix that is exclusively present in this domain. The structure of the DCC_{FN56} construct shows the fibronectin domains in an antiparallel β -sandwich organisation with an ABE strand on one side and a C'CFG strand on the other side (Fig. 18 A, pink and violet).

The complex that was observed in the crystal structure shows that each Netrin_{VIV} binds to two DCC_{FN56} molecules at distinct binding sites (Fig. 18 B). A distance of a minimum of 20 Å between the two receptor molecules is excluding direct contact between them. Both molecules bind to the same side of Netrin_{VIV}, but in a 90° angle to each other on the main axis of the V domain of Netrin_{VIV}. No interaction was observed between the VI domain or the glycosylation sites of Netrin_{VIV} and any of the

DCC_{FN56} molecules binding to the V-domain.

The binding site located at the EGF3 of the V-domain was defined as site 1. Here exclusively the FN5 domain of DCC is involved in direct protein-protein contact to residues of Netrin_{VIV}. The second binding site, subsequently named site 2, is located on EGF1 and EGF2 where a DCC molecule sits between these domains interacting mainly with FN5 and but also with parts of FN6.

The C-termini of both receptor molecules bound in the presented crystal structure (Fig. 18 B) point despite the angular tilt into the same direction. This conformation makes binding of two receptor molecules by one netrin-1 molecule close to the plasma membrane feasible. This could lead to dimerisation of the cytosolic domains to initiate signal transduction. This finding is supported by the fact that DCC mainly interacts with the FN5 domain with netrin-1. In both binding sites, this domain plays a major role, even if portions of FN6 are involved in site 2. However, the orientation of the DCC molecules also limits the possible size of a receptor-ligand cluster.

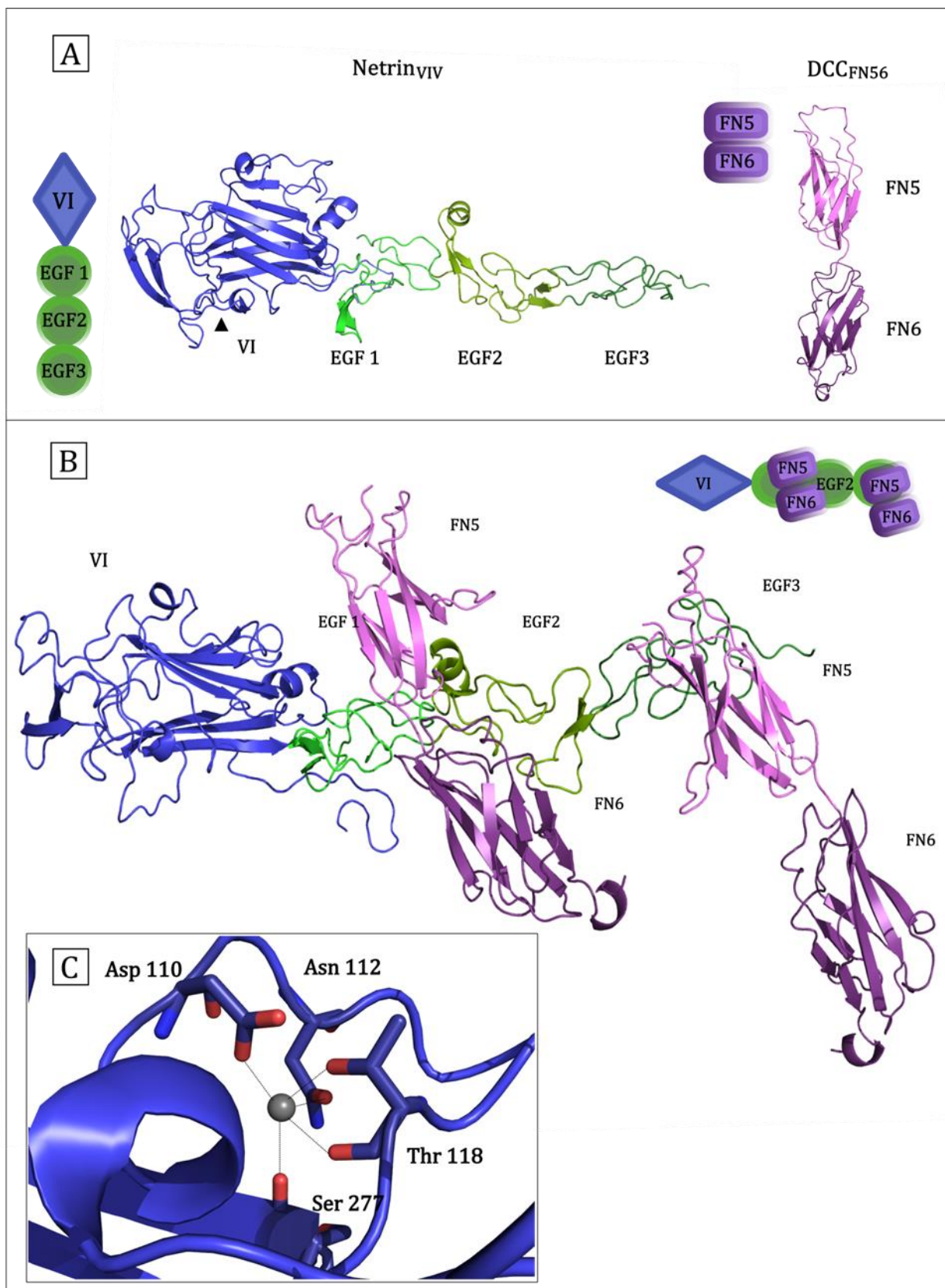
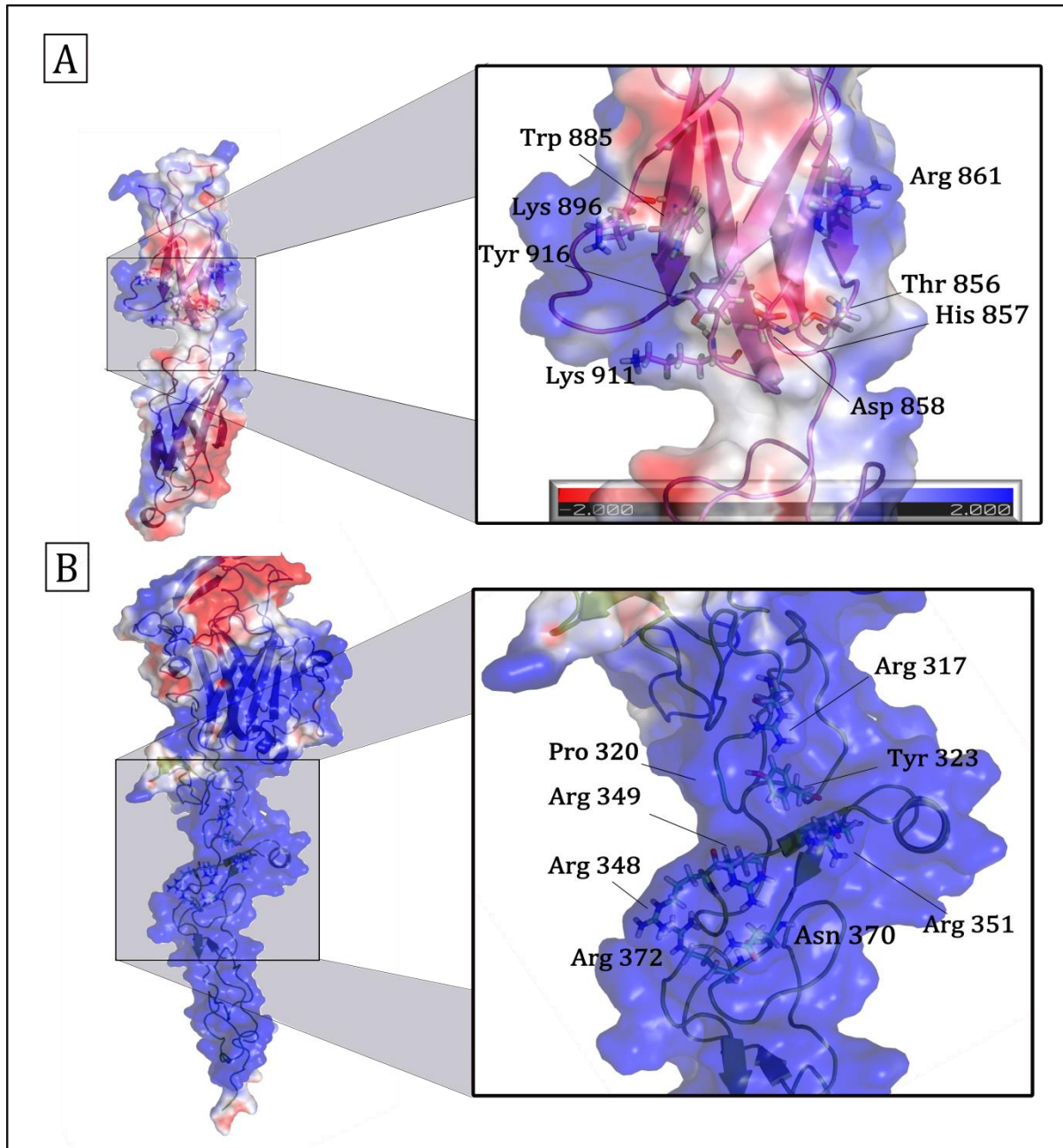


Figure 18 Crystal structure of the Netrin_{VIV}-DCC_{FN56} complex. The images were created with PyMOL (www.pymol.org) and Inkscape. **A** Domain organisation of Netrin_{VIV} and DCC_{FN56} separately shown as scheme and ribbon diagrams. Netrin domains; VI laminin domain : blue, V domain separated in EGF1-EGF3 : olive, green, dark green. Ca²⁺-binding site indicated by arrow head. Fibronectin domains of DCC, FN5: pink, FN6: violet. **B** Scheme and ribbon diagram of the Netrin_{VIV}-DCC_{FN56} complex showing two DCC molecules bound to two distinct sites of the V domain of one Netrin_{VIV} molecule. **C** Close view of calcium binding site located in the VI domain of Netrin_{VIV}.

4.b.4. A generic receptor binding site is mediated by a cluster of sulphate ions



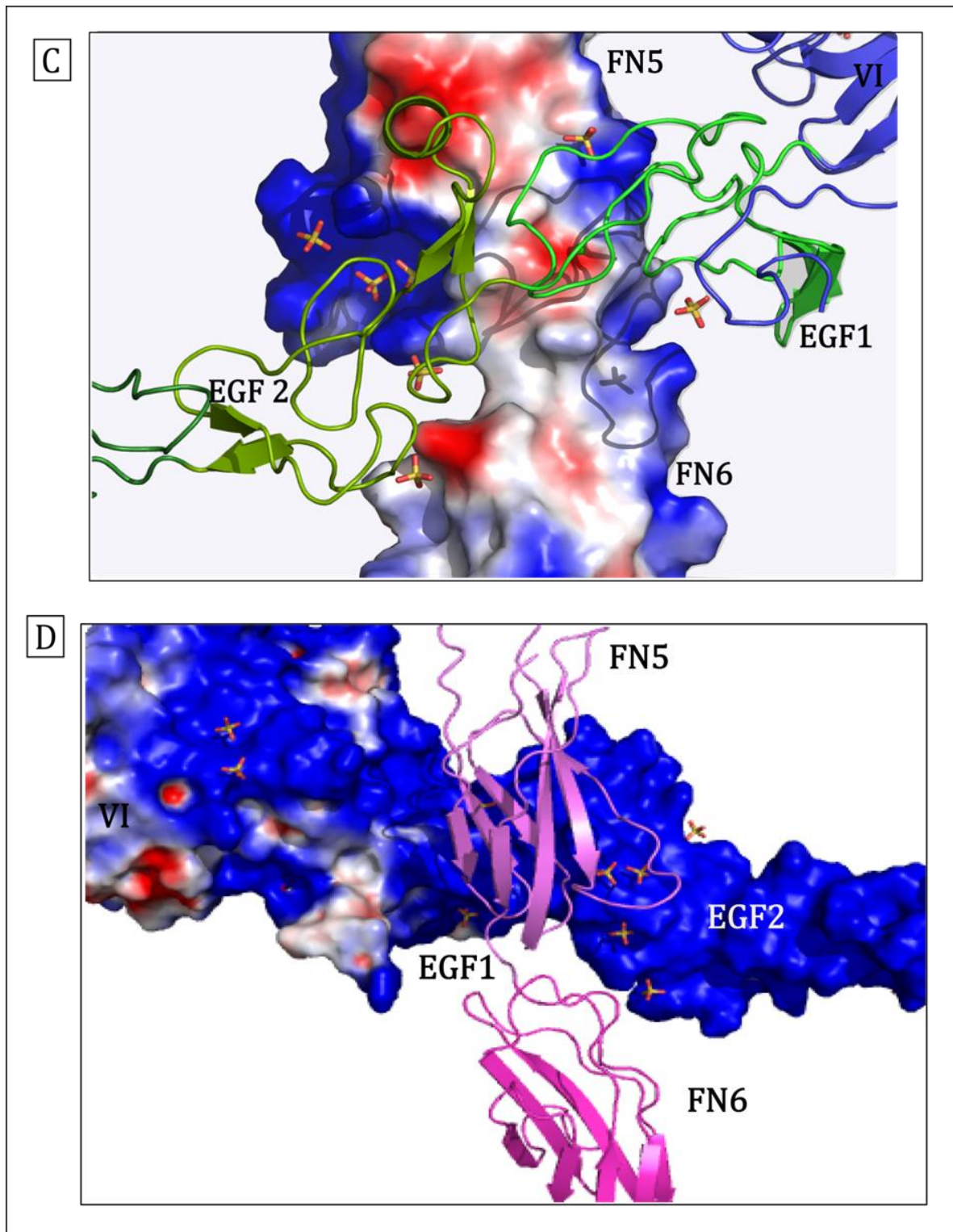


Figure 19 Detailed views into the universal binding site on netrin-1. The images were created with PyMOL (www.pymol.org), and the electrostatic surface representations were made using the Adaptive Poisson-Boltzmann Equation (APBS) plugin in PyMOL (Unni et al., 2011), Inkscape. **A-B** Representation of electrostatic surface potential of the binding site, residues involved shown as sticks. Charge of potential indicated on the diagram at the bottom (**A**), negative charges in red, positive charges in blue. **A** Charges of the DCC_{FN56} construct (small) and a close up view (grey and bigger box **B** Representation of Netrin_{VIV} (small) and close up view of the generic binding site (grey and bigger box). **C-D** Detailed view of the binding site showing a cluster of sulphate ions in the interface. Amino acid residues shown as sticks, sulphate ions shown as sticks in yellow/red. **C** DCC_{FN56} shown as surface representation of electrostatic charges, Netrin_{VIV} shown as ribbon (olive and green). **D** Netrin_{VIV} shown as surface representation of electrostatic charges, DCC_{FN5} shown as ribbon (pink).

The DCC_{FN56} molecule binding to the centre of the Netrin_{VIV} molecule at binding site 2 covers (Fig. 19 D) an area including portions of both, the EGF1 and EGF2 domain. It faces the netrin-1 binding site with the ABE β -sheet of domain FN5 and a few residues of the A and F strand of domain FN6. Calculations of the electrostatic surface potential of receptor (Fig. 19 A) and ligand (Fig. 19 B) revealed the presence of highly charged patches on both molecules, caused by positively charged amino acids. The accumulation of positively charged residues such as arginine (Arg), histidine (His) and lysine (Lys) and polar residues like threonine (Thr), asparagine (Asn) and glutamine (Gln) would make a direct contact between these regions of receptor and ligand implausible if they would not be neutralised by anions (Fig. 19 C and D).

Four sulphate ions are localised near the α -helical extension of the EGF2 domain (Fig. 19 C, Fig. 20 A) bridging the indirect contacts between five arginine residues of netrin-1, Arg 317 (Fig. 20 C), Arg 348, Arg 349, Arg 351 and Arg372 (Fig. 20A) and the DCC residues Lys 896, Lys 911 and Arg861. Arg 349 and Arg 351 (netrin-1) are also involved in hydrogen bonds. They seem to play a central role in mediating binding from netrin-1's site and were therefore chosen for substitution by site-directed mutagenesis (Fig. 11) to investigate the dynamics of molecular interactions of the receptor-ligand complex. These experiments are shown later in this section. Residues involved in the coordination of sulphate ions in the periphery are asparagine 370, histidine 373 and arginine 398 from Netrin_{VIV} and tryptophan (Trp) 885 and glutamine 972 of DCC_{FN56}. The residues involved in coordination of sulphate ions and formation of the positively charged regions on both receptor and ligand are evolutionary conserved among vertebrates (4.c, Fig. 30 and 31). This is as well true for the residues of the EGF1 domain (cysteine (Cys) 318, Arg 317, proline (Pro) 320 and tyrosine (Tyr) 323) and the FN5 domain (Asp 858 and Thr 856) which coordinate a potential chloride ion (Fig. 20 B). That the present ion is a negatively charged chloride ion is supported by the positive charged residue Arg 317 of Netrin_{VIV} and the presence of a chloride ion in a close position in the crystal structure of netrin-G2 (Brasch et al., 2011). The very few direct protein-protein interactions that were identified between Netrin_{VIV} and DCC_{FN56} are located around the aliphatic pyrrole ring of Pro 320 on the EGF1 domain (Fig. 20 B) which is forming hydrophobic interactions with the side chains of the residues Thr 856, His 857 and Asp 858 on the loop between the A and B strand of the FN5 domain.

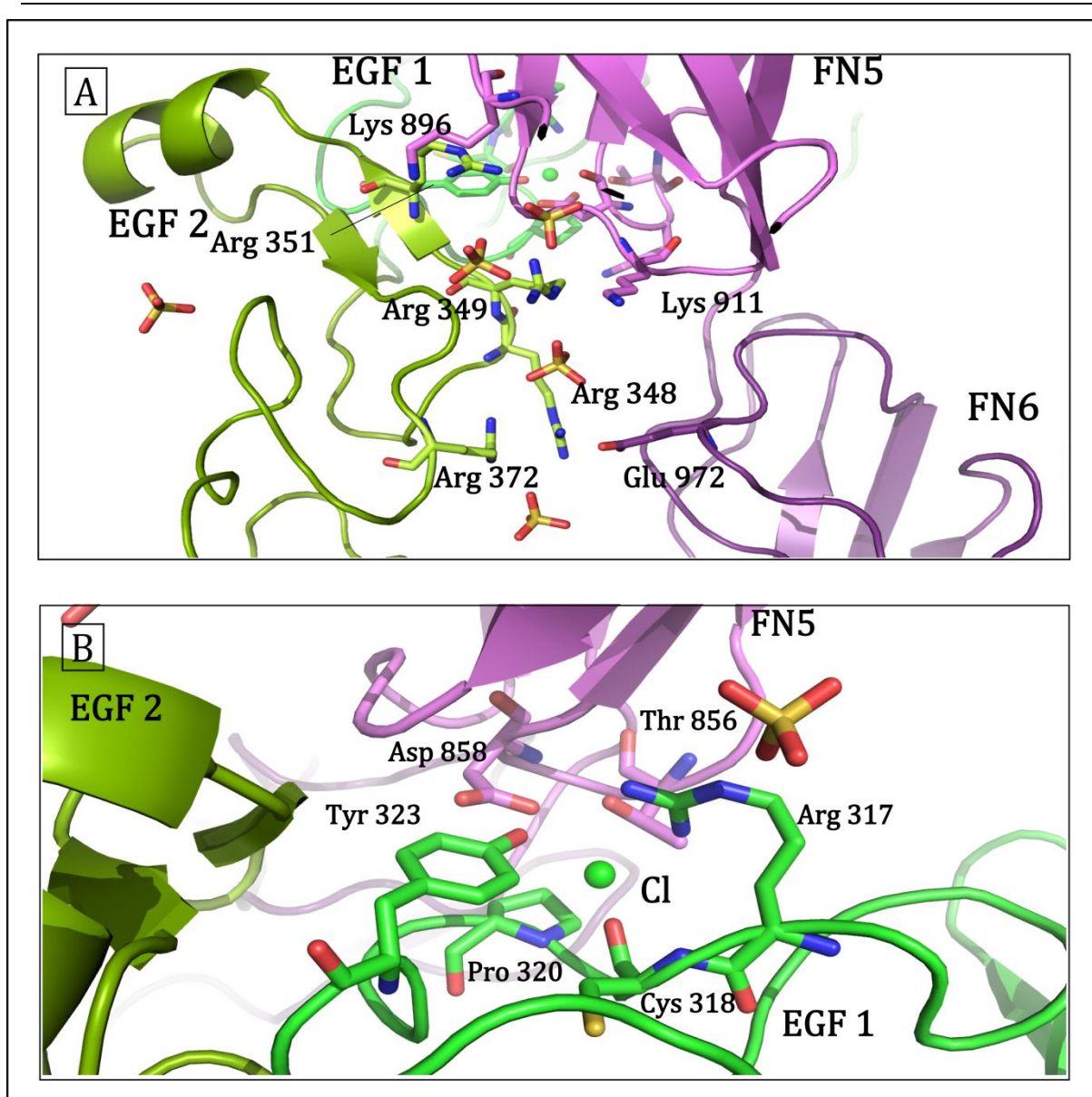


Figure 20 Close view into binding site 2 showing the sulphate cluster and a chloride ion. The images were created with PyMOL (www.pymol.org) and Inkscape. **A** Sulphate cluster mediating binding between Netrin_{VIV} EGF2 domain (olive) and DCC_{FN56} (pink) shown as ribbons, residues and sulphate ions shown as sticks. **B** Chloride ion (green ball) at the interface of direct protein-protein contact between Netrin_{VIV} EGF1 domain (green) and DCC_{FN56} (pink) shown as ribbons, residues and sulphate ions shown as sticks.

It is a striking feature of this binding site that only a few residues form direct contacts while the main binding is mediated by a cluster of negatively charged ions. The charged patches in the interface cover a large surface area of 950 Å² with sulphate ions present also at the periphery. This finding could make the accommodation of other molecules with similar charged patches to this binding site of Netrin_{VIV} conceivable. The rearrangement of ionic clusters by preferring the binding of certain heparan sulphate proteoglycans (Bennett et al., 1997; Shipp and Hsieh-Wilson, 2007) according to the different receptor molecules could alter the binding site depending on the receptors present.

4.b.5. The DCC specific binding site is a hydrophobic hot spot

Binding site 1 involves exclusively domain EGF3 (netrin-1) and FN5 (DCC). The orientation of the DCC_{FN56} is in contrast to binding site 2 rotated so that the edge of the FN5 β -sandwich is facing the EGF3 domain not involving the ABE strands containing β -sheet (Fig. 21 C). Direct interactions between the central residues methionine (Met) 933 and valine (Val) 848 of DCC (Fig. 21 A and B) and glutamine (Gln) 443 of Netrin_{VIV} (Fig. 21 A and C) identifies this binding site as a hydrophobic hot spot. A hydrophobic hot spot is characterised by a central hydrophobic region surrounded by hydrophilic, partially hydrated residues (Clackson and Wells, 1995). Met 933 (located at the start of the G strand) and Val848 (on the loop before the start of the A strand) protrude into the EGF3 domain of netrin-1 where the Met 933 forms together with another Val 850 from the DCC molecule, hydrogen bonds to the side chain of Gln 443. However, the key features of this binding site are hydrophobic interactions. They are formed between the side chain of Met 933 and the side chain of Gln 443, as well as the residues Val 409, Val 429, Pro 447 and Pro 450 of Netrin_{VIV} (Fig. 21 B). Further hydrogen bonds surround the hydrophobic centre of the hot spot. Residues involved are from the DCC side Gln 851, Asn867 and Thr 934 and from Netrin_{VIV} His 407 and, adjacent to the key residue 443, the Gln 442. This tight network of direct contacts between side chains differentiates binding site 1 from binding site 2, revealing the specificity of this site. Sulphate ions are only found in the periphery of binding site 1 (Fig. 21), engaging the positively charged residues Arg 436 and Lys 439 of netrin-1 (Fig. 21A and B). These ions are potentially necessary to help opening of the protected hydrophobic core of the hot spot to facilitate binding. Compared to binding site 2, a smaller number of residues has been resolved to participate in the interactions but according to Clackson and Wells the tight packed hydrophobic core of the binding interface accounts up to three-quarters of the binding energy and affinity, while the peripheral residues are less important (Clackson and Wells, 1995). Therefore, the loss of one of the binding partners could be sufficient to impair or reduce the function of this specific site. Guided by the studies of Clackson and Wells (Clackson and Wells, 1995) the Netrin_{VIV} key residue Gln 443 was chosen for alanine substitution by site-directed mutagenesis (Fig. 11) to further analyse the dynamics of this binding site.

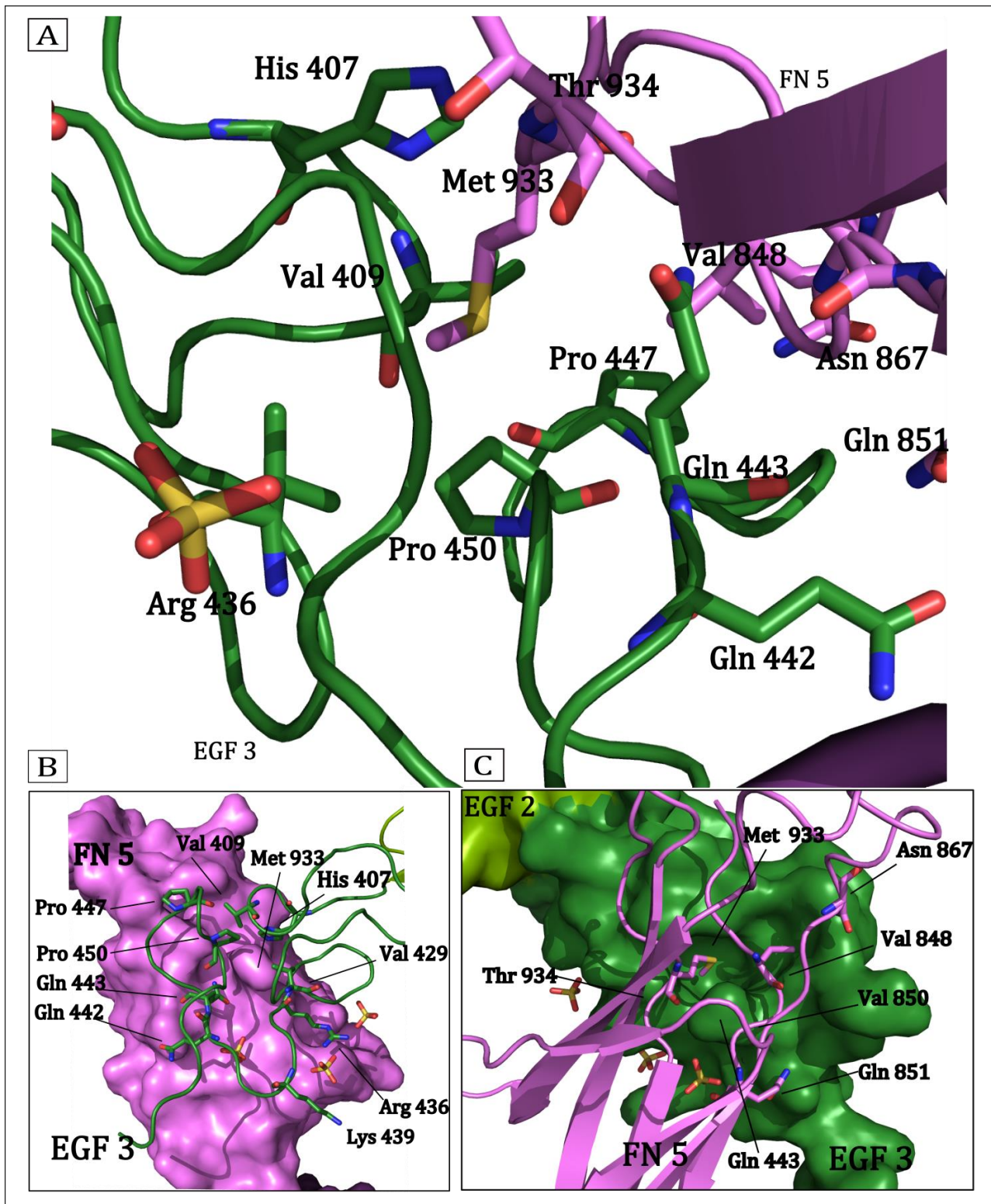


Figure 21 Detailed views into the DCC specific binding site involving the FN5 domain of DCC and EGF3 domain at the C-terminal portion of netrin-1s V domain. The images were created with PyMOL (www.pymol.org). **A** Amino acid residues (shown as sticks) involved in specific binding of DCC (pink) to the EGF3 domain (green) of Netrin_{VIV}. Sulphate ions shown in yellow/red. **B** Close view of the hot spot, DCC_{FN56} shown as surface representation (pink), the EGF3 of Netrin_{VIV} shown as ribbon (green), residues involved shown as sticks. **C** View into the hot spot with Netrin_{VIV} shown as surface representation (green) and DCC_{FN56} as ribbon diagram (pink), involved residues shown as sticks, sulphate ions in yellow/red.

4.b.6. The two receptor binding sites are differentiated by individual affinities

The binding affinities of a classic hydrophobic hotspot can be high. Values for the dissociation coefficient K_d are often observed to be below 1×10^{-7} M (Clackson and Wells, 1995; Green, 1990). The interactions defined for binding site 2 are believed to be less specific. They are mainly mediated by bridging anions that cover positive patches that would otherwise inhibit binding by electrostatic repulsion. This type of binding site is unique, but similar clusters of arginines and lysines have been reported to be involved in heparan sulphate binding of extra-cellular matrix proteins (Tan et al., 2008). Binding affinities between proteins, such as growth factors, receptors and adhesion molecules, and heparan sulphates have been determined ranging between 1×10^{-8} and 1×10^{-5} M (10 nM-10 μ M) (Capila and Linhardt, 2002). Microscale thermophoresis (MST) and isothermal titration calorimetry (ITC) experiments were performed to define binding affinities of the individual binding sites.

The detection of changes in the hydration shell upon complex formation between DCC_{FN56} and $Netrin_{VIV}$ and the subsequent changes of the particle movement was measured by MST. This method is suitable to determine binding affinities in a wide range of concentrations especially when the affinity is not yet known.

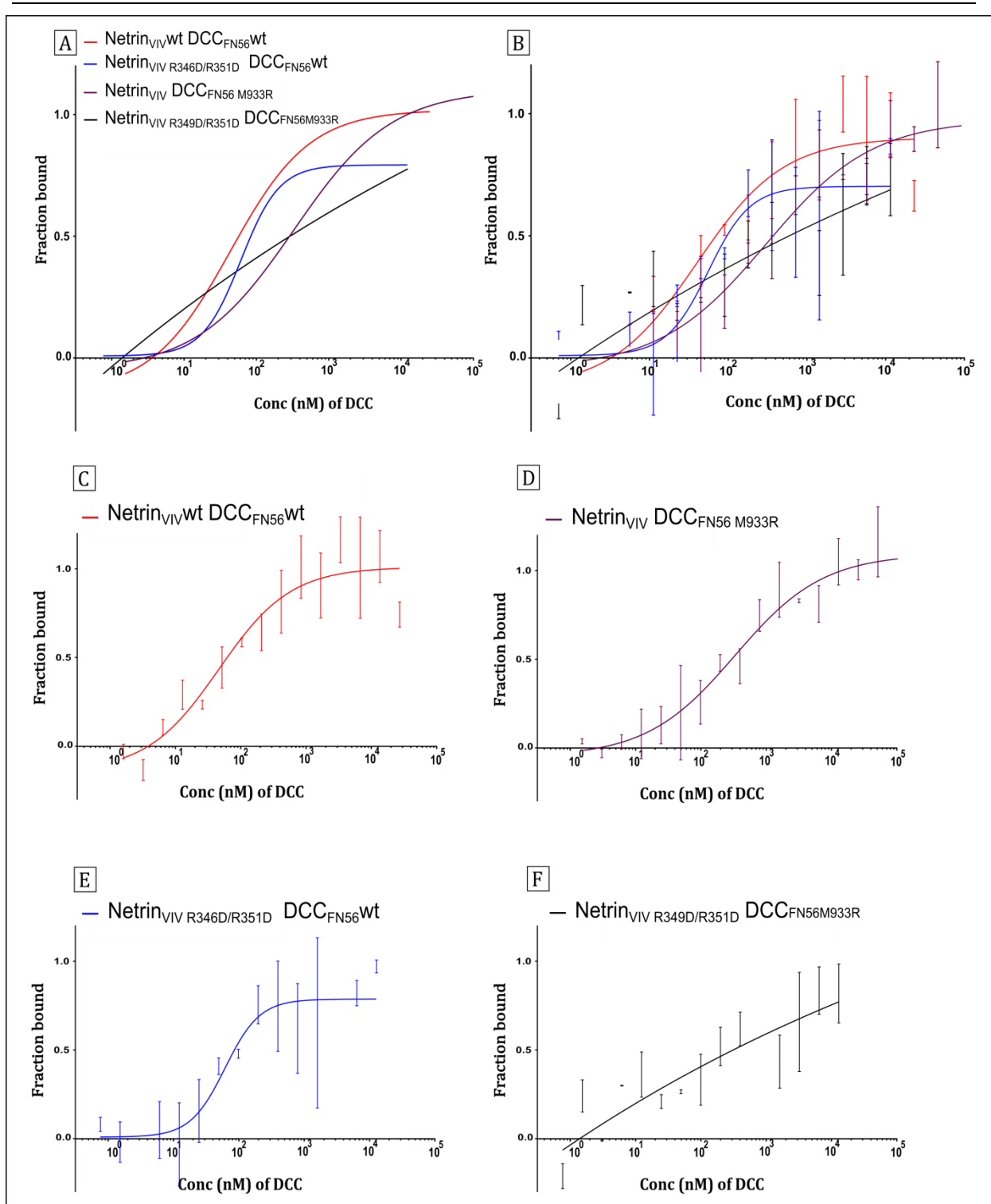


Figure 22 Thermophoresis experiment to determine the binding affinities between Netrin_{VIV} and DCC_{FN56}. Concentration of labelled ligand Netrin_{VIV} and Netrin_{VIV}R349D/R351D were kept at a constant concentration of 50nM, while the concentration of the non-labelled receptor was varied between 0.7 nM and 100μM. All experiments were performed in three individual pipetted measurements, apart from Netrin_{VIV}- DCC_{FN56}M933A (n=2) and Netrin_{VIV}- DCC_{FN56}M933D (n=1). **A** Graph of non-linear regression (Hill equation, Graph pad prism) of the titration curves, concentration of labelled ligand (Netrin_{VIV}) plotted against the fraction of bound receptor (DCC_{FN56}) in percent. Red curve shows binding between Netrin_{VIV}wt and DCC_{FN56}wt. Violet curve shows Netrin_{VIV}wt and DCC_{FN56}M933R binding site 1 mutant, blue curve shows binding of Netrin_{VIV}R349D/R351D binding site 2 mutant and DCC_{FN56}wt, black curve shows no binding between Netrin_{VIV}R349D/R351D and DCC_{FN56}M933R. **B** Graph of figure A with error bars shown. **C** Netrin_{VIV}wt and DCC_{FN56}wt. **D** Netrin_{VIV}wt and DCC_{FN56}M933R binding site 1 mutant. **E** Netrin_{VIV}R349D/R351D and DCC_{FN56}wt. **F** Netrin_{VIV}R349D/R351D and DCC_{FN56}M933R.

log(agonist) vs. response -- Variable slope (four parameters)	NetrinVIV R349D/R351 D DCC56wt	NetrinVIV R349D/R351D DCC56 M933R Ambiguous	NetrinVIV DCC56wt	NetrinVIV DCC56 M933R	NetrinVIV DCC56 M933A	NetrinVIV DCC56 M933D
Best-fit values						
Bottom	0,008329	~-57,66	-0,1414	-0,05061	-0,2464	-0,06859
Top	0,7934	~2,019	1,020	1,103	1,106	0,9257
LogEC50	1,785	~-26,38	1,641	2,519	2,203	2,313
HillSlope	1,634	~-0,05490	0,7912	0,6436	0,4820	1,066
EC50	60,97	~0,0	43,70	330,7	159,8	205,4
Span	0,7850	~-59,68	1,161	1,154	1,352	0,9943
Kd	84,26	51,2	296,33	255	255	122
	+/-12,72	+/-7,26	+/-21,06	+/-22,8	+/-22,8	+/-9
Std. Error						
Bottom	0,06462	~33306	0,1623	0,07360	0,2687	0,07577
Top	0,05844	~26,28	0,06120	0,06631	0,1469	0,04909
LogEC50	0,1316	~5303	0,2101	0,1326	0,3487	0,1497
HillSlope	0,6696	~1,734	0,2611	0,1462	0,2107	0,3083
Span	0,09348	~33332	0,1983	0,1232	0,3871	0,09958
Lower 90% conf. limit						
Bottom	-0,1011	(Very wide)	-0,4153	-0,1742	-0,7070	-0,2047
Top	0,6944	(Very wide)	0,9163	0,9916	0,8542	0,8375
LogEC50	1,562	(Very wide)	1,286	2,297	1,606	2,044
HillSlope	0,4996	(Very wide)	0,3507	0,3982	0,1209	0,5127
EC50	36,49	(Very wide)	19,32	198,0	40,35	110,6
Span	0,6267	(Very wide)	0,8265	0,9467	0,6891	0,8154
Upper 90% conf. limit						
Bottom	0,1178	(Very wide)	0,1324	0,07299	0,2142	0,06749
Top	0,8924	(Very wide)	1,123	1,214	1,358	1,014
LogEC50	2,008	(Very wide)	1,995	2,742	2,801	2,581
HillSlope	2,768	(Very wide)	1,232	0,8891	0,8430	1,620
EC50	101,9	(Very wide)	98,86	552,1	632,6	381,5
Span	0,9434	(Very wide)	1,496	1,360	2,016	1,173
Goodness of Fit						
Degrees of Freedom	32	33	37	45	23	11
R square	0,7891	0,7321	0,8639	0,9254	0,9063	0,9573
Absolute Sum of Squares	1,086	1,005	1,020	0,6513	0,3953	0,1113
Sy.x	0,1842	0,1745	0,1660	0,1203	0,1311	0,1006
Number of points Analyzed	36	37	41	49	27	15

Figure 23 Analysis of thermophoresis experiment to determine the binding affinities between Netrin_{VIV} and DCC_{FNS6}. Analysis was done by calculation of log of dose-response and statistics of 90% confidential limits (Hill equation, variable slope, Graphpad Prism). EC50 as 50% of maximal response, and R² as indication of goodness of fit of non-linear regression are indicated in red boxes. K_{d,s} of the experiments were calculated employing the fluorescent signal from thermophoresis and temperature jump using the NTAanalysis software (K_d fit).

To measure interactions between the wildtype (wt) constructs of Netrin_{VIV} and DCC_{FN56}, Netrin_{VIV} was labelled with the RED-NHS labelling kit (Nanotemper, described in chapter 3.b.) that labels free amine groups as present in lysine residues. The concentration of the Netrin_{VIV} was adjusted to 50 nM and DCC_{FN56} was titrated in the range of 3 nM to 50 μ M (3×10^{-9} - 5×10^{-5} M). The measured fluorescence was normalised for the baseline of the unbound state and the amplitude to plot the bound fraction (1 full binding, 0 no binding) against the concentration of the titrated receptor (Fig. 22 C). A binding curve was fitted with the dose-response Hill equation (Fig. 22 A, Fig. 23), giving a calculated EC₅₀ (50% of maximum response) of 43.7 nM and a K_d of 51.5 nM +/- 7.25 (Fig. 22 C). The mean error between the individual measurements is relatively high (Fig. 22 C, Fig 23) and the goodness of fit represented by R² is with 0.86 (1= curve resembles exactly the measured points, 0= not fit) not ideal (Fig. 23). However, the determined affinity is consistent with earlier studies of cell culture based assays where affinities in the same range were observed (Keino-Masu et al., 1996). According to the observations in the crystal structure, an equation for a two binding site model (Two sites, Fit logEC₅₀, Graphpad Prism) was also applied to the data. Equations to accommodate two binding sites are designed for enzymatic reactions with competitive binding or inhibition (Cheng and Prusoff, 1973), but were found to be difficult to apply to the MST binding curves. Nevertheless, two EC₅₀ values for DCC_{FN56}-Netrin_{VIV} wt were calculated; a lower EC₅₀ of 4.99 nM and a higher EC₅₀ of 122.4 nM. The goodness of fit R² = 0.86 resembled the one described for the dose-response equation, but the 90% confidential limits are very wide (0.04-810.1 nM).

Both binding sites contribute to the affinity measured and determined by the Hill equation. To separately evaluate the receptor-ligand binding of each binding site, MST measurements were performed using binding site specific mutant constructs. Residues of Netrin_{VIV} involved in sulphate coordination on binding site 2, Arg 349 and Arg 351 were mutated into aspartic acid (Asp, D) giving rise to the construct Netrin_{VIV} R349D/R351D. Netrin_{VIV} R349D/R351D was labelled in the same way as described before, and DCC_{FN56} was titrated in the range of 3 nM to 25 μ M (3×10^{-9} - 2.5×10^{-5} M). Aspartic acid is a negatively charged amino acid. The inversion of the electrostatic charge could mediate direct binding between residues of opposite charges on Netrin_{VIV} and DCC_{FN56}. The binding curve obtained from this experiment (Fig. 22 E) showed that this is not the case; there is no significant increase of affinity observed for this

reaction (Fig. 23). Actually, the values for the EC₅₀ of 61 nM and the K_d of 84.3 nM +/- 12.72 are slightly higher than for the wildtype and the binding curve does not reach the state of full saturation (Fig. 22 E). No binding was observed for experiments where DCC_{FN56} was labelled (data not shown). The dye used labels free amine groups of lysine residues. Two Lys are involved in the binding site 2 coming from DCC_{FN56}. Labelling could impair binding to this site and sterically hinder binding to site 1 as well.

The collaboration with Prof. Dr. JH. Wang's laboratory provided three mutants constructs of the binding site 1 key residue Met 933 of DCC_{FN56}. In the construct DCC_{FN56M933A} the methionine is substituted for an alanine, in DCC_{FN56M933D} changed into aspartic acid and in DCC_{FN56M933R} an arginine takes place at position 933. Alanine is, like methionine a hydrophobic amino acid, but with a shorter side chain, Asp and Arg are oppositely charged amino acids. The binding experiments with DCC_{FN56M933A} decreased the affinity to Netrin_{VIV} to an EC₅₀ of 159.8 nM and a K_d of 255 nM +/- 22.8 (Fig. 23). DCC_{FN56M933D} (EC₅₀ 205.5 nM, K_d 122 nM +/-9) and DCC_{FN56M933R} (EC₅₀ 330.7 nM, K_d 296.33 nM +/- 21.06) show a similar or even lower affinity. The errors of these measurements are low and the R² of > 0.9 indicate a good fit of the binding curves (Fig. 23). Performing binding experiments with the Netrin_{VIV} R349D/R351D and DCC_{FN56M933R} showed complete impairment of binding between receptor and ligand (Fig. 22 A and F). No binding curve could be calculated from the randomly distributed measure points.

These results allow the conclusion that each binding site contributes with distinct affinities to the total receptor-ligand binding dynamics. The wildtype clustering of receptor and ligand is dominated by the tight binding of the hydrophobic hot spot of binding site 1. Interruption of the positive patch involved in binding site 2 on the construct Netrin_{VIV} decreased the affinity only slightly, confirming the high affinity of site 1. The lower affinity of binding site 2 was only to be determined by impairment of the hydrophobic interactions of site 1. The higher affinity of binding site 1 is probably masking binding to site 2 in the experiment with the wildtype constructs. This led to the conclusion that with this kind of experiment it is not possible to separate the two binding affinities without eliminating one of them by mutation. The existence of both binding sites was further supported by the fact that no binding was measured when both sides are knocked out by mutations. It is worth mentioning, that the MST results presented above were only obtained after an extended series of measurement at

different pH. Measurements with an acceptable signal to noise ratio were measured at pH 7.5 to 8.0 in phosphate buffer or a buffer containing ammonium sulphate.

ITC was performed (Fig. 24, top graph) to confirm the binding affinity for Netrin_{VIV} to DCC_{FN56} determined by the MST and that were described previously in other studies (Keino-Masu et al., 1996). Netrin_{VIV} was concentrated to 9 μM and DCC_{FN56} was titrated into the solution to a molar ratio of 1:2. The binding curve showed a good fit (Fig. 24, bottom graph). However, a low affinity (K_d of 4.5 μM) was calculated by inversion of parameter K . This is inconsistent with the previous findings, but could be explained by the fact that the concentration range used did not lead to saturation of Netrin_{VIV} with DCC_{FN56} molecules. No inflection points at the bottom (no binding) or top (saturation) of the curve were reached, so the calculated K_d value is not reliable. This might be due to the design of the experiment and the concentrations used. For MST the highest ratio of concentrations was 1:2000, (50 nM Netrin_{VIV}: 100 μM DCC_{FN56}) guaranteeing saturation. The binding stoichiometry (parameter N) obtained from ITC supports a stoichiometry of 1:1, but only a 1:2 stoichiometry would show full saturation of both binding sites. To obtain reliable K_d values the experiment could be repeated in two steps, in lower and higher concentrations, to obtain the inflection points for a more reliable calculation of K_d .

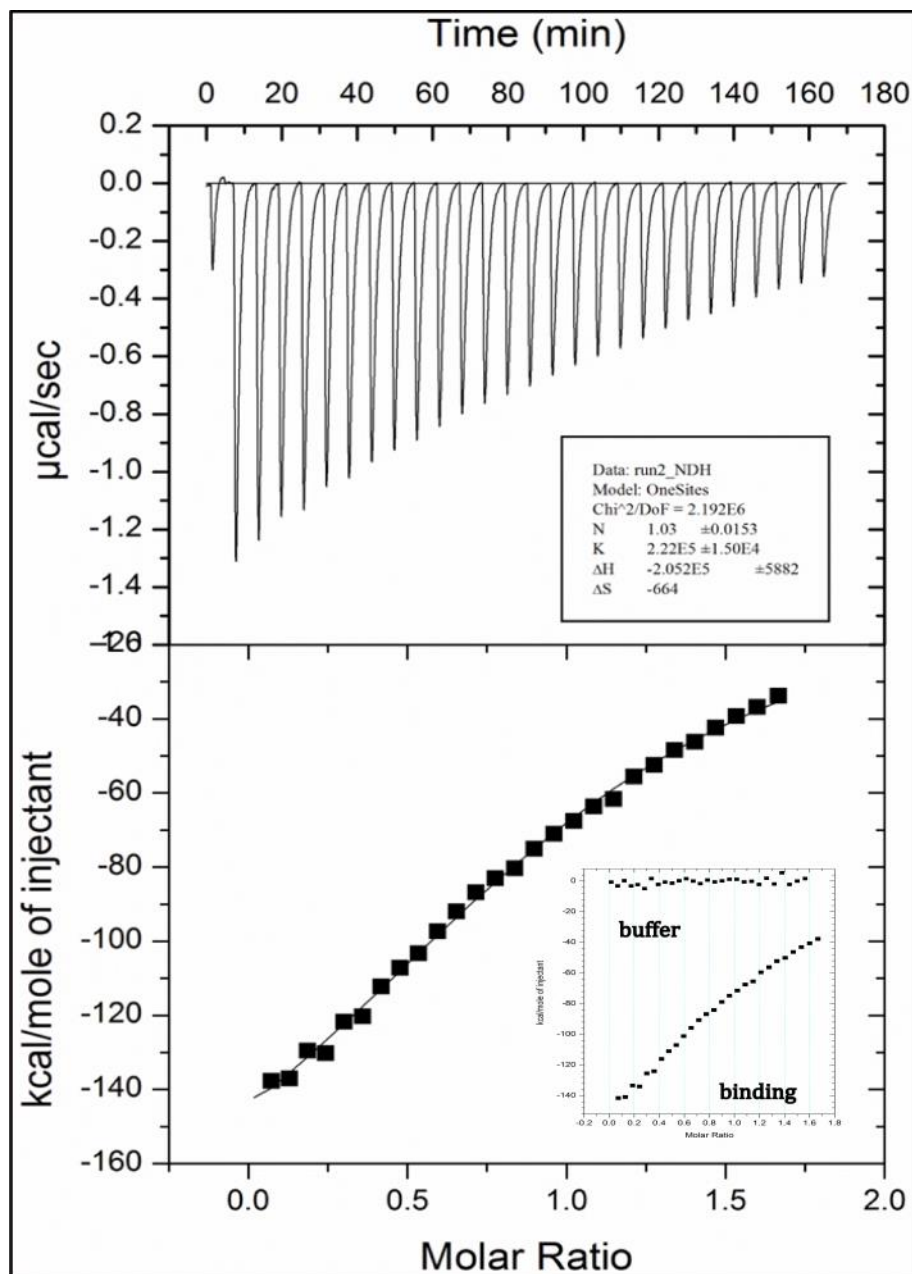


Figure 24 Isothermal titration calorimetry (ITC). Experiments were carried out with a VP-ITC system (MicroCal). Experiments were performed at 25°C in PBS, pH8.0, with 1mM DTT. Purified Netrin_{VIV} was placed in the reaction cell at a concentration of 9 μM and DCC_{FN56} at a concentration of 82 μM in the injection syringe to be titrated into the Netrin_{VIV} solution. Top graph: Peaks of individual measurements. Bottom graph: Data were processed with the Origin 7 software (MicroCal). Data were corrected by the heat of injection calculated from the basal heat remaining after saturation. This reference value was subtracted from the protein–ligand titration to nullify the heat of dissolution. The heat changes of the Netrin injections were plotted against the molar ratio of DCC. Small graph: Binding curve compared to control experiment.

4.b.7. Signal transduction is dependent on clustering by both binding sites of Netrin_{VIV}/DCC_{FN56}

It has been shown that the construct Netrin_{VIV} is sufficient to bind DCC_{FN56} (Fig.15) and that complex formation stabilises Netrin_{VIV} in solution *in-vitro* (Fig. 16). This complex is formed by binding of DCC_{FN56} (Fig. 18) to two distinct binding sites on Netrin_{VIV} showing differentiated binding mechanisms (Fig. 20 and Fig. 21) and dynamics (Fig. 22 and Fig. 23). To verify if the results obtained from crystallographic and biophysical characterisation resemble the mechanisms *in-vivo*, that lead to clustering of the DCC by netrin-1 to transduce a signal across the membrane, a series of cell based functional assays have been performed in collaboration with Dr. Yan Zhang (Peking University, China). Cloning, site-directed mutagenesis, expression and purification of Netrin_{VIV} and mutant constructs (Fig. 11) have been carried out at EMBL, Hamburg.

To confirm *in-vivo* binding of Netrin_{VIV} to DCC, COS cells transfected with constructs of the full-length wildtype DCC were incubated with Netrin_{VIV} and binding was detected with an antibody specific to netrin-1 (Fig. 25 A, Netrin_{VIV}). This experiment showed that Netrin_{VIV} is binding to the full-length receptor DCC in the same way as full-length netrin-1 wt does (Fig. 25 A DCC wt, C).

To investigate how mutations for binding site 1 affect *in-vivo* binding, valine 848 and methionine 933, the amino acids on the FN5 domain of DCC involved in hydrophobic interactions were mutated. For Val 848 there was either an alanine (V848A) or an arginine (V848R) introduced. The introduction of another hydrophobic amino acid (Ala) to this position did reduce binding by approximately 25% (Fig.25 A and C V848A), while introduction of a positively charged Arg impaired binding of netrin-1 to the DCC (Fig. 25 A and C V848R) completely. Similar observations were made for mutations of Met 933 (Fig. 25A). Introduction of an Ala (M933A) affected binding of netrin-1 only slightly (Fig. 25A and C), while mutations into positively (M933R) and negatively (M933D, aspartic acid) charged amino acids prevented netrin-1 from effective binding to DCC (Fig. 25 A and C).

On the netrin-1 side, Gln 443 takes the central role in hydrophobic interactions, and mutation of this residue into an alanine had a severe effect. No binding to DCC was observed (Fig. 25 A and C Q443A). Although single mutations of the hydrophobic amino acids from the DCC side showed little effect when the

hydrophobicity was preserved by the introduction of an alanine, on the Netrin_{VIV} side this substitution had a greater impact. This might be due to the fact that from the netrin-1 site Gln 443 is not only participates in hydrophobic interactions; it also builds hydrogen bonds to Val 850 and M933 of DCC. Although the importance of integrity of the hydrophobic interactions for binding was confirmed by the described binding studies, the question, if the ability of axon guidance would be also affected remained. Therefore, neuronal cells, isolated from E15 (embryonic day 15) DCC^(-/-) mice were injected with DCC wt and the mutated constructs described above. The chemotropic potency was evaluated by the number of axons attracted to immobilised netrin-1 or Netrin_{VIV} soaked beads (Fig. 25 B and D). This experiment also showed only minimal differences between netrin-1 full-length and the Netrin_{VIV} construct (Fig 25 B DCC wt and D), reconfirming that Netrin_{VIV} contains the domains responsible to bind DCC and generate a positive response in neuronal cells. The phenotype of the murine DCC^(-/-) neurons injected with DCC wt was rescued both, by netrin-1 and Netrin_{VIV}. The alteration of single, hydrophobic amino acids (Val848 and Met 933) showed, again, little effect when substituted by the hydrophobic alanine (Fig. 25 B and D) occurred on DCC, but reduced attraction drastically if Netrin_{VIV}s Gln 443 was altered (Fig. 25 B and D, Q443A). A similar effect was observed by the introduction of charged amino acids (M993R, M933D), which probably hinder the hydrophobic interactions and therefore impair clustering of DCC. This might prevent homo-dimerisation of the receptor necessary for signal transduction.

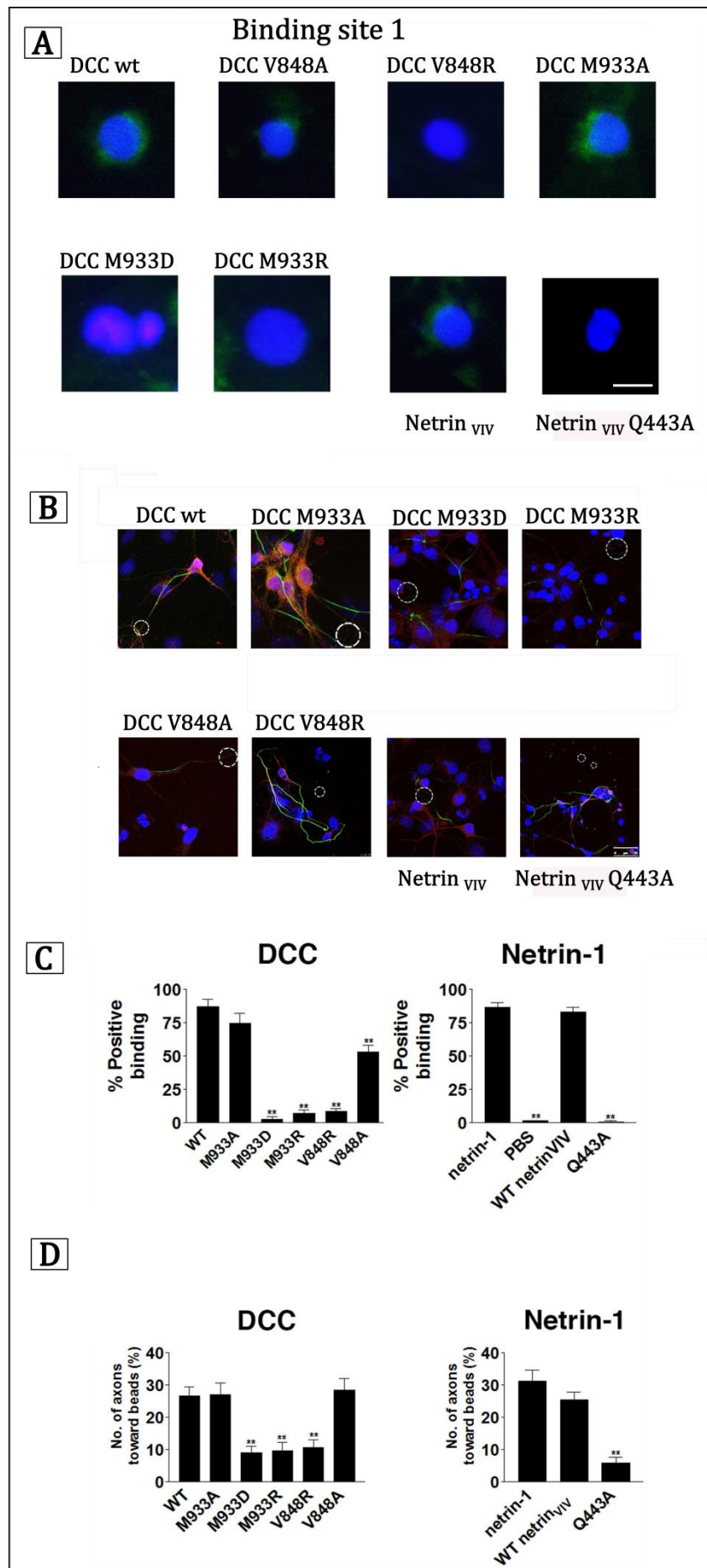


Figure 25 Cell binding assay and axon guidance assay to verify binding site 1. **A** Representative fluorescence microscopy images of netrin-1 (Enzo Life Sciences) or Netrin_{viv} and mutants binding to COS cells transfected with DCC wt or mutants receptors. Netrin-1 constructs were detected with a netrin-1 antibody. **B** Representative images of axon guidance assay for axons injected with DCC wt or mutants affecting binding site 1. Injected cells are coloured red, cells bodies were dyed with DAPI (blue). Growing axons are marked by AnkG-EGFP and appear green. Position of netrin-1/Netrin_{viv} mutants soaked beads indicated by circles. **C** Graph of cell binding assay showing the percentage of DCC wt or DCC mutant transfected cells binding to netrin-1, Netrin_{viv} or Netrin_{viv} Q443A. **D** Graph of axon guidance assay showing percentage of DCC wt and mutant injected axons attracted towards netrin-1, Netrin_{viv}, and Netrin_{viv}Q443A soaked beads. **Images are courtesy of Dr. Yan Zhang.**

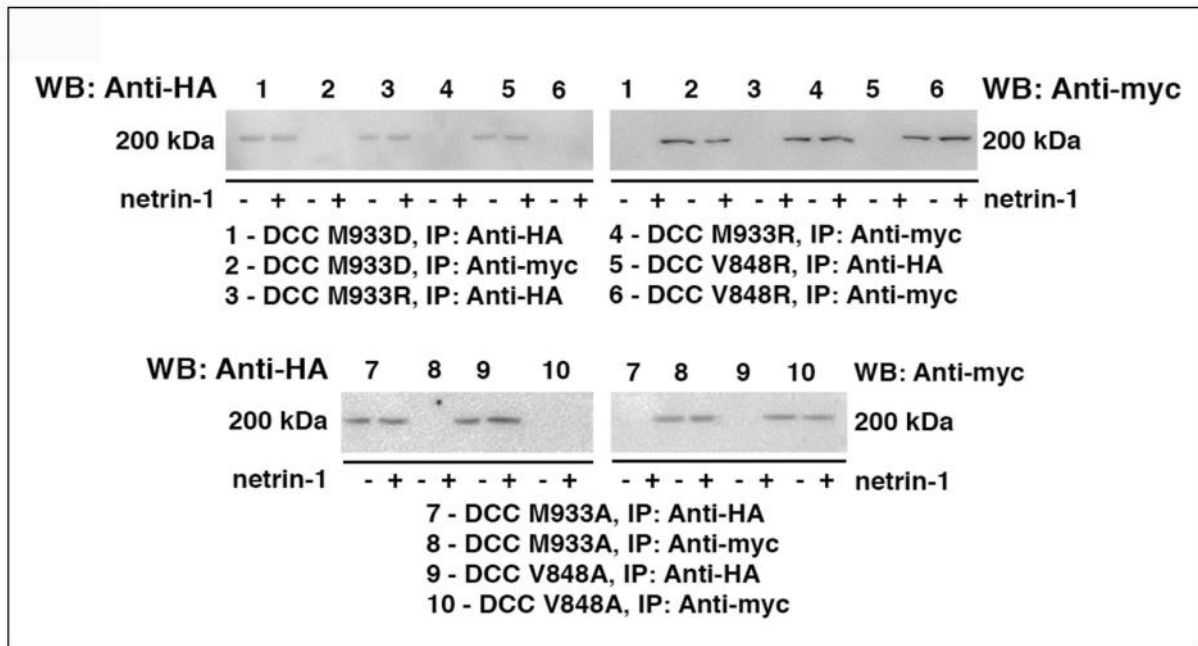


Figure 26 Western blot of clustering assay for oppositely tagged (myc-tag/HA-tag) DCC wt and mutant constructs pulled down by netrin-1 coupled beads. Sample detected by HA antibody and myc antibody. **Images are courtesy of Dr. Yan Zhang.**

To address the question, if the inhibition of clustering of DCC by impairing binding site 1 could be responsible for reduced binding and chemotropic attraction, an immune-precipitation pull down assay with isolated DCC constructs was performed. To test the ability of netrin-1 to cluster DCC wt and mutant constructs for binding site 1, two different tags (HA- and myc-tag) were introduced. None of the Western blots (Fig. 26) showed an enrichment of oppositely tagged receptors, leading to the conclusion that netrin-1 wt binds two DCC molecules and if one binding site (here binding site 1) is mutated to loss of function no clustering can be observed. This finding is excluding the possibility as well, that there are additional binding sites for DCC on full-length netrin-1.

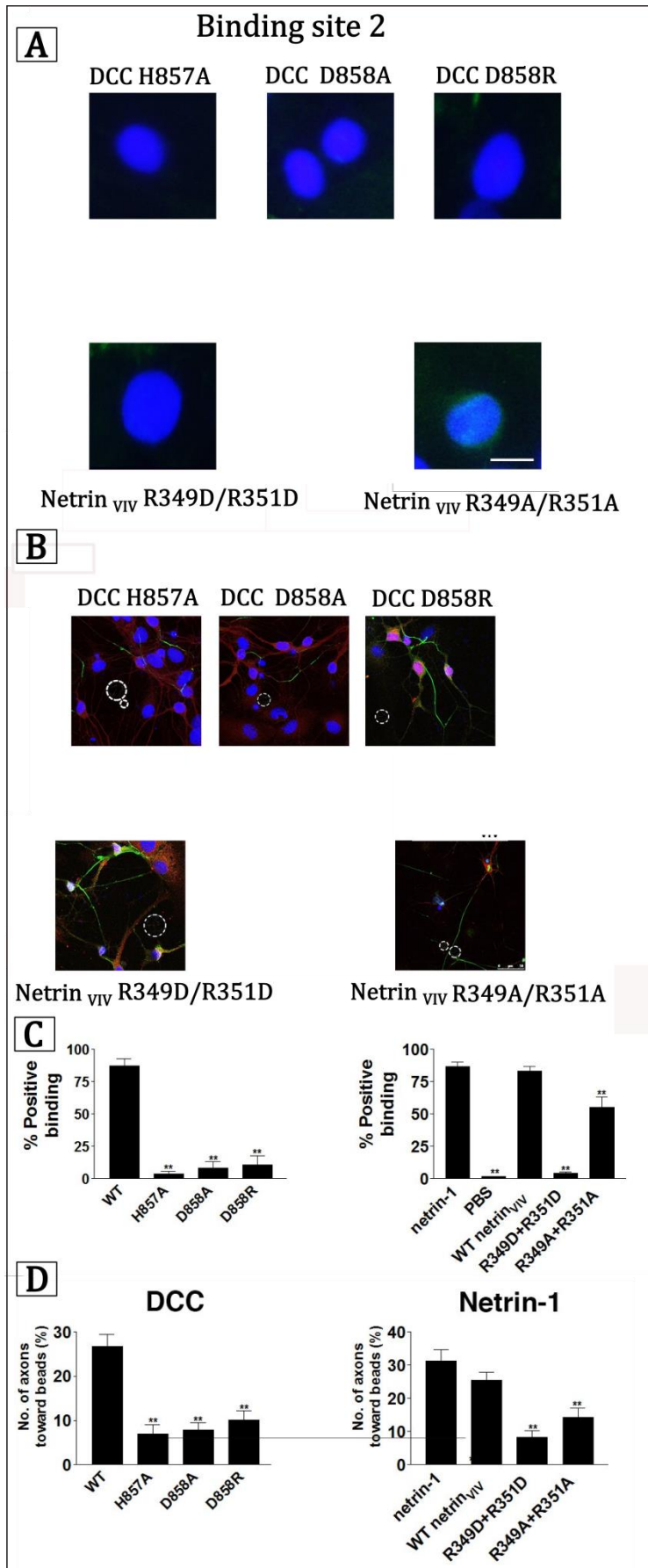


Figure 27 Cell binding assay and axon guidance assay to verify binding site 2. **A** Representative fluorescence microscopy images of netrin-1, Netrin_{viv} and mutants binding to COS cells transfected with DCC wt or mutant receptors. Netrin-1 constructs were detected with a netrin-1 antibody. **B** Representative images of axon guidance assay for axons injected with DCC wt or mutants affecting binding site 2. Injected cells are coloured red, cells bodies were dyed with DAPI (blue). Growing axons are marked by AnkG-EGFP and appear green. Position of netrin-1/Netrin_{viv} mutants soaked beads indicated by circles. **C** Graph of cell binding assay showing the percentage of DCC wt or DCC mutant transfected cells binding to netrin-1, Netrin_{viv}, Netrin_{viv} R349D/R351D and Netrin_{viv} R349A/R351A. **D** Graph of axon guidance assay showing percentage of DCC wt and mutant injected axons attracted towards netrin-1, Netrin_{viv}, Netrin_{viv} R349D/R351D and Netrin_{viv} R349A/R351A soaked beads. **Images are courtesy of Dr. Yan Zhang.**

The binding mechanisms of site 2 showed so far no similarity to binding site 1. Here, interactions are mediated by negatively charged anions rather by direct protein-protein interactions (Fig. 20). The finding, that binding site 1 is essential for functionality of the netrin-1 guidance cue (Fig.25 B and D) raised the question, how binding site 2 contributes to the signal transduction. The same experiments as described previously in this section were performed for DCC and Netrin_{VIV} constructs carrying mutations for binding site 2.

The few observed direct contacts between receptor and ligand on binding site 2 are centred around Pro 320 (Netrin_{VIV}, EGF1) interacting with the hydrophobic portions of His 857 and Asp 858, located on the AB loop of DCCs FN5 domain (Fig. 20 A). Asp 858 participates as well in the coordination of the chloride ion present in the receptor ligand interface (Fig. 20 B). To verify the role of these amino acids, they were chosen for site-directed mutagenesis. The positively charged His 857 was substituted by the hydrophobic amino acid alanine (H857A). The Asp 858, that has a double function in chloride ion coordination and hydrophobic interaction, was mutated into alanine (D858A) or a positively charged arginine (D858R). All three mutations have great effect on binding of netrin-1 to DCC mutant expressing COS cells (Fig. 27 A and C) compared to the DCC wt expressing cells. The mutation of His 857 (H857A) abolished binding completely. Axon attraction was affected in a comparable way (Fig. 27 B and D). Less than 10% of the injected axons were attracted to a netrin-1 gradient (Fig. 27 D).

The second important feature of binding site 2 is the sulphate cluster. Changes in the positive patch on netrin-1 were introduced by mutations of the Netrin_{VIV} residues Arg 349 and Arg 351 (R349A/R351A and R349D/R351D) as described before to identify the role of the sulphate mediated interaction on binding and axon guidance. Neutralising the arginine residues by alanine (R349A/R351A) reduced binding of Netrin_{VIVR349A/R351A} by approximately 25% (Fig. 27 A and C) compared to Netrin_{VIV} wt (Fig. 25 A and Fig. 27 C). Consistent with the reduction of binding ability, the number of axons growing in the direction of the gradient were halved (Fig. 27 C). The inversion of the electrostatic charge by introduction of aspartic acid prevented binding of Netrin_{VIVR349D/R351D} to COS cells expressing DCC wt (Fig. 27 A and C) and reduced the positive response of axons migrating towards a netrin-1 or Netrin_{VIV} gradient severely (Fig.27 B and D).

To confirm the contribution of binding site 2 to binding and axon guidance by clustering of DCC molecules on the plasma membrane, the binding site 2 mutants described previously were tested in the same way as the binding site 1 mutants by immune-precipitation (Fig. 28). Therefore the ability of the DCC mutants to be clustered by netrin-1 was compared with Netrin_{VIV} and Netrin_{VIV} mutants. Netrin_{VIV} bound DCC in the same way as netrin-1 and as described previously in this section (Fig. 28, 9B, 10B and 9C and 10C). The binding site 1 mutants completely inhibited clustering (Fig. 26). For the binding site 2 mutants the result is more complex. The mutation of His 857 and Asp 858 into alanine had no effect on the clustering experiment (Fig. 28, 2-6). Only the inversion of the charge of Asp 858 (D858R) abolished binding (Fig. 28, 7 and 8).

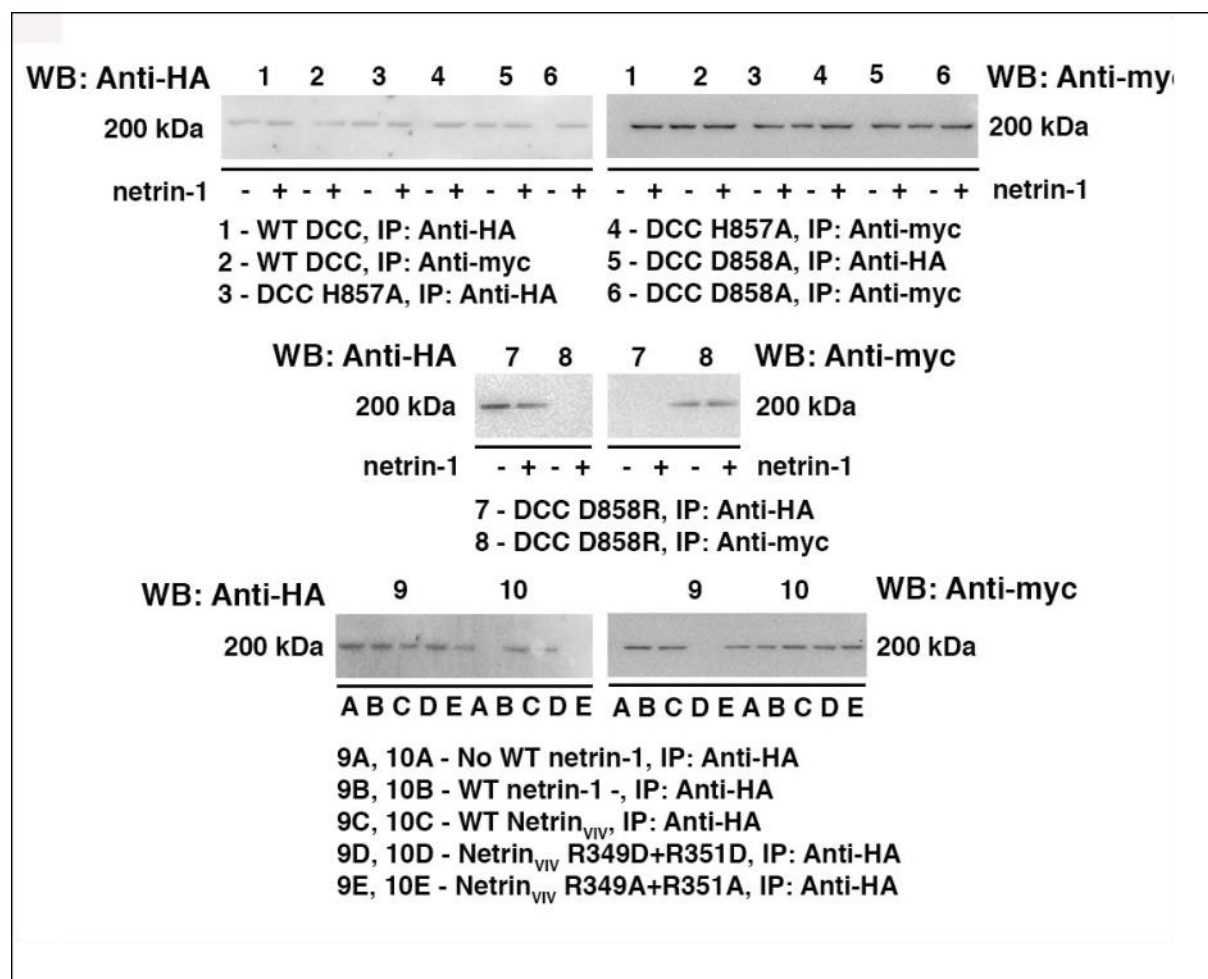


Figure 28 Western blot of clustering assay for oppositely tagged (myc-tag/HA-tag) DCC wt and mutant constructs affecting site 2 pulled down by netrin-1, Netrin_{VIV}, Netrin_{VIV} R349D/R351D and Netrin_{VIV} R349A/R351A coupled beads. Sample detected by HA antibody and myc antibody. **Images are courtesy of Dr. Yan Zhang.**

Furthermore, the mutations of the two adjacent arginine residues (Arg 349 and Arg 351) influenced the ability to cluster DCC wt. The R349A/R351A mutant of Netrin_{VIV} (Fig. 28 9E), as well as the charge inverting R349D/R351D mutant (Fig. 28 D) showed no binding of the respective oppositely tagged DCC wt.

Together these experiments further confirmed the existence of both binding sites *in-vivo* and *in-vitro*. Binding of netrin-1 to DCC *in-vitro* is not necessarily dependent on both binding sites. Some mutants still showed binding, although the affinity seemed to be reduced. These findings confirmed the observations made by MST, where changes of the binding affinity for the binding site 1 and binding site 2 mutants were observed. The role of clustering the ectodomains of DCC by netrin-1 for signal transduction was verified by the axon guidance assays. When the affinity of one of the binding sites was reduced by amino acid substitution, axon guidance was affected. In the most severe cases no attraction was observed anymore. This confirms the importance of both binding sites for the functionality of the netrin-1 guidance cue.

4.b.8. Clustering in solution requires both binding sites and is netrin-1 dependent

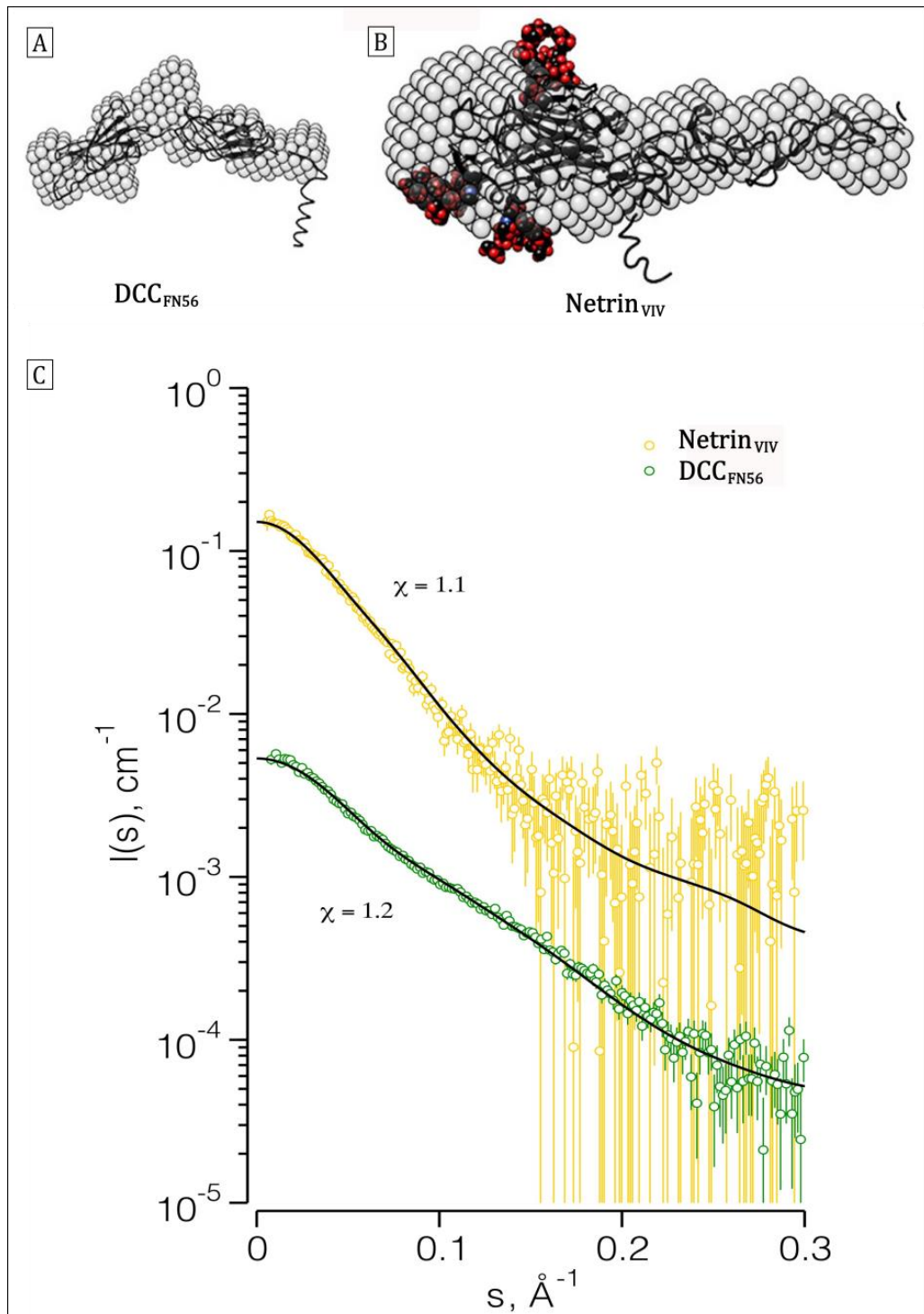


Figure 29 Molecular envelop and SAXS experimental and theoretical scattering curves. **A and B** *Ab initio* molecular envelopes (grey spheres) calculated from the SAXS data overlaid onto the crystal structure (ribbons) **A** DCC_{FN56} **B** Netrin_{VIV} with glycosylation sites (black and red balls). **C** Experimental curves of Netrin_{VIV} (yellow) and DCC_{FN56} (green) with fits of the theoretical curves calculated from the crystal structures. The Netrin_{VIV} curves have been scaled by a factor of 10 for visualisation. Data analysis has been performed by Dr. Haydyn Mertens (EMBL, Hamburg). **Figures are courtesy of Dr. Haydyn Mertens**

Small angle X-ray scattering (SAXS) uses the elastic X-ray scattering of a sample at very low angles to gain information about shape and size of molecules in solution (Glatter O, 1982). This technique is a suitable method to gain information about complex samples because stoichiometry and concentrations can be varied easily. SAXS data were collected at the P12 beamline at the PETRAIII beamline (EMBL, Hamburg) and data analysis has been performed in collaboration with Dr. Haydyn Mertens, Dr. Gundolf Schenk and Dr. Dmitri I. Svergun (all EMBL, Hamburg). Details of the data analysis and statistical calculations can be found in the appendix (Appendix 8.d.).

The results from binding and axon guidance assays, together with other studies (Stein et al., 2001) allow the conclusion that clustering of DCC is netrin-1 dependent and necessary for signal transduction. The assumption, that DCC alone is monomeric in solution in the absence of netrin-1 was tested by SAXS measurements of a concentration series of DCC_{FN56} (Fig.29 A and C). The experimental scattering curve was compared with a theoretical curve calculated from the crystal structure (Fig. 29 C). The good fit of the two curves confirms that the conformation in solution (Fig. 29 A) is consistent with the conformation observed in the crystal (Fig. 18 A).

To fit a theoretically calculated curve to the experimental data of Netrin_{VIV} the glycosylation sites had to be taken into account (Fig. 29 B and C). Therefore, a model was build containing glycosylation sites according to the crystal structure guided by the mass obtained by mass spectrometry. The fit of the model to the experimental data indicated that Netrin_{VIV} is also monomeric in solution. It has been observed earlier, that the mouse homologue of netrin-4 forms dimers (Koch et al., 2000), for netrin-1 this is not true. Moreover, this reduces the possibility, that netrin-1 forms dimers or multimers to initialise receptor clustering.

SAXS is a method that is not only suitable for homogenic samples. In a mixture of components each individual particle contributes to the scattering intensity. The volume fraction of each contributing particle can be calculated by the program OLIGOMER (P.V. Konarev, 2003). Netrin_{VIV} has an elongated rod-like conformation in solution (Fig. 29 A) and the expected changes of the radius of gyration upon complex formation should significantly differ from the individual components. The radius of gyration is a parameter measured by SAXS; it is defined as the root mean square distance between an object and its centre of mass. In proteins these objects are the atoms. Calculations have to take the molecular surface area and volume of

the protein or protein complex into account (Lobanov et al., 2008).

In a stoichiometry of 1:1 no saturation of both binding sites of Netrin_{VIV} was observed (Fig. 30, turquoise). Binding to site 1 contributes with 40% (Fig. 30, blue), binding site 2 (Fig. 30, red) with 20 % to the overall scattering. This is consistent with the observations from the MST experiments, where a higher affinity for binding site 1 than for binding site 2 was calculated. Interestingly, disrupting the integrity of binding site 1 (DCC_{FN56 M933R}) did not lead to a higher occupation of binding site 2 (Fig. 30 Netrin_{VIV} wt-DCC_{FN56M933R} 1:1). At higher concentrations of DCC_{FN56}, in a stoichiometry of 1:5, binding site 1 is still predominantly chosen over site 2 but no clustering was observed. While all free Netrin_{VIV} disappears from solution, DCC_{FN56} still contributed with ~30% volume fraction. It was only at a stoichiometry of 1:10 that 10% of the sample fit to a fully occupied Netrin_{VIV}. Binding to site 2 alone is no longer detected. The impairment of the hydrophobic hotspot prevents clustering even at abundance of DCC_{FN56} (1:10) as observed in previous experiments. These results show that complex formation is dependent on the integrity of both binding sites and abundance of DCC in solution (*in-vitro*).

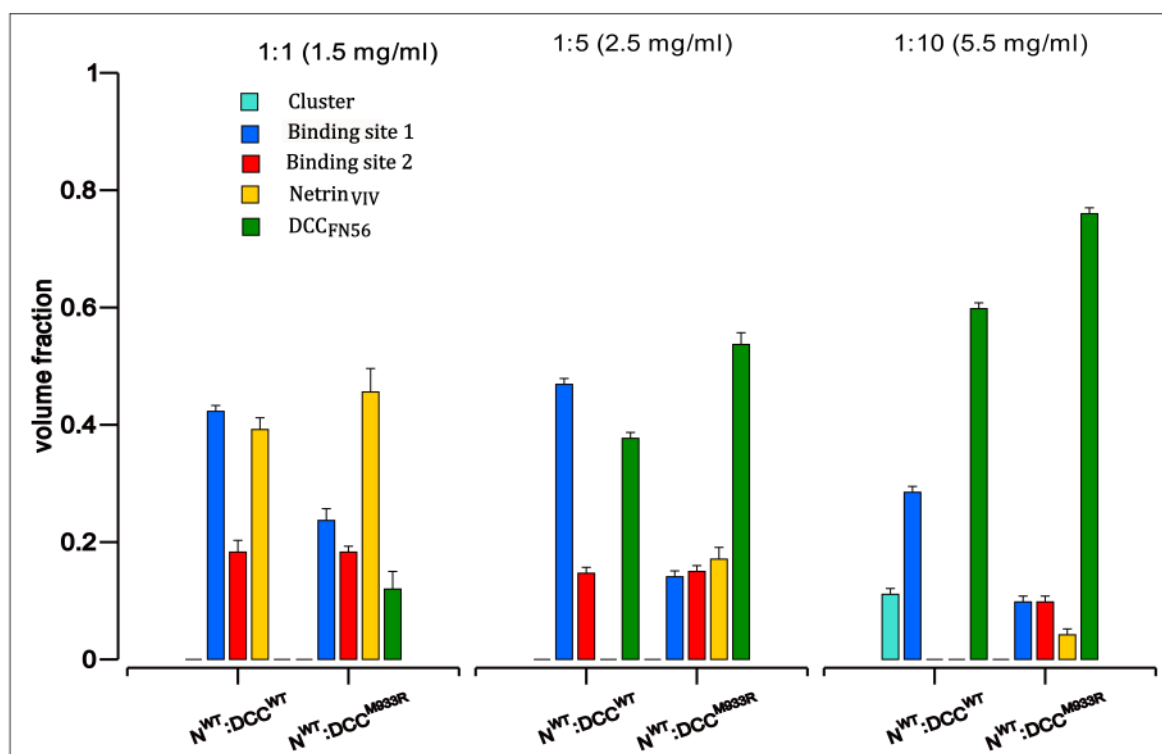


Figure 30 SAXS analysis of Netrin_{VIV}/DCC_{FN56} complex formation in solution. Bar diagram shows volume fractions of component distribution to the overall scattering of a solution containing a mixture of Netrin_{VIV}/DCC_{FN56} wt compared to Netrin_{VIV}/DCC_{FN56 M933R}. Stoichiometries of 1:1, 1:5 and 1:10 were measured and scattering patterns for the individual components were computed from the crystallographic models by CRY SOL(Svergun D.I., (1995)). Best fits from mixtures of individual species and relevant complexes were computed with OLIGOMER (P.V. Konarev, 2003).

4.c. Analysis of binding site conservation

4.c.1. Conservation of DCC binding sites on netrins

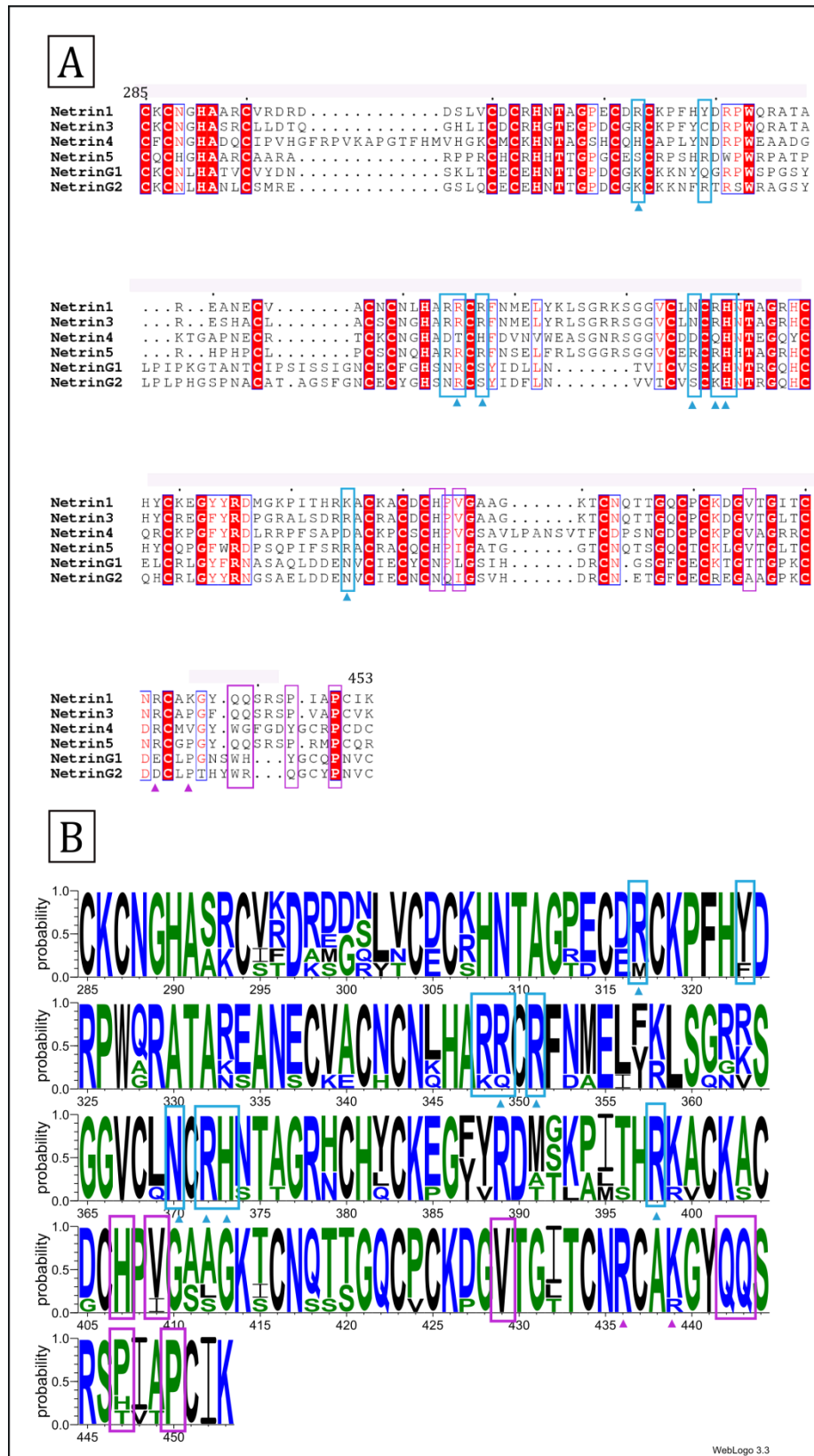


Figure 31 Sequence alignments of EGF domains of netrins. Residues of binding site 1 are marked in pink boxes, residues of binding site 2 in cyan boxes, residues involved in coordination of sulphate ions are marked with pink (site 1) and cyan (site 2) arrow heads for. Alignment was done with Clustal Omega (Sievers and Higgins, 2014) and ESPrnt (Gouet et al., 2003), sequence logo representation with WebLogo3 (Crooks et al., 2004) **A** Sequence alignment of human netrins. Fully conserved residues are in red boxes, conserved residues in red. **B** Logo representation of conservation of residues of domain V of netrin-1 of *H. sapiens*, *M. musculus* and *D. rerio*, *X. laevis*, *D. melanogaster* and *C. elegans*. Blue: hydrophilic residues, green: neutral residues, black: hydrophobic residues.

UNC-6, a netrin-1 homologue, was first discovered during a genome search in *C. elegans* (Hedgecock et al., 1990; Serafini et al., 1994). The worm is a model organism for neuronal development and was the first multicellular organism with a complete map of neuronal wiring (Chatterjee and Sinha, 2008). The presence of netrin homologues at this evolutionary stage indicates the high degree of conservation in neuronal development. To investigate whether the binding sites for DCC are evolutionary conserved among species and can also be found in other human netrins, sequences were obtained from Uniprot and compared by alignment.

Netrin-3 (Uniprot: O00634) is present on motor neurons and neurons in sensory and sympathetic ganglia implying a role in development of the peripheral nervous system (Seaman and Cooper, 2001). Netrin-4 (Uniprot: Q9HB63) has anti-angiogenic effects and stimulates vascular smooth muscle cells. Interaction with the common netrin-1 receptors are believed (Lejmi et al., 2014). There is not much known about the function of Netrin-5 (Uniprot: Q8WTR8). Netrin-G1 (Uniprot: Q9Y2I2) and netrin-G2 (Uniprot: Q96CW9) are GPI-anchored membrane proteins and do not interact with the same receptors (Rajasekharan and Kennedy, 2009).

The alignment of the V-domain (EGF1, EGF2 and EGF3) of the six human netrins (Fig. 31 A) showed, of course, the conservation of the cysteine residues responsible for the stabilisation of the domain structure.

The residues of binding site 2 involved in sulphate coordination, Arg 317, Arg 349, Arg 351, Asn 370 and Arg 372 are conserved (arginine, histidine or lysine) in netrin-1, netrin-3 and netrin-5. In netrin-4 the residues Arg 317, Arg 348, Arg 349 and Arg 372 are absent and not substituted with comparable residues. The amino acids involved in direct protein-protein interaction and chloride coordination on binding site 2, Pro 320, and Cys 318 are conserved in all secreted netrins, while Tyr 323 is not conserved at all. Netrin-3 contains a cysteine residue, netrin-4 an asparagine and netrin-5 an arginine at this position. The netrinG proteins do contain a chloride binding site close to that determined for netrin-1, but the residues that netrin-1 utilised are not conserved in them.

It is therefore concluded, that netrin-1, netrin-3 and netrin-5 bind DCC in the same way, while netrin-4 and the GPI-linked netrins do not. Due to the substitution of the Tyr 323 binding of a chloride ion at this position for netrin-3 and netrin-5 is questionable, but the substitution with cysteine and arginine would not make it impossible.

The hydrophobic residues of binding site 1 are conserved in netrin-1, netrin-3 and netrin-5 (Fig. 31 A, pink boxes). Netrin-4 has amino acid substitutions at Gln 442 and the hydrophobic key residue Gln 443. The sulphate binding residues are not fully conserved either. The anions are only present at the periphery and substitution of one of the sites must not lead to impair this binding site. Netrin-3 and netrin-5 may therefore interact with DCC in the same way and through two distinct binding sites like netrin-1.

Sequence alignment of netrin-1 and homologues of *H. sapiens*, *M. musculus* (Uniprot: O09118), *D. rerio* (Uniprot: O42203), *X. laevis* (Uniprot: O57339), *D. melanogaster* (Uniprot: Q24567) and *C. elegans* (UNC-6, Uniprot: P34710) revealed a complete conservation of binding site 2 from human to the frog *Xenopus laevis* (*X. laevis*) (Fig. 31 B, blue boxes). In *C. elegans* the arginine 317 is substituted by a methionine. UNC-6 is known to bind to UNC-40, the DCC homologue (Chan et al., 1996) therefore it does not seem to prevent binding but might change the chloride binding site. In *D. melanogaster* Tyr 323 is substituted by a phenylalanine and Arg 349 by a glutamine. The fruit fly homologue of the netrin receptor DCC is Frazzled and known to bind netrin (Hiramoto et al., 2000). Therefore, the amino acid substitutions of binding site 2 are not affecting binding or binding does not require binding site 2. Binding site 1 is conserved among the species to an even higher degree (Fig. 31 B, pink boxes). The residues Gln 443 and Val 409, Val 429, Pro 450, involved in hydrophobic interactions are present in all organisms. The sulphate binding residues Arg 436 and Lys 439 are conserved as well. The amino acid sequence alignment showed, that the mechanisms of binding between netrin-1 (UNC-6) and the receptor DCC (UNC-40 in *C. elegans*, Frazzled in *D. melanogaster*) are evolutionary conserved from the netrin-1 site. This allows the conclusion, that axon guidance during neuronal wiring is a highly conserved process during the development of bilaterally organised organisms. The knowledge obtained by the structural and functional analysis of human Netrin_{VIV} and DCC_{FN56} can be projected onto the mechanisms occurring during axon growth, tissue development and cancer involving netrin-1/DCC signalling in other organisms as well.

4.c.2. Conservation of netrin-1 binding sites on DCC and neogenin

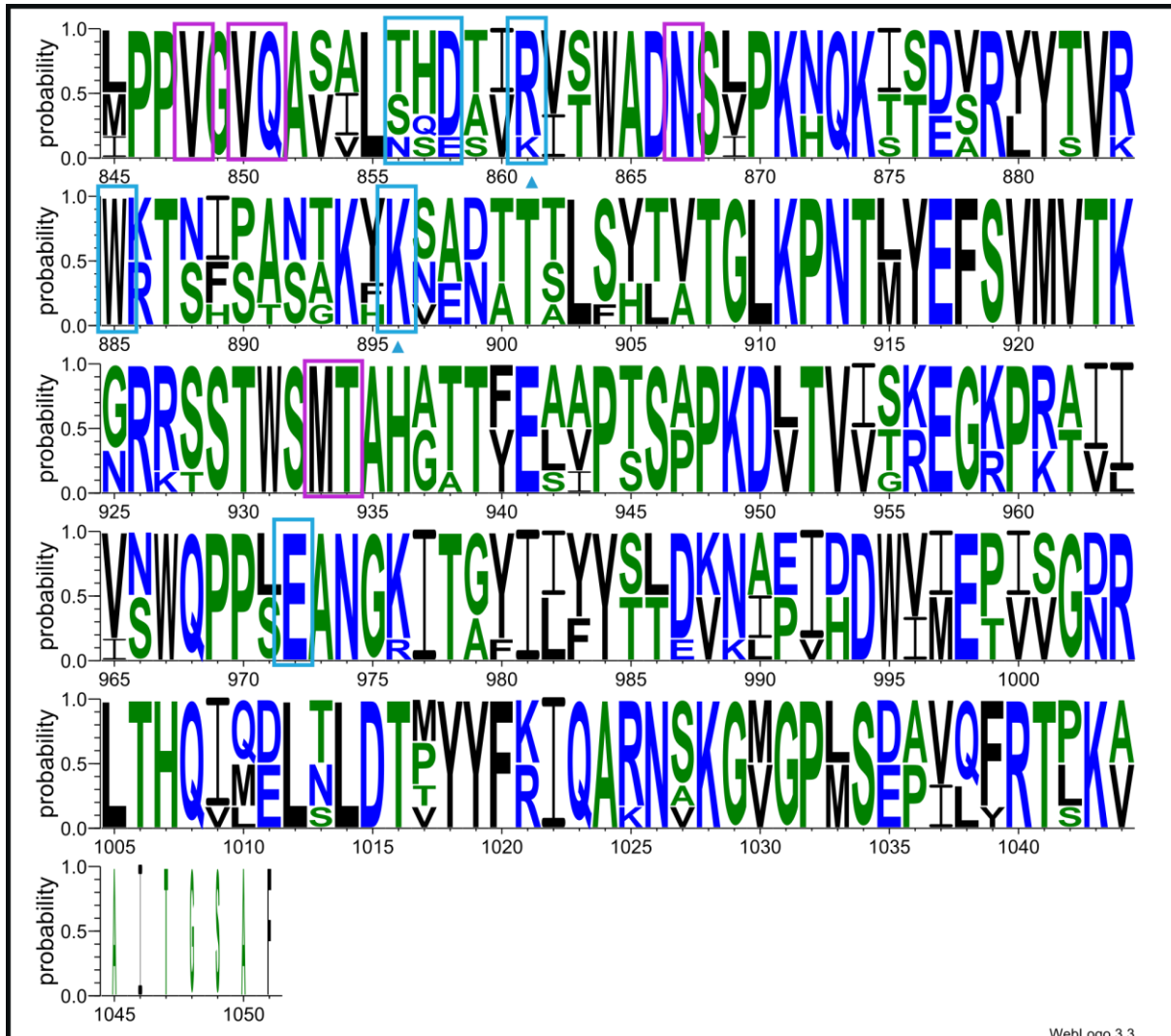


Figure 32 Sequence logo representation of residue conservation of domain FN5 and FN6 of DCC compared to neogenin from *H.sapiens* (Uniprot: P43146, Q92859), *M.musculus* (Uniprot: P70211, P97798), and *D.erio* (Uniprot: Q49BB0, Q801M2). Residues of binding site 1 are marked in pink boxes, residues of site 2 in cyan boxes, residues coordinating sulphate ions in binding site 2 are marked with cyan arrow heads. Blue: hydrophilic residues, green: neutral residues, black: hydrophobic residues. Alignment was done with Clustal Omega (Sievers and Higgins, 2014), sequence logo representation with Weblogo3 (Crooks et al., 2004)

Neogenin and DCC are closely related and have a sequence identity of more than 50% (Fig. 32). Studies of the axon guidance in chicken suggest that neogenin could act as a substitution for DCC (Phan et al., 2011) in binding to netrin and mediating a positive response. In mammals neogenin is involved in the development of the forebrain and the olfactory bulb (Bradford et al., 2010) and in interaction with netrin-4 to inhibit angiogenesis (Lejmi et al., 2008).

To evaluate, if neogenin could bind to netrin-1 through the same binding sites as DCC, the sequences of the FN5 and FN6 domain of human, murine and zebra fish DCC were aligned to the respective sequences of neogenin. Since netrin-4 does not contain the binding sites for DCC observed for netrin-1, 3 and 5 it must bind through other mechanisms to neogenin.

Binding site 1 is not only conserved among the vertebrate species, it is present as a conserved binding site in neogenin as well (Fig. 32, pink boxes).

The residues involved in sulphate binding on site 2, Arg 861, Trp 885, Lys 896, Lys 911, Tyr 916 and Glu 972 were confirmed to be highly conserved in vertebrates (Fig. 32, blue boxes). The residues that are involved in direct protein-protein contact and chloride coordination are not conserved to the same degree, but substitutions mainly occur with amino acids of comparable charge and size. The results of the sequence alignments led to the assumption, that neogenin interacts with netrin-1 through the same binding mechanisms like DCC. Therefore, it could take DCCs role and replace it in organisms or tissues that do not express DCC (Phan et al., 2011).

5. Discussion and Conclusion

5. a. Discussion

This study presents the expression and purification of a human netrin-1 construct (Netrin_{VIV}) that was confirmed to be sufficient to bind to the fibronectin domains 5 and 6 of DCC. Two distinct binding sites were found by structural analysis of Netrin_{VIV} in a complex with DCC_{FN56}. The affinities of both binding sites were investigated *in-vitro* and different preferences were observed. *In-vivo* experiments confirmed that the integrity of both binding sites is necessary for signal transduction and axon guidance. Sequence analysis revealed their evolutionary conservation between different species.

5.a.1. Expression, purification and characterisation of Netrin_{VIV}

In chapter 4.a. the establishment of a protocol for recombinant expression and purification of a human netrin-1 construct comprised of the VI domain followed by the three EGF-hands of the V domain is presented. This construct contains four predicted glycosylation sites and several, disulphide bonds forming cysteine residues. Therefore, Netrin_{VIV} was expressed in HEK293T cells. This adherent growing, human cell line was found in earlier studies to be robust, easy to transfect and reliable in expression yield (Aricescu et al., 2006b; Krüger, 2011). Expression was initiated by transient transfection and recombinant proteins were secreted into the culture medium. Since the expression yield of full-length netrin-1 was found to be low and not sufficient for structural studies, the substitution with a potentially more efficient secretion signal was tested. The change of the native signal peptide to the PSG1 signal peptide resulted in elevated expression of truncated netrin-1 constructs in small scale trials and led to protein yields in milligram quantities in large scale expression (> 1L). Human PSG1 is a highly expressing pregnancy hormone (Bohn, 1971), with top serum concentrations of 200–400 µg/ml at term (Lin et al., 1974) while netrin-1 is expressed to form local gradients during embryonic development to

guide migrating axons on a well-defined path. Therefore, it can be assumed that their expression is regulated in different ways. Among other factors the expression can be controlled by the secretion efficiency (Knappskog et al., 2007). Here, it was shown, that the composition of the signal peptide can influence secretion efficiency and therefore protein yield.

In a comparative study, the Netrin_{VIV} construct, containing the PSG1 signal peptide expressed better than the same construct with the native secretion signal. However, all constructs containing this N-terminal domain expressed better than the V domain alone. The laminin domain might aid in the stabilisation of the EGF-repeats, especially because it cannot be excluded, that the domain boundaries of the Netrin_V construct were not correctly chosen. This could result in poor expression yield, as well as instability of the protein (Hamill, Meekhof et al. 1998).

Along with protein aggregation and instability, the main challenge during the establishment of the purification protocol was the persistent contamination with BSA from the culture medium. Shortening the purification protocol by using Ni SepharoseTM excel and avoiding dialysis improved protein stability, as well as the reduction of the buffer pH to 6.0 and the addition of calcium chloride, but did not lead to reduction of BSA contamination. BSA contains 17 histidine residues (Uniprot: P02769), possibly explaining the continuous nonspecific pull down by different metal ion coupled affinity matrices. The molecular weights of BSA (66 kDa) and the Netrin_{VIV} construct (55.5 kDa) are too close to guarantee complete separation by size exclusion chromatography. The separation of glycoproteins from non-glycosylated contaminants by binding to a concanavalin A coupled matrix was shown to be functional, but protein loss during the procedure was high and reproducibility low. Also Ion exchange did not improve separation of the two, in theory oppositely charged proteins. The observation that Netrin_{VIV} eluted at least partially together with BSA indicated that it bound despite the predicted charge incompatibility to the ion exchange column. Theoretical net charges of glycosylated proteins can vary substantially from the actual net charges in solution (Sola and Griebenow, 2009). Therefore, the suitable matrix for ion exchange has to be determined experimentally and predicted charges might not be reliable.

Protein precipitation by salting out with agents such as ammonium sulphate or PEI did not lead to satisfying separation either. The concentration intervals chosen were possibly too wide to observe salting out of BSA and Netrin_{VIV} at different salt

concentrations. The only viable method to avoid BSA contamination was the reduction of FCS in the culture medium. Minimising the nutrients provided by the FCS supplementation of the culture medium bears the risk of severe reduction of expression efficiency, resulting in low recombinant protein yields. In this case the expression yield was not affected, in contrast the opposite was observed. Improved purification conditions and shortening of the turn-over times resulted in higher yields of proteins that were recovered to 95% purity and concentrated to the final concentration of 100 μ M for crystallisation. Therefore, the advantage of FCS reduction in the culture medium succeeded possible down-sides, especially when the loss of protein during complicated, multistep protocols is taken into account.

Glycosylation is necessary for correct folding (Chang et al., 2007), but working with glycosylated proteins confronts the investigator with a number of difficulties. The chemical conformation of carbohydrate moieties can be heterogeneous (Chang et al., 2007), subsequently variations between expression batches were observed by MS analysis. The main peaks shifted depending on the expression batch between 55000 and 56000 Da, and peaks appeared broad, an indication of heterogeneity within the sample. This inhomogeneity might be, apart from the chosen crystallisation conditions, the reason why crystallisation attempts with the fully glycosylated Netrin_{VIV} were not successful. The MS results showed as well, that the degree of heterogeneity within the samples varied between the batches, explaining why later crystallisation trials in the complex set-up might have been more successful. Here, randomly a more homogenous sample could have been obtained. Mass spectrometric analysis could therefore be a useful control technique to monitor the grade of glycosylation. Subsequently, only protein sample with higher, internal homogeneity should be further processed for crystallisation. An alternative possibility is the expression in cell lines, such as the HEK 293S cells that lack the *N*-acetylglucosaminyltransferase I (GnTI) activity resulting in less complex N-glycans (Reeves et al., 2002), leaving them more accessible to deglycosylation agents like endoglycosidase H. However, this cell line often shows reduced expression yields (Chang et al., 2007). Experiments with the Netrin_{VIV} construct (data not presented in this study) indicated along with lower yields, the destabilisation of the protein during the deglycosylating treatment. Therefore, it was not further considered, but future studies could engage in the optimisation of the deglycosylation treatment or the use of the α -mannosidase inhibitors kifunensine and swainsonine that were shown affect

expression yields less (Chang et al., 2007).

A stabilising effect of CaCl_2 was noticed in a thermofluor experiment (Fig. 10) after the presence of a calcium binding site in the laminin VI domain of Netrin_{VIV} (in complex with DCC_{FN56}) was confirmed in the crystal structure. Supporting evidence was obtained by the destabilisation of Netrin_{VIV} after addition of EDTA, a chelating agent that forms complexes with cations such as Ca^{2+} . A calcium binding motif was already proposed earlier, based on crystal structure of netrinG2 (Brasch et al., 2011). The addition of different sulphate salts in the thermofluor assay, among them ammonium sulphate (as present in the complex crystal condition) had no contributing effect on protein stability that exceeded those of pH reduction or CaCl_2 addition, although clusters of sulphate ions were observed in the crystal structure of binding site 2 and in the periphery of binding site 1. For SAXS, the presence of sulphate was necessary to prevent aggregation in higher concentrations ($>50 \mu\text{M}$), but these concentrations might not resemble physiological conditions. Therefore, it was concluded, that sulphate ions are not necessary for stabilisation in solutions of lower concentrations, but negatively charged ions are needed to bridge between positive patches on binding site 2 to mediate receptor-ligand binding. This finding supports the hypothetical model (Fig. 1) where specific HSPGs or heparin could be responsible for the recruitment of distinct receptor molecules.

Similar protein yields of the Netrin_{VIV} mutant constructs were obtained, despite the fact that reduced expression was observed for the binding site 2 mutants in small scale expression trails. This showed that the same purification protocol described for the Netrin_{VIV} wt can be used for the mutant constructs without compromising on the protein yield. Expression and function of GFP-fusion constructs were confirmed after purification. These constructs could be used in future binding studies and cell culture based assays to detect binding or netrin-1 localisation without labelling or antibody detection.

5.a.2. Netrin-1 and DCC

Chapter 4.b. presents a close investigation of the molecular binding mechanisms between the guidance cue molecule netrin-1 and its receptor DCC. An *in-vitro* binding experiment showed that the construct containing the fibronectin domains FN5 and FN6 is sufficient to bind Netrin_{VIV}. *In-vivo* binding studies and axon guidance experiments confirmed that Netrin_{VIV} is sufficient to mediate binding and signal transduction. This observation was confirmed by a thermofluor assay where thermal stability increased upon binding to DCC_{FN56}, while the addition of a construct containing the fourth fibronectin domain alone (DCC_{FN4}) or preceding the FN5 and FN6 (DCC_{FN456}) did not show any further stabilisation. The T_m shift observed for complex formation indicated a higher degree of stabilisation compared to CaCl₂ addition and buffer optimisation. This indicates that binding occurs within the domains FN5 and FN6, although it cannot be excluded, that FN4 or other domains contribute in binding (Kruger et al., 2004) and initiation of signal transduction *in-vivo*. Additional to the finding that a positive locomotive response of the growth cone requires a specific conformation of the Ig-domains of DCC, it was also shown that they do not participate in netrin-1 binding (Chen et al., 2013).

The structure of Netrin_{VIV} showed that the N-terminal domain has a typical laminin fold as observed previously for the laminin γ -1 LN-domain (Carafoli et al., 2012) which also contains a Ca²⁺ binding site. Ca²⁺ contributes to protein stability as observed in the thermofluor assay of Netrin_{VIV}, however, these results do not suggest a direct association of this ion binding site with the netrin-1 dependent increase of Ca²⁺ in the growth cone (Hong et al., 2000). The requirement of extracellular Ca²⁺ for axon branching coinciding with netrin-1 induced Ca²⁺ transients (Tang and Kalil, 2005) could indicate that netrin-1 half-life at sites of high extracellular calcium concentrations is increased and axon branching could therefore be promoted.

The structure of the fibronectin type III domains of the DCC_{FN56} construct revealed a linear arrangement in complex with Netrin_{VIV} similar to the arrangement of the FN5 and FN6 domains of neogenin. FN5 of neogenin shows the same positive surface charges as DCC proposed to interact with HSPGs (Bennett et al., 1997; Yang et al., 2011).

Deeper insight into the interactions between the FN5 and FN6 domains of DCC

and the EGF domains of netrin-1 was gained from the structural analysis of the Netrin_{VIV} / DCC_{FN56} complex. No information was obtained for constructs including the FN4 domain of DCC due to the lack of protein crystals from these set-ups. Therefore, no supporting evidence was found for the involvement of domain FN4 as suggested by other studies (Kruger et al., 2004).

Disproving studies stating no direct binding (Meyerhardt et al., 1999), Netrin_{VIV} binds DCC_{FN56} with two distinct binding sites located on the same side of the EGF-repeats of the V domain. The participation of intrinsic parts of the V domain in specific axon guidance events has been shown for *C. elegans* (Lim and Wadsworth, 2002), but confirmation for the also reported requirement of the VI domain was not observed in the crystal structure. Contacts to the glycosylation sites were not present and the distance between the two DCC molecules excluded direct contact of the basal receptor ectodomain parts during binding. The orientation of the DCC domains would not prohibit interaction of the N-terminal parts of the ectodomains *in-vivo*. Nevertheless, it was reported that dimerisation of the cytosolic domains is occurring independently from the ectodomains (Stein et al., 2001).

A 1:2 binding mode was observed where Netrin_{VIV} associated with two DCC_{FN56} molecules, despite the 1:1 stoichiometry in the crystallisation set-up. This finding was surprising and clearly differentiates netrin-1/DCC binding from other guidance cue complexes where a symmetric 2:2 stoichiometry is typically observed allowing the formation of extended signalling clusters (Bell et al., 2013; Janssen et al., 2010). The angular tilt of the DCC_{FN56} molecules bound to Netrin_{VIV} limits the size of receptor ligand clusters that could be obtained by binding of multiple netrin-1 molecules to receptors in close proximity. The formation of a modelled, extended zipper-like cluster of different receptors is not well supported by the orientation of the DCC_{FN56} molecules in complex with Netrin_{VIV}, but response to as little as five netrin-1 molecules was observed by Pinato and colleagues (Pinato et al., 2012). Together with the binding observed in the crystal structure, this indicates that an extend cluster of multiple netrin-1/DCC complexes could be non-essential to initiate signal transduction as previously proposed for other guidance cue signalling complexes (Bell et al., 2013).

SAXS studies showed that both sites exist and are occupied in solution with clear preference for binding site 1. The integrity of both binding sites is necessary for positive axon guidance *in-vivo* and receptor clustering by netrin-1 *in-vitro* and *in-vivo*.

Whether the concentration of a netrin-1 gradient is the driving force in clustering DCC to create a positive response or other mechanisms, such as interactions with cell surface proteoglycans promote the recruitment of netrin-1 molecules remains unclear from the experimental data.

Binding site 2 is characterised by the presence of highly positive charged patches on the binding interface of both, receptor and ligand. These surface charges would lead to electrostatic repulsion if they would not be covered by negatively charged sulphate ions and a chloride ion that bridge between amino acid side chains of the molecules. The close proximity of the residues involved in sulphate ion coordination provides a structural conformation that allows their embedding into the surface of the EGF1 and EGF2 domain of netrin-1. Sequence alignments of different human netrins showed that the residues for sulphate coordination are conserved in netrin-1, netrin-3 and netrin-5, indicating the presence of a similar binding site also on the other two netrins. These residues are evolutionary fully conserved within the netrin-1 homologues of vertebrates indicating the conservation of this binding mechanism.

Arginine/lysine/sulphate clusters have been linked before to heparan sulphate binding (Tan et al., 2008) and the residues that participate in ion coordination on netrin-1 could provide the flexibility necessary to accommodate HSPG or heparin molecules instead of single ions. Heparin and HSPGs are structurally related, highly-sulphated polysaccharides that are synthesised through the same pathways, but HSPGs remain connected to their core protein (Capila and Linhardt, 2002). HSPGs and heparin can act as co-receptors or activators to mediate binding between receptors and ligands involved in angiogenesis, cell migration and cell adhesion, to the extracellular matrix (Gallagher, 2001). HSPGs have even been shown to control cell migration and influence guidance cues by opening growth factor binding sites on fibronectin domains that were otherwise masked (Symes et al., 2010). The involvement of HSPGs or heparin could allow other receptors with similar positive patches (like DCC) to rearrange binding sites to adapt the interface according to the respective requirements depending on the structural context.

A model where the presence of specific sulphated polysaccharides mediates the recruitment and binding of a compatible second receptor to binding site 2 after binding site 1 has been occupied (Fig. 1) is supported by two experimental findings. Firstly, the binding of heparin and heparan sulphates has been confirmed for netrin-1 (Geisbrecht et al., 2003) and for DCC on, or close to, the binding domains (Bennett et

al., 1997) as well as for other fibronectin type III domains (McLellan et al., 2006). Secondly, predominance for occupation of binding site 1 in solution was observed in SAXS measurements and thermophoresis, supporting the theory that recruitment occurs by HSPGs or heparin mediation after netrin-1 bound with its specific site 1 to DCC. Furthermore, in SAXS only a small portion of the molecules in solution formed clusters with full occupation of both binding sites of Netrin_{VIV} indicating that factors other than single ions might be involved in receptor-ligand interactions.

UNC5 was shown to bind netrin-1 through heparin (Geisbrecht et al., 2003) and fits therefore in a scenario where the selection of receptors for functional dimerisation is influenced by sulphated sugar molecules. These observations could give a first indication on how netrin-1 signalling contributes in the fine-tuning orchestration of axon guidance by mediating attractive or repulsive responses depending on the receptors present.

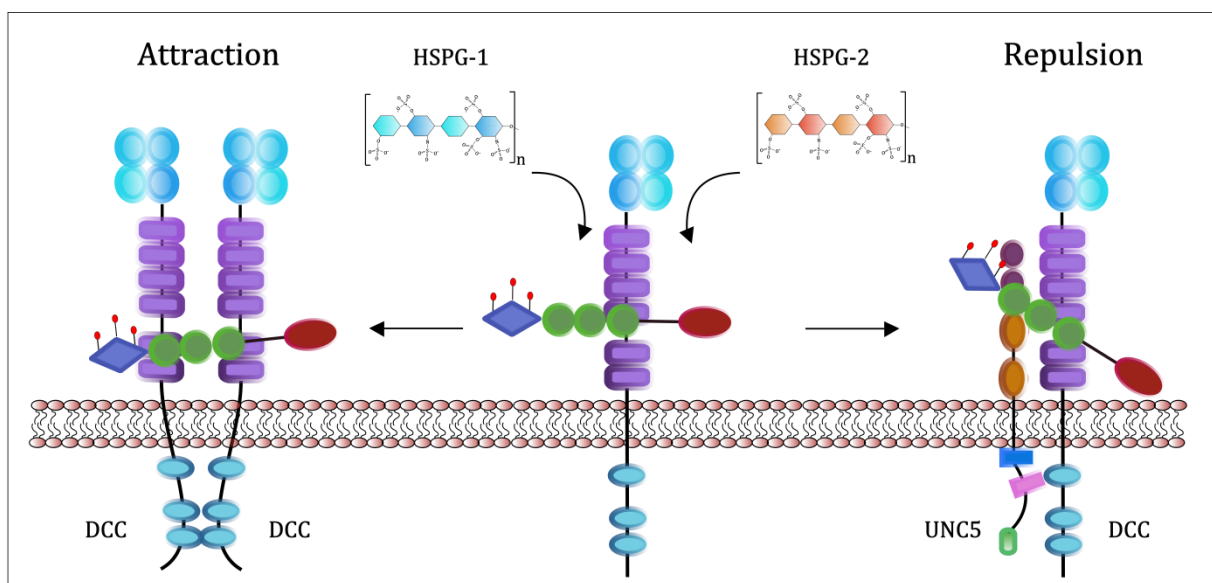


Figure 1 Modelled complex formation of DCC/DCC or DCC/UNC5 receptor complexes with netrin-1 mediated by specific heparan sulphate proteoglycans (HSPG) on a growth cone. **Attraction** Netrin-1 binds specifically to domain FN5 of the receptor DCC (binding site 1); the presence of a HSPG-1 molecule mediates the recruitment of a second DCC binding to site 2 on netrin-1 leading to homo-dimerisation of the intracellular receptor domains P3 and an attraction response of the growth cone. **Repulsion** the presence of a different HSPG-2 leads to recruitment of a UNC5 instead of a second DCC, resulting in intracellular hetero-dimerisation between the UPA-domain of UNC5 and the P1 of DCC.

The assistance of bridging molecules in the binding interface is further supported by occurrence of homo- and hetero-dimerisation on the cytosolic domains of DCC and UNC5 (Stein and Tessier-Lavigne, 2001; Stein et al., 2001; Xie et al., 2006). Netrin-1 represents an interesting modular concept of receptor pairing, where distinct

binding sites are arranged in close proximity to initiate certain cytosolic interactions with different receptors leading to alternate guidance events. The model described here could explain netrin-1's bi-functionality. The influence of heparin or HSPGs is a likely possibility during netrin-1 mediated axon guidance and should be investigated in future studies. Additionally, sequence alignment showed that binding site 2 is mostly conserved in DCC and neogenin. This binding site is located on neogenin at the border of the binding site to the repulsive guidance molecule B (RGMB) which is supposed to compete with netrin-1 (Bell et al., 2013) to suppress RGMB mediated growth cone collapses (Conrad et al., 2007). A sulphated saccharide was found on loop 5 of the FN5 domain of in the crystal structure of neogenin (Bell et al., 2013), the same region that on DCC is involved in binding site 2 (Geisbrecht et al. (2003), this study). Applying the model described above, netrin-1 could disrupt the 2:2 neogenin/RGMB complex by binding first to site 1 without interfering and then disintegrate the complex previously formed by binding to site 2. This would rearrange the orientation of the receptors and alter the signal transduced through the membrane. Similar to the observations for Netrin_{VIV}, that protein stability is supported at pH 6.0 but binding to DCC is only observed at neutral pH, binding of RGMA to neogenin to site 2 is pH dependent (Bell et al., 2013).

While binding site 2 could accommodate a wide range of receptor molecules, binding site 1 appears to be more specific to interactions between netrin-1 and DCC or neogenin (as the sequence alignment showed). The binding interface is characterised by direct protein-protein contacts rather than by bridging ions. Binding site 1 is conserved to an even higher degree than binding site 2 in netrins, DCC and neogenin supporting the evolutionary importance of this binding site. As seen for binding site 2, netrin-3 and netrin-5 are proposed to bind DCC and neogenin through binding site 1 in a similar way.

Thermophoresis showed that the binding affinity for site 1 dominates *in-vitro* in wildtype interactions and separation of the two binding sites could only be observed for constructs with mutations in one of the binding sites. Therefore, a dose-response equation was applied to obtain EC₅₀ and K_d values. The calculated affinities are consistent with earlier binding studies (Keino-Masu et al., 1996) and a higher, and therefore, dominating affinity for binding site 1 was supported by the predominant occupation of this site observed in SAXS studies.

5. b. Conclusion

The discovery that netrin-1 binds to two DCC receptor molecules with distinct binding sites and the unravelling of their different binding mechanisms and affinities provides an insight into how netrin-1 guidance cues can influence the path migrating cells take on their journey. The selection of receptors present together with the proposed effector molecules directly determines the outcome of signals created in response to a netrin-1 gradient. Although it was shown that extended netrin-1/DCC clusters are not supported, the interaction with other receptor molecules, possibly together with competing ligands as seen in the neogenin/RGMA complex for example, could provide a reasonable concept for netrin-1 mediated receptor clustering. These interactions could integrate different guidance cues in a hierarchical fashion, offering new explanations for sensitivity switches observed in axon turning (Stein and Tessier-Lavigne, 2001). This could be seen as an important step in the direction to understand how the essential connections in the nervous system are established during development and maintained in adult tissues. Furthermore, these findings could be transferable to multiple processes during organ development, angiogenesis and pathological conditions, such as certain cancers and neurodegenerative diseases where participation of netrin-1 and its receptors has been shown.

Therefore, the results of this study could lead to new impulses in a diverse number of research fields studying guidance cues and netrin-1 signalling. Future studies could question how heparin and heparan sulphate proteoglycans influence the receptor subset chosen to bind netrin-1 and if other receptors could utilise similar binding sites or developed other specific ways of interaction. The residue composition determined for the respective binding sites could lead to the identification of additional receptors for netrin-1, for instance by data base searches, leading to an even more detailed picture of the netrin guidance code.

6. Acknowledgements

Firstly, I would like to thank Dr. Rob Meijers for giving me the opportunity to carry out this research project under his supervision. I am grateful for his support, advice and critical discussion. I learnt a lot during this time.

I would also like to express my gratitude to JProf. Dr. Christian A. Voigt and Prof. Dr. Christian Lohr for agreeing to take part in my thesis committee

Prof. Dr. Jia-Huai Wang, I would like to thank for a very fruitful collaboration, critical discussion and for his motivating words. Dr. Lorenzo Finci, I show a lot of respect for his unbelievable dedication to this project and his travels around the world. I also thank him for his persisting will to assist, critical discussion and for reading this manuscript. Without him, this project would not have been the same; I wouldn't have tried Chinese chocolate or eaten the most expensive paella of my life.

Dr. Yan Zhang and Xiaqin Sun I would thank for their collaboration by performing the functional assays that finally confirmed the biological relevance of the samples and results. Dr. Dmitri Svergun, Dr. Gundolf Schenk and Dr. Haydyn Mertens I would like to thank for their help during the SAXS experiments and data analysis. I also thank Jie Zhang and Yu Wu for supporting this project. Dr. Jonathan Rapley I would like to thank for doing the first steps in this project and being a friend.

Magda Chegkazi, you have my honest respect for your strength. Your help, explanations and support really made a difference. I am grateful that we eventually started to work together. Dr. Anna Gieras and Matthew Dunne, I want to thank you for reading this manuscript and your advice. Your support and friendship was priceless, and I don't think that I would have handled the pressure without you, especially when tables are disappearing a few hours before the deadline. Furthermore, I would like to thank every current or former inhabitant of Meijers Island and the SPC team for assistance.

My love and my deep gratitude go to my family. You always kept me going on the many roads I travelled and taught me the meaning of "blood is thicker than water". C., you have been a great coach. Thank you for motivation. S., thank you for reminding me of Septoman and critical discussion of science. Finally, H., R. and H, thank you for your company during the endless nights of writing.

7. References

. PROTEIN CALCULATOR v3.3 (<http://www.scripps.edu/~cdputnam/protcalc.html>).

Afonine, P.V., Grosse-Kunstleve, R.W., Echols, N., Headd, J.J., Moriarty, N.W., Mustyakimov, M., Terwilliger, T.C., Urzhumtsev, A., Zwart, P.H., and Adams, P.D. (2012). Towards automated crystallographic structure refinement with phenix.refine. *Acta crystallographica Section D, Biological crystallography* 68, 352-367.

Ahmed, G., Shinmyo, Y., Ohta, K., Islam, S.M., Hossain, M., Naser, I.B., Riyadh, M.A., Su, Y., Zhang, S., Tessier-Lavigne, M., *et al.* (2011). Draxin inhibits axonal outgrowth through the netrin receptor DCC. *The Journal of neuroscience : the official journal of the Society for Neuroscience* 31, 14018-14023.

Alberts, J., Lewis, Raff, Roberts and Walter (2004). Neuronale Entwicklung. In *Molekularbiologie der Zelle*, W. Jacoby, ed. (Wiley-VCH Verlag), p. 1430 ff

Alcantara, S., Ruiz, M., De Castro, F., Soriano, E., and Sotelo, C. (2000). Netrin 1 acts as an attractive or as a repulsive cue for distinct migrating neurons during the development of the cerebellar system. *Development* 127, 1359-1372.

Aricescu, A.R., Assenberg, R., Bill, R.M., Busso, D., Chang, V.T., Davis, S.J., Dubrovsky, A., Gustafsson, L., Hedfalk, K., Heinemann, U., *et al.* (2006a). Eukaryotic expression: developments for structural proteomics. *Acta crystallographica Section D, Biological crystallography* 62, 1114-1124.

Aricescu, A.R., Lu, W., and Jones, E.Y. (2006b). A time- and cost-efficient system for high-level protein production in mammalian cells. *Acta crystallographica Section D, Biological crystallography* 62, 1243-1250.

Bagri, A., and Ashkenazi, A. (2010). UNCovering the molecular machinery of dependence receptor signaling. *Mol Cell* 40, 851-853.

Baldi, L., Hacker, D.L., Adam, M., and Wurm, F.M. (2007). Recombinant protein production by large-scale transient gene expression in mammalian cells: state of the art and future perspectives. *Biotechnology letters* 29, 677-684.

Banerjee, A.K. (1997). DCC expression and prognosis in colorectal cancer. *Lancet* 349, 968.

Barbosa, L.R., Ortore, M.G., Spinozzi, F., Mariani, P., Bernstorff, S., and Itri, R. (2010). The importance of protein-protein interactions on the pH-induced conformational changes of bovine serum albumin: a small-angle X-ray scattering study. *Biophys J* 98, 147-157.

Bell, C.H., Healey, E., van Erp, S., Bishop, B., Tang, C., Gilbert, R.J., Aricescu, A.R., Pasterkamp, R.J., and Siebold, C. (2013). Structure of the repulsive guidance molecule (RGM)-neogenin signaling hub. *Science* 341, 77-80.

Bennett, K.L., Bradshaw, J., Youngman, T., Rodgers, J., Greenfield, B., Aruffo, A., and Linsley, P.S. (1997). Deleted in colorectal carcinoma (DCC) binds heparin via its fifth fibronectin type III domain. *The Journal of biological chemistry* 272, 26940-26946.

Blow, D. (2010). *Outline of Crystallography for Biologists* (Ixford: Oxford University Press).

Bohn, H. (1971). [Detection and characterization of pregnancy proteins in the human placenta and their quantitative immunochemical determination in sera from pregnant women]. *Archiv fur Gynakologie* 210, 440-457.

Boivin, S., Kozak, S., and Meijers, R. (2013). Optimization of protein purification and characterization using Thermofluor screens. *Protein expression and purification* 91, 192-206.

Bradford, D., Faull, R.L., Curtis, M.A., and Cooper, H.M. (2010). Characterization of the netrin/RGMA receptor neogenin in neurogenic regions of the mouse and human adult forebrain. *The Journal of comparative neurology* 518, 3237-3253.

Brasch, J., Harrison, O.J., Ahlsen, G., Liu, Q., and Shapiro, L. (2011). Crystal structure of the ligand binding domain of netrin G2. *Journal of molecular biology* 414, 723-734.

Breasted, J.H. (1980). *The Edwin Smith surgical papyrus, Vol 2* (Chicago: Univ. Chicago Press).

Burgess, R.W., Jucius, T.J., and Ackerman, S.L. (2006). Motor axon guidance of the mammalian trochlear and phrenic nerves: dependence on the netrin receptor *Unc5c* and modifier loci. *The Journal of neuroscience : the official journal of the Society for Neuroscience* 26, 5756-5766.

Capila, I., and Linhardt, R.J. (2002). Heparin-protein interactions. *Angew Chem Int Ed Engl* 41, 391-412.

Carafoli, F., Hussain, S.A., and Hohenester, E. (2012). Crystal structures of the network-forming short-arm tips of the laminin beta1 and gamma1 chains. *PLoS one* 7, e42473.

Carter, C.W., Jr., and Carter, C.W. (1979). Protein crystallization using incomplete factorial experiments. *The Journal of biological chemistry* 254, 12219-12223.

Castets, M., Coissieux, M.M., Delloye-Bourgeois, C., Bernard, L., Delcros, J.G., Bernet, A., Laudet, V., and Mehlen, P. (2009). Inhibition of endothelial cell apoptosis by netrin-1 during angiogenesis. *Developmental cell* 16, 614-620.

Chan, S.S., Zheng, H., Su, M.W., Wilk, R., Killeen, M.T., Hedgecock, E.M., and Culotti, J.G. (1996). UNC-40, a *C. elegans* homolog of DCC (Deleted in Colorectal Cancer), is required in motile cells responding to UNC-6 netrin cues. *Cell* 87, 187-195.

Chang, V.T., Crispin, M., Aricescu, A.R., Harvey, D.J., Nettleship, J.E., Fennelly, J.A., Yu, C., Boles, K.S., Evans, E.J., Stuart, D.I., *et al.* (2007). Glycoprotein structural genomics: solving the glycosylation problem. *Structure* 15, 267-273.

Chatterjee, N., and Sinha, S. (2008). Understanding the mind of a worm: hierarchical network structure underlying nervous system function in *C. elegans*. *Progress in brain research* 168, 145-153.

Chen, Q., Sun, X., Zhou, X.H., Liu, J.H., Wu, J., Zhang, Y., and Wang, J.H. (2013). N-terminal horseshoe conformation of DCC is functionally required for axon guidance and might be shared by other neural receptors. *Journal of cell science* 126, 186-195.

Chen, V.B., Arendall, W.B., 3rd, Headd, J.J., Keedy, D.A., Immormino, R.M., Kapral, G.J., Murray, L.W., Richardson, J.S., and Richardson, D.C. (2010). MolProbity: all-atom structure validation for macromolecular crystallography. *Acta crystallographica Section D, Biological crystallography* 66, 12-21.

Cheng, Y., and Prusoff, W.H. (1973). Relationship between the inhibition constant (K_1) and the concentration of inhibitor which causes 50 per cent inhibition (I_{50}) of an enzymatic reaction. *Biochemical pharmacology* 22, 3099-3108.

Cho, K.R., and Fearon, E.R. (1995). DCC: linking tumour suppressor genes and altered cell surface interactions in cancer? *Eur J Cancer* 31A, 1055-1060.

Clackson, T., and Wells, J.A. (1995). A hot spot of binding energy in a hormone-receptor interface. *Science* 267, 383-386.

Coissieux, M.M., Tomsic, J., Castets, M., Hampel, H., Tuupainen, S., Andrieu, N., Comeras, I., Drouet, Y., Lasset, C., Liyanarachchi, S., *et al.* (2011). Variants in the netrin-1 receptor *UNC5C* prevent apoptosis and increase risk of familial colorectal cancer. *Gastroenterology* 141, 2039-2046.

Conrad, S., Genth, H., Hofmann, F., Just, I., and Skutella, T. (2007). Neogenin-RGMA signaling at the growth cone is bone morphogenetic protein-independent and involves RhoA, ROCK, and PKC. *The Journal of biological chemistry* 282, 16423-16433.

Cooper, H.M., Armes, P., Britto, J., Gad, J., and Wilks, A.F. (1995). Cloning of the mouse homologue of the deleted in colorectal cancer gene (mDCC) and its expression in the developing mouse embryo. *Oncogene* 11, 2243-2254.

Cowtan, K. (2012). Completion of autobuilt protein models using a database of protein fragments. *Acta crystallographica Section D, Biological crystallography* 68, 328-335.

Crooks, G.E., Hon, G., Chandonia, J.M., and Brenner, S.E. (2004). WebLogo: a sequence logo generator. *Genome research* 14, 1188-1190.

Culotti, J.G. (1994). Axon guidance mechanisms in *Caenorhabditis elegans*. *Current opinion in genetics & development* 4, 587-595.

Culotti, J.G., and Merz, D.C. (1998). DCC and netrins. *Current opinion in cell biology* 10, 609-613.

de la Torre, J.R., Hopker, V.H., Ming, G.L., Poo, M.M., Tessier-Lavigne, M., Hemmati-Brivanlou, A., and Holt, C.E. (1997). Turning of retinal growth cones in a netrin-1 gradient mediated by the netrin receptor DCC. *Neuron* 19, 1211-1224.

Del Rio, J.A., Gonzalez-Billault, C., Urena, J.M., Jimenez, E.M., Barallobre, M.J., Pascual, M., Pujadas, L., Simo, S., La Torre, A., Wandosell, F., *et al.* (2004). MAP1B is required for Netrin 1 signaling in neuronal migration and axonal guidance. *Current biology : CB* 14, 840-850.

Demeneix, B., and Behr, J.P. (2005). Polyethylenimine (PEI). *Adv Genet* 53PA, 215-230.

Derewenda, Z.S. (2004). The use of recombinant methods and molecular engineering in protein crystallization. *Methods* 34, 354-363.

Drescher, U., Kremoser, C., Handwerker, C., Loschinger, J., Noda, M., and Bonhoeffer, F. (1995). In vitro guidance of retinal ganglion cell axons by RAGS, a 25 kDa tectal protein related to ligands for Eph receptor tyrosine kinases. *Cell* 82, 359-370.

Emsley, P., Lohkamp, B., Scott, W.G., and Cowtan, K. (2010). Features and development of Coot. *Acta crystallographica Section D, Biological crystallography* 66, 486-501.

Englard, S., and Seifter, S. (1990). Precipitation techniques. *Methods in enzymology* 182, 285-300.

Evans, P. (2006). Scaling and assessment of data quality. *Acta crystallographica Section D, Biological crystallography* 62, 72-82.

Fearon, E.R., Cho, K.R., Nigro, J.M., Kern, S.E., Simons, J.W., Ruppert, J.M., Hamilton, S.R., Preisinger, A.C., Thomas, G., Kinzler, K.W., *et al.* (1990). Identification of a chromosome 18q gene that is altered in colorectal cancers. *Science* 247, 49-56.

Fitamant, J., Guenebeaud, C., Coissieux, M.M., Guix, C., Treilleux, I., Scoazec, J.Y., Bachelot, T., Bernet, A., and Mehlen, P. (2008). Netrin-1 expression confers a selective advantage for tumor cell survival in metastatic breast cancer. *Proceedings of the National Academy of Sciences of the United States of America* 105, 4850-4855.

Franke, D., and Svergun, D.I. (2009). (2009). DAMMIF, a program for rapid ab-initio shape determination in small-angle scattering. *J Appl Crystallogr* 42, 342-346.

Franke, D., Kikhney, A.G., and Svergun, D.I. (2012). (2012). Automated acquisition and analysis of small angle X-ray scattering data. *Nucl Instrum Methods Phys Res Sect Accel Spectrometers Detect Assoc Equip* 689, 52-59.

Gallagher, J.T. (2001). Heparan sulfate: growth control with a restricted sequence menu. *The Journal of clinical investigation* 108, 357-361.

GEHealthcare (2010). Ion Exchange Chromatography and Chromatofocusing.

GEHealthcare (2011). Con A Sepharose TM 4B Handbook.

GEHealthcare (2012). Ni SepharoseTM excel handbook.

Geisbrecht, B.V., Dowd, K.A., Barfield, R.W., Longo, P.A., and Leahy, D.J. (2003). Netrin binds discrete subdomains of DCC and UNC5 and mediates interactions between DCC and heparin. *The Journal of biological chemistry* 278, 32561-32568.

Glatter O, K.O., ed. (1982). *Small Angle X-ray Scattering*. Academic Press.

Gouet, P., Robert, X., and Courcelle, E. (2003). ESPript/ENDscript: Extracting and rendering sequence and 3D information from atomic structures of proteins. *Nucleic acids research* 31, 3320-3323.

Green, N.M. (1990). Avidin and streptavidin. *Methods in enzymology* 184, 51-67.

Han, Y., Shao, Y., Lin, Z., Qu, Y.L., Wang, H., Zhou, Y., Chen, W., Chen, Y., Chen, W.L., Hu, F.R., *et al.* (2012). Netrin-1 simultaneously suppresses corneal inflammation and neovascularization. *Invest Ophthalmol Vis Sci* 53, 1285-1295.

Harris, R., Sabatelli, L.M., and Seeger, M.A. (1996). Guidance cues at the Drosophila CNS midline: identification and characterization of two Drosophila Netrin/UNC-6 homologs. *Neuron* 17, 217-228.

He, K., Jang, S.W., Joshi, J., Yoo, M.H., and Ye, K. (2011). Akt-phosphorylated PIKE-A inhibits UNC5B-induced apoptosis in cancer cell lines in a p53-dependent manner. *Molecular biology of the cell* 22, 1943-1954.

Hedgecock, E.M., Culotti, J.G., and Hall, D.H. (1990). The unc-5, unc-6, and unc-40 genes guide circumferential migrations of pioneer axons and mesodermal cells on the epidermis in *C. elegans*. *Neuron* 4, 61-85.

Hedrick, L., Cho, K.R., Boyd, J., Risinger, J., and Vogelstein, B. (1992). DCC: a tumor suppressor gene expressed on the cell surface. *Cold Spring Harbor symposia on quantitative biology* 57, 345-351.

Hiramoto, M., Hiromi, Y., Giniger, E., and Hotta, Y. (2000). The Drosophila Netrin receptor Frazzled guides axons by controlling Netrin distribution. *Nature* 406, 886-889.

Hong, K., Hinck, L., Nishiyama, M., Poo, M.M., Tessier-Lavigne, M., and Stein, E. (1999). A ligand-gated association between cytoplasmic domains of UNC5 and DCC family receptors converts netrin-induced growth cone attraction to repulsion. *Cell* 97, 927-941.

Hong, K., Nishiyama, M., Henley, J., Tessier-Lavigne, M., and Poo, M. (2000). Calcium signalling in the guidance of nerve growth by netrin-1. *Nature* 403, 93-98.

Horn, K.E., Glasgow, S.D., Gobert, D., Bull, S.J., Luk, T., Girgis, J., Tremblay, M.E., McEachern, D., Bouchard, J.F., Haber, M., *et al.* (2013). DCC expression by neurons regulates synaptic plasticity in the adult brain. *Cell reports* 3, 173-185.

Horn, K.E., and Kennedy, T.E. (2012). Putting flesh on the bones: DCC combines membrane insertion with cytoskeletal reorganization to promote chemoattraction (commentary on Cotrufo *et al.*). *The European journal of neuroscience* 36, 3151.

Islam, S.M., Shinmyo, Y., Okafuji, T., Su, Y., Naser, I.B., Ahmed, G., Zhang, S., Chen, S., Ohta, K., Kiyonari, H., *et al.* (2009). Draxin, a repulsive guidance protein for spinal cord and forebrain commissures. *Science* 323, 388-393.

Janssen, B.J., Robinson, R.A., Perez-Branguli, F., Bell, C.H., Mitchell, K.J., Siebold, C., and Jones, E.Y. (2010). Structural basis of semaphorin-plexin signalling. *Nature* **467**, 1118-1122.

Jarjour, A.A., Manitt, C., Moore, S.W., Thompson, K.M., Yuh, S.J., and Kennedy, T.E. (2003). Netrin-1 is a chemorepellent for oligodendrocyte precursor cells in the embryonic spinal cord. *The Journal of neuroscience : the official journal of the Society for Neuroscience* **23**, 3735-3744.

Jin, Z., and Strittmatter, S.M. (1997). Rac1 mediates collapsin-1-induced growth cone collapse. *The Journal of neuroscience : the official journal of the Society for Neuroscience* **17**, 6256-6263.

Kabsch, W. (2010a). Integration, scaling, space-group assignment and post-refinement. *Acta crystallographica Section D, Biological crystallography* **66**, 133-144.

Kabsch, W. (2010b). Xds. *Acta crystallographica Section D, Biological crystallography* **66**, 125-132.

Kanehisa, M., Goto, S., Sato, Y., Kawashima, M., Furumichi, M., and Tanabe, M. (2014). Data, information, knowledge and principle: back to metabolism in KEGG. *Nucleic acids research* **42**, D199-205.

Keino-Masu, K., Masu, M., Hinck, L., Leonardo, E.D., Chan, S.S., Culotti, J.G., and Tessier-Lavigne, M. (1996). Deleted in Colorectal Cancer (DCC) encodes a netrin receptor. *Cell* **87**, 175-185.

Keleman, K., and Dickson, B.J. (2001). Short- and long-range repulsion by the *Drosophila* Unc5 netrin receptor. *Neuron* **32**, 605-617.

Kennedy, T.E., Serafini, T., de la Torre, J.R., and Tessier-Lavigne, M. (1994). Netrins are diffusible chemotropic factors for commissural axons in the embryonic spinal cord. *Cell* **78**, 425-435.

Knappskog, S., Ravneberg, H., Gjerdrum, C., Trosse, C., Stern, B., and Pryme, I.F. (2007). The level of synthesis and secretion of Gaussia princeps luciferase in transfected CHO cells is heavily dependent on the choice of signal peptide. *Journal of biotechnology* **128**, 705-715.

Ko, S.Y., Dass, C.R., and Nurgali, K. (2012). Netrin-1 in the developing enteric nervous system and colorectal cancer. *Trends Mol Med* **18**, 544-554.

Koch, M., Murrell, J.R., Hunter, D.D., Olson, P.F., Jin, W., Keene, D.R., Brunken, W.J., and Burgeson, R.E. (2000). A novel member of the netrin family, beta-netrin, shares homology with the beta chain of laminin: identification, expression, and functional characterization. *The Journal of cell biology* **151**, 221-234.

Kolodkin, A.L., and Tessier-Lavigne, M. (2011). Mechanisms and molecules of neuronal wiring: a primer. *Cold Spring Harbor perspectives in biology* **3**.

Krissinel, E. (2011). Macromolecular complexes in crystals and solutions. *Acta Crystallogr D Biol Crystallogr* **67**, 376–385.

Krüger, N. (2011). Recombinant Expression of Pregnancy-specific Glycoproteins. In *Fachbereich Biologie (Universität Hamburg)*.

Kruger, R.P., Lee, J., Li, W., and Guan, K.L. (2004). Mapping netrin receptor binding reveals domains of Unc5 regulating its tyrosine phosphorylation. *The Journal of neuroscience : the official journal of the Society for Neuroscience* **24**, 10826-10834.

Lai Wing Sun, K., Correia, J.P., and Kennedy, T.E. (2011). Netrins: versatile extracellular cues with diverse functions. *Development* **138**, 2153-2169.

Larrivee, B., Freitas, C., Trombe, M., Lv, X., Delafarge, B., Yuan, L., Bouvree, K., Breant, C., Del Toro, R., Brechot, N., *et al.* (2007). Activation of the UNC5B receptor by Netrin-1 inhibits sprouting angiogenesis. *Genes & development* **21**, 2433-2447.

Lejmi, E., Bouras, I., Camelo, S., Roumieux, M., Minet, N., Lere-Dean, C., Merkulova-Rainon, T., Autret, G., Vayssettes, C., Clement, O., *et al.* (2014). Netrin-4 promotes mural cell adhesion and recruitment to endothelial cells. *Vascular cell* 6, 1.

Lejmi, E., Leconte, L., Pedron-Mazoyer, S., Ropert, S., Raoul, W., Lavalette, S., Bouras, I., Feron, J.G., Maitre-Boube, M., Assayag, F., *et al.* (2008). Netrin-4 inhibits angiogenesis via binding to neogenin and recruitment of Unc5B. *Proceedings of the National Academy of Sciences of the United States of America* 105, 12491-12496.

Leonardo, E.D., Hinck, L., Masu, M., Keino-Masu, K., Ackerman, S.L., and Tessier-Lavigne, M. (1997a). Vertebrate homologues of *C. elegans* UNC-5 are candidate netrin receptors. *Nature* 386, 833-838.

Leonardo, E.D., Hinck, L., Masu, M., Keino-Masu, K., Fazeli, A., Stoeckli, E.T., Ackerman, S.L., Weinberg, R.A., and Tessier-Lavigne, M. (1997b). Guidance of developing axons by netrin-1 and its receptors. *Cold Spring Harbor symposia on quantitative biology* 62, 467-478.

Lesnick, T.G., Papapetropoulos, S., Mash, D.C., Ffrench-Mullen, J., Shehadeh, L., de Andrade, M., Henley, J.R., Rocca, W.A., Ahlskog, J.E., and Maraganore, D.M. (2007). A genomic pathway approach to a complex disease: axon guidance and Parkinson disease. *PLoS genetics* 3, e98.

Lesnick, T.G., Sorenson, E.J., Ahlskog, J.E., Henley, J.R., Shehadeh, L., Papapetropoulos, S., and Maraganore, D.M. (2008). Beyond Parkinson disease: amyotrophic lateral sclerosis and the axon guidance pathway. *PloS one* 3, e1449.

Lim, Y.S., and Wadsworth, W.G. (2002). Identification of domains of netrin UNC-6 that mediate attractive and repulsive guidance and responses from cells and growth cones. *The Journal of neuroscience : the official journal of the Society for Neuroscience* 22, 7080-7087.

Lin, T.M., Halbert, S.P., and Spellacy, W.N. (1974). Measurement of pregnancy-associated plasma proteins during human gestation. *The Journal of clinical investigation* 54, 576-582.

Liu, L., Xie, S., Liao, X., Zhang, L., and Zhong, L. (2013). Netrin-1 pretreatment protects rat kidney against ischemia/reperfusion injury via suppression of oxidative stress and neuropeptide Y expression. *J Biochem Mol Toxicol* 27, 231-236.

Liu, Y., Stein, E., Oliver, T., Li, Y., Brunken, W.J., Koch, M., Tessier-Lavigne, M., and Hogan, B.L. (2004). Novel role for Netrins in regulating epithelial behavior during lung branching morphogenesis. *Current biology : CB* 14, 897-905.

Lobanov, M., Bogatyreva, N.S., and Galzitskaia, O.V. (2008). [Radius of gyration is indicator of compactness of protein structure]. *Molekuliarnaia biologii* 42, 701-706.

Lu, X., Le Noble, F., Yuan, L., Jiang, Q., De Lafarge, B., Sugiyama, D., Breant, C., Claes, F., De Smet, F., Thomas, J.L., *et al.* (2004). The netrin receptor UNC5B mediates guidance events controlling morphogenesis of the vascular system. *Nature* 432, 179-186.

Ly, A., Nikolaev, A., Suresh, G., Zheng, Y., Tessier-Lavigne, M., and Stein, E. (2008). DSCAM is a netrin receptor that collaborates with DCC in mediating turning responses to netrin-1. *Cell* 133, 1241-1254.

Manitt, C., Mimee, A., Eng, C., Pokinko, M., Stroh, T., Cooper, H.M., Kolb, B., and Flores, C. (2011). The netrin receptor DCC is required in the pubertal organization of mesocortical dopamine circuitry. *The Journal of neuroscience : the official journal of the Society for Neuroscience* 31, 8381-8394.

Manitt, C., Nikolakopoulou, A.M., Almarino, D.R., Nguyen, S.A., and Cohen-Cory, S. (2009). Netrin participates in the development of retinotectal synaptic connectivity by modulating axon arborization and synapse formation in the developing brain. *The Journal of neuroscience : the official journal of the Society for Neuroscience* 29, 11065-11077.

-
- Matus, D.Q., Pang, K., Marlow, H., Dunn, C.W., Thomsen, G.H., and Martindale, M.Q. (2006). Molecular evidence for deep evolutionary roots of bilaterality in animal development. *Proceedings of the National Academy of Sciences of the United States of America* 103, 11195-11200.
- Mazelin, L., Bernet, A., Bonod-Bidaud, C., Pays, L., Arnaud, S., Gespach, C., Bredesen, D.E., Scoazec, J.Y., and Mehlen, P. (2004). Netrin-1 controls colorectal tumorigenesis by regulating apoptosis. *Nature* 431, 80-84.
- McLellan, J.S., Yao, S., Zheng, X., Geisbrecht, B.V., Ghirlando, R., Beachy, P.A., and Leahy, D.J. (2006). Structure of a heparin-dependent complex of Hedgehog and Ihog. *Proceedings of the National Academy of Sciences of the United States of America* 103, 17208-17213.
- Mehlen, P., Delloye-Bourgeois, C., and Chedotal, A. (2011). Novel roles for Slits and netrins: axon guidance cues as anticancer targets? *Nature reviews Cancer* 11, 188-197.
- Meijers, R., Puettmann-Holgado, R., Skinotis, G., Liu, J.H., Walz, T., Wang, J.H., and Schmucker, D. (2007). Structural basis of Dscam isoform specificity. *Nature* 449, 487-491.
- Meyerhardt, J.A., Caca, K., Eckstrand, B.C., Hu, G., Lengauer, C., Banavali, S., Look, A.T., and Fearon, E.R. (1999). Netrin-1: interaction with deleted in colorectal cancer (DCC) and alterations in brain tumors and neuroblastomas. *Cell growth & differentiation : the molecular biology journal of the American Association for Cancer Research* 10, 35-42.
- Millard, S.S., and Zipursky, S.L. (2008). Dscam-mediated repulsion controls tiling and self-avoidance. *Current opinion in neurobiology* 18, 84-89.
- Moore, S.W., Tessier-Lavigne, M., and Kennedy, T.E. (2007). Netrins and their receptors. *Advances in experimental medicine and biology* 621, 17-31.
- Murshudov, G.N., Skubák, P., Lebedev, A.A., Pannu, N.S., Steiner, R.A., Nicholls, R.A., Winn, M.D., Long, F., and Vagin, A.A. (2011). REFMAC5 for the refinement of macromolecular crystal structures. *Acta Crystallogr D Biol Crystallogr* 67, 355–367.
- Nelson&Cox (2005). *Lehninger Biochemie, Vol 3. Auflage* (Springer Verlag Heidelberg).
- Newquist, G., Hogan, J., Walker, K., Lamanuzzi, M., Bowser, M., and Kidd, T. (2013). Control of male and female fertility by the netrin axon guidance genes. *PloS one* 8, e72524.
- Nguyen, A., and Cai, H. (2006). Netrin-1 induces angiogenesis via a DCC-dependent ERK1/2-eNOS feed-forward mechanism. *Proceedings of the National Academy of Sciences of the United States of America* 103, 6530-6535.
- Oeser, E. (2010). *Geschichte der Hirnforschung. Von der Antike bis zur Gegenwart*.
- P.V. Konarev, V.V.V., A.V. Sokolova, D.I. Svergun, (2003). OLIGOMER. *J Appl Cryst* 36, 1277-1282.
- Petit, A., Sellers, D.L., Liebl, D.J., Tessier-Lavigne, M., Kennedy, T.E., and Horner, P.J. (2007). Adult spinal cord progenitor cells are repelled by netrin-1 in the embryonic and injured adult spinal cord. *Proceedings of the National Academy of Sciences of the United States of America* 104, 17837-17842.
- Petoukhov, M.V., and Svergun, D.I. (2005). Global Rigid Body Modeling of Macromolecular Complexes against Small-Angle Scattering Data. *Biophys J* 89, 1237–1250.
- Petoukhov, M.V., Franke, D., Shkumatov, A.V., Tria, G., Kikhney, A.G., Gajda, M., Gorba, C., Mertens, H.D.T., Konarev, P.V., and Svergun, D.I. (2012). New developments in the ATSAS program package for small-angle scattering data analysis. *J Appl Crystallogr* 45, 342–350.
- Phan, K.D., Croteau, L.P., Kam, J.W., Kania, A., Cloutier, J.F., and Butler, S.J. (2011). Neogenin may functionally substitute for Dcc in chicken. *PloS one* 6, e22072.

-
- Pierce, M.M., Raman, C.S., and Nall, B.T. (1999). Isothermal titration calorimetry of protein-protein interactions. *Methods* 19, 213-221.
- Pinato, G., Cojoc, D., Lien, L.T., Ansuini, A., Ban, J., D'Este, E., and Torre, V. (2012). Less than 5 Netrin-1 molecules initiate attraction but 200 Sema3A molecules are necessary for repulsion. *Sci Rep* 2, 675.
- Qu, C., Dwyer, T., Shao, Q., Yang, T., Huang, H., and Liu, G. (2013). Direct binding of TUBB3 with DCC couples netrin-1 signaling to intracellular microtubule dynamics in axon outgrowth and guidance. *Journal of cell science*.
- Rajasekharan, S., Baker, K.A., Horn, K.E., Jarjour, A.A., Antel, J.P., and Kennedy, T.E. (2009). Netrin 1 and Dcc regulate oligodendrocyte process branching and membrane extension via Fyn and RhoA. *Development* 136, 415-426.
- Rajasekharan, S., and Kennedy, T.E. (2009). The netrin protein family. *Genome biology* 10, 239.
- Ramesh, G. (2012). Role of Netrin-1 Beyond the Brain: From Biomarker of Tissue Injury to Therapy for Inflammatory Diseases. *Recent Pat Biomark* 2, 202-208.
- Ramesh, G., Kwon, O., and Ahn, K. (2010). Netrin-1: a novel universal biomarker of human kidney injury. *Transplantation proceedings* 42, 1519-1522.
- Reeves, P.J., Callewaert, N., Contreras, R., and Khorana, H.G. (2002). Structure and function in rhodopsin: high-level expression of rhodopsin with restricted and homogeneous N-glycosylation by a tetracycline-inducible N-acetylglucosaminyltransferase I-negative HEK293S stable mammalian cell line. *Proceedings of the National Academy of Sciences of the United States of America* 99, 13419-13424.
- Rigato, C., Buckinx, R., Le-Corronc, H., Rigo, J.M., and Legendre, P. (2011). Pattern of invasion of the embryonic mouse spinal cord by microglial cells at the time of the onset of functional neuronal networks. *Glia* 59, 675-695.
- Round, J., and Stein, E. (2007). Netrin signaling leading to directed growth cone steering. *Current opinion in neurobiology* 17, 15-21.
- Schmucker, D., Clemens, J.C., Shu, H., Worby, C.A., Xiao, J., Muda, M., Dixon, J.E., and Zipursky, S.L. (2000). *Drosophila* Dscam is an axon guidance receptor exhibiting extraordinary molecular diversity. *Cell* 101, 671-684.
- Seaman, C., and Cooper, H.M. (2001). Netrin-3 protein is localized to the axons of motor, sensory, and sympathetic neurons. *Mechanisms of development* 101, 245-248.
- Serafini, T., Colamarino, S.A., Leonardo, E.D., Wang, H., Beddington, R., Skarnes, W.C., and Tessier-Lavigne, M. (1996). Netrin-1 is required for commissural axon guidance in the developing vertebrate nervous system. *Cell* 87, 1001-1014.
- Serafini, T., Kennedy, T.E., Galko, M.J., Mirzayan, C., Jessell, T.M., and Tessier-Lavigne, M. (1994). The netrins define a family of axon outgrowth-promoting proteins homologous to *C. elegans* UNC-6. *Cell* 78, 409-424.
- Shipp, E.L., and Hsieh-Wilson, L.C. (2007). Profiling the sulfation specificities of glycosaminoglycan interactions with growth factors and chemotactic proteins using microarrays. *Chemistry & biology* 14, 195-208.
- Siebert, J.R., and Osterhout, D.J. (2011). The inhibitory effects of chondroitin sulfate proteoglycans on oligodendrocytes. *Journal of neurochemistry* 119, 176-188.
- Sievers, F., and Higgins, D.G. (2014). Clustal Omega, accurate alignment of very large numbers of sequences. *Methods Mol Biol* 1079, 105-116.

Sola, R.J., and Griebenow, K. (2009). Effects of glycosylation on the stability of protein pharmaceuticals. *Journal of pharmaceutical sciences* 98, 1223-1245.

Sperry, R.W. (1963). Chemoaffinity in the Orderly Growth of Nerve Fiber Patterns and Connections. *Proceedings of the National Academy of Sciences of the United States of America* 50, 703-710.

Srinivasan, K., Strickland, P., Valdes, A., Shin, G.C., and Hinck, L. (2003). Netrin-1/neogenin interaction stabilizes multipotent progenitor cap cells during mammary gland morphogenesis. *Developmental cell* 4, 371-382.

Stein, E., and Tessier-Lavigne, M. (2001). Hierarchical organization of guidance receptors: silencing of netrin attraction by slit through a Robo/DCC receptor complex. *Science* 291, 1928-1938.

Stein, E., Zou, Y., Poo, M., and Tessier-Lavigne, M. (2001). Binding of DCC by netrin-1 to mediate axon guidance independent of adenosine A2B receptor activation. *Science* 291, 1976-1982.

Stryer, L. (1988). *Biochemistry*, Third edition edn (W.H. Freeman & Company).

Su, M., Merz, D.C., Killeen, M.T., Zhou, Y., Zheng, H., Kramer, J.M., Hedgecock, E.M., and Culotti, J.G. (2000). Regulation of the UNC-5 netrin receptor initiates the first reorientation of migrating distal tip cells in *Caenorhabditis elegans*. *Development* 127, 585-594.

Svergun, D., Barberato, C., and Koch, M.H.J. (1995). CRY SOL – a Program to Evaluate X-ray Solution Scattering of Biological Macromolecules from Atomic Coordinates. *J Appl Crystallogr* 28, 768–773.

Svergun D.I., B.C.a.K.M.H.J. ((1995)). CRY SOL - a Program to Evaluate X-ray Solution Scattering of Biological Macromolecules from Atomic Coordinates. *J Appl Cryst* 28, , 768-773.

Symes, K., Smith, E.M., Mitsi, M., and Nugent, M.A. (2010). Sweet cues: How heparan sulfate modification of fibronectin enables growth factor guided migration of embryonic cells. *Cell adhesion & migration* 4, 507-510.

Tan, K., Duquette, M., Liu, J.H., Shanmugasundaram, K., Joachimiak, A., Gallagher, J.T., Rigby, A.C., Wang, J.H., and Lawler, J. (2008). Heparin-induced cis- and trans-dimerization modes of the thrombospondin-1 N-terminal domain. *The Journal of biological chemistry* 283, 3932-3941.

Tang, F., and Kalil, K. (2005). Netrin-1 induces axon branching in developing cortical neurons by frequency-dependent calcium signaling pathways. *The Journal of neuroscience : the official journal of the Society for Neuroscience* 25, 6702-6715.

Tessier-Lavigne, M., and Goodman, C.S. (1996). The molecular biology of axon guidance. *Science* 274, 1123-1133.

Thiebault, K., Mazelin, L., Pays, L., Llambi, F., Joly, M.O., Scoazec, J.Y., Saurin, J.C., Romeo, G., and Mehlen, P. (2003). The netrin-1 receptors UNC5H are putative tumor suppressors controlling cell death commitment. *Proceedings of the National Academy of Sciences of the United States of America* 100, 4173-4178.

Trisler, G.D., Schneider, M.D., and Nirenberg, M. (1981). A topographic gradient of molecules in retina can be used to identify neuron position. *Proceedings of the National Academy of Sciences of the United States of America* 78, 2145-2149.

Tsai, H.H., Macklin, W.B., and Miller, R.H. (2006). Netrin-1 is required for the normal development of spinal cord oligodendrocytes. *The Journal of neuroscience : the official journal of the Society for Neuroscience* 26, 1913-1922.

Unni, S., Huang, Y., Hanson, R.M., Tobias, M., Krishnan, S., Li, W.W., Nielsen, J.E., and Baker, N.A. (2011). Web servers and services for electrostatics calculations with APBS and PDB2PQR. *Journal of computational chemistry* 32, 1488-1491.

-
- Vagin, A., and Teplyakov, A. (2010). Molecular replacement with MOLREP. *Acta Crystallogr D Biol Crystallogr* 66, 22–25.
- Vielmetter, J., Chen, X.N., Miskevich, F., Lane, R.P., Yamakawa, K., Korenberg, J.R., and Dreyer, W.J. (1997). Molecular characterization of human neogenin, a DCC-related protein, and the mapping of its gene (NEO1) to chromosomal position 15q22.3-q23. *Genomics* 41, 414-421.
- Vogelstein, B., Fearon, E.R., Hamilton, S.R., Kern, S.E., Preisinger, A.C., Leppert, M., Nakamura, Y., White, R., Smits, A.M., and Bos, J.L. (1988). Genetic alterations during colorectal-tumor development. *The New England journal of medicine* 319, 525-532.
- Volkov, V.V., and Svergun, D.I. (2003). Uniqueness of ab initio shape determination in small-angle scattering. *J Appl Crystallogr* 36, 860–864.
- Wang, G.X., and Poo, M.M. (2005). Requirement of TRPC channels in netrin-1-induced chemotropic turning of nerve growth cones. *Nature* 434, 898-904.
- Wienken, C.J., Baaske, P., Rothbauer, U., Braun, D., and Duhr, S. (2010). Protein-binding assays in biological liquids using microscale thermophoresis. *Nature communications* 1, 100.
- Wilson, B.D., Li, M., Park, K.W., Suli, A., Sorensen, L.K., Larrieu-Lahargue, F., Urness, L.D., Suh, W., Asai, J., Kock, G.A., *et al.* (2006). Netrins promote developmental and therapeutic angiogenesis. *Science* 313, 640-644.
- Xie, Y., Hong, Y., Ma, X.Y., Ren, X.R., Ackerman, S., Mei, L., and Xiong, W.C. (2006). DCC-dependent phospholipase C signaling in netrin-1-induced neurite elongation. *The Journal of biological chemistry* 281, 2605-2611.
- Yam, P.T., Langlois, S.D., Morin, S., and Charron, F. (2009). Sonic hedgehog guides axons through a noncanonical, Src-family-kinase-dependent signaling pathway. *Neuron* 62, 349-362.
- Yamakawa, K., Huot, Y.K., Haendelt, M.A., Hubert, R., Chen, X.N., Lyons, G.E., and Korenberg, J.R. (1998). DSCAM: a novel member of the immunoglobulin superfamily maps in a Down syndrome region and is involved in the development of the nervous system. *Human molecular genetics* 7, 227-237.
- Yang, F., West, A.P., Jr., and Bjorkman, P.J. (2011). Crystal structure of a hemojuvelin-binding fragment of neogenin at 1.8Å. *Journal of structural biology* 174, 239-244.
- Yang, L., Garbe, D.S., and Bashaw, G.J. (2009). A frazzled/DCC-dependent transcriptional switch regulates midline axon guidance. *Science* 324, 944-947.
- Zhang, Y., Goodyer, C., and LeBlanc, A. (2000). Selective and protracted apoptosis in human primary neurons microinjected with active caspase-3, -6, -7, and -8. *The Journal of neuroscience : the official journal of the Society for Neuroscience* 20, 8384-8389.
- Zipursky, S.L., and Sanes, J.R. (2010). Chemoaffinity revisited: dscams, protocadherins, and neural circuit assembly. *Cell* 143, 343-353.

8. Appendix

8.a. Publication

The results presented in the chapters 4.b.2, 4.b.3, 4.b.4, 4.b.5, 4.b.7, 4.b.8 and 4.c. have been accepted for publication in **NEURON**:

The crystal structure of netrin-1 in complex with DCC reveals the bifunctionality of netrin-1 as a guidance cue

Lorenzo I. Finci^{1,2†}, Nina Krüger^{3†}, Xiaqin Sun^{1†}, Jie Zhang¹, Magda Chegkazi³, Yu Wu¹, Gundolf Schenk³, Haydyn D. T. Mertens³, Dmitri I. Svergun³, Yan Zhang^{1,4*}, Jia-huai Wang^{1,2*} and Rob Meijers^{3*}

Affiliations:

¹State Key Laboratory of Biomembrane and Membrane Biotechnology, College of Life Sciences, Peking University, Beijing, 100871, China

²Dana-Farber Cancer Institute, Harvard Medical School, Boston, MA. 02215, USA

³European Molecular Biology Laboratory (EMBL), Hamburg Outstation, Notkestrasse 85, 22607, Hamburg, Germany.

⁴PKU-IDG/McGovern Institute for Brain Research, Peking University, Beijing, 100871, China

Contact:

Rob Meijers: r.meijers@embl-hamburg.de, and Jia-huai Wang: jwang@red.dfci.harvard.edu

Additional Footnotes:

†These authors contributed equally to this work

*Correspondence to: Rob Meijers r.meijers@embl-hamburg.de, Jia-huai Wang jwang@red.dfci.harvard.edu, and Yan Zhang yanzhang@pku.edu.cn.

Abstract

Netrin-1 is a guidance cue that can trigger either attraction or repulsion effects on migrating neurons, depending on the repertoire of receptors available on the growth cone. How a single chemotropic molecule can act in such contradictory ways has long been a puzzle at the molecular level. Here we present the crystal structure of netrin-1 in complex with the Deleted in Colorectal Cancer (DCC) receptor. We show that one netrin-1 molecule can simultaneously bind to two DCC molecules through a DCC-specific site and through a unique generic receptor binding site, where sulfate ions staple together positively charged patches on both DCC and netrin-1. Furthermore, we demonstrate that UNC5A can replace DCC on the generic receptor binding site to switch the response from attraction to repulsion. We propose that the modularity of binding allows for the association of other netrin receptors at the generic binding site, eliciting alternative turning responses.

8.b. Eidesstattliche Versicherung

Hiermit erkläre ich an Eides statt, dass ich die vorliegende Dissertationsschrift selbst verfasst und keine anderen als die angegebenen Quellen und Hilfsmittel benutzt habe.

Hamburg, den 18.03.2014

Nina Krüger

8.c. SAXS data table

Table SI SAXS Data collection and derived parameters for Netrin_{VIV}, DCC_{FN56} and Netrin_{VIV} / DCC_{FN56}.

	Netrin _{VIV}	DCC _{FN56}	Netrin _{VIV} / DCC _{FN56} wt	Netrin _{VIV} / DCC _{FN56} M933R
Data collection parameters				
Instrument	EMBL P12 (PETRA-III)			
Beam geometry (mm ²)	0.2 x 0.12			
Wavelength (Å)	1.24			
s range (Å ⁻¹) ^a	0.005-0.35	0.002-0.40	0.005-0.35	0.005-0.35
Exposure time (s)	0.045-20	0.05-20	0.045-20	0.045-20
Concentration range (mg/mL)	0.3-1.2	0.8-9.9	0.3-2.9	0.3-3.9
Temperature (K)	283			
Structural parameters				
$I(0)$ (relative) [from $p(r)$]	1420± 20	810± 20	1450± 20	1260± 20
R_g (Å) [from $p(r)$]	40±1	34±1	51±2	40±1
$I(0)$ (relative) (from Guinier)	1400 ± 20	800 ± 20	1450 ± 20	1270 ± 20
R_g (Å) (from Guinier)	39±1	32 ± 1	51 ± 2	40 ± 1
D_{max} (Å)	135±10	110±10	170±20	140±10
Porod volume (10 ³ Å ³)	100±10	38±5	120± 15	95± 10
Dry volume (10 ³ Å ³) calculated [from sequence]	66	31	N/A	N/A

Molecular mass M_r (kDa) [from $I(0)$]	48 ± 6	27 ± 3	49 ± 7	42 ± 6
Molecular mass M_r (kDa) [from Porod volume ($V_p/1.7$)]	58 ± 8	24 ± 3	70 ± 10	56 ± 8
Calculated monomeric M_r (kDa) [from sequence]	49.3 ^b	25.5	N/A	N/A

Software employed

Primary data reduction	Automated pipeline (Franke et al., 2012)
Data processing	ALMERGE, AUTORG, DATGNOM, DATPOROD
Ab initio analysis	DAMMIF, DAMMIN
Validation and averaging	SUPCOMB, DAMAVER
Rigid-body modeling	BUNCH
Computation of model intensities	CRYSOL, FFMAKER, OLIGOMER
3D graphics representations	UCSF Chimera (Pettersen et al., 2004)

Abbreviations: M_r : molecular mass; R_g : radius of gyration; D_{max} : maximal particle dimension; V_p : Porod volume. ^aMomentum transfer $|s| = 4\pi\sin(\theta)/\lambda$. ^bwith added glycans, 54.6 kDa

CRYSOL: Svergun D.I., Barberato C. & Koch M.H.J. (1995) *J. Appl. Cryst.* **28**, 768-773.

OLIGOMER: P.V.Konarev, V.V.Volkov, A.V.Sokolova, M.H.J.Koch and D. I. Svergun (2003) *J Appl Cryst.* **36**, 1277-1282.

BUNCH: Petoukhov, M.V. & Svergun, D.I. (2005) *Biophys J.* **89**, 1237-1250.

SUPCOMB: M.Kozin & D.Svergun (2001) *J Appl Cryst.* **34**, 33-41.

DAMAVER: V. V. Volkov and D. I. Svergun (2003) *J. Appl. Cryst.* **36**, 860-864.

DAMMIF: D. Franke and D. I. Svergun (2009) *J Appl Cryst.* **42**, 342-346.

DAMMIN: D. I. Svergun (1999) *Biophys J.* **77**, 2879-2886.

Pipeline: Franke, D., Kikhney, A.G. and Svergun, D.I. (2012) *Nuc Inst Meth A* **689**, 52-59

AUTORG, DATGNOM: M. V. Petoukhov, P. V. Konarev, A. G. Kikhney and D. I. Svergun (2007) *J Appl Cryst.* 40, s223-s228.

DATPOROD: Petoukhov, M.V., Franke, D., Shkumatov, A.V., Tria, G., Kikhney, A.G., Gajda, M., Gorba, C., Mertens, H.D.T., Konarev, P.V. and Svergun, D.I. (2012) *J. Appl. Cryst.* 45, 342-350

8.d. Crystallisation data table

Table S2 Data collection and refinement statistics

	Netrin _{VIV} /DCC _{FN56} complex
Data collection	
Space group	P2 ₁ 2 ₁ 2 ₁
Unit cell dimensions	
<i>a</i> , <i>b</i> , <i>c</i> (Å)	84.6 87.4 155.3
α , β , γ (°)	90.0, 90.0, 90.0
Resolution (Å)	30 – 3.10 (3.31 – 3.10) *
<i>R</i> _{merge}	14.8 (82.0)
<i>I</i> / <i>sI</i>	10.8 (1.8)
Completeness (%)	99.3 (96.0)
Redundancy	8.3 (3.7)
CC _{1/2} at 3.10 Å (Karplus and Diederichs, 2012)	0.64
Refinement	
Resolution (Å)	30 – 3.10
No. reflections	20291
<i>R</i> _{work} / <i>R</i> _{free}	23.8 (28.5)
No. atoms	
Protein	5038
Ligand/ion	91
Water	N/A
<i>B</i> -factors	
Protein	81
Ligand/ion	101
Water	N/A
RMS deviations	
Bond lengths (Å)	0.02
Bond angles (°)	0.68
Ramachandran Statistics	
Favored (%)	91.5
Disallowed (%)	0.5

*Values in parentheses are for the highest-resolution shell.
